Yukikazu Itikawa

SPRINGER SERIES IN ATOMIC, OPTICAL AND PLASMA PHYSICS 43

Molecular Processes in Plasmas

Collisions of Charged Particles with Molecules

Springer

Springer Series on

ATOMIC, OPTICAL, AND PLASMA PHYSICS 43

Springer Series on

ATOMIC, OPTICAL, AND PLASMA PHYSICS

The Springer Series on Atomic, Optical, and Plasma Physics covers in a comprehensive manner theory and experiment in the entire field of atoms and molecules and their interaction with electromagnetic radiation. Books in the series provide a rich source of new ideas and techniques with wide applications in fields such as chemistry, materials science, astrophysics, surface science, plasma technology, advanced optics, aeronomy, and engineering. Laser physics is a particular connecting theme that has provided much of the continuing impetus for new developments in the field. The purpose of the series is to cover the gap between standard undergraduate textbooks and the research literature with emphasis on the fundamental ideas, methods, techniques, and results in the field.

36 **Atom Tunneling Phenomena in Physics, Chemistry and Biology**
Editor: T. Miyazaki

37 **Charged Particle Traps**
Physics and Techniques of Charged Particle Field Confinement
By V.N. Gheorghe, F.G. Major, G. Werth

38 **Plasma Physics and Controlled Nuclear Fusion**
By K. Miyamoto

39 **Plasma-Material Interaction in Controlled Fusion**
By D. Naujoks

40 **Relativistic Quantum Theory of Atoms and Molecules**
Theory and Computation
By I.P. Grant

41 **Turbulent Particle-Laden Gas Flows**
By A.Y. Varaksin

42 **Phase Transitions of Simple Systems**
By B.M. Smirnov and S.R. Berry

43 **Collisions of Charged Particles with Molecules**
By Y. Itikawa

44 **Collisions of Charged Particles with Molecules**
Editors: T. Fujimoto and A. Iwamae

Vols. 10–35 of the former Springer Series on Atoms and Plasmas are listed at the end of the book

Y. Itikawa

Molecular Processes in Plasmas

Collisions of Charged Particles with Molecules

With 84 Figures

Springer

Dr. Yukikazu Itikawa
3-16-3 Miwamidoriyama
Machida
Tokyo 195-0055
Japan
E-mail: yukitikawa@nifty.com

ISSN 1615-5653

ISBN 978-3-540-72609-8 Springer Berlin Heidelberg New York

Library of Congress Control Number: 2007927102

Typesetting and prodcution: SPI Publisher Services
Cover design: eStudio Calmar Steinen

Printed on acid-free paper SPIN: 11578727 57/3180/SPI - 5 4 3 2 1 0

Preface

When I was a graduate student, I studied plasma physics. My thesis for D.Sc. was concerned with transport properties of plasmas. This study needed information of elementary collision processes in the plasma. Since the plasma considered was a fully ionized, hydrogen plasma, collisions were only the Coulomb scattering among plasma particles (i.e., electrons and protons). Therefore, no atomic physics was involved in the study. After my graduation, I started a theoretical study of atomic collisions. Among a variety of collision processes, I was particularly interested in electron–molecule collisions. Molecules are much more complicated than atoms. A detailed study of electron–molecule collisions was somewhat behind the study of electron–atom collisions. At first, my study of atomic collisions had no relation to plasma physics. Eventually, however, I realized that the electron–molecule collision is a fundamental elementary process in gaseous discharges. In fact, scientists engaged in the research of gaseous discharges, or more generally weakly ionized plasmas, are very much interested in electron–molecule collisions. I began to contact those scientists.

Then came an era of plasma processing. In the 1990s, a weakly ionized plasma found a wide range of applications. Requests of information of electron–molecule collisions and related subjects have arisen from industry. Personally, I have been asked to give a talk of atomic collisions to the community of application fields. They often want to have a text book on atomic collisions they can refer to. The present book is my answer to the request.

Many text books on plasma physics include sections for atomic collision processes, but usually they give only a general feature of the processes. On the other hand, many text books are available on the atomic and molecular collisions. Usually, however, they are too much detailed to be referred for application problems. This book has been written from the stand points of atomic physics. Nothing is mentioned about plasma physics. But the examples shown have been selected with an intension to the application in molecular plasmas. The description of atomic physics is as much compact as possible. But, if anyone wants to know more details, he/she is directed to a proper reference. In this sense, this book serves as a guide to atomic physics that is

necessary to understand the molecular processes in plasmas. From the side of applications, the items sought after are cross-section data. Considering that situation, this book would also serve as a guide for cross-section data on molecular processes.

During the preparation of this book, many scientific colleagues in the world provided the results of their theoretical and experimental research on atomic collisions. I am very much grateful, particularly, to Professor H. Tanaka of the Sophia University, Tokyo. He not only made available the detailed results of the experiments of his group, but also kindly offered me technical help for the preparation of the manuscript.

Tokyo, March 2007 *Yukikazu Itikawa*

Contents

1

Introduction

Plasma is an ionized gas which contains equal amounts of positive and negative charges. Positive charges are carried by positive ions. Negative charges are usually supplied by electrons, but in some cases negative ions have a contribution. Plasmas are broadly classified into two classes. One is a high-temperature, fully ionized plasma. The other is a low-temperature, weakly ionized one. This book is concerned with a molecular plasma, i.e., a plasma containing neutral molecules. In most cases, a molecular plasma belongs to the class of low-temperature, weakly ionized plasmas. But, although belonging to the class, plasmas composed only of atoms (e.g., rare gases) are not dealt with in this book. Some of the high-temperature, fully ionized plasmas have a supply of molecules from outside and partly become a molecular plasma. For example, a plasma in a fusion device has a very hot core region, but also contains a large amount of molecules in its boundary region (see Sect. 2.4).

This book deals with molecular processes in the molecular plasmas. A molecular process literally means an elementary collision process involving molecules. In this book, however, it means a collision between charged particles (i.e., ions and electrons) and molecules. Electron collisions with molecular ions are also discussed in this book. Collisions involving only neutral molecules are primarily a subject of chemistry and less concerned with plasmas.

One of the typical examples of molecular plasmas is the ionosphere on the Earth and other planets. In the ionosphere, atoms and molecules are ionized mainly by the UV or X-ray photons from the Sun. Most regions of the Universe are in a state of plasmas. A stellar atmosphere, for example, is a kind of high-temperature plasmas, but molecules are often found there. Interstellar space is filled with very-low density matter. In the space, a clump of matter is found and called an interstellar cloud. Those clouds contain a variety of molecules. They also have ions and electrons. In that sense, the interstellar clouds are molecular plasmas. Although their fraction is very small, the charged particles play an important role in the interstellar cloud. Many of the laboratory plasmas are low-temperature, weakly ionized ones and generated from a molecular gas. In recent years, plasmas are utilized for a wide range of industrial

purposes. Many of these plasmas are molecular. Fluorocarbon molecules, for instance, are used for plasma etching of microelectronics. Hydrocarbon molecules are the main ingredient of the plasma for the deposition of carbon layers. Atmospheric plasmas (i.e., plasmas generated from atmospheric gases) are widely used for pollution control or surface modification.

Molecular processes play fundamental roles in the plasmas. The production of positive ions (and free electrons) is of primary importance in generating and maintaining plasmas. An electron-impact ionization of molecules is the main process for that. In laboratory plasmas, electrons are accelerated by an applied electric field. On the other hand, those electrons lose their energy through collisions with plasma particles (mainly with molecules). As a result of balance of these two processes (i.e., acceleration and deceleration), the electrons have a stationary distribution of their energies. The resulting electron energy distribution function (EEDF) determines the transport properties of electrons and the rates of various electron–collision processes. In some cases (e.g., in the ionosphere), ions are produced by photoionization processes. The photoelectrons produced usually have a finite kinetic energy. Upon collisions with plasma particles, the photoelectrons degrade their energy to reach a thermal distribution of energies. The last, but not the least, important role of the molecular processes is the production of active species. Those products are ions, excited atoms and molecules, radicals, reactive atoms such as O and F, and high-energy photons. Some of the products even have a significant amount of kinetic energy (i.e., being "hot"). These species are the source of actions of practical importance.

The aim of this book is to list up all possible processes of collisions between charged particles (i.e., ions and electrons) and neutral molecules (and molecular ions). A brief description with figures of examples is given for each process. The descriptions are not too much detailed, but are intended to give an overall picture of the process. An emphasis is placed on the features which are tended unnoticed when the processes are considered for applications. Keeping in mind those collisions in a molecular plasma, discussions are concentrated on low-energy collisions. Collision energies considered are mostly in the range from thermal energy at room temperature (=0.026 eV) to 100 eV for electrons and to 10 eV for ions. For the understanding of the collision processes, the basic ideas and the fundamental quantities in the physics of atomic collisions are presented. Furthermore, specific features of molecular targets are summarized and a simple theory of electron–molecule collisions is given.

The plan of this book is as follows. Chapter 2 presents four examples of molecular plasmas: Earth's ionosphere (Sect. 2.1), interstellar clouds (Sect. 2.2), gaseous discharges (mainly for plasma processing) (Sect. 2.3), and edge plasmas in fusion devices (Sect. 2.4). Chapters 3 and 4 give the fundamental ideas and quantities in the physics of atomic collisions and, in particular, a brief theory of electron–molecule collisions. These are the minimum essence of the atomic collision physics, necessary for understanding the molecular processes described in the following chapters. Chapter 5 is devoted to the

electron–molecule collision processes. Seven different processes are stated separately. Four related subjects (i.e., the total scattering, momentum–transfer, emission, and stopping cross-sections) are also described in additional sections. Most of the collision processes described in this chapter are those for the target molecules in their ground state. In the practical applications, the information is needed about the collisions involving targets in excited states. Those information are scarcely available. The situation is summarized in the last section of Chap. 5. Next chapter (Chap. 6) deals with ion collisions with molecules. The ion–molecule collisions are much more complicated than the electron–molecule ones. Besides the same processes as in the electron–molecule collisions, charge changing processes and rearrangement of atomic components are possible in the ion–molecule collisions. The description of the ion–molecule collisions are broadly divided into three parts: momentum–transfer processes (Sect. 6.2), inelastic collisions with no change of collision system (Sect. 6.3), and rearrangements, including charge changing processes (Sect. 6.4). Chapter 7 briefly reviews the electron collisions with molecular ions. This process is not necessarily major in molecular plasmas, but has a special feature as a collision of two charged particles. After the description of the general feature of the electron collisions with molecular ions, recombination processes are separately described in Sect. 7.2. To make this book more informative, useful tables and a guide for cross-section data are attached as appendices. Appendix A gives tables showing magnitudes of typical macroscopic quantities derived from cross-sections. Appendix B tabulates molecular parameters needed to understand the cross-section data. A simple theory of cross-section calculation is the Born approximation. It is not necessarily accurate, but very useful to analyze the physics under the collision process. Appendix C presents how to use the Born approximation, particularly for the electron-impact excitation of rotational and vibrational states of a molecule. For the demonstration of the variety of electron–molecule collisions, Appendix D graphically shows sets of cross-sections for four simple molecules (H_2, N_2, H_2O, and CO_2). The last three appendices (Appendices E, F, and G) are a guide to readers who want to find cross-section data. It is not a complete guide, but gives a clue when they search necessary data.

A few important collision processes in molecular plasmas or related phenomena are out of the scope of this book. In a weakly ionized plasma, collisions among neutral particles (i.e., molecule–molecule collisions) may have as much a significance as the collisions involving charged particles. In particular, collisions of active neutral species (particularly, radicals and excited molecules) with other molecules often play a decisive role for plasma activity in applications. Those neutral–neutral collisions are too complicated to summarize in a chapter or two and hence totally excluded from this book. Another processes not mentioned here are the elementary processes on the surface of the apparatus or electrodes. The surface processes are sensitively dependent on the condition of the surface. It is difficult to state those processes without specifying the surface conditions.

In this book, many examples of cross-sections are shown graphically or tabulated. These examples are primarily presented to show the general feature of the respective processes. Although they have been carefully selected as reliable data, they are not necessarily the best (i.e., the most accurate) values for applications. In other words, this book is not a compilation of cross-section data. This would, however, serve as a guide to find and understand the cross-section data.

2

Plasmas Involving Molecules

2.1 Ionosphere

A part of the atmosphere of the Earth and other planets is ionized by solar radiation and precipitating particles from outside. The part of rather high density of electrons is called an ionosphere. This is a typical example of molecular plasmas in nature. Here we consider the ionosphere on the Earth. For the ionospheres on the other planets, as well as details of the Earth's ionosphere, see the text book of Schunk and Nagy [144].

The Earth's ionosphere is located at the height of 60–1,000 km. The structure of the ionosphere is different for the day side and night side (more precisely, depending on the local time). It is severely affected by the solar activity. Figure 2.1 shows one example of ionic composition and electron density of the day side ionosphere at the minimum of solar activity [85]. This is a composite picture based on a few rocket and satellite measurements in 1963 and 1964. The absolute value of ion number density is normalized to the electron number density measured separately. Typical value of the electron density is $\sim 10^5\,\mathrm{cm}^{-3}$ at 100 km and $\sim 10^6\,\mathrm{cm}^{-3}$ at 200 km. These values are compared with the density of atmosphere: $\sim 10^{13}\,\mathrm{cm}^{-3}$ at 100 km and $\sim 10^{10}\,\mathrm{cm}^{-3}$ at 200 km. In the region of ionosphere, the Earth's atmosphere is composed mainly of N_2, O_2, and O. Above about 200 km, atomic oxygen dominates over the molecular components.

In the day side region at the height of about 100 km, the ionospheric plasma is maintained in the following manner:

(1) Ionization by solar radiation, particularly by the radiation of short wavelength

$$\text{Solar radiation} + \mathrm{N_2} \rightarrow \mathrm{N_2^+} + \mathrm{e(ph)}$$

$$\text{Solar radiation} + \mathrm{O_2} \rightarrow \mathrm{O_2^+} + \mathrm{e(ph)}$$

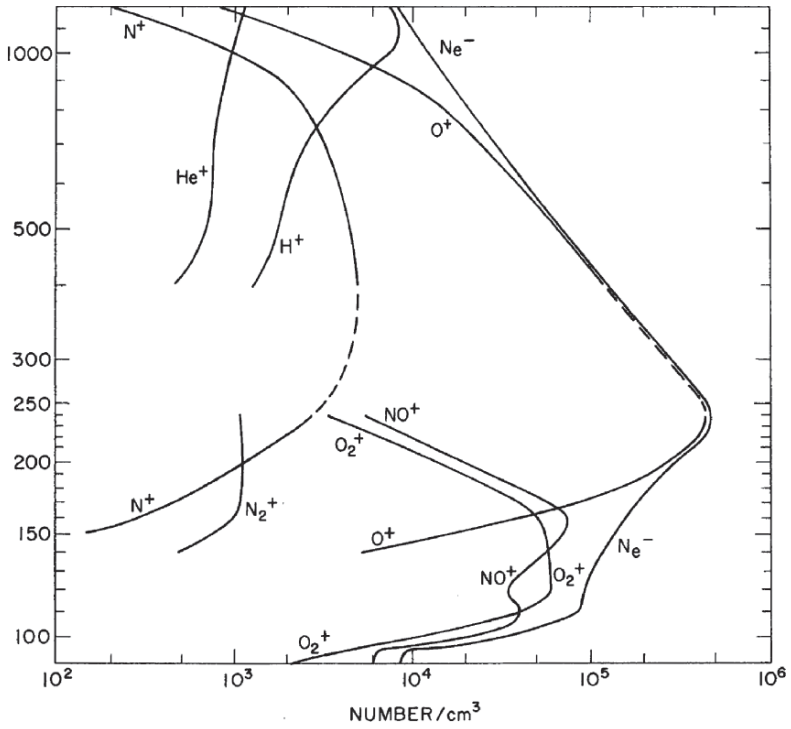

Fig. 2.1. Ion composition and electron density of the day side ionosphere on the Earth, reproduced from [85]. Ordinate is the height in km above the ground

The electrons produced are called photoelectrons (denoted by e(ph)). They have a rather high kinetic energy (20–30 eV or more). The N_2^+ is, however, immediately transformed into NO^+ by the reaction

$$N_2^+ + O \rightarrow NO^+ + N$$

As a result, the most abundant ions at the height around 100 km are O_2^+ and NO^+ as is shown in Fig. 2.1. Above about 150 km, an atomic ion, O^+, dominates. This ion is produced by the photoionization of atomic oxygen.

(2) Recombination of ions with the thermal electrons.

The photoelectrons lose their energy through the collisions with the atmospheric particles (N_2, O_2, O). They eventually join the thermal electrons, whose temperature is around 1,000 K. This slowed-down photoelectron is the source of the thermal electrons in the ionosphere. The energy degradation process of photoelectrons is discussed later in this section. The ions produced in (1) are recombined with the thermal electrons (denoted here by e(th))

$$NO^+ + e(th) \rightarrow N + O$$

$$O_2^+ + e(th) \rightarrow O + O$$

Even O^+ disappears through these recombination processes. First it is transformed into molecular ions through the processes:

$$O^+ + N_2 \rightarrow NO^+ + N$$

$$O^+ + O_2 \rightarrow O_2^+ + O$$

Then the molecular ions, NO^+ and O_2^+, recombine with electrons as above.

In the region at around 100 km, these processes (i.e., photoionization, electron energy-degradation, and electron–ion recombination) take place locally. As the height increases, the atmospheric density decreases rapidly and the transport (diffusion) of electrons dominates over those collision processes. In other words, nonlocal effects must be considered for the maintenance of the ionosphere.

Electron–molecule collisions play a significant role in the ionosphere. Examples are the following.

2.1.1 Energy Degradation of Photoelectrons

The photoelectrons lose their energy by the collisions with atmospheric atoms, molecules, ions, and electrons. Because of the large density of the neutral particles, the degradation process is so fast that a steady-state distribution of electron energy is established. The resulting distribution (i.e., the electron energy spectrum) can be observed by rockets or satellites. One example is shown in Fig. 2.2. The figure shows the energy distribution observed with a satellite at the height of 150–282 km by Lee et al. [99]. It corresponds to the daytime ionosphere at the solar minimum condition. Most of the structure in the distributions reflects the structure in the spectrum of solar radiation. To understand the energy degradation, we need information of all the collision processes between the electrons (in the energy range 1–100 eV) and the molecules N_2 and O_2 (and O) (see, for example, [155]). With the use of the information, calculations of the energy distribution of ionospheric electrons have been performed several times (see, for example [8]). Those calculations generally could reproduce the observed spectra of electron energy. For example, the sharp dip at around 2 eV in the energy spectra at the lower altitudes (e.g., at 150 km) was ascribed to the large cross-section of the vibrational excitation of N_2 due to the resonance process (see Sect. 5.5). Once electrons acquire the energy ($\sim$2 eV) for the resonance to occur, they quickly lose that energy through the resonant vibrational excitation of N_2.

2.1.2 Optical Emission

Optical emission from the atmosphere (called airglow) is caused by various processes. One of them is the excitation (and excitation following dissociation) of molecules by energetic photoelectrons (see [110]). (Others are resonant

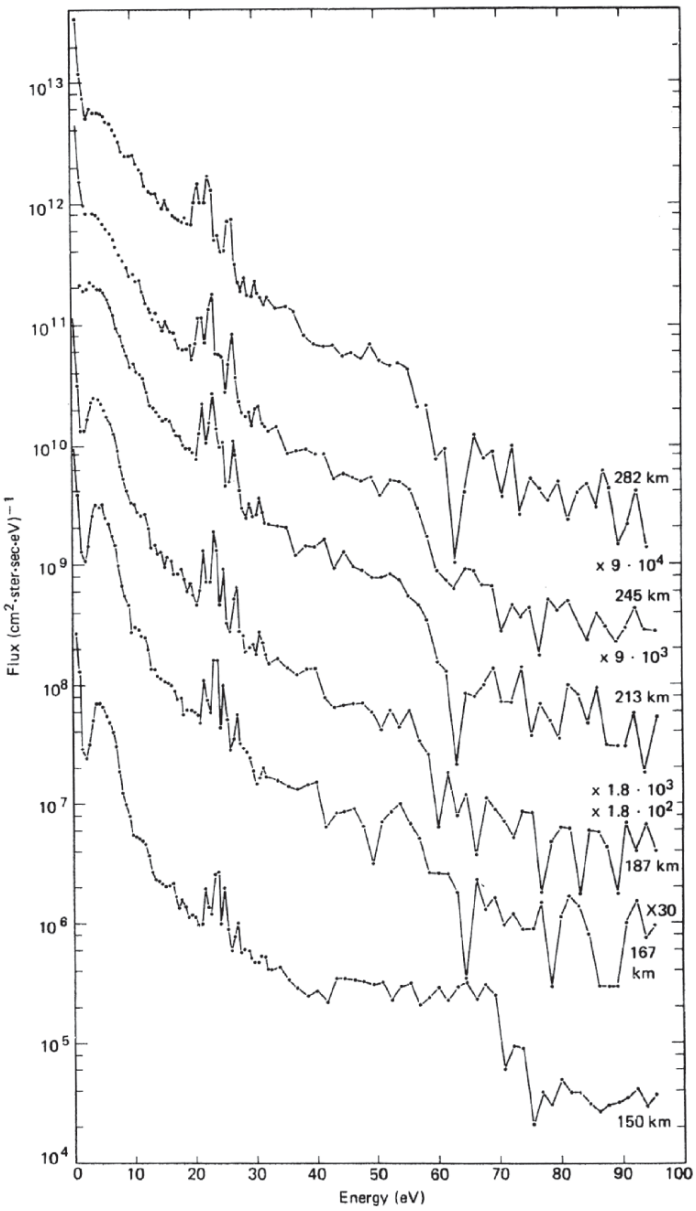

Fig. 2.2. Energy distribution of photoelectrons in the Earth's ionosphere, reproduced from [99]. The photoelectron flux per unit energy, observed by a satellite, is shown for the heights from 150 to 282 km

scattering of sunlight, photoexcitation by solar radiation, chemical reactions of atmospheric atoms and molecules, etc.)

For example, Broadfoot et al. [16] observed the emission in the range 115–900 nm. They identified some part of the spectra as the emission from N_2 induced by electron impact. They were the emissions associated with the transitions:

$$C^3\Pi_u \rightarrow B^3\Pi_g$$
$$B^3\Pi_g \rightarrow A^3\Sigma_u^+$$
$$a^1\Pi_g \rightarrow X^1\Sigma_g^+$$

The emission cross-sections for these transitions are dealt with in Sect. 5.9. If the emission mechanism is known, the observed spectra can be used for the diagnostics of the atmosphere. That is, we can deduce atmospheric composition, density, temperature, etc. from the analysis of the observed spectra of airglow.

Aurora is another example of atmospheric emission (see, for example, [162]). It is caused by high-energy charged particles (usually electrons) precipitating from outside of the atmosphere. Those charged particles (with energies above about 1 keV) are generated in the magnetosphere, transported along the line of magnetic field, and injected into the high-latitude atmosphere. The roles of the electron–molecule collisions in the auroral emission is twofold: energy degradation of fast electrons and emission of radiation. The incoming high-energy electrons quickly reach the lower-range of the ionosphere. Since the atmospheric density increases rapidly with decreasing height, those electrons lose their energies mostly in the lower region (at around 100 km). During the slowing down processes, the electrons collide with molecules to emit radiation. The radiation intensity is proportional to the emission cross-section and the number of emitting molecules. The emission cross-section depends on the electron energy, which, in turn, is determined by the degradation processes.

To understand aurora, modeling calculations have been performed many times. One example is the Monte Carlo simulation by Onda et al. [126]. Starting from the measured energy spectra of the incident high-energy electrons, they simulated the thorough behavior of the electrons until they join the thermal electrons of the ionosphere. They obtained the emission spectra, particularly for the transition:

$$N_2^+(B^2\Sigma_u^+) \rightarrow N_2^+(X^2\Sigma_g^+)$$

This transition is mainly caused by an electron-impact ionization–excitation process:

$$e + N_2 \rightarrow e + N_2^+(B^2\Sigma_u^+) + e$$

The agreement between the calculated and observed spectra was fairly good. The emission spectra are sensitively dependent on the energy spectra of the

incident high-energy electrons. The notable point of the work of Onda et al. is that the energy spectra of the incident electrons was simultaneously measured with the observation of the auroral spectra and used as an input of the model calculation. By doing so, they could avoid any ambiguity associated with the incident high-energy electrons. Most of other modeling studies assume some model spectra for the incident electrons.

2.1.3 Energy Balance and Transport Phenomena in Thermal Electrons

The thermal electrons in the ionosphere are usually assumed to have a Maxwell distribution of energy. The electron temperature is determined by the balance of heating and cooling. The source of heating is the collision with photoelectrons produced by the solar radiation. Cooling of the thermal electrons is due to the collision with atmospheric molecules. Since the electron temperature is not high ($\sim$1,000 K), the dominant processes are elastic scattering and rotational and vibrational excitations. In the higher region of ionosphere, electron–ion collisions are the dominant cooling process of electrons. Electric conductivity of the ionosphere is determined by the electron collisions with the atmospheric molecules. More generally, the propagation of radio wave in the ionosphere is governed by the electron–molecule collisions. In these cases, the most important process is a momentum–transfer collision (see Sect. 5.3).

As is already shown, ion–molecule collisions are also important in the ionosphere. The ions produced by the solar radiation are transformed into other ions, through the following processes:

$$N_2^+ + O \rightarrow NO^+ + O$$

$$O^+ + N_2 \rightarrow NO^+ + N$$

These reactions often result in the products in their excited state. Such reactions, therefore, act as a source of airglow emission. Ions in the ionosphere are heated by the collision with the thermal electrons. The cooling of the ions is mostly due to the collisions between ions and the neutral molecules. The most important process in this case is the momentum–transfer collisions between ions and molecules.

2.2 Interstellar Cloud

Matter in the Universe is mostly in the state of a plasma. On the other hand, molecules are found in many places in the Universe (see [156]). It is natural, therefore, to encounter a molecular plasma in the Universe. One example is the interstellar cloud.

The space between the stars is empty, but not entirely so. It is filled with matter, although very tenuous. Its density is not uniform. Some part of the interstellar space has rather dense matter and is called interstellar cloud. Most of the interstellar clouds are molecular and ionized. They are composed mostly of (atomic and molecular) hydrogen. Its density is 10^2–$10^4\,\mathrm{cm}^{-3}$. The gas temperature of the cloud is extremely low (10–100 K). The degree of ionization is very low ($\sim 10^{-8}$), but the charged particles still play a significant role.

A wide variety of molecules have been found in the interstellar clouds. Molecular species found are different depending on the cloud and the condition of the observation. For illustration, we present in Table 2.1 a list of abundant molecules. The abundance shown is the result of a model calculation [113], but generally consistent with observation. In the model, the cloud is assumed to have H_2 density of $10^4\,\mathrm{cm}^{-3}$ and temperature of 10 K. It should be noted that some of the molecules (e.g., N_2) obtained by the model calculation have not yet been observed. They have no transitions of the energy states suitable for spectroscopic observation.

The formation of the interstellar molecules are thought to follow the scheme described below. Here we consider the so-called molecular cloud, which is of a rather high density ($\sim 10^4$ cm^{-3}) and a low temperature ($\sim$10 K). Table 2.2 shows the molecular abundance observed in a typical molecular cloud TMC-1 (cited in [113]). In such a cloud, very unsaturated species such as radicals C_nH are dominant. The molecular clouds are important as a source of star formation. Because of the low gaseous density, only two-body collision occurs in the cloud. (In contrast to this, three-body collisions are the main process of molecule formation in laboratories.) Furthermore, only the reactions

Table 2.1. Fractional abundance (with respect to H_2) of interstellar molecules based on a model calculation [113]

Species	Abundance	Species	Abundance	Species	Abundance
H_2	1.0	CO_2	3.0(−6)[a]	CHOOH	2.6(−8)
CO	1.4(−4)	H_2O	2.3(−6)	H_2CO	1.4(−8)
O_2	8.4(−5)	SO_2	3.0(−8)	C_4H	7.1(−9)
N_2	2.0(−5)	HNC	6.8(−9)	C_3H_2	5.7(−9)
NO	3.3(−6)	HNO	4.1(−9)	C_3H	2.2(−9)
OH	9.6(−7)	HCN	4.0(−9)	HCO^+	1.3(−8)
SiO	5.5(−9)	NH_2	3.7(−9)	H_3^+	7.1(−9)
SO	5.2(−9)	OCN	2.4(−9)	H_3O^+	2.4(−9)
PO	2.9(−9)	NH_3	1.4(−7)	e	4.4(−8)
CS	2.7(−9)	CH_4	1.3(−7)		
HCl	2.1(−9)	C_2H_2	6.2(−8)		

[a] $3.0(-6)=3.0 \times 10^{-6}$.

Table 2.2. Fractional abundance (with respect to H_2) of interstellar molecules observed in the cloud TMC-1

Species	Abundance	Species	Abundance	Species	Abundance
CO	8(−5)[a]	CH	2(−8)	NH_3	2(−8)
OH	3(−7)	HCN	2(−8)	CS	1(−8)
C_2	5(−8)	HNC	2(−8)	C_3H_2	1(−8)
C_2H	5(−8)	CCCCH	2(−8)	HCO^+	8(−9)
CN	3(−8)	H_2CO	2(−8)		

[a] $8(-5)=8 \times 10^{-5}$.

with no activation energy are possible in such a cold space. The two-body ion–molecule reaction satisfies this condition (see Sect. 6.4). The possible scheme of molecule formation in the interstellar cloud is as follows [62]:

(1) Ions are produced by collisions of cosmic-rays with interstellar atoms and molecules. Reflecting the abundance, most of the nascent ions are H_2^+. Because of the rapid reaction

$$H_2^+ + H_2 \rightarrow H_3^+ + H \tag{2.1}$$

the H_2^+ is immediately transformed into H_3^+, which is, therefore, the starting point of a series of ion–molecule reactions in the interstellar cloud.
(2) Through a chain of ion–molecule reactions, larger, as well as complex, molecules are created.
(3) A part of ions disappear through the collision with electrons (i.e., the electron–ion recombination). The recombination is mostly dissociative, so that some simple molecules are produced as a product of this process.

One simple route to the formation of water molecules is as follows:

$$H_3^+ + O \rightarrow OH^+ + H_2 \tag{2.2}$$

$$OH^+ + H_2 \rightarrow H_2O^+ + H \tag{2.3}$$

$$H_2O^+ + H_2 \rightarrow H_3O^+ + H \tag{2.4}$$

$$H_3O^+ + e \rightarrow H_2O + H \tag{2.5a}$$

$$OH + H_2 \tag{2.5b}$$

$$OH + H + H \tag{2.5c}$$

$$O + H + H_2 \tag{2.5d}$$

In the interstellar clouds, the ion–molecule reactions involving H or H_2 are of primary importance. Such processes as (2.3) and (2.4) above produce new molecules having an additional hydrogen. The electron–ion collisions like (2.5)

are very rare in the interstellar clouds, but still very important, because they produce such small molecules as OH, CO, and H_2O. For example, the formation of CO proceeds through the route:

$$H_3^+ + C \rightarrow CH^+ + H_2 \tag{2.6}$$

$$CH^+ + H_2 \rightarrow {CH_2}^+ + H \tag{2.7}$$

$${CH_2}^+ + H_2 \rightarrow {CH_3}^+ + H \tag{2.8}$$

$${CH_3}^+ + O \rightarrow HCO^+ + H_2 \tag{2.9}$$

$$HCO^+ + e \rightarrow CO + H \tag{2.10}$$

In the last process (2.10), productions of $C + OH$ and $CH + O$ are also possible, but their probability is known to be very small (see Sect. 7.2).

Finally it should be noted that recent, more refined, models include additional processes: two-body neutral–neutral collisions involving radicals and reactions on a surface of interstellar grains [63, 64].

2.3 Gaseous Discharges

Discharge in a molecular gas is a typical example of molecular plasmas. The discharge plasmas are widely used in applications, some of which are:

- Production of active molecules (e.g., ozone synthesis)
- Pollution control (destruction of NO_x and SO_x, cleaning of flue gas, etc.)
- Light sources (lightings, gaseous lasers and plasma displays)
- Deposition of materials (production of thin films)
- Etching for semiconductor devices
- Surface modification and treatment
- Plasma sterilization (inactivation of microorganisms)

These applications are possible, because the plasma is in the state of nonequilibrium. That is, the mean energy of electrons much exceeds the gaseous temperature. An applied electromagnetic field supplies energy to keep the nonequilibrium state of the plasma. Thus the plasma serves as a converter of electromagnetic energy into useful materials. Depending on the purposes, different plasmas are produced. It is impossible to fully describe the details of all those plasmas. Here we summarize the roles of molecular processes in those plasmas. More details of the discharge plasmas can be found, for example, in the text book of Lieberman and Lichtenberg [100].

2.3.1 Production and Maintenance of Plasmas

Production of ions needs energy. The energy is supplied from outside mainly through the application of electromagnetic field. Electrons are accelerated

by the field to have enough energy to produce ions. There are two ways of ionization: direct and indirect. Direct ionization is

$$\mathrm{e} + \mathrm{AB} \rightarrow \mathrm{AB}^{+} + 2\mathrm{e}$$

The incident electron must have an energy above the ionization potential of AB. Indirect process of ionization takes place through an excitation of a molecule followed by an ionization of the excited molecule:

$$\mathrm{e} + \mathrm{AB} \rightarrow \mathrm{AB}^{*} + \mathrm{e}$$

$$\mathrm{e} + \mathrm{AB}^{*} \rightarrow \mathrm{AB}^{+} + 2\mathrm{e}$$

In this case the excited molecule must have a long lifetime. Or more precisely, the lifetime of AB^{*} should be longer than the mean collision time for the ionization process. In the indirect ionization, the electron energy is not necessarily above the ionization potential. When the gaseous pressure is high, the following process is also possible:

$$\mathrm{AB}^{*} + \mathrm{AB} \rightarrow (\mathrm{AB})_2{}^{+} + \mathrm{e}$$

This is called an associative ionization of molecules. It should be noted that, even when the associative ionization dominates, the ionization process is started by the collision of accelerated electrons with the gaseous molecules (for the production of excited molecules).

In a discharge plasma, ions (and electrons also) disappear on the surface of the apparatus. Electron–ion recombinations in a bulk plasma usually play a minor role in the annihilation of ions in a laboratory plasma. But the recombination process may be effective for the production of small radicals, as in the case of the formation of interstellar molecules (see Sect. 2.2).

2.3.2 Determination of Electron Energy Distribution Function

The statistical behavior of electrons in a plasma is governed by the electron energy distribution function (EEDF). Transport properties of electrons are directly dependent on EEDF. Rate coefficients of any electron–molecule collision process are evaluated with the EEDF. In the nonequilibrium plasma used for applications, the EEDF is normally non-Maxwellian. Theoretically EEDF can be obtained by solving the Boltzmann equation. According to the equation, the EEDF is determined by the balance between the acceleration of the electrons by the applied field and the deceleration of them through the collisions with plasma particles (i.e., electrons, ions, and neutral molecules). In a low-temperature, molecular plasma, the electron–molecule collisions play the central role in determining EEDF. Particularly important are the elastic scattering and the rotational and vibrational excitations of molecules. The latter two processes are specific to a molecular gas. To show that, Capitelli

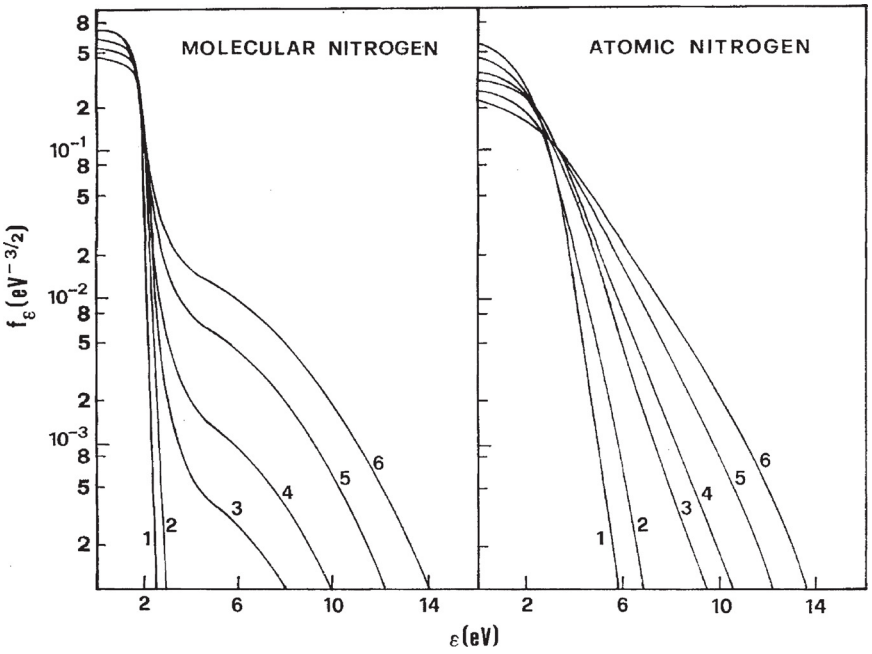

Fig. 2.3. Electron energy distribution functions for N_2 and N plasmas, calculated at different $\mathcal{E}/N$ values (in 10^{-16} V cm^2) (reproduced from [21])

et al. [21] solved the Boltzmann equation separately for molecular nitrogen (N_2) and atomic nitrogen (N). The resulting EEDF is presented in Fig. 2.3.

In the Boltzmann equation, the strength of the applied field $\mathcal{E}$ appears only in the combination with the gas density N in the form $\mathcal{E}/N$. The EEDF is calculated at a constant value of $\mathcal{E}/N$. The figure shows EEDF for several different values of $\mathcal{E}/N$. According to the convention, this EEDF has been normalized as

$$\int_0^\infty \sqrt{\epsilon}\, f(\epsilon)\, \mathrm{d}\epsilon = 1\,, \tag{2.11}$$

where ϵ is the electron energy. In both the cases of atomic and molecular nitrogens, the gaseous temperature was assumed to be so low that all the atoms and molecules are in the ground states. The EEDF in the molecular plasma has a peculiar feature compared with the atomic case. In the energy region below about 6 eV, the number of electrons is remarkably reduced. This reflects the significant energy loss of electrons due to the rotational and vibrational excitations of nitrogen molecules. Because of this effect, the mean energy of electrons in the molecular plasma is smaller than the corresponding value in the atomic plasma. (For example, at $\mathcal{E}/N = 3 \times 10^{-16}$ V cm^2, the mean electron energies for the molecular and atomic plasmas are 1.06 and 1.78 eV, respectively.) In an actual plasma of nitrogen molecules, an accumulation of

vibrationally excited molecules has a significant effect on EEDF. Electrons can gain an energy by the collision with the vibrationally excited molecules (i.e., the super-elastic collision). The behavior of the excited molecules are also affected by their collisions with neutral molecules. In a weakly ionized molecular plasma, therefore, the EEDF and the kinetics of molecules should be treated simultaneously (see, e.g., [21]).

2.3.3 Production of Active Species

Energy supplied from outside through the applied field mainly goes to the electrons. Those electrons (and sometime ions) collide with molecules to produce various active species in the plasma. They are ions, radicals, active atoms, excited atoms and molecules, and high-energy photons. Those active species are utilized for practical applications mentioned above. They collide with other plasma particles to generate secondary products. In this manner, the electron and ion collisions serve as a trigger of a series of chemical reactions.

To show what kinds of active species are produced, we present in Fig. 2.4 the result of a model calculation of CH_4 plasma by Tachibana et al. [153]. This is an RF plasma and the gas pressure is 0.22 Torr. The number density of the species shown was determined by solving a set of rate equations. The rate coefficient of each reaction was evaluated with the EEDF observed by themselves (i.e., not a theoretical one). All possible reactions were taken into account. But some of them have a rate coefficient of large uncertainty, because of a lack of relevant experimental data. The most abundant radical is CH_3. It is produced mainly by the collision of electrons with CH_4. The other radicals, CH_2, CH, and C, are also produced by the electron collision with CH_4. But, due to the fast radical–molecule reactions, the number density of those radicals is small. The authors investigated the effect of attachment of radicals on the surface. There was no definite information about the sticking probability of CH_3 on a surface. They took two different values for the sticking probability to see the effect. They found that the radical density is very sensitive to the surface condition.

Later a similar modeling calculation of CH_4 plasma was made by Herrebout et al. [65]. They obtained the electron energy distribution function by solving the Boltzmann equation. The result of Herrebout et al. is not necessarily the same as that of Tachibana et al. The most abundant radical in the model of Herrebout et al. is CH_3 as in the model of Tachibana et al. But, in the model of Herrebout et al., higher order hydrocarbons (i.e., C_2H_4 and C_2H_6) are relatively more abundant than the model of Tachibana et al. Herrebout et al. produced even C_3H_8, which was not included in the calculation of Tachibana et al. Herrebout et al. ascribed the difference to the fact that different reactions were considered in the two models. This confirms the importance of the reliable knowledge of the elementary processes.

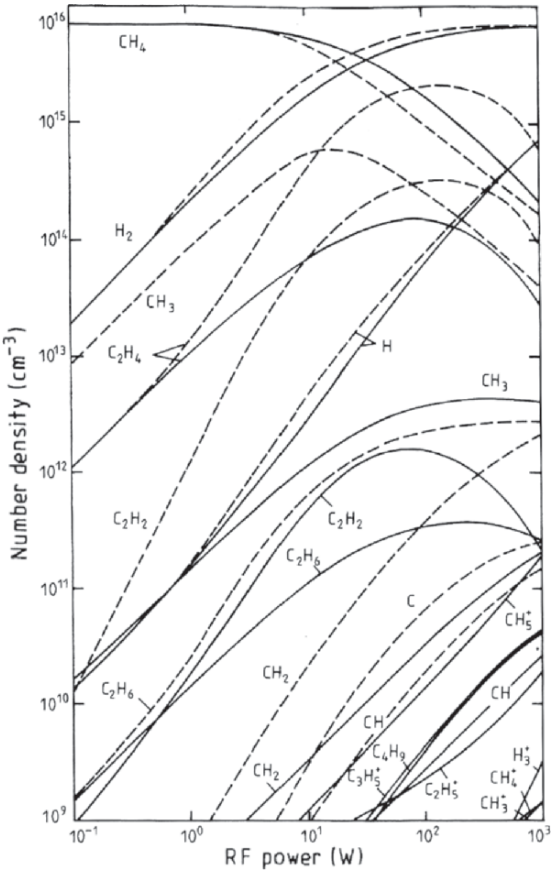

Fig. 2.4. Number densities of radicals and other species produced in a CH_4 plasma. They are plotted as a function of the RF power applied, for two different values of sticking probability of CH_3 on a surface: unity (*solid line*) and 10^{-3} (*dashed line*). (Reproduced from [153])

2.4 Fusion Plasma

Fusion plasma is the plasma developed for achieving thermonuclear fusion. The central part of the fusion plasma has a temperature of as high as 10 keV (or 10^8 K) and is fully ionized. The plasma in the boundary region is relatively cool and includes neutral particles. Most of the large fusion devices are now equipped with a divertor, which pulls out the ash of the burnt material and the generated heat from the core plasma. Since contacting special boundary plates (divertor plates), the plasma in the divertor includes molecules originated from the plate. The plasma in the boundary region, including the divertor, is often called the edge plasma. It is a kind of molecular plasma, whose temperature

is normally less than 100 eV. The following two molecular species are involved in the edge plasma:

(1) H_2. It is ejected from the wall of the fusion device (or divertor) as a result of an H^+ impact. When a H^+ hits on the wall, it reacts with hydrogen atoms on the wall surface or in the wall materials to produce H_2. The resulting molecule is ejected from the surface promptly or at the impact of another H^+.
(2) C_nH_m. This is generated by a chemical sputtering of H^+ on the carbon coated surface, which is widely used in the current fusion devices.

The study of edge plasma is important (see, e.g., [28]):

(1) To establish the boundary condition of the whole fusion plasma. The temperature and density of the bulk plasma are controlled by the boundary condition.
(2) To investigate the interaction between the plasma and the wall of the device. This is necessary for the protection of the wall materials.
(3) To understand the behavior of the impurities (e.g., C atoms) in the plasma. They are originated from the bounding surface.

The study of the molecular processes in the edge plasma is different from other cases. Here the plasma itself is given as an extension of the bulk plasma. We investigate the behavior of neutral molecules in such a plasma. The density of molecules is usually smaller than the density of electrons, which is equal to the ion density. To know the behavior of hydrogen molecules (or any other neutral particles) in the plasma, we always resort to spectroscopy. From the analysis of the spectra of the radiation measured, we directly obtain the population of the molecules in particular states. To deduce plasma parameters from the population, we need the knowledge of the mechanism of generating the population. The best way to do so is to solve the equations of the collisional-radiative model of the molecule [58]. It is a set of rate equations for electron-impact and ion-impact excitations (and de-excitations, if necessary) and radiative transitions. We need cross-sections (or rate coefficients) for all possible processes of excitation (and de-excitation) of rotational, vibrational, and electronic states of the relevant molecule. An example of the collisional-radiative model was the study of hydrogen plasma by Sawada and Fujimoto [141].

One particular topic of molecular processes in the edge plasma is the behavior of hydrocarbon molecules in a divertor. This study is needed to understand the erosion mechanism of wall materials and the behavior of the C-impurity in the bulk plasma. It is also of significance in the estimate of the loss of hydrogen atoms. Hydrocarbon molecules are ionized in the plasma and eventually return to the wall. Hydrogen atoms are lost as a component of the molecules deposited on the wall. For example, Alman et al. [6] made a model calculation of the behavior of C_nH_m in the edge plasma. They took into account all the possible processes of electron- and proton-collisions

with 16 hydrocarbon molecules (i.e., CH_n with $n = 1$–4, C_2H_m and C_3H_m with $m = 1$–6). They also included the (dissociative) recombination processes between electrons and hydrocarbon ions, leading to the production of small hydrocarbon radicals.

Another special topic of the molecular process in the edge plasma is the molecule assisted recombination. The main component of the fusion plasma, i.e., H^+, is annihilated through the recombination with the plasma electrons in such a way as

$$H^+ + e \rightarrow H + h\nu$$

This is a radiative process and very slow. If a molecular hydrogen is present in the plasma, a charge transfer collision can transform H^+ into a molecular ion

$$H^+ + H_2 \rightarrow H_2^+ + H$$

Then the molecular ion induces the dissociative recombination

$$H_2^+ + e \rightarrow H + H$$

This process is much faster than the radiative recombination of H^+. Furthermore the last two processes may be enhanced, if the molecules or molecular ions are vibrationally excited. This two-step recombination process of H^+ is called a molecule assisted recombination (MAR). In a real plasma, many other processes compete with MAR. To estimate the effect of MAR, we need a complicated model calculation of hydrogen plasmas. Krasheninnikov [93], for example, carried out one such calculation. He obtained the frequency of the recombination through MAR at the electron temperature $T_e \sim 1$–$4\,\mathrm{eV}$ and the electron density $N_e = 10^{14}\ \mathrm{cm}^{-3}$ to be

$$\nu_{\mathrm{MAR}} = 3 \times 10^{-10}\,\mathrm{cm}^3\,\mathrm{s}^{-1} \times N_{\mathrm{H_2}}\ (\mathrm{in\ cm}^{-3})$$

When we assume the number density of hydrogen molecules to be of the order of N_e (i.e., $\sim 10^{14}\,\mathrm{cm}^{-3}$), the ν_{MAR} has the value by about 100 times larger than the frequency of the radiative recombination. Kubo et al. [94] investigated the behavior of H_2 in the divertor of a large fusion device, JT-60U, with using spectroscopy. They confirmed that the MAR is, at least, as important as the radiative recombination of H^+.

One of the methods of heating the fusion plasma is an injection of fast neutral (usually atomic hydrogen) beam into the plasma. To produce the fast ($\sim 1\,\mathrm{MeV}$) H beam, a fast H^- beam is used, because an acceleration of ions is easy and H^- has a high neutralization ($H^- \rightarrow H$) efficiency even at such a high beam energy. For that purpose, we need an ion source which efficiently generates a large amount of H^-. It is now well known that an electron (dissociative) attachment of H_2 has a large cross-section, once the hydrogen molecule is vibrationally excited (see Sect. 5.13)

$$e + H_2(v > 0) \rightarrow H^- + H$$

If we have any efficient method to produce vibrationally excited H_2, then we can adopt this process for the H^- source we need. The direct vibrational excitation of H_2 by electron impact is not efficient. One promising process is the two-step process such as

$$e + H_2\ (X,\ v = 0) \rightarrow H_2(n,\ v') + e$$

$$H_2(n,\ v') \rightarrow H_2(X, v > 0) + h\nu$$

The electronic state, n, is connected with the ground state, X, through a dipole-allowed transition. An H^- source based on this mechanism has been developed and tested (see a review by Bacal et al. [9]). To understand the physics in the ion source and to improve its operation, a modeling of H_2 plasma has been made by a number of authors (e.g., [22]). In the modeling, a knowledge is needed for the collision processes involving H_2 in its vibrationally excited state. One controversial problem is whether the electronically excited molecule can also enhance the production of H^-. To make clear this problem, we need information about the collision processes involving H_2 in its electronically excited state.

3

Collision Cross-Sections and Related Quantities

3.1 Definitions and Fundamental Relations

Consider a collision between particles A and B (see Fig. 3.1). Here B is a target fixed in space and A is a projectile incident along z-axis. (Collisions between two moving particles are treated in Sect. 3.4.) The flux of the incident particle is denoted by $j_{\rm in}$. The number of particles coming out per unit time and per unit solid angle in the direction $(\theta,\, \phi)$ is denoted by $J_{\rm out}(\theta, \phi)$. (Note that Fig. 3.1 shows a case of axial symmetry and the ϕ-dependence is omitted.) The quantity $J_{\rm out}$ is proportional to the incident flux $j_{\rm in}$. We denote the proportionality constant by $q(\theta, \phi)$, namely

$$q(\theta,\, \phi) = \frac{J_{\rm out}(\theta,\, \phi)}{j_{\rm in}}\,. \tag{3.1}$$

This is the definition of the differential cross-section (DCS) for the collision. The integral cross-section is defined by

$$Q = \int q(\theta, \phi)\, {\rm d}\Omega\,, \tag{3.2}$$

where Ω is the solid angle and ${\rm d}\Omega = \sin\theta\, {\rm d}\theta\, {\rm d}\phi$.

The corresponding collision frequency can be defined as

$$\nu_{\rm coll} = \int J_{\rm out}(\theta, \phi) {\rm d}\Omega\,. \tag{3.3}$$

With the use of (3.1) and (3.2), $\nu_{\rm coll}$ is expressed in terms of the cross-section by

$$\nu_{\rm coll} = j_{\rm in}\, Q\,. \tag{3.4}$$

When a beam of particles A with a constant velocity $v_{\rm in}$ collides with the target B (Fig. 3.2), the incident flux is obtained as

$$j_{\rm in} = N v_{\rm in}\,, \tag{3.5}$$

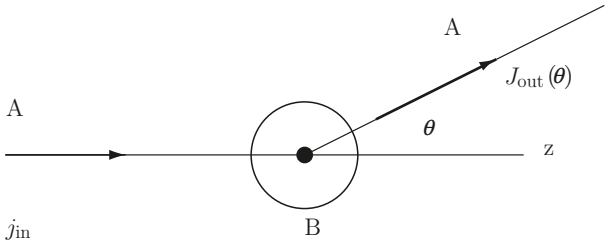

Fig. 3.1. Collision system for the definition of cross-section

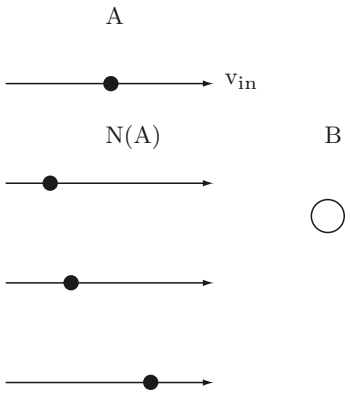

Fig. 3.2. A beam of particles A colliding with a fixed target B

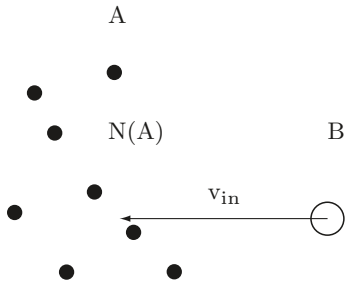

Fig. 3.3. A particle B colliding with a group of particles A fixed in space

where N is the number density of particle A. In this case (i.e., Fig. 3.2), the (3.4) is rewritten in the form

$$\nu_{\text{coll}} = N v_{\text{in}} Q \,. \tag{3.6}$$

Let us consider inversely the case where a particle B (with velocity v_{in}) comes into a group of particles A, which are now fixed in space (Fig. 3.3). The number density of A is given by N. The frequency for B to collide with

the field particles A is given by the same equation as (3.6). The number of collisions per unit path-length of B is given by

$$\xi = \nu_{\rm coll} \times \frac{1}{v_{\rm in}} = NQ\,. \tag{3.7}$$

Then the mean free path of the particle B moving in a group of particles A is calculated to be

$$\lambda_{\rm mfp} = \frac{1}{\xi} = \frac{1}{N\,Q}\,. \tag{3.8}$$

The mean collision time, which is defined as an inverse of collision frequency, is given by

$$\tau_{\rm coll} = \frac{1}{\nu_{\rm coll}} = \frac{1}{N v_{\rm in} Q}\,. \tag{3.9}$$

The mean collision time is a useful quantity, when we ask if the collision process dominates over other dynamic processes (e.g., transport of particles). Also we can use the mean collision time to estimate the life of an excited state. Usually an excited state decays through an emission of radiation. But, if the collision time is shorter than the radiative lifetime of the state, the state decays through collisions with other particles. This is the case shown in Fig. 3.2 and N in (3.9) is taken as the number density of the colliding particles.

As is shown in the later sections, there are various kinds of collision processes (i.e., excitation, ionization, dissociation, etc.). We have the same definition of the cross-section for each process as above. That is, instead of (3.1), we have

$$q_s(\theta,\,\phi) = \frac{J_{{\rm out},s}(\theta,\,\phi)}{j_{\rm in}}\,, \tag{3.10}$$

where the subscript s specifies each collision process and $J_{{\rm out},s}$ is the number of the particles coming out after the collision process s. Equation (3.2) is replaced by

$$Q_s = \int q_s(\theta,\,\phi)\,{\rm d}\Omega\,. \tag{3.11}$$

When we are not interested in the details of the collision process, the total scattering cross-section, $Q_{\rm tot}$, is a useful quantity. It is defined by

$$Q_{\rm tot} = \sum_s Q_s\,. \tag{3.12}$$

This cross-section is simply a measure of the strength of the collision (i.e., how strongly or how often the collision occurs). The related quantities introduced above (i.e., ν, ξ, λ, τ) can be defined either with Q_s or with $Q_{\rm tot}$.

Sometimes collision cross-section is interpreted as a collision "probability". Strictly speaking, however, a probability, which is a number between 0 and 1, should be defined more rigorously. Consider a beam of particles B (of velocity v

and intensity I) passing through a group of particles A (of density N and fixed in space). The number of collisions of B with A during an infinitesimally short path $\mathrm{d}x$ is given by $\mathrm{d}x/\lambda_{\mathrm{mfp}}$, where λ_{mfp} is the mean free path given by (3.8). As a consequence of collisions, the beam loses its intensity by $(\mathrm{d}x/\lambda_{\mathrm{mfp}})I$. Or we have a relation

$$\frac{\mathrm{d}I}{I} = -\frac{\mathrm{d}x}{\lambda_{\mathrm{mfp}}}\,. \tag{3.13}$$

The minus sign on the right-hand side of (3.13) means that the intensity decreases with increasing x. After passing over a finite distance L, the beam intensity becomes

$$I(L) = I_0\,\exp\left(-\frac{L}{\lambda_{\mathrm{mfp}}}\right)\,, \tag{3.14}$$

where I_0 is the intensity at $x = 0$. With the use of (3.8), we have

$$I(L) = I_0\,\exp(-NQL)\,. \tag{3.15}$$

Inversely, the beam intensity remaining after passing through the distance L is

$$(1\,-\exp(-NQL))\;I_0\,. \tag{3.16}$$

The factor in front of I_0 can be interpreted as the collision probability, i.e.,

$$P_{\mathrm{coll}} = 1 - \exp(-NQL)\,. \tag{3.17}$$

This relation implies that, if the cross-section is large, we have a large (almost unity) collision probability, but there is no proportionality between the two quantities.

Consider collisions (of process s) between a group of particles B (whose number density is N_{B}) and a group of particles A (with number density N_{A}). In a case where particles A are fixed in space but particles B have a velocity distribution $f(\boldsymbol{v})$, the number of collisions per unit time (i.e., the rate of the collision) is given by

$$R_s = N_{\mathrm{A}}\,N_{\mathrm{B}}\int v\,Q_s(\boldsymbol{v})\,f(\boldsymbol{v})\,\mathrm{d}\boldsymbol{v}\,. \tag{3.18}$$

Defining the rate coefficient by

$$k_s = \int v\,Q_s(\boldsymbol{v})\,f(\boldsymbol{v})\,\mathrm{d}\boldsymbol{v}\,. \tag{3.19}$$

we have a relation

$$R_s = N_{\mathrm{A}}\,N_{\mathrm{B}}\,k_s\,. \tag{3.20}$$

This can be applied to the case of chemical reaction

$$\mathrm{A} + \mathrm{B} \rightarrow \mathrm{C} + \mathrm{D}\,.$$

In this case, the velocity $\boldsymbol{v}$ is meant to be the relative velocity between A and B. Since the velocity distribution depends on the gas temperature, the "reaction rate coefficient" $k_{\mathrm{A+B\to C+D}}$ is a function of the temperature.

To help a quantitative estimate of the effect of a certain collision process, we show in Appendix A the representative values of mean free path (λ_{mfp}), mean collision time (τ_{coll}), and collision frequency (ν_{coll}). There we assume a typical value of the cross-section to be $10^{-16}\,\mathrm{cm}^2$ (i.e., the size of typical atoms). The order of magnitude of rate coefficient is also shown there.

In this book, differential cross-sections (DCSs) are not explicitly shown, except in a few special cases. Lots of data are available on DCSs, but they are too detailed to be summarized in a compact form. Typical examples of DCS can be found in a review paper on electron collisions with diatomic molecules written by Brunger and Buckman [17]. DCS is not less important than the integral cross-sections. The angular dependence of the cross-section reflects the physics underlying the collision process. DCS is of importance also as basic data. Monte Carlo simulation needs the information of angular distribution of scattering. In solving the Boltzmann equation, DCS is needed if inelastic collisions are expected to dominate. In such instances, the angular distribution is often assumed to be isotropic or concentrated in the forward direction. These assumptions, however, are normally not valid (see the review by Brunger and Buckman). When DCSs are needed, one should find them in the relevant original literature.

3.2 Cross-Section in the Quantum Theory

Here the collision is considered as a stationary problem. A group of particles (with mass μ) constantly flow over a fixed target B. The wavefunction of the colliding system, A + B, is set to have the following boundary condition at the separation of the two particles:

$$\Psi \overset{r\to\infty}{\longrightarrow} \mathrm{e}^{\mathrm{i}\boldsymbol{k}\cdot\boldsymbol{r}} + f_s(\boldsymbol{k}\to\boldsymbol{k}_s|\theta,\phi)\frac{\mathrm{e}^{\mathrm{i}k_s r}}{r}\,. \tag{3.21}$$

Here the origin of the coordinates is taken at the position of particle B and $\boldsymbol{r}$ is the position vector of particle A from the origin. The first term of the right-hand side of (3.21) represents the incident free particle (i.e., a plane wave) and the second one the scattered particle (i.e., an outgoing spherical wave). The quantity f_s is called a scattering amplitude (with subscript s indicating the collision process considered) and $\boldsymbol{k}$ and $\boldsymbol{k}_s$ are the wave vectors of the incident and scattered particles, respectively.

To evaluate the DCS (i.e., (3.1) or (3.10)), we need j_{in} and J_{out}. In the quantum mechanics, a particle flux is obtained by

$$\boldsymbol{j} = \frac{\hbar}{2\mu\mathrm{i}}\left(\Phi^*\,\nabla\Phi - \Phi\nabla\Phi^*\right). \tag{3.22}$$

Inserting $\Phi = \exp(\mathrm{i}\boldsymbol{k}\cdot\boldsymbol{r})$ into (3.22), we have the incident flux. By definition, the flux is along the z axis. Its magnitude is calculated to be

$$j_{\mathrm{in}} = \frac{\hbar k}{\mu}\,. \tag{3.23}$$

To calculate J_{out}, we first evaluate the outgoing flux j_{out}, which is directed in the direction (θ,ϕ) from the origin. The flux is obtained by inserting $\Phi = f_s\,\exp(\mathrm{i}k_s r)\,/r$ into (3.22). We only need the flux in the limit $r\to\infty$. Then we have

$$j_{\mathrm{out}}(r\to\infty) = \frac{\hbar k_s}{\mu}\,\frac{1}{r^2}\,|f_s|^2\,. \tag{3.24}$$

This is the number of outgoing particles *per unit area* on the surface of a sphere of radius r. The quantity J_{out} has been defined as the number of outgoing particles *per unit solid angle*. Thus we have

$$J_{\mathrm{out}} = r^2\,j_{\mathrm{out}} = \frac{\hbar k_s}{\mu}\,|f_s|^2\,. \tag{3.25}$$

From (3.10), (3.23), and (3.25), we finally have the DCS in the form

$$q_s(\theta,\phi) = \frac{k_s}{k}\,|f_s(\boldsymbol{k}\to\boldsymbol{k}_s\,|\theta,\phi)|^2\,. \tag{3.26}$$

The integral cross-section is obtained by integrating $q_s(\theta,\phi)$ over the scattering angles. It should be noted that the present formula of the cross-section (3.26) has been derived under the boundary condition (3.21). We can set other boundary condition to the wavefunction, but in that case we have a different form of cross-section.

3.3 Scattering from a Spherical Potential

To illustrate how to evaluate cross-sections quantum mechanically, we here consider a particle (with mass μ and energy E) scattered from a spherical potential, $V(r)$. The motion of the particle is determined by a wave equation (i.e., the Schrödinger equation)

$$\left(-\frac{\hbar^2}{2\mu}\nabla^2 + V(r)\right)\Psi = E\Psi\,. \tag{3.27}$$

According to the standard way of solving a partial differential equation, we separate the variables. In the present case, it is natural to expand the wave function in terms of angular basis functions. Because of the axial symmetry of the problem, we now expand the solution in terms of the Legendre function P_ℓ:

$$\Psi = \frac{1}{r}\sum_{\ell} u_\ell(r)\,P_\ell(\cos\theta)\,. \tag{3.28}$$

Here ℓ is regarded as an angular momentum quantum number of the incoming particle. Inserting this into (3.27) and using the orthonormality of the Legendre functions, we have an equation for the radial function u_ℓ in the form

$$\left[\frac{\mathrm{d}^2}{\mathrm{d}r^2} - \frac{\ell(\ell+1)}{r^2} - \frac{2\mu}{\hbar^2}(V-E)\right] u_\ell = 0\,. \tag{3.29}$$

When we assume

$$V(r) \overset{r\to\infty}{\longrightarrow} 0, \tag{3.30}$$

we can set an asymptotic form of the solution of (3.29) as

$$u_\ell \overset{r\to\infty}{\longrightarrow} A_\ell \sin(kr - \frac{\ell\pi}{2} + \eta_\ell)\,, \tag{3.31}$$

or, with using (3.28),

$$\Psi \overset{r\to\infty}{\longrightarrow} \frac{1}{r}\sum_\ell A_\ell \sin(kr - \frac{\ell\pi}{2} + \eta_\ell) P_\ell(\cos\theta)\,. \tag{3.32}$$

In (3.31) and (3.32), A_ℓ is a normalization constant, and k is the wave number of the incident particle and related to the energy by

$$E = \frac{\hbar^2\, k^2}{2\,\mu}\,. \tag{3.33}$$

The quantity η_ℓ in (3.31) and (3.32) is called a phase shift and represents the amount of distortion of the incoming wave due to the presence of the target potential. To derive the scattering cross-section, we compare (3.32) with (3.21). Then we have (see, for example, [117])

$$f(k|\theta) = \frac{1}{k}\sum_\ell (2\ell+1)\exp(\mathrm{i}\eta_\ell)(\sin\eta_\ell) P_\ell(\cos\theta)\,. \tag{3.34}$$

From this, the differential cross-section is calculated to be

$$q(\theta) = \frac{1}{4k^2}\left|\sum_\ell (2\ell+1)\left[\exp(2\mathrm{i}\eta_\ell) - 1\right] P_\ell(\cos\theta)\right|^2\,. \tag{3.35}$$

Because of the axial symmetry of the system, the differential cross-section does not depend on ϕ. The integral cross-section is obtained as

$$Q = \frac{4\pi}{k^2}\sum_\ell (2\ell+1)(\sin\eta_\ell)^2\,. \tag{3.36}$$

Thus the cross-section in this particular case can be calculated only with the phase shift η_ℓ, which in turn is determined from the solution of (3.29) under the boundary condition (3.31).

In principle the summation over ℓ in (3.28) (and other equations) should be taken over $0-\infty$. But, in practice, the upper limit of ℓ (denoted by $\ell_{\max}$) is finite. To estimate $\ell_{\max}$, we simply take a classical picture. The scattered particle follows a trajectory specified by an initial condition of impact parameter b and velocity v. The scattering is possible only if the impact parameter is smaller than the size (denoted by a) of the interaction potential. The orbital angular momentum of the incident particle can be obtained by a relation

$$L = \mu v\, b = \hbar k b\,. \tag{3.37}$$

Using the definition of the quantum number, i.e., $L = \ell\hbar$, we have

$$b = \frac{\ell}{k}\,. \tag{3.38}$$

From the above condition for the scattering (i.e., $b < a$), we simply have

$$\ell < ka = 5.12\sqrt{\frac{\mu}{m_{\mathrm{e}}}}\,\sqrt{E(\mathrm{eV})}a(\mathrm{nm})\,, \tag{3.39}$$

where m_{e} is the electron mass. When an electron of 1 eV collides with a molecule and a typical value $a = 0.5$ nm is taken as a size of the interaction region, then we have $\ell < 3$. Therefore, we need to consider only a few partial waves in this case. As can be seen from the relation (3.39), many partial waves have to be taken into account in the collision between an ion and a molecule, but even in that case, the total number of the partial waves can be finite.

3.4 One-Body vs. Two-Body Problems

So far in the present chapter, we have assumed that the target particle is fixed in space. Now we consider a more general case: a collision of two moving particles. The two particles have masses m_1 and m_2 and velocities $\boldsymbol{v}_1$ and $\boldsymbol{v}_2$. Define their velocities in the center of mass (CM) frame of reference by

$$\boldsymbol{g}_1 = \boldsymbol{v}_1 - \boldsymbol{G}\,, \tag{3.40}$$

$$\boldsymbol{g}_2 = \boldsymbol{v}_2 - \boldsymbol{G}\,, \tag{3.41}$$

where $\boldsymbol{G}$ is the velocity of the gravity center

$$\boldsymbol{G} = \frac{m_1}{M}\,\boldsymbol{v}_1 + \frac{m_2}{M}\,\boldsymbol{v}_2 \tag{3.42}$$

with

$$M = m_1 + m_2\,. \tag{3.43}$$

Inserting (3.42) into (3.40) and (3.41), we have

$$\boldsymbol{g}_1 = \frac{m_2}{M}\,\boldsymbol{v}\,, \tag{3.44}$$

$$\boldsymbol{g}_2 = -\frac{m_1}{M}\,\boldsymbol{v} \tag{3.45}$$

with the relative velocity

$$\boldsymbol{v} = \boldsymbol{v}_1 - \boldsymbol{v}_2\,. \tag{3.46}$$

Or we have

$$\boldsymbol{v}_1 = \boldsymbol{g}_1 + \boldsymbol{G} = \frac{m_2}{M}\boldsymbol{v} + \boldsymbol{G}, \tag{3.47}$$

$$\boldsymbol{v}_2 = \boldsymbol{g}_2 + \boldsymbol{G} = -\frac{m_1}{M}\boldsymbol{v} + \boldsymbol{G}\,. \tag{3.48}$$

Thus a set of two independent variables, $(\boldsymbol{v}_1, \boldsymbol{v}_2)$, is expressed by another set of variables, $(\boldsymbol{v}, \boldsymbol{G})$.

Now we define the total kinetic energy in the laboratory and the CM frames in such a way as

$$E_{\rm lab}({\rm tot}) = \frac{1}{2}m_1 v_1^2 + \frac{1}{2}m_2 v_2^2\,, \tag{3.49}$$

$$E_{\rm CM}({\rm tot}) = \frac{1}{2}m_1 g_1^2 \;+\; \frac{1}{2}m_2 g_2^2\,. \tag{3.50}$$

Further we introduce the kinetic energy of relative motion defined by

$$E_{\rm rel} = \frac{1}{2}\mu_{12} v^2\,, \tag{3.51}$$

where μ_{12} is the so-called reduced mass

$$\mu_{12} = \frac{m_1 m_2}{M}\,. \tag{3.52}$$

Inserting (3.44) and (3.45) into (3.50), we have

$$E_{\rm CM}({\rm tot}) = E_{\rm rel}\,. \tag{3.53}$$

Recalling the relation (3.42), we finally have

$$\begin{aligned} E_{\rm lab}({\rm tot}) &= E_{\rm CM}({\rm tot}) + E_{\rm G} \\ &= E_{\rm rel} + E_{\rm G}\,, \end{aligned} \tag{3.54}$$

where $E_{\rm G}$ is the energy of the motion of the gravity center and defined by

$$E_{\rm G} = \frac{1}{2}MG^2\,. \tag{3.55}$$

During the collision, the motion of the gravity center does not change. We cannot use that part (i.e., $E_{\rm G}$) of the total collision energy for any activity (e.g., excitation, ionization, etc.). Only the other part (i.e., $E_{\rm CM}({\rm tot})$ or equivalently $E_{\rm rel}$) is physically usable.

In the quantum mechanics, the same relation as (3.54) holds for the kinetic-energy operator, i.e.,

$$\frac{1}{m_1}\nabla_1^2 + \frac{1}{m_2}\nabla_2^2 = \frac{1}{\mu_{12}}\nabla_{\rm r}^2 + \frac{1}{M}\nabla_{\rm G}^2 \,. \tag{3.56}$$

Here the coordinates of the relative position of the two particles, $\boldsymbol{r}$, and the gravity center, $\boldsymbol{r}_{\rm G}$, are introduced by

$$\boldsymbol{r} = \boldsymbol{r}_1 - \boldsymbol{r}_2 \,, \tag{3.57}$$

$$\boldsymbol{r}_{\rm G} = \frac{m_1}{M}\,\boldsymbol{r}_1 + \frac{m_2}{M}\boldsymbol{r}_2 \,, \tag{3.58}$$

where $\boldsymbol{r}_1$ and $\boldsymbol{r}_2$ denote the positions of the two particles. The corresponding Laplacian operators are $\nabla_{\rm r}^2$ and $\nabla_{\rm G}^2$. The relation (3.56) can be easily derived in the differential calculus or simply from the correspondence principle in the quantum mechanics. When we solve a general 2-body problem, we need a solution of the equation

$$\left(-\frac{\hbar^2}{2m_1}\,\nabla_1^2 - \frac{\hbar^2}{2m_2}\,\nabla_2^2 + V(\boldsymbol{r}_1,\boldsymbol{r}_2)\right)\Psi(\boldsymbol{r}_1,\boldsymbol{r}_2) = E\,\Psi(\boldsymbol{r}_1,\boldsymbol{r}_2)\,. \tag{3.59}$$

With use of the relation (3.56), this equation is separated into two: one for the motion of the gravity center and the other for the relative motion of the two particles. Since we do not need to solve the former equation, we have to solve only the latter (i.e., the equation of the relative motion). Now we have the following conclusion. Whenever we consider a collision of two particles (2-body problem), we only need to solve the equation of relative motion (1-body problem) in the form

$$\left(-\frac{\hbar^2}{2\mu_{12}}\,\nabla_r^2 + V(\boldsymbol{r})\right)\Psi(\boldsymbol{r}) = E_{\rm rel}\,\Psi(\boldsymbol{r})\,. \tag{3.60}$$

Note that the interaction between the two particles depends only on their relative position, $\boldsymbol{r}$. The equation (3.60) is a wave equation for one particle in the potential V, but the mass of the particle is μ_{12}, instead of either m_1 or m_2.

The definition of the cross-section presented in the previous sections do not need to be changed for the collisions of two moving particles, if we replace the mass with the relevant reduced one. In other words, cross-section is a quantity defined for a relative motion of the colliding particles. Other quantities introduced in Sect. 3.1 need to change their definitions, if necessary. For example, let us consider the case of Fig. 3.3, but with the field particles A

moving with the velocity distribution $f(\boldsymbol{v}_{\rm A})$. The collision frequency is now evaluated in the form

$$\nu_{\rm coll}({\rm B} \to {\rm A}) = N({\rm A}) \int {\rm d}\boldsymbol{v}_{\rm A}\, v\, Q(v)\, f(\boldsymbol{v}_{\rm A})\,, \tag{3.61}$$

where v $(= |\boldsymbol{v}_{\rm B} - \boldsymbol{v}_{\rm A}|)$ is the absolute magnitude of the relative velocity. The mean free path of the incoming particle B is obtained with this collision frequency in such a way as

$$\lambda_{\rm mfp}({\rm B} \to {\rm A}) = \frac{v_{\rm B}}{\nu_{\rm coll}({\rm B} \to {\rm A})}\,. \tag{3.62}$$

Now we consider an experiment where particle 1 collides with particle 2, but particle 2 is fixed in space before collision. Then we have

$$\boldsymbol{v}_2 \;=\; 0\,, \tag{3.63}$$

$$\boldsymbol{v}_1 \;=\; \boldsymbol{v}\,. \tag{3.64}$$

The total kinetic energies in the laboratory and CM frames are given by

$$E_{\rm lab}({\rm tot}) = \frac{1}{2} m_1 v_1^2\,, \tag{3.65}$$

$$E_{\rm CM}({\rm tot}) = E_{\rm rel} = \frac{1}{2}\mu_{12} v_1^2\,. \tag{3.66}$$

Then we have a relation

$$E_{\rm rel} = \frac{m_2}{M}\, E_{\rm lab}({\rm tot})\,. \tag{3.67}$$

Only a fraction (i.e., m_2/M) of the collision energy given before collision can be spent on the process induced by the collision. In this sense, cross-sections in the literature are often expressed as a function of $E_{\rm rel}$, instead of $E_{\rm lab}$. The former is called the collision energy in the CM frame, or simply the CM energy. It should be noted that the relation (3.67) can be used only in the case where the conditions (3.63) and (3.64) are satisfied before the collision. When we consider "electron–molecule" collisions, the reduced mass can be regarded as the electron mass and $E_{\rm CM}$ and $E_{\rm lab}$ have essentially the same values.

Following the above statement, we have a relation:

$$E_{\rm rel} - E'_{\rm rel} = W\,, \tag{3.68}$$

where the superscript "prime" denotes the quantity after the collision and W represents the inelasticity of the collision or the *increase* of the internal energy of the colliding system (either in particle 1, particle 2, or both). Again we consider the collision in the laboratory frame specified by (3.63) and (3.64). We denote the initial kinetic energies of particle 1 (projectile) and 2 (target) in the laboratory frame by E_1 and E_2, respectively. In the present collision

system, $E_2 = 0$. Those energies after the collision are denoted by ${E_1}'$ and ${E_2}'$. The change of the kinetic energy of particle 1 (projectile) is calculated in the form

$$\Delta E_1 = E_1 - {E_1}' = {E_2}' + W\,, \tag{3.69}$$

where ${E_2}'$ is the recoil energy of the target. This relation means that the change (e.g., a loss) of the incident–particle energy (in laboratory frame) consists of two parts: the change (e.g., a gain) of internal energies and the recoil energy of the target.

Let us evaluate W in terms of the energies of the incident particle. After the collision, the relative velocity becomes (see (3.47))

$$\boldsymbol{v}' = \frac{M}{m_2}\,(\boldsymbol{v}_1{}' - \boldsymbol{G})\,. \tag{3.70}$$

In the present case, the velocity of gravity center is given by (see (3.42) with $\boldsymbol{v}_2 = 0$)

$$\boldsymbol{G} = \frac{m_1}{M}\,\boldsymbol{v}_1\,. \tag{3.71}$$

From (3.70) and (3.71), we have

$$\boldsymbol{v}' = \frac{M}{m_2}\,\boldsymbol{v}_1{}' - \frac{m_1}{m_2}\,\boldsymbol{v}_1\,. \tag{3.72}$$

Then the square of (3.72) gives

$${v'}^2 = \left(\frac{M}{m_2}\right)^2 {v_1{}'}^2 + \left(\frac{m_1}{m_2}\right)^2 v_1^2 - 2\frac{Mm_1}{m_2^2}\,v_1{}' v_1\,\cos\theta_{\rm lab}\,, \tag{3.73}$$

where $\theta_{\rm lab}$ is the scattering angle of particle 1 with respect to its incident direction (i.e., the scattering angle in the laboratory frame). Rewriting (3.68) into the form

$$W = \frac{1}{2}\mu_{12}\,(v^2 - {v'}^2) = \frac{1}{2}\mu_{12}(v_1^2 - {v'}^2)\,, \tag{3.74}$$

and using (3.73), we finally have

$$W = (1-\gamma)\,E_1 - (1+\gamma)\,{E_1}' + 2\gamma\sqrt{E_1\,{E_1}'}\,\cos\theta_{\rm lab}\,, \tag{3.75}$$

where $\gamma = m_1\,/\,m_2$.

Consider an experiment under the laboratory conditions, (3.63) and (3.64). Measure the intensity I_1 of particle 1 after the collision as a function of its energy ${E_1}'$, at fixed values of incident energy E_1 and scattering angle $\theta_{\rm lab}$. When we plot I_1 against ${E_1}'$, we have peaks at the positions ${E_1}' = {E_1}'(W)$, which is derived from the relation (3.75) with a certain internal energy change W (due to excitation or de-excitation of the particles). This is the principle of the translational energy spectroscopy.

One specific example of (3.75) is the elastic scattering (i.e., $W = 0$) of electrons from molecules (i.e., $\gamma \ll 1$). In this case, the energy loss of the incident electron can be calculated from (3.75), to the first-order of γ, as

$$\begin{aligned}\Delta E_1 &= E_1 - {E_1}' \\ &= 2\gamma E_1 \left(1 - \cos\theta_{\rm lab}\right) \qquad \text{for elastic electron collisions.} \end{aligned} \tag{3.76}$$

3.5 Experimental Methods to Obtain Cross-Sections

There are a variety of methods to experimentally determine cross-sections. To provide accurate cross-section data, it is necessary to have reliable experimental methods. From this point of view, experimental methods for atomic collisions were reviewed in a special volume of Advances in Atomic, Molecular, and Optical Physics [73]. To help the understanding of the following chapters, we briefly summarize in this section the principles of five representative methods used for electron collisions. All of them are used also for ion collisions, for which more sophisticated methods are employed for specific processes. Here an emphasis is placed on the points to be considered when we evaluate the accuracy of the cross-sections obtained by the respective methods. An issue of particular importance is how to determine the absolute value of the cross-section. Technical details of the experimental methods are found in the review articles mentioned above.

3.5.1 Measurement of Energy Loss of Electrons

The most straightforward manner to obtain cross-sections is the measurement of energy loss of electrons. The principle exactly follows the definition of the DCS (see Fig. 3.1) (see [161]). Prepare an electron beam with energy E. Shoot the beam into a box filled with target molecules. (Many of the experiments use a beam of target molecules to clearly define the collision point. It is called a crossed-beam experiment.) Detect electrons scattered in the direction (θ, ϕ) with respect to the incident beam. Analyze the energy (E') of the scattered electrons and draw a diagram of the intensity of the scattered electrons (ordinate) against the amount of energy loss of the electrons $(= E - E'$, abscissa). This diagram is called an electron energy loss spectrum (EELS). The spectrum shows several peaks corresponding to the excitation of discrete states of the molecule. This is a special example of the translational energy spectroscopy described in Sect. 3.4. If a continuous energy-loss (e.g., ionization) occurs, we have a broad peak. The intensity of the nth peak is written in the form

$$I_n(\theta, \phi\,|E) = q_n(\theta, \phi\,|E) I_{\rm e} F(E') G(\boldsymbol{r}_{\rm coll}). \tag{3.77}$$

Here $I_{\rm e}$ is the current of the incident electron, the function F is the apparatus function determining the transmission efficiency of the scattered electron, and

G is the number of target molecule at the collision point $\boldsymbol{r}_{\rm coll}$. To obtain an absolute value of the differential cross-section for the excitation of the nth state, $q_n(\theta, \phi)$, we need to know the functions F and G. They are difficult to determine. In many cases, the same experiment is carried out with a standard collision system (e.g., electron collisions with He) for which an accurate cross-section is already known. The relative intensity for the elastic scattering (i.e., $n = 0$) from the target gas A and the standard gas (say, He) is obtained as

$$\frac{I_0^{\rm A}(\theta, \phi\,|E)}{I_0^{\rm He}(\theta, \phi\,|E)} = \frac{q_0^{\rm A}(\theta, \phi\,|E)}{q_0^{\rm He}(\theta, \phi\,|E)} \, \frac{I_{\rm e}^{\rm A}\, F^{\rm A}\, G^{\rm A}}{I_{\rm e}^{\rm He}\, F^{\rm He}\, G^{\rm He}} \,. \tag{3.78}$$

Here $I_{\rm e}^{\rm A}$ and $I_{\rm e}^{\rm He}$ can be accurately measured. Since the function F is specific to the apparatus, we simply have $F^{\rm A} = F^{\rm He}$. By adjusting the flow condition of the target gas, we can determine $G^{\rm A}/G^{\rm He}$ from the relative pressure measurement. Finally we obtain $q_0^{\rm A}$ from the measured ratio $I_0^{\rm A}/I_0^{\rm He}$, provided that we have $q_0^{\rm He}$. This is called the relative flow method. The inelastic cross-sections are determined from the relative measurement of $I_n^{\rm A}/I_0^{\rm A}$ with the elastic cross-section now obtained.

With varying the detection angle (θ, ϕ), we can determine the angular distribution of the cross-section. Integrating the DCS over the scattering angles, we finally have the (integral) cross-section Q. In ordinary beam-type experiments, forward (near $\theta = 0°$) and backward (near $\theta = 180°$) scatterings cannot be measured, because of the geometrical constraint of the apparatus. To get the integral cross-section, we need extrapolations of the measured DCS to the forward and backward directions. This introduces uncertainty in the resulting cross-section. To avoid this problem, a new technique, called the magnetic angle changer (MAC), has been developed [137]. In this method, the electron trajectory is changed by an applied magnetic field so that the DCS can be measured all over the scattering angles (i.e., 0–180°). Because of technical difficulties, this method has not been extensively used yet, particularly for molecular targets.

3.5.2 Detection of Collision Products

Cross-section can be determined by a detection of the collision product. Let us consider an ionization as an example. We introduce an electron beam with energy E into a gas of target molecules (see Fig. 3.4). Along the beam trajectory, electron collides with molecules. Some of the collisions produce ions. The number of ions produced per unit time is evaluated as

$$I_{\rm ion} = Q_{\rm ion}\, NLI_{\rm e} \,. \tag{3.79}$$

Here $Q_{\rm ion}$ is the ionization cross-section, N is the number density of target molecules, L is the length of the collision region, and $I_{\rm e}$ is the current of the incident electron. By using (3.79), we can determine the cross-section $Q_{\rm ion}$ from the measurement of the product ion, provided that we have N, L, $I_{\rm e}$.

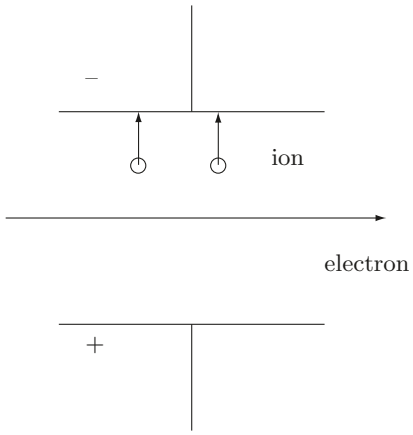

Fig. 3.4. A method of measurement of ionization cross-section

To have a correct value of the cross-section, we have to be careful about detecting all the ions produced. A problem may arise, when the collision product has a kinetic energy (e.g., in the case of dissociative ionization). When several different ions are produced, we can identify them with a mass spectrometer installed in front of the ion collector.

3.5.3 Beam Attenuation Method

When an electron beam passes through a molecular gas of density N, the beam intensity I decreases due to the collision with the molecule (Fig. 3.5). The intensity decrease over a distance L can be evaluated by the formula (see (3.14) and the discussion about the equation)

$$\frac{I(L)}{I(0)} = \exp(-\frac{L}{\lambda})\,. \tag{3.80}$$

Here λ is the mean free path of the incoming electron and given by

$$\lambda = \frac{1}{N\,Q}\,. \tag{3.81}$$

(Note that, in the case of electron–molecule collisions, we can ignore the velocity distribution of molecules in (3.61), unless the electron energy is too small.) From the measurement of I, we can obtain the cross-section Q, provided that we know the density of the molecule N. It is clear from the principle that the quantity measured is the total scattering cross-section $Q_{\rm tot}$ introduced in (3.12). One of the advantages of this method is that we can obtain the absolute value of the cross-section without any normalization procedure. Furthermore, we do not need to measure the absolute value of the beam intensity I. It is sufficient to measure the relative change of the beam intensity.

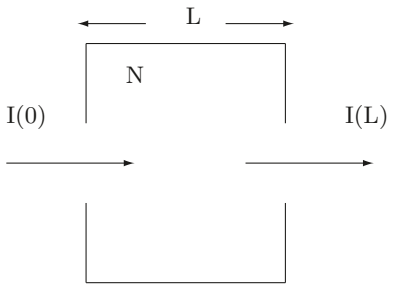

Fig. 3.5. Beam attenuation experiment

In this experiment, it is assumed that electrons must be lost from the beam once they collide with molecules. Some electrons move in the forward direction even after the collision. The intensity $I(L)$ should not include these scattered electrons. It is not easy to make corrections for this effect. The reliability of the resulting cross-section, therefore, can be judged by asking if this forward-scattering effect is properly taken into account or not.

3.5.4 Merged Beam Method

In this method, two interacting beams of particles are made to travel in parallel with each other for some finite distance (see the review by Phaneuf et al. [131]). By so doing, the chance of collisions is increased. When collisions involve active species, it is difficult to accumulate them dense enough for a collision experiment and hence a merged beam technique is often employed. The best example is the electron collisions with ions. The most unique advantage of the method is its ability to access low relative (or, in other words, center-of-mass) energies. Since the two beams are collinear, the relative speed can be set arbitrarily small with controlling the laboratory speeds of the beams. Collision cross-sections depend only on the relative energy (or velocity) of the colliding particles. The merged beam method, therefore, is particularly useful for the process having a large cross-section at very low relative energies (e.g., electron–ion recombination). When fast primary beams are used, the collision products are also travelling fast. Those fast products are easily detectable, even when they are neutral particles. Compared with other experimental methods, the merged beam method has several inherent difficulties. The method needs to have high-quality fast beams and we should precisely control those beams. It is usually difficult to know accurately the effective number of the target density. Because of these and other difficulties of the method, we need special care when we use the result obtained by the method.

3.5.5 Swarm Experiment

This method is completely different from others. Prepare a chamber filled with target molecules. Introduce an ensemble of electrons into the chamber. Apply a uniform electric field from outside. The electrons are continuously accelerated by the field, but occasionally collide with the molecules. When colliding with a molecule, an electron loses its energy and deviates from its trajectory. After the collision, the electron is again accelerated by the field and recovers its energy and momentum. As a whole a swarm of electrons move towards the anode with a constant mean velocity (called a drift velocity). The electrons also spatially spread by diffusion. We measure the drift velocity and the diffusion coefficient as a function of the strength of the applied field, $\mathcal{E}$. More precisely those quantities (called the transport coefficients) depend on the so-called reduced field $\mathcal{E}/N$, N being the number density of the gaseous molecules. In principle the transport coefficients are resulted from the balance between the applied field and the degree of electron–molecule collisions. We can, therefore, relate the measured values of the transport coefficients to the cross-sections of relevant collision processes. In other words, we can derive cross-sections from the measurement of the transport coefficients. For a general review, see [32].

The electron transport in a gas involves various collision processes. All of them should be considered simultaneously when we derive cross-sections. This results in an ambiguity of the cross-sections derived (i.e., a non-uniqueness problem). Transport properties of electrons are primarily determined by the electron energy distribution function (EEDF). The EEDF is a solution of the Boltzmann equation. It is almost established how to solve the equation, although approximately. Before solving the equation, however, we need to have sufficient knowledge of the collision processes involved. Otherwise the non-uniqueness problem makes the resulting cross-sections less reliable.

The mean energy of electrons, $< \epsilon >$, depends on $\mathcal{E}/N$. Usually when $\mathcal{E}/N$ decreases, $< \epsilon >$ decreases. Since it is rather easy to decrease $\mathcal{E}/N$ (compared to the lowering of electron energies in the ordinary EELS measurement), the swarm method is suitable to obtain cross-sections for low-energy collisions. Furthermore, at the lower energies, fewer inelastic processes occur so that the non-uniqueness problem becomes less serious. Accordingly, more reliable cross-sections are derived from the swarm experiment at the low collision energies. Another advantage of the swarm method is that an absolute value of the cross-section is obtained without any additional procedure such as normalization. For these reasons, the swarm method may serve as a complementary to the EELS measurement.

4

Molecule as a Collision Partner

4.1 Molecular Structure and Energy Levels

Compared with an atom, a molecule has two or more nuclei. This leads to the following characteristics of a molecule:

1. We have to consider a relative motion of nuclei. The motion appears as a rotational and vibrational degrees of freedom of the molecule.
2. The wave function of the molecule depends on the configuration (i.e., the relative positions) of the nuclei. Accordingly the molecular energy and the distribution of molecular electrons are dependent on the nuclear configuration. In particular, the charge distribution of the molecule becomes anisotropic.
3. As an extreme case of vibration, a molecule can dissociate into two or more fragments. It is noted that dissociation is regarded as a continuum state of vibrational motion, in such a way as an ionization is regarded as a continuum state of the motion of the bound electron.

The energy levels of a molecule are composed of three parts: rotational, vibrational, and electronic components. Each of them is briefly described below for the understanding of the following chapters. More details can be found in any textbook of molecular structure or quantum chemistry. A simple explanation of molecular structure and spectra is found in the book of Khristenko et al. [90]. For more details, see the textbooks of Herzberg [66–68].

The rotational motion of a molecule is classified into three types, according to the relative magnitudes of the three moments of inertia of the molecule. They are a linear rotor, a symmetric top, and an asymmetric top. If all three moments of inertia are equal, the molecule is called a *spherical top*, but this is a special case of symmetric top. The energy levels of each type are given below. Here we assume a rigid rotor (i.e., no coupling between the rotational and vibrational motions) and no angular momentum for bound electrons. More general cases are described, for example, in a textbook of Herzberg [67].

(a) *Linear rotor*
In this case, the molecule has only one moment of inertia, I_{B}. The energy level is given by

$$E_{\mathrm{rot}}(J) = BJ(J+1), \tag{4.1}$$

where B is the rotational constant and J is the rotational quantum number of the molecule. We have a relation

$$B = \frac{1}{2I_{\mathrm{B}}}. \tag{4.2}$$

(b) *Symmetric top*
Here two of the moments of inertia have the same value (I_{B}). The third one is denoted by I_{A}. Then the rotational constants are defined by

$$A = \frac{1}{2I_{\mathrm{A}}}, \quad B = \frac{1}{2I_{\mathrm{B}}}. \tag{4.3}$$

The rotational energy is given in the form

$$E_{\mathrm{rot}}(J,K) = BJ(J+1) + (A-B)K^2, \tag{4.4}$$

where K is the quantum number of the angular momentum component along the symmetry (top) axis of the molecule. For a given J, the quantum number K takes a value in the range $(-J, -J+1, \ldots, J-1, J)$. If $K \neq 0$, the states with K and $-K$ are degenerate.

(c) *Spherical top*
This is a symmetric top, but with $A = B$. The energy is specified only by the quantum number J as

$$E_{\mathrm{rot}}(J) = BJ(J+1). \tag{4.5}$$

All the states with same J but different K are degenerate.

(d) *Asymmetric top*
The energy level is labeled by a quantum number J and a pseudoquantum number τ. The pseudoquantum number takes a value in the range $(-J, -J+1, \ldots, J-1, J)$. The structure of the energy levels is a complicated function of the three moments of inertia $(I_{\mathrm{A}}, I_{\mathrm{B}}, I_{\mathrm{C}})$. As an example, the rotational energy of H_2O is tabulated in Table 4.1 (from the review by Itikawa and Mason [81]). Due to the molecular symmetry, the rotational energy levels of H_2O are separated into two groups: one with even values of τ (called *para levels*) and the other with odd values of τ (called *ortho levels*). Transitions between the two groups can occur neither by photoabsorption nor by electron impact. Table 4.1 gives all the levels with $J = 0$–3. They cannot be expressed with any simple function of J and τ.

Table 4.1. Rotational energy levels of H_2O

Para		Ortho	
J_τ	Energy (meV)	J_τ	Energy (meV)
0_0	0.0	1_{-1}	2.950
1_0	4.604	1_1	5.253
2_{-2}	8.690	2_{-1}	9.856
2_0	11.800	2_1	16.726
2_2	16.882	3_{-3}	16.956
3_{-2}	17.640	3_{-1}	21.495
3_0	25.578	3_1	26.304
3_2	35.363	3_3	35.387

When the molecular gas is in thermal equilibrium with temperature $T_{\rm gas}$, the rotational states satisfy the Maxwell–Boltzmann distribution. In the case of linear rotor, for example, the fraction of a state with J is given by

$$f_J = F_{\rm rot} g_J \exp\left(-\frac{E(J)}{k_{\rm B} T_{\rm gas}}\right), \tag{4.6}$$

where $k_{\rm B}$ is the Boltzmann constant,

$$E(J) = BJ(J+1), \tag{4.7}$$

and $F_{\rm rot}$ is a normalization constant to give

$$\sum_J f_J = 1. \tag{4.8}$$

In (4.6), g_J is the statistical weight of the state J. For a nonsymmetric linear molecule (e.g., a heteronuclear diatomic molecule), we have

$$g_J = 2J + 1. \tag{4.9}$$

As an example, we show in Fig. 4.1 the distribution of rotational states of HCl at 300 K. The most probable state is $J = 3$. At 300 K, only 5% of HCl are populated in the ground rotational state.

In the case of homonuclear diatomic molecules, we have to take into account the symmetry property of the wave function. An interchange of nuclei does not change the wave equation of the molecule. The rotational wave function, therefore, is either symmetric or antisymmetric with the interchange of nuclei. Accordingly the rotational states are separated into two sets. Transitions between the states belonging to the different sets are forbidden. This rule

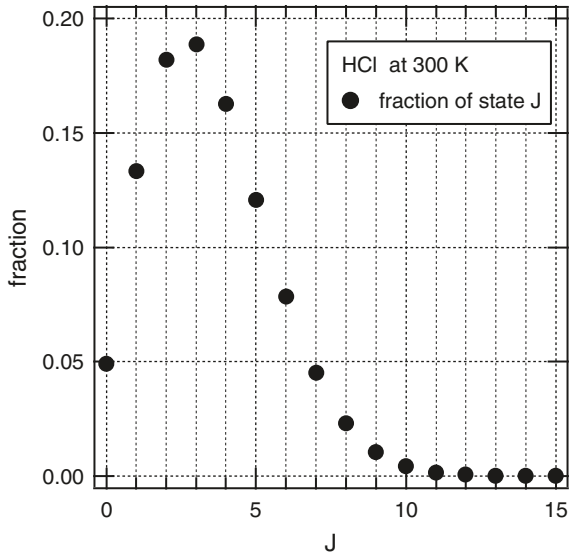

Fig. 4.1. Fraction of the rotational states of HCl at 300 K

is applied to the transition induced by electron collisions, as well as photoabsorption. Consider the case of N_2. The rotational states are separated into the group with even J (called "ortho" states) and that with odd J (called "para" states). Any electron impact cannot change an even-J state into an odd-J state or vice versa. Furthermore, we have to consider nuclear spins, which affect the nuclear symmetry. The statistical weight is now given by [66]

$$\begin{aligned} g_J &= 2\,(2J+1) \quad \text{for } J = \text{even} \\ &= 2J+1 \quad \text{for } J = \text{odd}. \end{aligned} \tag{4.10}$$

Figure 4.2 shows the fraction of the rotational states of N_2 at 300 K. In this case the state with $J = 6$ has the largest population.

The vibrational energy of a diatomic molecule is written by

$$E_{\text{vib}}(v) = hc\,G(v). \tag{4.11}$$

Here v is the vibrational quantum number and G is the corresponding term value, which is given by, to the first order of anharmonicity,

$$G(v) = \omega_{\text{e}}\left(v+\frac{1}{2}\right) - \omega_{\text{e}}x_{\text{e}}\left(v+\frac{1}{2}\right)^2. \tag{4.12}$$

We call ω_{e} and $\omega_{\text{e}}x_{\text{e}}$ the vibrational frequency and the anharmonicity constant, respectively. The transition energy from the state v to $v+1$ is given by

$$\Delta E(v \to v+1) = hc\,\Delta G_{v+1/2}, \tag{4.13}$$

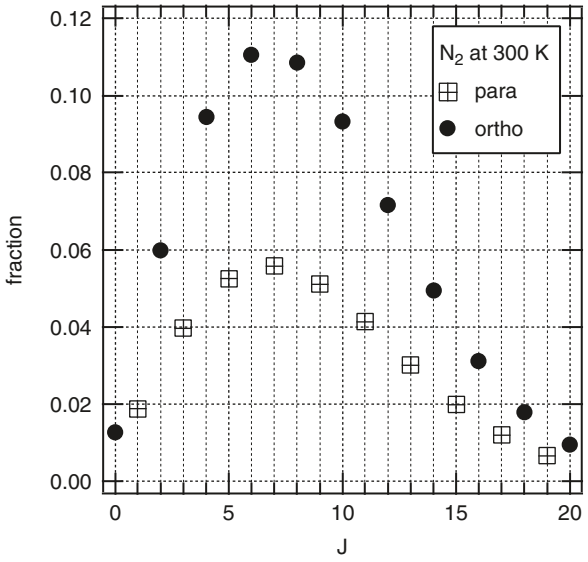

Fig. 4.2. Fraction of the rotational states of N_2 at 300 K

with

$$\begin{aligned}\Delta G_{v+1/2} &= G(v+1) - G(v) \\ &= \omega_e - 2\omega_e x_e(v+1). \end{aligned} \tag{4.14}$$

It is noted that, once the anharmonicity is taken into account, the level separation decreases with increasing v. The energy of the lowest vibrational transition is

$$\Delta E(v = 0 \to 1) = hc(\omega_e - 2\omega_e x_e). \tag{4.15}$$

We show in Appendix B $\Delta E(v = 0 \to 1)$ for some molecules.

A polyatomic molecule has two or more normal modes of vibration. The number of modes is given by

$$m_{\text{vib}} = 3N_{\text{nuc}} - 6 \text{ (or 5 for a linear molecule)}, \tag{4.16}$$

where N_{nuc} is the number of nuclei in the molecule. It should be noted that some of the modes are often degenerate and the number of independent modes is less than the value given by (4.16). If we ignore anharmonicity, each mode (designated by index s) has an energy

$$E_{\text{vib},s} = hc\,\omega_e \left(v_s + \frac{1}{2}\right). \tag{4.17}$$

Due to possible couplings among different modes, anharmonicity effects are very complicated in polyatomic molecules. There have been extensive studies of the vibrational motion of polyatomic molecules (see [67]). The result

depends sensitively on the structure (nuclear configuration) of the molecule. It is impossible to make any general statement here. We only show in Appendix B the energy of the lowest (i.e., fundamental) transition of each vibrational mode, $\Delta E(v_s = 0 \to 1)$, of several polyatomic molecules. They have been determined from the infrared or the Raman spectroscopy.

As in the case of rotation, the distribution of vibrational states in thermal equilibrium is determined by the Maxwell–Boltzmann formula. Particularly the ratio of the number of molecules in the first to that in the ground vibrational state is given by

$$\frac{n(v=1)}{n(v=0)} = \exp\left(-\frac{\Delta E(v=0\to 1)}{k_{\mathrm{B}}T_{\mathrm{gas}}}\right). \tag{4.18}$$

Table 4.2 gives the ratio for some molecules. At room temperature most of the molecules are populated in the vibrationally ground state. But, even at room temperature, some polyatomic molecules (e.g., CF_4 in the table) have a relatively large population of vibrationally excited states.

The electronic energy levels of a molecule depend on the nuclear configuration of the molecule. In the case of a diatomic molecule, the electronic energy levels can be drawn as curves in the graph of the electronic energy $\mathcal{E}_{\mathrm{e}}$ against the internuclear distance R (see Fig. 4.3). Since the electronic energy serves as a potential for the nuclear motion, these curves are called *potential diagrams*. For the state to be stable, the potential curve must have a minimum as a function of R. The states 1 and 2 in Fig. 4.3 have their minima at $R = \bar{R}_1$ and $R = \bar{R}_2$, respectively. The quantities $\bar{R}_1$ and $\bar{R}_2$ are called the *equilibrium internuclear distances*. Usually the molecule is located at its equilibrium position. In most cases, $\bar{R}_2$ does not coincide with $\bar{R}_1$. When an

Table 4.2. Population ratio of the first ($v = 1$) to the ground ($v = 0$) vibrational states

Molecule	Mode of vibration[a]	$n(v=1)/n(v=0)$	
		T_{gas} =300 K	T_{gas} =1,000 K
H_2		2.15×10^{-9}	2.51×10^{-3}
N_2		1.40×10^{-5}	3.50×10^{-2}
CO_2	ν_1	1.69×10^{-3}	0.147
	ν_2	4.03×10^{-2}	0.382
	ν_3	1.29×10^{-5}	3.42×10^{-2}
CF_4	ν_1	1.26×10^{-2}	0.269
	ν_2	0.124	0.534
	ν_3	2.13×10^{-3}	0.158
	ν_4	4.89×10^{-2}	0.404

[a] For modes and energies of vibrational states, see Appendix B.

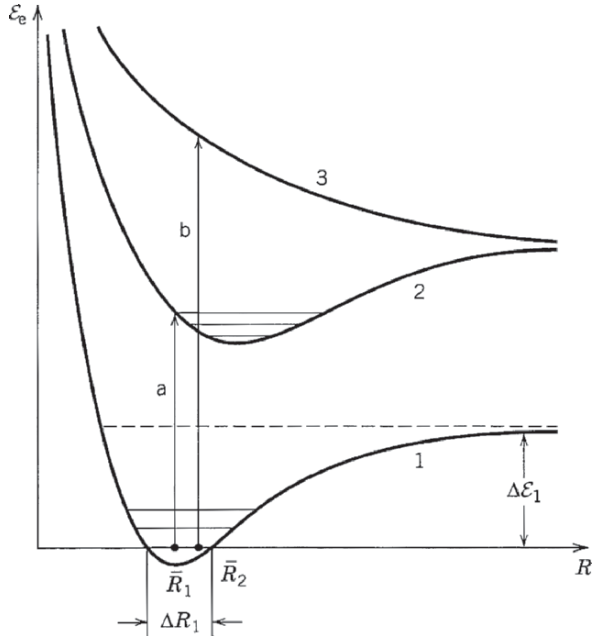

Fig. 4.3. Electronic energy levels of a diatomic molecule, reproduced from [100]

electric dipole transition is allowed between state 2 and state 1, state 2 is unstable against the radiative decay (i.e., having a short lifetime). Otherwise state 2 is designated to be metastable. State 3 in Fig. 4.3 is repulsive. Once the molecule is excited to state 3, it promptly dissociates into two atoms. Each attractive electronic state accompanies a series of rotational and vibrational energy levels. Strictly speaking a transition between state 2 and state 1 takes place between one rotational–vibrational level of state 1 and one rotational–vibrational level of state 2. In other words, any transition of electronic states accompanies transitions of rotational–vibrational states. In the figure, $\Delta\mathcal{E}_1$ is the dissociation energy of the molecule. Above this energy (i.e., the horizontal dashed line in Fig. 4.3), the vibrational levels belonging to state 1 become continuum. The dissociation of the molecule can also occur through the transition to this continuum.

4.2 Interaction of Charged Particles with Molecules

The main part of the interaction between an incident charged particle (electron or ion) and a molecule consists of electrostatic (Coulomb) interactions between the incident particle and the electrons and nuclei in the molecule. Other parts of the interaction, particularly for electron–molecule collisions, are described

in Sect. 4.3. For simplicity, we consider a diatomic molecule as a target. Then the electrostatic interaction is expressed in the form

$$V(\boldsymbol{r};\boldsymbol{R}) = qe\int \mathrm{d}\boldsymbol{s}\,\rho(\boldsymbol{s};\boldsymbol{R})\frac{1}{|\boldsymbol{r}-\boldsymbol{s}|}. \tag{4.19}$$

Here $\boldsymbol{r}$ and qe denote, respectively, the position and the charge of the incident particle (e.g., $q = -1$ for an electron). The quantities $\boldsymbol{s}$ and $\rho(\boldsymbol{s})$ represent a position in the target and the charge density at the position, respectively. The origin of the coordinates $\boldsymbol{r}$ and $\boldsymbol{s}$ is located at the gravity center of the molecule. The internuclear vector is denoted by $\boldsymbol{R}$. The molecular charge density and, hence, the interaction potential depend on the nuclear configuration of the target molecule (i.e., $\boldsymbol{R}$ in this case). The molecular charge density is written as

$$\rho(\boldsymbol{s};\boldsymbol{R}) = -e\,\rho_{\mathrm{e}}(\boldsymbol{s};\boldsymbol{R}) + \sum_n Z_n e\delta(\boldsymbol{s}-\boldsymbol{R}_n), \tag{4.20}$$

where $\rho_{\mathrm{e}}(\boldsymbol{s};\boldsymbol{R})$ is the density of molecular electrons, and $Z_n e$ and $\boldsymbol{R}_n$ are the charge and the position of the nth nucleus in the molecule. Now we introduce a relation

$$\frac{1}{|\boldsymbol{r}-\boldsymbol{s}|} = \sum_{\lambda,\mu}\frac{r_<^\lambda}{r_>^{\lambda+1}}\frac{4\pi}{2\lambda+1}{Y_{\lambda\mu}}^*(\hat{\boldsymbol{r}})Y_{\lambda\mu}(\hat{\boldsymbol{s}}), \tag{4.21}$$

where Y is the spherical harmonic function and $r_<$ ($r_>$) is the smaller (larger) of (r, s). The quantity $\hat{\boldsymbol{r}}$ represents the angular part of $\boldsymbol{r}$ (or, equivalently, the unit vector in the direction of $\boldsymbol{r}$). The $\hat{\boldsymbol{s}}$ has the same meaning. When we take the z-direction along the molecular axis, the molecular charge density is symmetric around the z-axis. Hence only the term with $\mu = 0$ appears in the summation and we have

$$V(\boldsymbol{r};\boldsymbol{R}) = qe\int \mathrm{d}\boldsymbol{s}\,\rho(\boldsymbol{s};\boldsymbol{R})\sum_\lambda\frac{r_<^\lambda}{r_>^{\lambda+1}}P_\lambda(\cos\hat{\boldsymbol{r}}\cdot\hat{\boldsymbol{R}})P_\lambda(\cos\hat{\boldsymbol{s}}\cdot\hat{\boldsymbol{R}}), \tag{4.22}$$

where $\hat{\boldsymbol{r}}\cdot\hat{\boldsymbol{R}}$ and $\hat{\boldsymbol{s}}\cdot\hat{\boldsymbol{R}}$ indicate the angles of the vectors, $\boldsymbol{r}$ and $\boldsymbol{s}$, with respect to the molecular axis. Equation (4.22) can be written as

$$V(\boldsymbol{r};\boldsymbol{R}) = \sum_\lambda v_\lambda(r;R)P_\lambda(\cos\hat{\boldsymbol{r}}\cdot\hat{\boldsymbol{R}}), \tag{4.23}$$

with

$$v_\lambda(r;R) = qe\int \mathrm{d}\boldsymbol{s}\,\rho(\boldsymbol{s};\boldsymbol{R})\frac{r_<^\lambda}{r_>^{\lambda+1}}\,P_\lambda(\cos\hat{\boldsymbol{s}}\cdot\hat{\boldsymbol{R}}). \tag{4.24}$$

When the incident particle is located far from the molecule (i.e., $r \gg s$), we have

$$V \approx V^{\mathrm{L}} = \sum_\lambda v_\lambda^{\mathrm{L}}(r;R)P_\lambda(\cos\hat{\boldsymbol{r}}\cdot\hat{\boldsymbol{R}}), \tag{4.25}$$

with

$$v_\lambda^{\mathrm{L}}(r;R) = qe \int \mathrm{d}\boldsymbol{s}\, \frac{s^\lambda}{r^{\lambda+1}}\, \rho(\boldsymbol{s};\boldsymbol{R})\, P_\lambda(\cos\hat{\boldsymbol{s}}\cdot\hat{\boldsymbol{R}}). \tag{4.26}$$

We call V^{L} the long-range part of the interaction or simply the long-range interaction. Here we introduce a quantity M_λ, which is defined by

$$M_\lambda(R) = \int \mathrm{d}\boldsymbol{s}\, s^\lambda \rho(\boldsymbol{s};\boldsymbol{R}) P_\lambda(\cos\hat{\boldsymbol{s}}\cdot\hat{\boldsymbol{R}}). \tag{4.27}$$

With use of this, (4.26) is rewritten in the form

$$v_\lambda^{\mathrm{L}}(r;R) = \frac{qe\, M_\lambda(R)}{r^{\lambda+1}}. \tag{4.28}$$

The quantity M_λ is the permanent electric multipole moment, i.e., M_1, $M_2, \ldots$ are the dipole, quadrupole, ... moments of the molecule. The interaction (4.28) decays with a power law of the distance. This is in contrast to the electron–atom interaction, which decays exponentially with the distance.

Summarizing the formulation presented so far, we have the following conclusions.

First, for electron–molecule collisions:

1. The interaction potential (see (4.23)) has a term with $\lambda \neq 0$. This term causes rotational transition.
2. The interaction potential V, or more precisely v_λ, depends on the nuclear configuration (in the present case, the internuclear distance R). When nuclear configuration changes, the charge distribution in the molecule changes. Through this change of the charge distribution, the interaction potential changes. In a reverse manner, a change in the interaction potential induces a change of nuclear configuration. This is the mechanism of vibrational excitation of molecules.
3. An electron interaction with electric multipole moments of the molecule gives rise to a long-ranged interaction. This interaction is particularly important at low energies of incident electron, because most of the low-energy electrons cannot come close to the target.

For ion–molecule collisions, the situation is much more complicated. The projectile ion has its own electrons and nuclei. The electrostatic interaction between the ion and the molecule consists of the Coulomb interactions between the *electrons and nuclei* of the ion and the *electrons and nuclei* of the target molecule. The term (4.19) is only a part of it. The above conclusions about electron–molecule collisions also hold for ion–molecule ones. But they are not the dominant features of ion–molecule collisions. For ion–molecule collisions, a more general treatment as atom–molecule or molecule–molecule interactions is necessary (see, e.g., [117]).

4.3 Electron Collision with a Diatomic Molecule

An outline of the treatment of electron–molecule collisions is presented here for a diatomic molecule as a target. Special features of polyatomic molecules are summarized in Sect. 4.4. Details of the theory for electron–molecule collisions (including polyatomic molecules) can be found, for example, in a review by Gianturco et al. [54].

The Hamiltonian for the collision system is given by (see (3.60))

$$H = -\frac{\hbar^2}{2m_\mathrm{e}}\,\nabla_r^2 \,+\, H_\mathrm{mol} + V. \tag{4.29}$$

The first term on the right-hand side of (4.29) is the kinetic energy operator of the relative motion of the electron and the target molecule. In the present case, the reduced mass of the collision system can be taken as the electron mass. The position of the electron relative to the target is denoted by $\boldsymbol{r}$. The second term, H_mol, is the Hamiltonian of the target molecule, including its nuclear motion. As the interaction between the electron and the molecule, we assume here the electrostatic interaction introduced in Sect. 4.2. Other parts of the interaction are mentioned at the end of the present section. The total wave function of the system is expanded in terms of the molecular wave function (i.e., the eigenfunction of the molecular Hamiltonian) in the form

$$\Psi(\boldsymbol{r},\, \boldsymbol{r}_\mathrm{m},\, \boldsymbol{R}) = \sum F(n, v, JM|\boldsymbol{r})\, \psi_n(\boldsymbol{r}_\mathrm{m})\, \chi_v(R)\, Y_{JM}(\hat{\boldsymbol{R}}). \tag{4.30}$$

The nuclear coordinates of a diatomic molecule are denoted by the internuclear vector $\boldsymbol{R}$. Its angular part is represented by $\hat{\boldsymbol{R}}$. The coordinates of molecular electrons are collectively given by $\boldsymbol{r}_\mathrm{m}$. The wave functions for the electronic and vibrational motions of the molecule are denoted by ψ and χ, respectively. The rotational motion is expressed by the spherical harmonic function, Y. The function F in (4.30) describes the motion of the incident electron relative to the molecule. The summation on the right-hand side of (4.30) is taken over all the quantum numbers.

Inserting (4.30) into (4.29) and using the orthonormality of the molecular wave functions, we have a set of coupled equations for F

$$\begin{aligned}&\left(\nabla_r^2 \,+\, k_{nvJ}^2\right)\, F(n, v, JM|\boldsymbol{r}) \\ &\quad = \frac{2m_\mathrm{e}}{\hbar^2} \sum_{n', v', J'M'} \langle n, v, JM\,|V|n', v', J'M'\rangle\, F(n', v', J'M'|\boldsymbol{r}).\end{aligned} \tag{4.31}$$

The wave number of electron on the left-hand side is defined by

$$k_{nvJ}^2 = \frac{2m_\mathrm{e}}{\hbar^2}\,\left(E \,-\, E_{nvJ}\right), \tag{4.32}$$

where E_{nvJ} is the energy of the molecule in the state specified by the quantum number (nvJ). The quantity on the right-hand side of (4.31) is the interaction matrix defined by

$$\begin{aligned}&\langle n, v, JM\,|V|n', v', J'M'\rangle\\ &\quad = \int \mathrm{d}\boldsymbol{r}_{\mathrm{m}} \int \mathrm{d}R \int \mathrm{d}\hat{\boldsymbol{R}}\,\{\psi_n\,\chi_v\,Y_{JM}\}^*\,V\,\{\psi_{n'}\,\chi_{v'}\,Y_{J'M'}\}. \end{aligned} \tag{4.33}$$

To obtain the cross-section for the transition $\nu_0 \to \nu$ (ν being the collective expression of (n, v, JM)), we set an asymptotic condition

$$\Psi \overset{r\to\infty}{\longrightarrow} \mathrm{e}^{\mathrm{i}\boldsymbol{k}_{\nu_0}\cdot\boldsymbol{r}}\,\{\psi_{n_0}\,\chi_{v_0}\,Y_{J_0M_0}\} + \sum_{\nu'} f_{\nu_0\to\nu'}(\boldsymbol{k}_{\nu'})\,\frac{\mathrm{e}^{\mathrm{i}k_{\nu'}r}}{r}\,\{\psi_{n'}\,\chi_{v'}\,Y_{J'M'}\}. \tag{4.34}$$

Correspondingly the asymptotic form of the solution of (4.31) is set to be

$$F(\nu') \overset{r\to\infty}{\longrightarrow} \mathrm{e}^{\mathrm{i}\boldsymbol{k}_{\nu_0}\cdot\boldsymbol{r}}\,\delta_{\nu_0\nu'} + f_{\nu_0\to\nu'}(\boldsymbol{k}_{\nu'})\,\frac{\mathrm{e}^{\mathrm{i}k_{\nu'}r}}{r}. \tag{4.35}$$

Solving the set of (4.31) to have a solution with the asymptotic form (4.35), we calculate the differential cross-section for the transition in the form

$$q_{\nu_0\to\nu} = \frac{k_\nu}{k_{\nu_0}}\,|f_{\nu_0\to\nu}(\boldsymbol{k}_\nu)|^2. \tag{4.36}$$

It is noted that $\boldsymbol{k}_\nu$ is the electron wave vector after the collision and specifies the scattering angle. Usually target molecules are randomly oriented in the space. Correspondingly to that, an average of the cross-section, (4.36), is taken over the azimuthal components of the rotational angular momentum.

For further discussions, we derive here a formal solution of (4.31). When expressing (4.31) in the form

$$\left(\nabla_r^2 + k_\nu^2\right)\,F(\nu|\boldsymbol{r}) = \frac{2m_{\mathrm{e}}}{\hbar^2}\,\sum_{\nu'}\langle\nu\,|V|\nu'\rangle\,F(\nu'|\boldsymbol{r}), \tag{4.37}$$

we can derive a formal solution with an asymptotic form of outward spherical wave, $\exp(\mathrm{i}k_{\nu'}r)/r$, as (see, e.g., [117])

$$\begin{aligned}F(\nu'|\boldsymbol{r}) \;&= -\frac{m_{\mathrm{e}}}{2\pi\hbar^2}\int \mathrm{d}\boldsymbol{r}' \int \mathrm{d}\boldsymbol{r}_{\mathbf{m}} \int \mathrm{d}\boldsymbol{R}\,\frac{\exp(\mathrm{i}k_{\nu'}|\boldsymbol{r}-\boldsymbol{r}'|)}{|\boldsymbol{r}-\boldsymbol{r}'|}\\ &\quad\times\{\psi_{n'}\,\chi_{v'}\,Y_{J'M'}\}^*\,V\,\Psi(\boldsymbol{r}', \boldsymbol{r}_{\mathbf{m}}, \boldsymbol{R}).\end{aligned} \tag{4.38}$$

Here the function Ψ on the right-hand side of (4.38) is meant to have the correct asymptotic form (4.34). From the asymptotic form of this solution, we obtain the scattering amplitude for the transition $\nu_0 \to \nu$

$$\begin{aligned}f(\boldsymbol{k}_\nu) \;&= -\frac{m_{\mathrm{e}}}{2\pi\hbar^2}\int \mathrm{d}\boldsymbol{r} \int \mathrm{d}\boldsymbol{r}_{\mathbf{m}} \int \mathrm{d}\boldsymbol{R}\,\exp(-\mathrm{i}\boldsymbol{k}_\nu\cdot\boldsymbol{r})\\ &\quad\times\{\psi_n\,\chi_v\,Y_{JM}\}^*\,V\,\Psi(\boldsymbol{r}, \boldsymbol{r}_{\mathbf{m}}, \boldsymbol{R}).\end{aligned} \tag{4.39}$$

Since this expression includes an unknown function Ψ in the integral, this does not directly give the cross-section we want. However, this can be used to provide an approximate value of the cross-section, if an approximate solution is inserted into the Ψ in the integral.

The interaction matrix (4.33) includes an integral over the molecular orientation

$$\int \mathrm{d}\hat{\boldsymbol{R}}\, Y_{JM}(\hat{\boldsymbol{R}})^*\, V\, Y_{J'M'}(\hat{\boldsymbol{R}}). \tag{4.40}$$

As is shown in (4.23), the interaction potential includes the function $P_\lambda(\cos\hat{\boldsymbol{r}}\cdot\hat{\boldsymbol{R}})$. Through this, the potential V depends on the molecular orientation $\hat{\boldsymbol{R}}$. The above integral indicates that the transition among the rotational states are induced by this part of the interaction.

For the vibrational excitation, we have the interaction matrix

$$\int \mathrm{d}R\, \chi_v(R)^*\, V\, \chi_{v'}(R). \tag{4.41}$$

Equation (4.23) indicates that the potential depends also on the internuclear distance R through the function $v_\lambda(r;R)$. The above integral shows that this R-dependence of V causes the transition among the vibrational states of the molecule.

Since the electron mass is much smaller than the nuclear mass, the collision duration (i.e., the time spent by the incident electron during the interaction with the target) is smaller than the time scale of nuclear motion, unless the electron speed is extremely low. In the first-order approximation, therefore, the nuclei can be assumed to be fixed in space during the collision. This is the principle of "adiabatic approximation of nuclear motion". Now we consider the adiabatic approximation of the rotational–vibrational transition. First, in the fixed-nuclei approximation, we have the wave function of the collision system in the form

$$\Psi^{\mathrm{FN}} = F^{\mathrm{FN}}(\boldsymbol{r}\,|\,\boldsymbol{R})\,\chi_v(R)\,Y_{JM}(\hat{\boldsymbol{R}}). \tag{4.42}$$

Here F^{FN} represents the wave function for the incident electron elastically scattered from the molecule fixed in space (with the internuclear vector $\boldsymbol{R}$). We insert Ψ^{FN} into the general expression of scattering amplitude (4.39). Then we have the scattering amplitude for the relevant rotational–vibrational transition in the form

$$f^{\mathrm{AN}}(v, JM \,\rightarrow\, v', J'M') = \int \mathrm{d}\boldsymbol{R}\,\{\chi_{v'}\,Y_{J'M'}\}^*\, f^{\mathrm{FN}}(\boldsymbol{k}\rightarrow\boldsymbol{k'}\,|\,\boldsymbol{R})\,\{\chi_v\,Y_{JM}\}. \tag{4.43}$$

The quantity f^{FN} is the amplitude of the electron scattered elastically from the molecule fixed in space and derived from the asymptotic form of the function $F^{\mathrm{FN}}(\boldsymbol{r}\,|\,\boldsymbol{R})$. With the formula (4.43), we can obtain cross-sections for

any inelastic processes of rotational and vibrational transition of a molecule. Only we need is the calculation of elastic scattering. The elastic-scattering calculation is carried out for the molecule fixed in space. But, to evaluate the integral in (4.43), we have to repeat the elastic-scattering calculation with varying the molecular orientation $\hat{\boldsymbol{R}}$ and the internuclear distance R.

It should be noted here that the adiabatic approximation can be used only when the electron energy is much above the respective threshold of the rotational–vibrational transition. When the collision energy is not high compared with the vibrational energy but still much exceeds the rotational energy, the adiabatic approximation is applied only to the calculation of rotational transitions. In this case, the method is called the *adiabatic-nuclear rotation* (ANR) approximation. Since the rotational energy of a molecule is very small (i.e., of the order of meV), this approximation is widely used and found successful.

The threshold energy of the excitation of electronic states is relatively high. For the excitation of electronic states, electrons must be fast and the nuclear motion in the molecule can be assumed to be fixed during the collision. Analogously to the adiabatic approximation for the rotational–vibrational transition, we can obtain the amplitude for the excitation of electronic states in the form

$$f^{\mathrm{AN}}(n, v, JM \;\rightarrow\; n', v', J'M') = \int \mathrm{d}\boldsymbol{R}\, \{\chi_{v'}^{n'}\, Y_{J'M'}\}^*\, f^{\mathrm{FN}}(n \rightarrow n' \,|\, \boldsymbol{R})\, \{\chi_v^n\, Y_{JM}\}. \tag{4.44}$$

It should be noted that the vibrational function χ_v depends on the electronic state. The quantity $f^{\mathrm{FN}}(n \rightarrow n' \,|\, \boldsymbol{R})$ is the scattering amplitude for the excitation $n \;\rightarrow\; n'$ of the molecule fixed in space. If we evaluate the scattering amplitude $f^{\mathrm{FN}}(n \rightarrow n' \,|\, \boldsymbol{R})$ at the equilibrium internuclear distance $R = \bar{R}$ for all the transitions $n \;\rightarrow\; n'$ (i.e., ignoring the R-dependence of f^{FN}), we have the excitation cross-section in the form

$$q(n, v \;\rightarrow\; n', v') = F_{vv'}^{nn'}\; q^{\mathrm{FN}}(n \rightarrow n'), \tag{4.45}$$

where

$$q^{\mathrm{FN}}(n \rightarrow n') = \frac{k_{n'}}{k_n} \left| f^{\mathrm{FN}}(n \rightarrow n' \,|\, \bar{R}) \right|^2 \tag{4.46}$$

and

$$F_{vv'}^{nn'} = \left| \int \mathrm{d}R\, \chi_{v'}^{n'}(R)^*\, \chi_v^n(R) \right|^2 . \tag{4.47}$$

Here rotational transitions have been ignored. The quantity (4.47) is called the Franck–Condon factor and the relation (4.45) is named the Franck–Condon factor approximation.

Finally we summarize the interaction between an electron and a diatomic molecule. Generally we consider three different types of interaction:

1. *Electrostatic interaction*
   This is the Coulomb interaction between the incoming electron and the molecular electrons and nuclei. It is given by (4.19) and fully discussed in Sect. 4.2. Particularly important is its long-range part (see (4.25) and (4.28))
   $$V^{\mathrm{L}} = \sum_{\lambda} \frac{-e\, M_\lambda}{r^{\lambda+1}}\, P_\lambda(\cos\hat{\boldsymbol{r}} \cdot \hat{\boldsymbol{R}}). \tag{4.48}$$
   This is the interaction between the incident electron and the electric multipoles of the molecule. This does not exist in the case of electron–atom collisions.
2. *Electron-exchange effect*
   In the quantum theory, we cannot distinguish the incoming electron from the bound electrons in the target molecule. To properly take into account this, we should antisymmetrize the right-hand side of (4.30) with respect to all the electronic coordinates. This leads to a set of coupled integrodifferential equations, instead of coupled differential ones (4.31). It is possible to solve the resulting equations, but the calculation is very time-consuming. There are several approaches to approximately take into account the exchange effect. The simplest way is to introduce a model (local) potential. A number of models have been proposed (see, for example, [54]). The exchange effect is important only when the electron comes close to the target.
3. *Polarization interaction*
   When an electron approaches the target molecule, the molecule gets polarized. The polarized molecule in turn exerts an attractive force to the incoming electron. This gives rise to the polarization interaction. If we include all the target states in the sum on the right-hand side of (4.30), this interaction is automatically taken considered. In fact the polarization interaction is caused as a virtual excitation of the energetically inaccessible states of the target. Since, in practice, it is impossible to consider all the inaccessible states, several approximate methods have been proposed to take into account the polarization interaction effectively (see, for example, [54]). The simplest way is the model of the adiabatic polarization potential. If we fix the incident electron at a distance r from the target, we can easily calculate the target polarization. Then an interaction is evaluated between the electron and the polarized molecule. This interaction depends on r. When $r \to \infty$, the potential of the polarization interaction has an asymptotic form such as
   $$V^{\mathrm{pol}} \to -\frac{e^2\alpha}{2r^4} - \frac{e^2\alpha'}{2r^4}\, P_2(\cos\hat{\boldsymbol{r}} \cdot \hat{\boldsymbol{R}}). \tag{4.49}$$

In the case of molecule, the target polarizability depends on the direction relative to the molecular axis. A diatomic molecule has two different components of the polarizability: the polarizability in the direction parallel to the molecular axis ($\alpha_\parallel$) and that perpendicular to the axis ($\alpha_\perp$). Those in (4.49) are the isotropic and anisotropic parts of the polarizability defined, respectively, by

$$\alpha = \frac{1}{3}\,(\alpha_\parallel + 2\alpha_\perp) \tag{4.50}$$

and

$$\alpha' = \frac{2}{3}\,(\alpha_\parallel - \alpha_\perp). \tag{4.51}$$

An effective model potential of the polarization interaction is taken as the asymptotic form (4.49) with a cut-off at a certain distance near the origin. This and other approximate methods are summarized in a compact form in a paper by Feng et al. [41].

4.4 Remarks on the Collision with Polyatomic Molecules

Polyatomic molecules are different from diatomic ones in the following aspects:

(A) *Rotational states*
Except for linear molecules, rotational motion of polyatomic molecules is represented by either a symmetric or an asymmetric top. Although the structure of the energy levels is complicated, the rotational wave function is well known. Essentially those wave functions are expressed by a linear combination of spherical harmonic functions. The interaction matrix includes the term like (4.40). The electron impact excitation of rotational states of polyatomic molecules, therefore, involves no new physics compared with that of diatomic molecules.

(B) *Vibrational states*
Polyatomic molecules have multiple normal modes of vibration. Once normal coordinates are introduced for nuclear motion, vibrational wave function is expressed as a harmonic function defined separately for individual modes. If we consider each normal mode independently, the treatment of the vibrational excitation of polyatomic molecules is almost similar to the case of diatomic one. Real vibrational motion has a deviation from the harmonic motion. Because of this anharmonicity, different normal modes can couple with each other. This mode coupling may give rise to a new phenomenon, which does not exist in the case of diatomic molecule.

(C) *Electronic states*
The nuclear configuration of polyatomic molecules is complicated. Even in the simplest case of a triatomic molecule, three independent variables are needed to specify its nuclear configuration. Furthermore, the equilibrium nuclear configuration of electronically excited states may be different from that of the ground state. In other words, the symmetry of

the molecule may be different for each electronic state. In principle, the Franck–Condon factor approximation can also be applied to the transition of electronic states of polyatomic molecules. But, in reality, it is very difficult to calculate the relevant Franck–Condon factors for polyatomic molecules.

4.5 The Born Approximation

One of the simplest ways to solve the wave equations (4.31) (or (4.37)) is the Born approximation. Assume that the right-hand side of (4.31) is very small. Then we can apply the perturbation theory to solve the equations. This method is called the *Born approximation*. It does not always provide an accurate value of the cross-section. (Its validity is discussed later in this section.) But the method is useful in the following points. First the Born cross-section is very easy to calculate. Once the interaction potential is given analytically, it is only needed to evaluate integrals. It is not needed to solve differential equations. When neither experimental nor theoretical cross-sections are available, the Born approximation is sometimes used to estimate the magnitude of the relevant cross-section. The simplicity of the calculation means the easiness of the understanding of the physics involved. The Born cross-section is directly proportional to the interaction potential squared. Hence it is easy to relate the result to the cause.

Now a general formula in the Born approximation is derived for an electron scattering from a diatomic molecule. (Polyatomic molecules can be similarly treated. See Chap. 5.) Furthermore only the transitions among rotational and vibrational states of the molecule are considered. It is straightforward to extend the method to the excitation of electronic states. For simplicity of presentation, the system of atomic units (a.u.) is used in the present section. The definition of the units is given in Appendix C.

When we ignore the right-hand side of (4.37), we have a zeroth-order solution in the form

$$F^{(0)}(\nu) = \delta_{\nu 0} \exp(\mathrm{i}\boldsymbol{k}_\nu \cdot \boldsymbol{r}), \tag{4.52}$$

where $\nu = 0$ means the initial channel. Insert this into the general form of the scattering amplitude (4.39) and the first-order solution in the Born approximation is obtained as

$$f_{0\to\nu}^{\mathrm{Born}} = -\frac{1}{2\pi} \int \mathrm{d}\boldsymbol{r} \, \exp(\mathrm{i}\boldsymbol{K}_{0\nu} \cdot \boldsymbol{r}) \, \langle \nu | V | 0 \rangle, \tag{4.53}$$

where $\boldsymbol{K}_{0\nu} = \boldsymbol{k}_0 - \boldsymbol{k}_\nu$ and

$$\langle \nu | V | 0 \rangle = \int \mathrm{d}\boldsymbol{R} \, \{\chi_v \, Y_{JM}\}^* \, V \, \{\chi_{v_0} \, Y_{J_0 M_0}\}. \tag{4.54}$$

From (4.53), we obtain the differential cross-section as

$$q^{\mathrm{Born}}(0 \to \nu) = \frac{1}{4\pi^2} \frac{k_\nu}{k_0} \left| \int \mathrm{d}\boldsymbol{r} \, \exp(\mathrm{i}\boldsymbol{K}_{0\nu} \cdot \boldsymbol{r}) \, \langle \nu | V | 0 \rangle \right|^2 . \tag{4.55}$$

In Chap. 5, we apply this formula to the long-range interaction, i.e., we take the form (see (4.25) and (4.28))

$$V = V^{\mathrm{L}} = -\sum_\lambda \frac{M_\lambda(R)}{r^{\lambda+1}} P_\lambda(\cos \hat{\boldsymbol{r}} \cdot \hat{\boldsymbol{R}}). \tag{4.56}$$

Here M_λ is the electric multipole moment of the target molecule. The matrix element of the interaction potential can be evaluated from

$$\langle \nu | V | 0 \rangle = \sum_\lambda \frac{-1}{r^{\lambda+1}} \langle v | M_\lambda | v_0 \rangle \, \langle JM | P_\lambda | J_0 M_0 \rangle, \tag{4.57}$$

with

$$\langle v | M_\lambda | v_0 \rangle = \int \mathrm{d}R \, \chi_v^* \, M_\lambda(R) \chi_{v_0}, \tag{4.58}$$

and

$$\langle JM | P_\lambda | J_0 M_0 \rangle = \int \mathrm{d}\hat{\boldsymbol{R}} \, Y_{JM}^* \, P_\lambda(\cos \hat{\boldsymbol{r}} \cdot \hat{\boldsymbol{R}}) \, Y_{J_0 M_0}. \tag{4.59}$$

Detailed formulas for the rotational and vibrational transitions are given in the respective sections (i.e., the rotational cross-section in Sect. 5.4 and the vibrational one in Sect. 5.5).

Finally we summarize the validity of the Born method. In principle the Born approximation can be employed whenever the right-hand side of (4.31) is very small compared with other terms on the left-hand side of the equation. This condition is satisfied in the following cases:

(1) *A high-energy collision*
When the collision energy (i.e., k^2 on the left-hand side of (4.31)) is very large compared with the interaction potential, the Born method gives a good result. Although depending on the process, the Born approximation can give a reliable result at the collision energy of 1,000 eV or higher.

(2) *A distant collision*
When the colliding electron is located far from the target, the interaction is weak so that the perturbation theory can be used. In other words, the Born approximation can be applied to the collision process where the long-range interaction dominates. As is shown in Sect. 4.2, an electrostatic long-range interaction (through the electric multipoles) exists between an electron and a molecule. It dominates in the low-energy collision. (When the incoming electron is very slow, it is difficult to come close to the target.) The Born method, therefore, is expected to give a good result in such a low-energy electron–molecule collision.

5

Electron Collisions with Molecules

5.1 Collision Processes

When an electron collides with a molecule, the following processes take place. Here, for simplicity of illustration, the target molecule is assumed to be diatomic. The attached symbols ($Q_{\rm elas}$, etc.) are used to represent the relevant cross-sections in this chapter:

(1) Elastic scattering ($Q_{\rm elas}$)

$$\mathrm{e} + \mathrm{AB} \rightarrow \mathrm{e} + \mathrm{AB}.$$

(2) Rotational transition ($Q_{\rm rot}$)

$$\mathrm{e} + \mathrm{AB}(J) \rightarrow \mathrm{e} + \mathrm{AB}(J'),$$

where J (J') is the rotational quantum number of the initial (final) state of the molecule.

(3) Vibrational transition ($Q_{\rm vib}$)

$$\mathrm{e} + \mathrm{AB}(v) \rightarrow \mathrm{e} + \mathrm{AB}(v'),$$

where v (v') is the vibrational quantum number of the initial (final) state of the molecule.

(4) Excitation of electronic state ($Q_{\rm exc}$)

$$\mathrm{e} + \mathrm{AB} \rightarrow \mathrm{e} + \mathrm{AB}^{*}.$$

(5) Dissociation ($Q_{\rm dis}$)

$$\mathrm{e} + \mathrm{AB} \rightarrow \mathrm{e} + \mathrm{A} + \mathrm{B}^{(*)}.$$

(6) Ionization ($Q_{\rm ion}$)

$$\mathrm{e} + \mathrm{AB} \rightarrow 2\mathrm{e} + \mathrm{AB}^{+(*)}$$

or

$$\mathrm{e} + \mathrm{AB} \rightarrow 2\mathrm{e} + \mathrm{A} + \mathrm{B}^{+(*)}.$$

(7) Electron attachment (Q_{att})

$$\mathrm{e} + \mathrm{AB} \rightarrow \mathrm{A} + \mathrm{B}^{-}$$

or

$$\mathrm{e} + \mathrm{AB} + \mathrm{M} \rightarrow \mathrm{AB}^{-} + \mathrm{M}.$$

Here we denote a molecule (or an atom) in its electronically excited state by AB* (or B*). The asterisk in brackets (*) means that the particle is either in its ground or in its excited state.

When an electron collides with a polyatomic molecule, a similar, but more complicated, process occurs. For instance, a dissociation of a triatomic molecule ABC can be in the form

$$\begin{aligned} \mathrm{e} + \mathrm{ABC} \rightarrow\ & \mathrm{e} + \mathrm{A} + \mathrm{BC} \\ & \mathrm{e} + \mathrm{AB} + \mathrm{C} \\ & \mathrm{e} + \mathrm{AC} + \mathrm{B} \\ & \mathrm{e} + \mathrm{A} + \mathrm{B} + \mathrm{C}. \end{aligned}$$

Each product of the dissociation may be in its excited state.

In the present chapter, the above seven processes are described separately in each section. Furthermore, four sections are added for the following related subjects.

(8) Momentum–transfer cross-section (Q_{m})
This quantity gives the degree of momentum–transfer during the collision. It plays a fundamental role in determining electron transport in plasmas.

(9) Emission cross-section (Q_{emis})
In some collision processes, the final product (molecule, atom, or ion) emits radiation immediately after the collision. This emission can be easily detected. The cross-section for the emission of particular radiation is called an *emission cross-section*. This cross-section is not necessarily the same as the cross-section for the excitation of a specific state (i.e., the process (4)). There may be a cascade contribution to the emission. The relation between Q_{emis} and Q_{exc} is given in the relevant section (Sect. 5.9).

(10) Total scattering cross-section (Q_{tot})
This is defined as a sum of all the cross-sections for the individual processes (1)–(7). This cross-section can be measured independently from any individual processes.

(11) Stopping cross-section (S)
This indicates the amount of energy transfer during the collision. Or more precisely it shows how much the incoming electron loses its energy.

Most of the experimental studies have been made at room temperature and concerned with the target molecules in the ground state. In the following

sections, therefore, we implicitly assume the target molecules in the ground state, unless otherwise stated. In a real plasma, excited molecules may be present and the information is needed for the electron collisions with those excited molecules. Section 5.13 is devoted to the information.

In the following sections, typical examples of the cross-sections are graphically shown for a number of simple molecules. There are many papers reporting cross-sections for electron collisions with molecules. It is not easy to select one for presentation. As far as possible, the cross-sections are selected from those recommended or suggested in the reviews or data compilations published recently. A list of the data reviews and compilations is given in Appendix E. It should be noted, however, that the data shown here are not necessarily regarded as the best values available at present. Because of constant development of experimental techniques and theoretical methods, the quality of the cross-sections is continuously improved. When one wants to have the best value of some cross-section, a resurvey of the original, particularly more recent, literature should be strongly recommended.

5.2 Elastic Scattering

In the elastic scattering, the internal state of the molecule does not change during the collision. In other words, the kinetic energy of the relative motion is conserved. In the laboratory frame, the kinetic energy of each partner of the collision system can be changed even in elastic collisions. Consider the laboratory frame where the target molecule is fixed in space before collision. According to the theory in Sect. 3.4, the change in the kinetic energy of electron ΔE_{e} is given by (see (3.69))

$$\Delta E_{\mathrm{e}} = E_{\mathrm{e}} - E'_{\mathrm{e}} = E'_{\mathrm{mol}} + W, \tag{5.1}$$

where E_{e} (E'_{e}) is the energy of the electron before (after) the collision, E'_{mol} is the energy of the target molecule after the collision (i.e., the recoil energy), and W is the gain of the internal energy of the molecule. In the elastic collision, $W = 0$, but, due to the recoil of the target, ΔE_{e} is not equal to zero. With use of the fact of small mass ratio of the electron and the molecule, we have (see (3.76))

$$(\Delta E)_{\mathrm{elas}} = 2\,\frac{m_{\mathrm{e}}}{M}\,E_{\mathrm{e}}\,(1 - \cos\theta\,). \tag{5.2}$$

Here m_{e} and M are the masses of electron and the molecule, respectively, and θ is the scattering angle. It should be noted that, in the electron–molecule collision, the scattering angle in the laboratory frame is the same as that in the CM frame. Equation (5.2) has been derived to the first order of the mass ratio m_{e}/M. For most of molecules, the ratio has a value of the order of 10^{-4}. Because of a finite energy resolution, the energy loss $(\Delta E)_{\mathrm{elas}}$ is regarded to be zero in any measurement of electron energy loss spectra (EELS).

The transition energy of rotational state of a molecule $(\Delta E)_{\rm rot}$ is normally of the order of meV or less (see Appendix B). It is much smaller than the experimental energy resolution, so that it is difficult to discriminate the rotational transition from the elastic scattering in the electron energy loss measurement. Thus the elastic cross-section determined with an EELS measurement includes the cross-section for rotational transitions. The measured value of the elastic cross-section is therefore expressed as

$$Q_{\rm elas}^{\rm exp} = \sum_J Q_{\rm rot}(J_0 \to J), \tag{5.3}$$

where the initial and final rotational states of the molecule are denoted by J_0 and J, respectively. As shown in Sect. 4.1, molecules are populated over a wide range of rotational states. The distribution of rotational states is specified by the gas temperature $T_{\rm gas}$. When we consider this, the experimental value of the elastic cross-section should be regarded as

$$Q_{\rm elas}^{\rm exp} = \sum_{J_0} F_{J_0}(T_{\rm gas}) \sum_J Q_{\rm rot}(J_0 \to J), \tag{5.4}$$

where F_{J_0} is the fraction of the molecule in the rotational state J_0. We often call this cross-section a "vibrationally" elastic cross-section. In the present section, $Q_{\rm elas}$ means $Q_{\rm elas}^{\rm exp}$, unless otherwise noted. In the same manner, the pure elastic cross-section is given by

$$\langle Q_{\rm elas} \rangle = \sum_{J_0} F_{J_0}(T_{\rm gas})\, Q_{\rm rot}(J_0 \to J_0). \tag{5.5}$$

Here the angle brackets indicate the average over the rotational states. This is sometime called "rotationally" elastic cross-section. Examples of this are presented in Sect. 5.4.

Figure 5.1 shows examples of elastic (or more precisely, vibrationally elastic) cross-sections for typical diatomic molecules (H_2, N_2, O_2, CO, and NO). Examples for polyatomic molecules (CO_2, CH_4, and H_2O) are shown in Fig. 5.2. All of them but those for H_2O are the cross-sections recommended by Buckman et al. [19] in their data compilation. For H_2O, improved values are taken from the review by Itikawa and Mason [81]. Here the figures show the cross-sections at the energies above 1 eV. All the recommended values have been determined on the basis of the data obtained with beam-type experiments (i.e., the EELS measurement).

Many of the $Q_{\rm elas}$ shown in the figures have a clear peak. Cross-sections for N_2 and CO have a large peak at around 2–3 eV. Cross-section for CH_4 has a peak at 8 eV and CO_2 has a small one at 3 eV. Cross-section for H_2 shows a broad peak at 3 eV. All of these peaks are attributed to a shape resonance. A molecule forms an electrostatic potential for an incoming electron. In some cases, the potential may have a bound state with positive binding energy. In other words, an electron having a specific energy (i.e., the energy matching

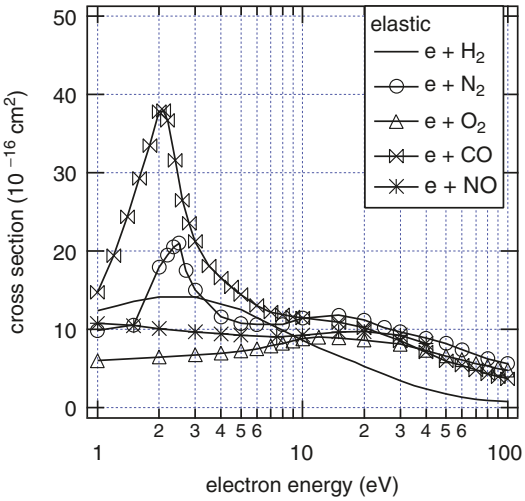

Fig. 5.1. Elastic scattering cross-sections for H_2, N_2, O_2, CO, and NO. For N_2, the fine structure in the resonance peak is smoothed out

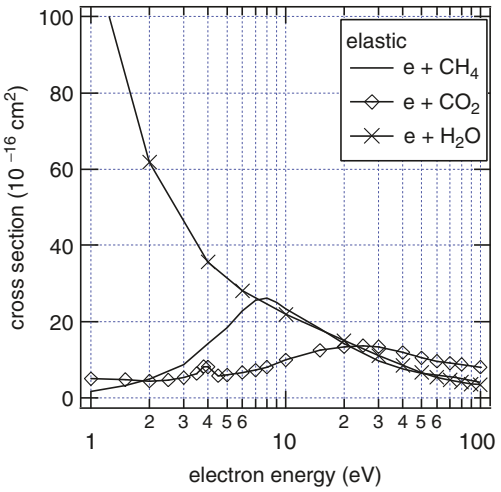

Fig. 5.2. Elastic scattering cross-sections for H_2O, CO_2, and CH_4

to the binding energy) can be captured by the molecule and forms a negative ion

$$\mathrm{e} + \mathrm{AB} \rightarrow (\mathrm{AB}^-)^{**}.$$

Here the right-hand side indicates such a negative ion. This ion is in an unstable excited state (indicated by the double asterisk) and eventually decays into an electron and the molecule

$$(\mathrm{AB}^-)^{**} \rightarrow \mathrm{AB}^{(*)} + \mathrm{e}.$$

The resulting molecule AB may be either in its ground state (i.e., elastic scattering) or in excited one. This is called a *shape resonance* (for details, see [143]).

In many cases, the shape resonance enhances the respective cross-section (see Figs. 5.1 and 5.2). Moreover, the cross-sections for N_2 have a complicated structure as a function of electron energy. That structure arises from a subtle interaction between electronic and nuclear motions. It is discussed in Sect. 5.5 in relation to vibrational excitations. The $Q_{\rm elas}$ for N_2 in Fig. 5.1 are those with the structure smoothed out. As is understood from the above statement, the shape resonance can appear also in the cross-sections for the excitation of rotational and vibrational states. Those are discussed in Sects. 5.4 and 5.5, respectively.

Another peculiar feature is seen in the $Q_{\rm elas}$ for H_2O (Fig. 5.2). The cross-section increases prominently with decreasing energy. This is an effect of rotational transition. Due to its large electric dipole moment, H_2O has a large rotational cross-section (see Sect. 5.4). CO and NO are also polar molecules, but their dipole moments are small (see Appendix B). They also show an increase of $Q_{\rm elas}$ with decreasing energy, but only at very low energies of electrons (not shown in the figure). In the electron collisions with CO and NO at the energy of 1 eV or above, other (shorter-ranged) interactions dominate over the (long-ranged) electron–dipole interaction.

Since the elastic scattering has no threshold, $Q_{\rm elas}$ has a considerable magnitude even at a very low energy. As the electron energy decreases below 1 eV, it becomes very difficult to do an EELS measurement. Some special technique is required to obtain reliable experimental data on $Q_{\rm elas}$ at $E_{\rm e} < 1\,{\rm eV}$. Two of them are the following:

1. *Total scattering cross-section*
   When $E_{\rm e}$ is below the threshold of vibrational excitation, the total scattering cross-section, $Q_{\rm tot}$, is given by (see Sect. 5.11)

$$Q_{\rm tot} = Q_{\rm elas} + Q_{\rm rot}. \tag{5.6}$$

   The right-hand side of (5.6) is equal to the definition of $Q_{\rm elas}^{\rm exp}$ (i.e., (5.3)). As is described in Sect. 5.11, $Q_{\rm tot}$ can be measured directly with a beam attenuation method. The method is rather simple and relatively easy to extend to lower energy. For example, Ferch et al. [42] measured $Q_{\rm tot}$ for H_2 at the energies down to 0.02 eV. Considering the data, Buckman et al. [19] extended their recommended value of $Q_{\rm elas}$ for H_2 to the lower energy region, as is shown in Fig. 5.3. (In this and the following two figures, momentum–transfer cross-sections are also shown for a comparison. They are explained in Sect. 5.3.)
2. *Modified effective range theory*
   In the case of spherical potential, cross-sections are calculated with the scattering phase shift (see Sect. 3.3). For a short-range potential, the low-energy limit of the phase shift is well known. The energy dependence of

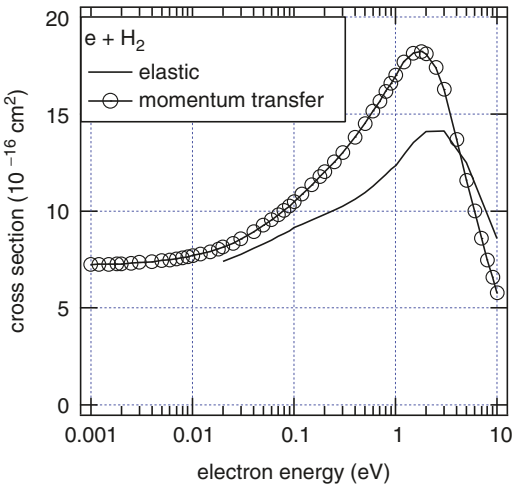

Fig. 5.3. Elastic scattering ($Q_{\rm elas}$) and momentum–transfer ($Q_{\rm m}$) cross-sections for H_2. The $Q_{\rm elas}$ above 1 eV is the same as in Fig. 5.1

the phase shift at low energies is obtained with the use of the effective range theory (see, for example, [117]). O'Malley et al. [124] extended the theory to the scattering of a charged particle by a polarizable target. It is called the modified effective range theory (MERT). According to the theory, the phase shift at a small electron energy can be analytically expressed as a function of energy (or more precisely, wave number). For the s- and p-wave phase shifts, we have

$$\tan\eta_0 = -A\,k \;-\; \frac{\pi}{3a_0}\,\alpha k^2 \;-\; \frac{4}{3a_0}\,\alpha A k^3\,\ln(ka_0) + O(k^3), \tag{5.7}$$

$$\tan\eta_1 = \frac{\pi}{15a_0}\,\alpha k^2 \;-\; A_1\,k^3 + O(k^4). \tag{5.8}$$

Here k is the wave number of the electron, α is the polarizability of the molecule, and a_0 is the Bohr radius. The coefficients A (called a *scattering length*) and A_1 are numerical constants. The phase shifts of higher partial waves are calculated by using the perturbation theory.

Mann and Linder [106] measured elastic cross-sections for CF_4 at the energies down to 0.3 eV, by using a crossed-beam EELS experiment. Assuming a spherical interaction potential, they derived phase shifts from their experiment. They fitted the experimental phase shifts to the formulas (5.7) and (5.8) to obtain the unknown coefficients in the formulas (i.e., A and A_1, and higher-order terms, if necessary). With the use of the resulting analytical expression, they extended their phase shifts to the energies below 0.3 eV. Then they obtained the elastic cross-sections in the lower energy region. As is easily understood, Mann and Linder ignored rotational transitions in their derivation of phase shifts. If we consider the symmetry of the molecule, it is not

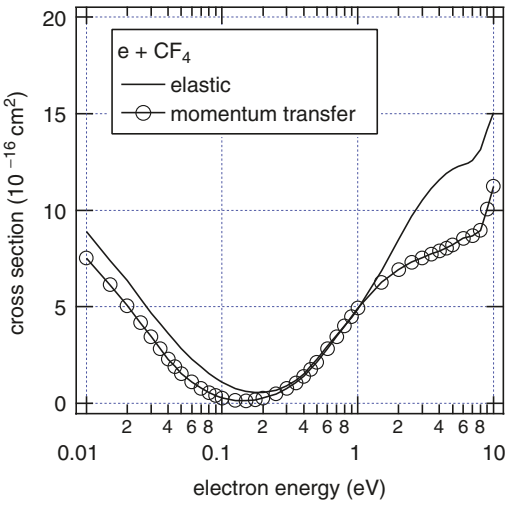

Fig. 5.4. Elastic scattering and momentum–transfer cross-sections for CF_4

likely to have a significant rotational transition in CF_4. Figure 5.4 shows the $Q_{\rm elas}$ for CF_4 recommended by Christophorou et al. [24]. In the energy region below 0.5 eV, they totally relied on the result of Mann and Linder.

In the electron collisions with heavy rare gas atoms (i.e., Ar, Kr, and Xe), the elastic cross-section has a minimum at a certain energy below 1 eV. This is known as the *Ramsauer minimum*. Retain the first two terms on the right-hand side of (5.7). If we have a negative scattering length (A) and a not too small polarizability, the s-wave phase shift can become zero at a finite value of k. This results in the Ramsauer minimum [125]. The Ramsauer minimum is also observed in the electron–molecule collisions. Figure 5.5 shows the $Q_{\rm elas}$ for CH_4 recommended by Buckman et al. [19]. This cross-section shows a minimum at around 0.6 eV, which is interpreted as the Ramsauer effect. Buckman et al. determined their cross-section in the low-energy region mainly from the total scattering cross-section measured by Ferch et al. [43]. Gianturco et al. [53] made a detailed theoretical study of the electron scattering from CH_4. They concluded that the polarization interaction is the main reason for the cross-section minimum. The minimum of $Q_{\rm elas}$ for CF_4 (in Fig. 5.4) is also suggested to be the Ramsauer effect (see [74]).

5.3 Momentum–Transfer

The momentum–transfer cross-section for elastic scattering is defined by

$$Q_{\rm m} = 2\pi \int_0^{\pi} (1 - \cos\theta)\, q_{\rm elas}(\theta)\, \sin\theta \, {\rm d}\theta, \tag{5.9}$$

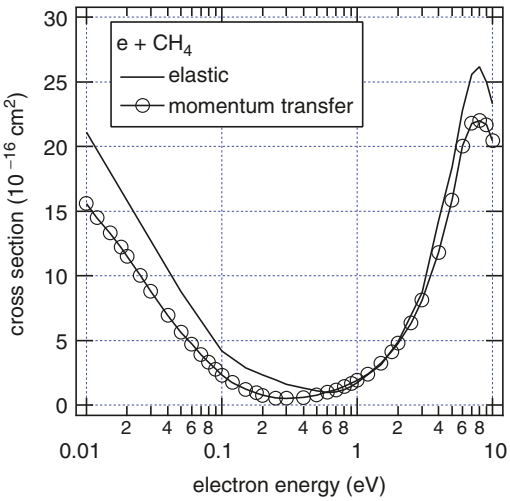

Fig. 5.5. Elastic scattering ($Q_{\rm elas}$) and momentum–transfer ($Q_{\rm m}$) cross-sections for CH_4. The $Q_{\rm elas}$ above 1 eV is the same as in Fig. 5.2

where $q_{\rm elas}(\theta)$ is the differential cross-section for the elastic scattering. In the present section, we consider only the elastic momentum–transfer cross-section. The momentum–transfer in inelastic processes is discussed at the end of this section.

In a plasma, electron transport is primarily governed by $Q_{\rm m}$. Consider, for instance, electric conduction. Under the application of electric field, electrons move along the direction of the field. Upon a collision with a molecule, the electron starts to move away from the field direction. The deviation of the electron trajectory from the field direction is determined by the momentum–transfer during the collision. Thus $Q_{\rm m}$ comes to enter into the formula of electric conductivity. If $Q_{\rm m}$ is large, the deviation from the field direction is large and the electron motion less contributes to the conduction of electricity. In a simple theory (see, for example, [75]), the DC conductivity is given by

$$\sigma_{\rm DC} = \frac{N_{\rm e} e^2}{m_{\rm e} \nu_{\rm eff}}, \tag{5.10}$$

with

$$\nu_{\rm eff}^{-1} = \frac{8}{3\pi^{1/2} N} \left(\frac{m_{\rm e}}{2k_{\rm B} T_{\rm e}} \right)^{5/2} \int_0^\infty \frac{v^3}{Q_{\rm m}(v)} \exp\left(- \frac{m_{\rm e}\, v^2}{2k_{\rm B} T_{\rm e}} \right) {\rm d}v, \tag{5.11}$$

where $m_{\rm e}$, $T_{\rm e}$, and $N_{\rm e}$ are the electron mass, temperature, and density, respectively, $k_{\rm B}$ is the Boltzmann constant, and N is the number density of the gaseous particles. The quantity $\nu_{\rm eff}$ is an effective frequency of momentum

–transfer collisions. Another effective collision frequency has been introduced for AC conductivity, which is expressed in the form [75]

$$\sigma_{\mathrm{AC}} = \frac{N_{\mathrm{e}} e^2}{m_{\mathrm{e}}(\langle \nu_{\mathrm{eff}} \rangle + \mathrm{i}\omega)}, \tag{5.12}$$

with

$$\langle \nu_{\mathrm{eff}} \rangle = \frac{8\,N}{3\pi^{1/2}} \left(\frac{m_{\mathrm{e}}}{2k_{\mathrm{B}}T_{\mathrm{e}}} \right)^{5/2} \int_0^\infty v^5\, Q_{\mathrm{m}}(v)\, \exp\left(- \frac{m_{\mathrm{e}}\, v^2}{2k_{\mathrm{B}}T_{\mathrm{e}}} \right) \mathrm{d}v. \tag{5.13}$$

Here ω is the frequency of the AC field and (5.12) has been obtained for a high-frequency field (i.e., $\omega \gg \langle \nu_{\mathrm{eff}} \rangle$). More generally, propagation (reflection and attenuation) of radio wave in a plasma is controlled by Q_{m} (see [163]). The formulas (5.10)–(5.13) have been derived for a Maxwellian distribution of electron velocity. (Conventionally the electric conductivity is defined for a small deviation from the equilibrium.) Other transport properties of a plasma (e.g., thermal conductivity) also depends on the momentum–transfer cross-section, but the form of dependence on Q_{m} is different for different properties. It should be noted that different definitions of the effective collision frequency of momentum–transfer are used in different literature. Whatever definition is used, however, we need the detailed knowledge of the momentum–transfer cross-section.

There are two different ways of experimental determination of Q_{m}: beam method and swarm experiment. In the beam method, the differential cross-section for the elastic scattering, q_{elas}, is measured first. Then the differential cross-section is inserted into (5.9) to obtain Q_{m}. As is described in Sect. 5.2, the experimental elastic cross-section includes an effect of rotational transition. Another problem inherent in the beam method is the uncertainty of the cross-section for the backward scattering (i.e., the scattering at the angles near 180°). It is clear from the definition (5.9) that the backward scattering contributes much to the integral. In a standard beam method, the backward scattering cannot be measured because of the geometrical constraints of the apparatus. The measured values of the differential cross-section have to be extrapolated toward the backward angles. This introduces an uncertainty in the resulting q_{elas}, which affects much the reliability of the resulting Q_{m}. For the same reason, the differential cross-section for the forward directions (near $\theta = 0°$) also cannot be measured. (At $\theta = 0°$, the elastically scattered electron beam cannot be separated from the unscattered incident beam, so that the measurement of q_{elas} at $\theta = 0°$ is intrinsically impossible.) From the definition (5.9), however, the uncertainty in the forward direction has a much less effect on the determination of Q_{m}.

In principle, a swarm technique is suitable for the experimental determination of Q_{m}. If no inelastic collision occurs, the Boltzmann equation depends solely on the quantity Q_{m}. Therefore, we can reliably derive Q_{m} from a swarm experiment, as far as we can assume less importance of any inelastic processes.

In the low-energy region (say, $< 1\,\mathrm{eV}$), the most significant inelastic process is the rotational transition. Effects of rotation can be separated out in the swarm analysis, though approximately. For this reason, the swarm method has been applied to the determination of Q_m for a number of molecules.

Figure 5.6 shows the Q_m for several diatomic molecules (N_2, O_2, and CO). Examples of Q_m for polyatomic molecules (H_2O and CO_2) are given in Fig. 5.7. In Sect. 5.2 Q_m is compared with Q_elas in the low-energy region (for

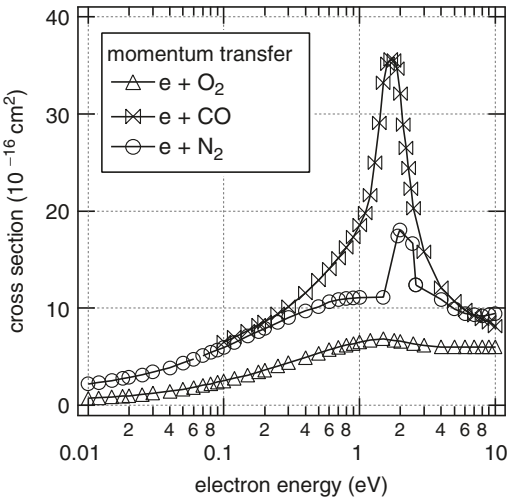

Fig. 5.6. Momentum–transfer cross-sections for N_2, O_2, and CO. For N_2, the fine structure in the resonance peak is smoothed out

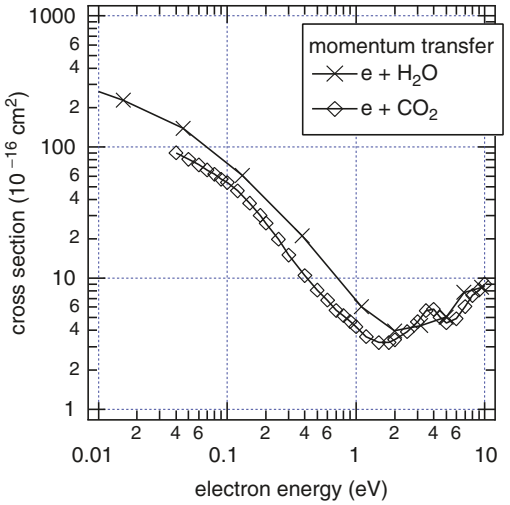

Fig. 5.7. Momentum–transfer cross-sections for H_2O and CO_2

H_2 in Fig. 5.3, CF_4 in Fig. 5.4, and CH_4 in Fig. 5.5). The Q_m shown for H_2, O_2, CO, CO_2, and CH_4 are those recommended by Elford et al. [34] in their compilation. The cross-sections for N_2, H_2O, and CF_4 are taken, respectively, from [83], [81], and [24]. All the recommendations are based on a combination of the results of the beam and swarm methods. Elford et al. [34] give a brief, but useful, review on the momentum–transfer cross-section. As in the case of Q_{elas}, some molecules show a peak of shape resonance. In particular, the cross-sections of N_2 have a peak with complicated structure. The Q_m shown in Fig. 5.6 are the cross-sections with the structure smoothed out.

Here it is worth noting the relation between Q_m and Q_{elas}. By definition, these two are different quantities. Depending on the angular distribution of elastic scattering, we have the following relations between them:

$$Q_m = Q_{elas} \quad \text{for isotropic scattering,}$$

$$Q_m < Q_{elas} \quad \text{for the dominance of small-angle scattering,}$$

$$Q_m > Q_{elas} \quad \text{for the dominance of large-angle scattering.}$$

In Figs. 5.3–5.5, we compare Q_m with Q_{elas} for three different molecules. Different molecules have different relations between Q_m and Q_{elas}.

Finally we discuss the momentum–transfer in inelastic collisions. Considering the relation $m_e/M \ll 1$, the velocity change of the incident electron is given by

$$(\Delta \boldsymbol{v})_e = \left(1 - \frac{v'}{v}\cos\theta\right)\boldsymbol{v}. \tag{5.14}$$

Here v and v' are the electron speeds before and after the collision. Then the momentum–transfer cross-section for inelastic processes is obtained by

$$Q_m^{inel} = 2\pi \int_0^\pi \left(1 - \frac{v'}{v}\cos\theta\right) q(\theta)\,\sin\theta\,\mathrm{d}\theta, \tag{5.15}$$

where $q(\theta)$ is the differential cross-section for the respective inelastic process. In the analysis of electron transport in a plasma, momentum–transfer in inelastic processes is treated in several different ways, depending on how to solve the Boltzmann equation:

Case A. Contributions of inelastic processes are completely neglected for momentum–transfer. This may cause a significant error at least for a high reduced electric field, $\mathcal{E}/N$.

Case B. Inelastic cross-sections are assumed to be much less than the elastic one. Furthermore, the inelastic scattering is assumed to be isotropic. Instead of (5.15), the integral cross-section

$$Q = 2\pi \int_0^\pi q(\theta)\,\sin\theta\,\mathrm{d}\theta \tag{5.16}$$

is used for momentum–transfer in inelastic scattering.

Case C. When $\mathcal{E}/N$ increases, contributions of inelastic processes become large and the velocity distribution of electrons is getting highly anisotropic. In such a case, angular distributions of scattered electrons, both for elastic and inelastic processes, must be taken into account more explicitly (see, for example, [132]).

Usually the Boltzmann equation is solved under the assumption that elastic collisions dominate over inelastic ones. In this assumption, the momentum–transfer in the inelastic process is ignored (Case A). When $\mathcal{E}/N$ increases, inelastic processes have more importance. Then the effect is considered approximately (Case B, see [59]). In the case of high $\mathcal{E}/N$, the momentum change in the collision cannot be taken into account by the quantity $Q_{\mathrm{m}}^{\mathrm{inel}}$ (neither (5.15) nor (5.16)). More sophisticated treatment of the angular distribution is necessary (see [132]).

5.4 Rotational Transition

Itikawa and Mason [82] published a comprehensive review on the electron-impact rotational transition of molecules. They surveyed theoretical and experimental studies on the subject through the end of 2004. The present section is mostly based on this review article.

Level spacings of the rotational states of a molecule are very small (except for hydrogen). It is difficult to experimentally resolve individual rotational states. As is stated in Sect. 4.1, molecules are distributed over a wide range of rotational states, even at room temperature. This leads to an additional difficulty in measuring state-to-state cross-sections for rotational transition.

Rotational cross-sections are not necessarily small (see the following figures in this section). Since the charge distribution in a molecule is anisotropic, the incoming electron exerts a torque on any molecule to rotate. When the molecule has a permanent electric dipole moment, the electron–dipole interaction is the primary cause of the rotational transition (see Sect. 4.2). This interaction has a long range so that the electron collision at low energies can have a large cross-section. This is shown later in this section. The smallness of the transition energy is also favorable to the collisions at low energies.

As is described in Sect. 5.2, the elastic peak in the measured electron energy loss spectra includes a contribution of rotational transitions. That is, the intensity of the elastic peak is proportional to the cross-section in such a way as

$$I_{\mathrm{elas}} \propto q_{\mathrm{elas}}^{\mathrm{exp}} = \sum_{J_0} F_{J_0} \sum_{J'} q_{\mathrm{rot}}(J_0 \rightarrow J'). \tag{5.17}$$

Here F_{J_0} is the fraction of the molecule in the rotational state J_0 and $q_{\mathrm{rot}}(J_0 \rightarrow J')$ is the differential cross-section for the rotational transition $J_0 \rightarrow J'$. If the incident energy is sufficiently large compared with the rotational transition energies, we can apply the adiabatic approximation to

the rotational motion (see Sect. 4.3). In this approximation (so-called the adiabatic-nuclear rotation (ANR) approximation), we can express a rotational cross-section for any transition $J_0 \to J'$ as a linear combination of the cross-sections for the transitions from the ground state (i.e., $0 \to J$) in the form (see [82])

$$q_{\rm rot}^{\rm ANR}(J_0 \to J') = \sum_J A(J_0, J' : J)\, q_{\rm rot}^{\rm ANR}(0 \to J). \tag{5.18}$$

The coefficient A depends only on the rotational quantum numbers and the associated energies, and not on the details of the electron–molecule interaction. Using this relation, we have

$$I_{\rm elas} \propto \sum_J a_J\, q_{\rm rot}^{\rm ANR}(0 \to J), \tag{5.19}$$

with

$$a_J = \sum_{J_0} \sum_{J'} F_{J_0}\, A(J_0, J' : J). \tag{5.20}$$

If the experimental energy resolution is sufficiently high, it is possible to deconvolute the elastic peak (i.e., $I_{\rm elas}$) to derive individual terms, $q_{\rm rot}^{\rm ANR}(0 \to J)$. Once we obtain the cross-section for the transition $0 \to J$, it is easy to evaluate rotational cross-section for any transition with the use of (5.18) within the ANR approximation. With this procedure, Ehrhardt and his group succeeded to measure the differential cross-section for the rotational transitions $0 \to J$ in the molecules N_2, CO, Cl_2, HCl, HF, and CH_4 [57, 118, 136]. (They reported, however, no integral cross-sections.) They made their experiment at the energies above 0.5 eV.

When an electron energy is very low (or more precisely below the threshold of any vibrational excitation), only possible inelastic process is rotational transition. The swarm technique, therefore, is expected to be suitable to derive rotational cross-sections in the low-energy region. Since molecules are populated over a number of rotational states, however, several different rotational transitions can occur. Furthermore a possible interference between elastic scattering and rotational transition may make it difficult to separately determine the cross-sections for the two processes. Despite these problems, a swarm method has been employed to obtain rotational cross-sections at low energies.

To see the general feature of the rotational cross-section, two examples of the molecule (H_2 and N_2) are selected. Figure 5.8 shows the cross-section for the rotational transition $J = 0 \to 2$ of H_2, recommended by England et al. [38]. (Due to the molecular symmetry, only the transition with $\Delta J =$ even occurs in a homonuclear diatomic molecule.) England et al. carried out a swarm experiment of parahydrogen (i.e., hydrogen molecules with even J) at 77 K. Since the rotational level spacing of H_2 is exceptionally large, almost all the molecules in this case are populated in the rotationally ground (i.e., $J = 0$) state. Thus they could derive $Q_{\rm rot}(J = 0 \to 2)$ accurately, provided that the electron energy is below the vibrational threshold (i.e., 0.5 eV).

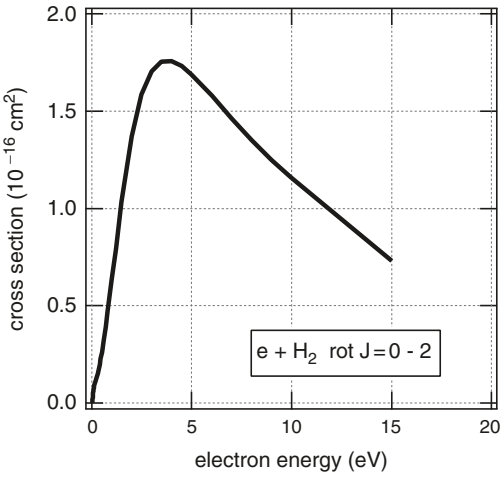

Fig. 5.8. Rotational cross-section $Q_{\rm rot}(J = 0 \rightarrow 2)$ for H_2

England et al. found that their swarm result is in good agreement with the theoretical cross-section obtained by Morrison et al. [115], which is thought to be the most elaborate calculation so far performed (see [82]). Then England et al. determined their recommended cross-section by smoothly merging their swarm data for $E < 0.5\,\text{eV}$ to the theoretical values in the higher energy region. The resulting cross-sections are those shown in Fig. 5.8. England et al. also reported cross-sections for the transitions $1 \rightarrow 3$, $2 \rightarrow 4$, and $3 \rightarrow 5$.

Robertson et al. [138] made an elaborate swarm experiment with N_2. They measured the electron transport coefficients in a gas mixture of N_2 and Ne at 77 K. In this case, 12 rotational states of N_2 had a significant population. Among them, only the transitions with $\Delta J = \pm 2$ were assumed to occur. They chose the fraction of Ne so much that the elastic momentum–transfer of electrons was determined mainly by the collision with Ne, for which an accurate cross-section was known at that time. Thus, when Robertson et al. solved the Boltzmann equation, only unknown quantities were rotational cross-sections of N_2. In this way, they could obtain the $Q_{\rm rot}(J = 0 \rightarrow 2)$ for N_2 with less ambiguity at the collision energies below 0.2 eV. The result is shown in Fig. 5.9.

In the higher energy region, no experimental data are available for $Q_{\rm rot}$ of N_2. To see the general trend of the cross-section, we show in Fig. 5.9 the result of a calculation by Kutz and Meyer [95]. They did a comprehensive calculation and reported the rotational cross-section of N_2 for the transitions $J = 0 \rightarrow 0, 2, 4, 6$ over a wide energy range (0.01–1,000 eV). Figure 5.9 shows their result for $J = 0 \rightarrow 0, 2, 4$. They found several specific features of $Q_{\rm rot}$ for N_2:

1. In the energy region above 1 eV, $Q_{\rm rot}(J = 0 \rightarrow 2)$ has a considerable magnitude (of the order of $10^{-16}\,\text{cm}^2$).

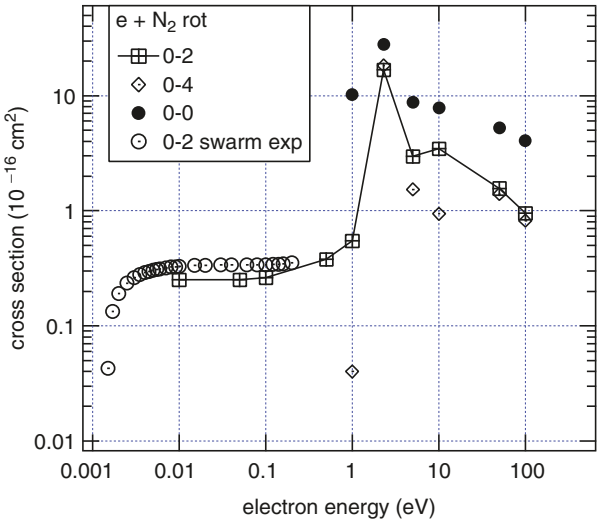

Fig. 5.9. Rotational cross-sections $Q_{\rm rot}(J = 0 \to J')$ for N_2. The result of swarm experiment for $J' = 2$ [138] and theoretical cross-sections for $J' = 0, 2, 4$ [95] are shown

2. The cross-section has a sharp peak at around 2.3 eV. This is due to the shape resonance described in Sect. 5.2.
3. At the resonance, $Q_{\rm rot}$ for higher-order transitions ($\Delta J > 2$) have a magnitude comparable to $Q_{\rm rot}(J = 0 \to 2)$. Below the resonance region, those cross-sections are much smaller than $Q_{\rm rot}(J = 0 \to 2)$, but above the region the difference is small.

In their review article [82], Itikawa and Mason made detailed discussions about $Q_{\rm rot}$ for HCl, H_2O, and CH_4, as well as for H_2 and N_2. There are very few experimental data available on $Q_{\rm rot}$, but a large number of theoretical calculations have been performed for the rotational transitions in those molecules. Figure 5.10 compares the theoretical cross-sections selected by Itikawa and Mason ($Q_{\rm rot}$ for H_2O from [40, 55], HCl from [130, 146], N_2 from [95], H_2 from [115], and CH_4 from [109]). For N_2, the values recommended by Brunger et al. [18] are also shown for comparison. Their recommendation is mainly based on the swarm result shown in Fig. 5.9. All the cross-sections are for the lowest rotational transition from the ground state. (Due to the molecular symmetry, the lowest transition for CH_4 is $J = 0 \to 3$.) For more details of each cross-section, see the review article by Itikawa and Mason [82]. It is seen from the figure that $Q_{\rm rot}$ for polar molecules (e.g., HCl and H_2O) have a peculiar feature. They increase enormously with decreasing energy. This is due to the electron interaction with the molecular dipole. As is stated in Sect. 4.2, the electron–dipole interaction is strongly anisotropic and of long range. Due to this interaction, even the electrons passing very far from the

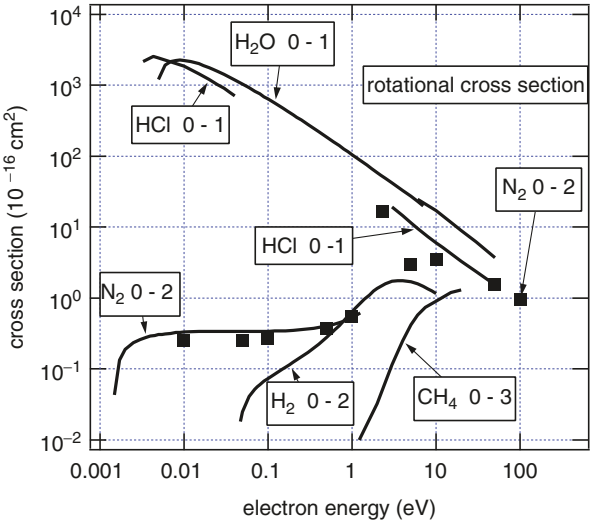

Fig. 5.10. Comparison of the rotational cross-sections for H_2, N_2, HCl, H_2O, and CH_4. Theoretical cross-sections for the lowest transition from the ground state are shown (see text). For N_2, the recommended values by Brunger et al. [18] (*solid line* for N_2) are also shown

target can induce rotational transition. As the electron energy decreases, the contribution of such a distant collision increases in the rotational transition. From the propensity rule of the electron–dipole interaction, transitions with $\Delta J = \pm 1$ dominates over others. (In the first-order perturbation theory, only the transition with $\Delta J = \pm 1$ can occur. See (5.22).) As is seen in Fig. 5.10, $Q_{\rm rot}(J = 0 \to 1)$ for polar molecules reach the value as much as $10^{-13}\,{\rm cm}^2$ at the electron energy of about 0.01 eV.

As is stated in Sect. 4.5, the Born approximation is expected to be well applied to the low-energy electron–molecule collision. Consider an electron scattering from a diatomic molecule. (Polyatomic molecules can be treated similarly. See [52].) Assuming an electron–multipole interaction, the Born cross-section for the rotational and vibrational transition is obtained from (4.55) with (4.57). (Note that all the Born cross-sections are expressed in atomic units. See Appendix C for atomic units.) With ignoring the vibrational transition, the Born cross-section becomes

$$q_{\rm rot}^{\rm Born}(J_0 \to J) = \frac{1}{4\pi^2}\,\frac{k_J}{k_0}\,\frac{1}{2J_0+1} \times \sum_{M_0}\sum_{M}\left|\int {\rm d}\boldsymbol{r}\,\exp({\rm i}\boldsymbol{K}_{0J}\cdot\boldsymbol{r})\sum_{\lambda}\frac{\langle M_\lambda\rangle}{r^{\lambda+1}}\,\langle JM|P_\lambda|J_0M_0\rangle\right|^2, \quad (5.21)$$

where k_0 and k_J are the electron wave numbers before and after the collision, and $\langle M_\lambda\rangle$ is the multipole moment of the molecule evaluated at its

equilibrium internuclear distance. Since, in experiments, target molecules are oriented randomly in space, an average has been taken in (5.21) over the azimuthal quantum numbers of the rotational state. From the matrix element $\langle JM|P_\lambda|J_0M_0\rangle$, each term of the interaction potential induces the rotational transition satisfying the relation

$$|J_0 - J| \le \lambda \le J_0 + J, \quad J_0 + J + \lambda = \text{even}. \tag{5.22}$$

For the first few terms, we have:

1. For $\lambda = 1$ (dipole interaction), $J = J_0 \pm 1$.
2. For $\lambda = 2$ (quadrupole interaction), $J = J_0 \pm 2$, J_0. (But $0 \to 0$ is not allowed.)

We consider the contribution of each term of interaction separately. For the dipole interaction, (5.21) gives the differential cross-section for the rotational transition $J_0 \to J_0 + 1$ in the form (see, for example, [154])

$$q_{\text{rot}}^{\text{Born,dipole}}(J_0 \to J_0 + 1; \theta) = \frac{4}{3}\frac{k_J}{k_0}\langle M_1\rangle^2 \frac{J_0 + 1}{2J_0 + 1}\frac{1}{K^2}, \tag{5.23}$$

where

$$K^2 = (K_{0J})^2 = k_0^2 + k_J^2 - 2k_0k_J\cos\theta. \tag{5.24}$$

The corresponding integral cross-section is (see [154])

$$Q_{\text{rot}}^{\text{Born,dipole}}(J_0 \to J_0 + 1) = \frac{8\pi}{3k_0^2}\langle M_1\rangle^2 \frac{J_0 + 1}{2J_0 + 1}\ln\left|\frac{k_0 + k_J}{k_0 - k_J}\right|. \tag{5.25}$$

Similarly we have

$$Q_{\text{rot}}^{\text{Born,dipole}}(J_0 \to J_0 - 1) = \frac{8\pi}{3k_0^2}\langle M_1\rangle^2 \frac{J_0}{2J_0 + 1}\ln\left|\frac{k_0 + k_J}{k_0 - k_J}\right|. \tag{5.26}$$

The long-range dipole interaction dominates in the electron collision with a polar molecule at low energies. The Born method must be satisfactorily applied to the calculation of the rotational cross-section of the polar molecule. Figure 5.11 compares the Born cross-section and the result of the best theoretical calculations shown in Fig. 5.10 for the $0 \to 1$ transition of HCl. (See Appendix C for the numerical calculation of the Born cross-section.) The Born cross-section well reproduces the theoretical one up to about 10 eV. There are no experimental data to be compared with them. A beam-type measurement, however, was made to obtain differential cross-sections (DCS) at the energies above 0.5 eV. Figure 5.12 shows the differential cross-section $q_{\text{rot}}(J = 0 \to 1)$ for HCl at 5 eV. The figure compares the results of the Born calculation, an elaborate calculation by Shimoi and Itikawa [146], and the experimental data obtained by Gote and Ehrhardt [57]. At the scattering angles smaller than 90°, the Born result agrees well with the experimental values. When the long-range dipole interaction dominates, collisions at a long

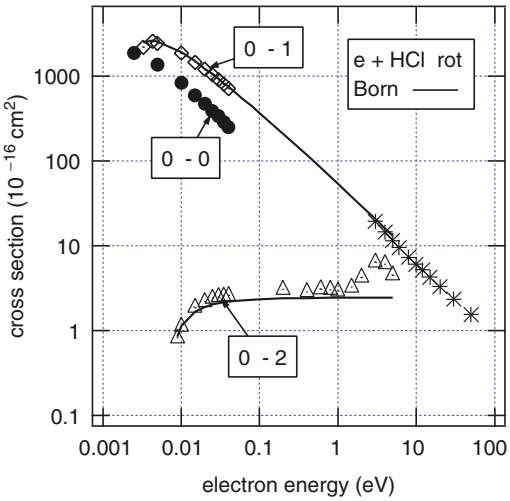

Fig. 5.11. Rotational cross-sections for HCl. Theoretical values [130, 146] are compared with the Born result

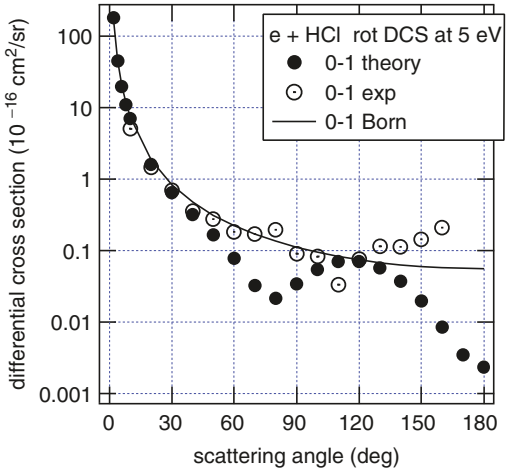

Fig. 5.12. Differential cross-sections for the rotational transition $J = 0 \rightarrow 1$ in HCl at 5 eV. Theoretical [146] and experimental [57] results are compared with the Born calculation

distance give the main contribution. Those collisions are so weak that most of the electrons are slightly scattered from the forward direction. In the Born formula (5.23), the angular dependence is given by

$$\frac{1}{K^2} = \left(\frac{1}{(k_0 - k_J)^2 \, + \, 2k_0 k_J (1 - \cos\theta)} \right)^2 . \tag{5.27}$$

When $k_0 \approx k_J$ (i.e., when the collision energy much exceeds the rotational transition energy), this term becomes very large at the forward scattering angle (i.e., $\theta \approx 0°$). This is seen in Fig. 5.12 as a sharp peak at $\theta = 0°$. In the small-angle region (say, $\theta < 30°$), the Born cross-section almost completely coincides with the theoretical value of Shimoi and Itikawa. There is some difference between the theory and the experiment in the large-angle region. This may arise from the experimental uncertainty (see [82]).

For the quadrupole interaction, the Born cross-sections are obtained as (see [154])

$$Q_{\mathrm{rot}}^{\mathrm{Born,quad}}(J_0 \to J_0 + 2) = \frac{8\pi}{15}\frac{k_J}{k_0}\frac{(J_0+1)(J_0+2)}{(2J_0+1)(2J_0+3)}\langle M_2\rangle^2, \tag{5.28}$$

$$Q_{\mathrm{rot}}^{\mathrm{Born,quad}}(J_0 \to J_0 - 2) = \frac{8\pi}{15}\frac{k_J}{k_0}\frac{(J_0-1)(J_0)}{(2J_0-1)(2J_0+1)}\langle M_2\rangle^2, \tag{5.29}$$

$$Q_{\mathrm{rot}}^{\mathrm{Born,quad}}(J_0 \to J_0) = \frac{16\pi}{45}\frac{k_J}{k_0}\frac{(J_0)(J_0+1)}{(2J_0-1)(2J_0+3)}\langle M_2\rangle^2. \tag{5.30}$$

Since the process $J_0 \to J_0$ is a rotationally elastic transition, k_J should be equal to k_0 in (5.30). Here $\langle M_2\rangle$ is the quadrupole moment (in a.u.) of the molecule. Figure 5.11 presents also the cross-sections for the $0 \to 2$ transition of HCl. The Born cross-section shows a fairly good agreement with the theoretical one in the threshold region, but the agreement deteriorates with increasing energy. The range of the interaction of the electron with the quadrupole moment of a molecule is not so long as in the case of dipole interaction. Probably shorter-range interactions may compete with the quadrupole term for the $0 \to 2$ transition.

A comment is given here on the treatment of rotational transition in the solution of the Boltzmann equation. To derive the electron energy distribution function (EEDF), the Boltzmann equation is solved. In principle, rotational transition should be taken into account in the collision term of inelastic processes. In practice, however, the following simple approximation is often employed (see, for example, [49]). First, because of small value of transition energy, the rotational transition is regarded as a continuous process like elastic scattering. Then Q_{rot} is replaced with the corresponding value calculated in the Born approximation. As is shown above, the Born method gives a good cross-section for the rotational transition in polar molecules. Even for nonpolar molecules, it gives fairly reasonable result at least near threshold. Accordingly the second part of the approximate method of the treatment of rotational transitions seems not much unreliable. However, the first part of the approximation needs some caution. The assumption of ignoring the inelasticity of rotational transitions is not valid near the threshold of the rotational transition.

When rotational cross-sections are derived from a swarm experiment, rotational transitions are treated as inelastic processes. However, in that case, an

assumption is often made that the energy dependence of the cross-section is the same as that of the Born cross-section. Then the absolute magnitude of the cross-section is determined so as to reproduce the measured values of transport coefficients. The resulting cross-section may be not much different from the correct value, but its validity should be tested in some way (e.g., with the help of any elaborate theory).

Finally we mention the rotationally elastic cross-section, $Q_{\mathrm{rot}}(J = 0 \to 0)$. As is stated in Sect. 5.2, the elastic cross-sections obtained experimentally are mostly the vibrationally elastic ones (see (5.4)). On the other hand, theory can give information about the pure elastic (or rotationally elastic) cross-section. Figures 5.9 and 5.11 show theoretical values of $Q_{\mathrm{rot}}(J = 0 \to 0)$ for N_2 and HCl, respectively. In the case of nonpolar molecules (e.g., N_2), the $Q_{\mathrm{rot}}(J = 0 \to 0)$ is always larger than any rotationally inelastic cross-sections. For polar molecules (e.g., HCl), however, $Q_{\mathrm{rot}}(J = 0 \to 1)$ exceeds the rotationally elastic one at least in the low-energy region (say, $< 1\,\mathrm{eV}$), except in the region near threshold of the rotational excitation. This means that the experimental elastic cross-section for polar molecules, at least in the low-energy region, is composed mostly of the contribution of rotationally inelastic processes.

5.5 Vibrational Transition

It is possible to measure vibrational cross-sections with a beam-type experiment (i.e., an EELS measurement). Since the threshold of vibrational excitation is located below 1 eV, however, it is difficult to do the measurement near threshold. Instead a swarm technique is often applied to the measurement of the cross-section near threshold. To derive vibrational cross-sections from a swarm experiment, rotational transitions should be taken into account simultaneously. In many cases of swarm analysis, however, vibrational cross-sections are obtained simply with ignoring rotational processes. The resulting vibrational cross-section must have some uncertainty.

As an example, Fig. 5.13 shows the vibrational cross-sections for $v = 0 \to 1$ for several diatomic molecules (H_2, O_2, CO, and NO). The cross-sections for O_2, NO, and CO are those recommended by Brunger et al. [18]. The data for H_2 are taken from a more recent review by Yoon et al. [167]. All the cross-sections shown in Fig. 5.13 have a peak as a function of electron energy. They are ascribed to the shape resonance (see Sect. 5.2). If the experimental energy resolution is high enough, the resonance peak often shows complicated structure. In this regards, the vibrational cross-section of N_2 is discussed later. An envelop of those structured cross-sections are plotted in Fig. 5.13.

As is stated in Sect. 4.1, a polyatomic molecule has multiple modes of vibration. Some of the modes have very close transition energies. It is difficult to resolve those modes experimentally. For example, the lowest excited levels of the symmetric (ν_1) and antisymmetric (ν_3) stretching vibrations of

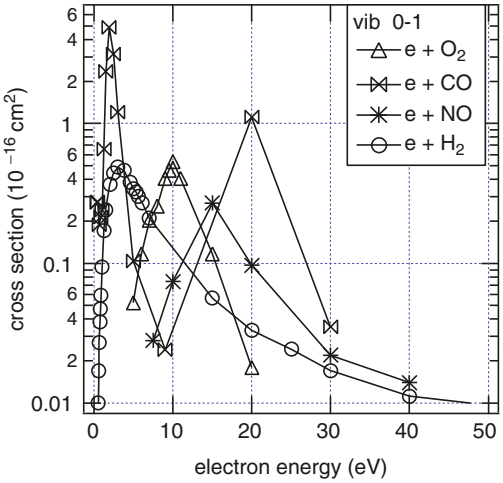

Fig. 5.13. Vibrational excitation cross-sections for $v = 0 \rightarrow 1$ for H_2, O_2, NO, and CO

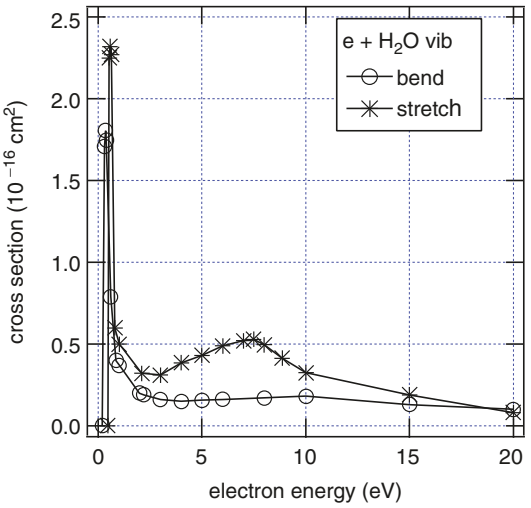

Fig. 5.14. Vibrational excitation cross-sections for the lowest transition in H_2O. *Bend*: bending mode, *stretch*: combined cross-sections for the symmetric and antisymmetric stretching modes

H_2O are located at 0.4534 and 0.4659 eV, respectively. The excitations of the two levels cannot be experimentally separated, unless an elaborate technique is used. Experimental data are obtained as a sum of the cross-sections for the two vibrational excitations. Figure 5.14 presents the vibrational cross-sections for H_2O recommended by Itikawa and Mason [81]. The figure shows

the cross-section for the bending mode (ν_2) and the combined cross-section for the symmetric and antisymmetric stretching modes. Both the cross-sections have a sharp peak at the respective thresholds. Immediately above the threshold, the electron after collision is very slow and interacts strongly with the molecular dipole. This strong interaction may make the threshold peak. For hydrogen halides (e.g., HF), this kind of threshold phenomena are studied in details [70].

Another example of vibrational cross-section of polyatomic molecules is given in Fig. 5.15. The figure shows the vibrational cross-sections for CH_4. Methane molecule has four normal modes of vibration: ν_1 with the transition energy of 0.362 eV, ν_2 of 0.190 eV, ν_3 of 0.374 eV, and ν_4 of 0.162 eV. Experiment cannot resolve ν_1 and ν_3, and ν_2 and ν_4. Experimental data are given for the combined cross-section for ν_1 and ν_3 (indicated as ν_{13}) and that for ν_2 and ν_4 (ν_{24}). Figure 5.15 shows those combined cross-sections recommended by Brunger et al. [18].

In the electron-impact excitation, different modes of vibration show different behaviors. In particular an infrared (IR)-active mode has a relatively large cross-section in the low-energy region. An IR-active mode is the vibrational mode which can be excited through an absorption of IR radiation. This implies that the mode of vibration can be strongly coupled with the electromagnetic field of radiation. A collision with an electron, particularly at a long distance, can be interpreted as a sort of application of electric field. As is stated below, the Born approximation shows that the vibrational cross-section for an IR-active mode is proportional to the IR absorption intensity of the mode. Among the four normal modes of vibration of CH_4, ν_3, and ν_4 are

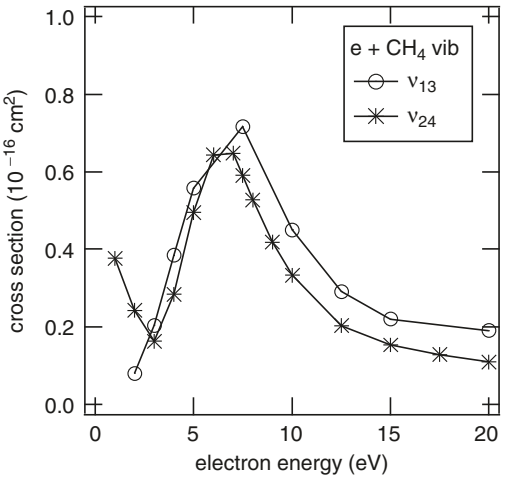

Fig. 5.15. Vibrational excitation cross-sections for the lowest transitions in CH_4. ν_{13}: combined cross-sections for the ν_1 and ν_3 modes, ν_{24}: those for the ν_2 and ν_4 modes

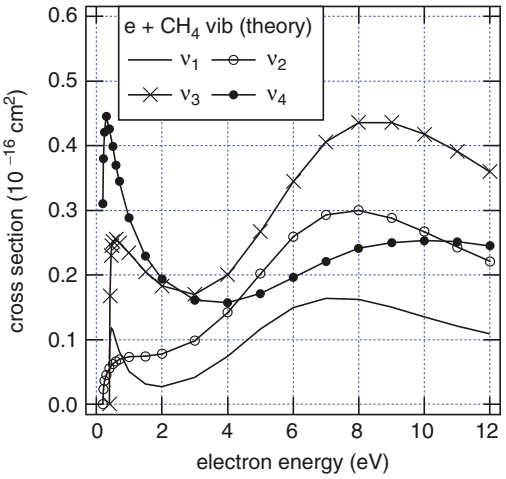

Fig. 5.16. Theoretical values of the vibrational excitation cross-sections for the lowest transitions of each mode in CH_4 [123]

IR-active. Figure 5.16 presents the vibrational cross-sections for each mode of CH_4, calculated by Nishimura and Gianturco [123]. (Experimentally those four modes cannot be fully separated, as is seen in Fig. 5.15.) Near the respective thresholds, the IR-active modes have a large cross-section compared with other modes. As the collision energy increases, other effects (especially the shape resonance) mask the dominance of the IR-active modes. This is a general trend of an IR-active mode of vibration (see, for more details, a review by Itikawa [80]).

The Born cross-sections for the rotational transitions, derived in Sect. 5.4, can easily be extended to the vibrational transitions. Here we consider only the dipole interaction between the incident electron and the molecule. Taking into account the vibrational transition $v_0 \to v$, the Born cross-section for $J_0 \to J_0 + 1$ in (5.25) is rewritten as (all the Born results being expressed in atomic units)

$$Q^{\mathrm{Born,dipole}}(v_0, J_0 \to v, J_0 + 1) = \frac{8\pi}{3k_0^2} \left|\langle v|M_1|v_0\rangle\right|^2 \frac{J_0 + 1}{2J_0 + 1} \ln\left|\frac{k_0 + k_\nu}{k_0 - k_\nu}\right| . \tag{5.31}$$

Similarly we have

$$Q^{\mathrm{Born,dipole}}(v_0, J_0 \to v, J_0 - 1) = \frac{8\pi}{3k_0^2} \left|\langle v|M_1|v_0\rangle\right|^2 \frac{J_0}{2J_0 + 1} \ln\left|\frac{k_0 + k_\nu}{k_0 - k_\nu}\right| . \tag{5.32}$$

If we do not discriminate any rotational transition (i.e., we ignore the rotational energy compared with the vibrational one), we take a sum of these two cross-sections to obtain the vibrational cross-section in the form

$$Q_{\rm vib}^{\rm Born,dipole}(v_0 \to v) = \frac{8\pi}{3k_0^2} \, |\langle v|M_1|v_0\rangle|^2 \, \ln\left|\frac{k_0 + k_v}{k_0 - k_v}\right|. \tag{5.33}$$

Here k_v is the wave number of the electron after the collision and $\langle v|M_1|v_0\rangle$ is the matrix element of the dipole moment with respect to the initial and final vibrational states. This matrix element also determines the absorption and emission of IR radiation by the molecule. In fact, the IR absorption intensity A is given by the formula (see, e.g., [14])

$$A(v \leftarrow v_0) = \frac{2\pi\omega}{3\hbar c} \, |\langle v|M_1|v_0\rangle|^2 \,, \tag{5.34}$$

where ω is the corresponding IR frequency and c is the speed of light. The IR intensity is generally obtained from the IR spectroscopy [14]. The dipole matrix element for the fundamental transition (i.e., $v = 0 \to 1$) can be obtained from the spectroscopic data on the IR intensity with the relation

$$|\langle v = 1|M_1|v = 0\rangle|^2 \ \text{(a.u.)} \ = 0.061757 \, \frac{A(\text{km mol}^{-1})}{\omega(\text{cm}^{-1})}. \tag{5.35}$$

The values of the dipole matrix element squared are tabulated in Table B.5 for a number of molecules.

So far the Born cross-section for the vibrational transition (5.33) has been derived for a diatomic molecule (i.e., from the corresponding formula (4.55)). A more general derivation of the Born cross-section has been given by Itikawa [76] for vibrational transitions in polyatomic molecules. The vibrational cross-section for any IR-active mode of any polyatomic molecule can be expressed in the same form as (5.33), if the Born approximation is employed. The matrix element $\langle v|M_1|v_0\rangle$ in this case is evaluated with respect to the respective IR-active modes. Or it is replaced with the corresponding IR intensity according to the relation (5.34). Itikawa [76] also derived the Born cross-section for vibrational transitions through other types of interaction (e.g., the quadrupole interaction).

To understand the mechanism of the vibrational excitation, we investigate some details of the interaction matrix element (for more details, see [77]). Consider only the long-range dipole interaction. The matrix element for the transition in the sth normal mode is written as

$$\langle v^{(s)}|M_1|v_0^{(s)}\rangle = \int \mathrm{d}\xi^{(s)} \, \chi_v^{(s)}(\xi^{(s)})^* \, M_1 \, \chi_{v_0}^{(s)}(\xi^{(s)}). \tag{5.36}$$

Here $\xi^{(s)}$ is the normal coordinates of the sth mode and $\chi_v^{(s)}$ is the vibrational wave function of the mode. (In the case of diatomic molecule, the normal coordinate corresponds to $R - \bar{R}$, with $\bar{R}$ being the equilibrium internuclear distance.) Unless we consider transitions involving very high vibrational states,

all molecular nuclei are located near their equilibrium positions (i.e., $\xi^{(s)} = 0$). Then we expand the dipole moment M_1 in terms of $\xi^{(s)}$ around the position $\xi^{(s)} = 0$. To the first order, we have

$$M_1(\xi^{(s)}) = M_1(\xi^{(s)} = 0) + \left(\frac{\partial M_1}{\partial \xi^{(s)}}\right)_{\xi^{(s)}=0} \xi^{(s)}. \tag{5.37}$$

It should be noted that M_1 depends also on the normal coordinates of other modes, but those coordinates are assumed to take their equilibrium values. Inserting (5.37) into (5.36), the matrix element becomes

$$\begin{aligned}\langle v^{(s)}|M_1|v_0^{(s)}\rangle \; &= M_1(0)\,\langle v^{(s)}|v_0^{(s)}\rangle \\ &\quad + \left(\frac{\partial M_1}{\partial \xi^{(s)}}\right)_{\xi^{(s)}=0} \langle v^{(s)}|\xi^{(s)}|v_0^{(s)}\rangle. \end{aligned} \tag{5.38}$$

Because of the orthogonality of the vibrational wave functions, we have

$$\langle v^{(s)}|v_0^{(s)}\rangle = \delta_{v^{(s)}v_0^{(s)}}, \tag{5.39}$$

and hence the first term on the right-hand side of (5.38) vanishes. The vibrational transition of the respective mode can occur only under the condition

$$\left(\frac{\partial M_1}{\partial \xi^{(s)}}\right)_{\xi^{(s)}=0} \neq 0. \tag{5.40}$$

This is equivalent to the statement that the sth mode is IR-active. It is clear from the present argument that the vibrational transition is concerned not with the dipole moment itself, but with the derivative of the dipole moment with respect to the nuclear coordinates. There are many polyatomic molecules which have no dipole moment (i.e., $M_1(0) = 0$) but have a number of IR-active vibrational modes satisfying the condition (5.40). This conclusion is extended to more general cases. Any interaction term can be put into the place of M_1 in (5.36). Vibrational transitions through the interaction can occur, if we have a nonzero value of the derivative of the term with respect to the nuclear coordinates.

To see the effectiveness of the Born approximation, we show in Fig. 5.17 the cross-sections for the vibrational excitations of the two IR modes (ν_3 and ν_4) of CH_4. (See Appendix C for the calculation of the Born cross-section.) In the figure, the Born cross-section is compared with the calculation by Nishimura and Gianturco [123] (the same as shown in Fig. 5.16). In the energy region near threshold, the Born cross-section for the ν_3 mode agrees well with the theoretical one. The agreement becomes worse with increasing energy. This is probably due to the effect of resonance (see Fig. 5.16). For the ν_4 mode, the Born result is by about a factor of 2 smaller than the cross-section of Nishimura and Gianturco. After a survey of many other cases, Itikawa [80] concluded that, for the electron-impact vibrational transition of IR-active

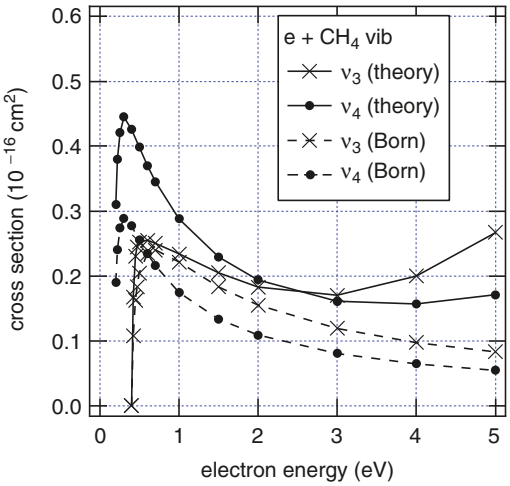

Fig. 5.17. Vibrational excitation cross-sections for the lowest transition of IR-active modes of CH_4. The Born cross-sections are compared with the theoretical result of Nishimura and Gianturco [123]

mode, the Born method gives a fairly reasonable result (probably within a factor of 2) at the collision energies near threshold. Furthermore, also for the vibrational transition, the Born approximation always provides an accurate value of differential cross-section at the small scattering angles (see the discussion for the rotational transition in Sect. 5.4). How large a scattering angle at which the Born method can be applied depends on the competition between the dipole and other interactions.

As is mentioned before, a shape resonance is a common phenomenon in the electron-impact vibrational excitation of molecules. Almost all the vibrational cross-sections have peaks as a function of electron energy. Most of them are interpreted as a shape resonance. Some of the peaks have fine structure. A typical example is the cross-section of N_2, which is shown in Fig. 5.18. The figure shows two sets of cross-sections. One is the recommended cross-section by Brunger et al. [18], who determined the cross-section from the results of beam-type measurements. In a beam experiment, DCS at a fixed collision energy are measured first with varying scattering angles. After the integration of the resulting DCS over the scattering angles, the integral cross-section at the energy is obtained. Thus, it is difficult to derive a detailed form of energy dependence of the (integral) cross-section with a beam-type experiment. Figure 5.18 presents another set of cross-sections, which was obtained by a swarm experiment. In a swarm experiment, cross-sections are derived directly as a function of collision energy. Campbell et al. [20] analyzed the swarm result very carefully to derive accurate values of the vibrational cross-section. The resulting cross-section shows fine structure. The two sets of the cross-section in Fig. 5.18 are generally consistent with each other. The difference can be

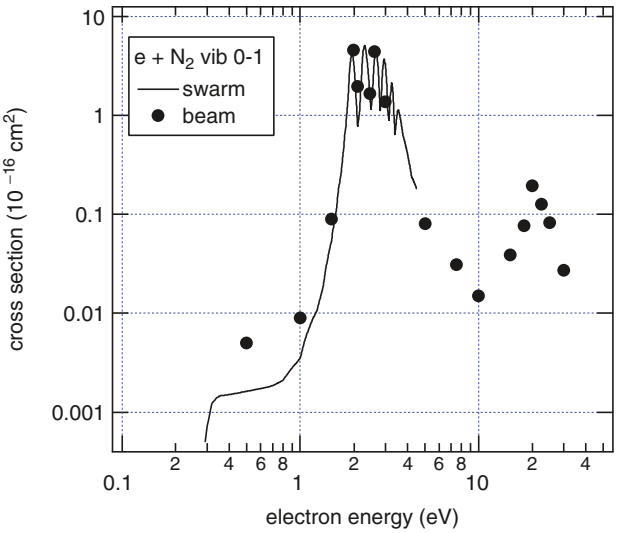

Fig. 5.18. Vibrational excitation cross-section, $Q_{\rm vib}(v = 0 \rightarrow 1)$, for N_2. Two sets of experimental data are shown: one by beam-type experiments and the other from swarm experiment

ascribed to the uncertainty of both the experiments. The structure was first found by Schulz in 1964 [142]. Since then many theoretical studies have been performed to understand the structure. Briefly summarizing those theoretical results, the structure is caused by a strong interference between the electronic and nuclear motions in the molecule. In this case, the lifetime of the resonance state (i.e., an electronically excited state of the negative molecular ion, N_2^-) is comparable to the period of the vibrational motion. In other words, the decay of the electron captured competes with the nuclear motion. Some time the molecule establishes a stationary state of vibrational motion before ejecting the electron, but other time it does not. It depends on the incident electron energy. One of the specific features of the resonance is the excitation of high vibrational states (i.e., $v > 1$). In the resonance region, the electron collision is known to induce an excitation of vibrational states up to $v = 17$ (see Table 5.1).

Finally, comments are given on the role of vibrational excitation in the electron transport in a molecular plasma. The vibrational cross-section has a sizable magnitude in the energy region below about 10 eV. The transition energy is not so small as in the case of rotational excitation. In this sense the vibrational excitation is the most important energy loss process of electrons in a low-temperature molecular plasma (see the discussion of stopping cross-section in Sect. 5.12). Or it is the most significant process of deposition of the electron energy to the plasma. Once vibrationally excited, the molecule decays to the lower state through emission of radiation. If the vibrational mode is not IR-active, the excited molecule remains for a long time. The vibrationally

Table 5.1. Vibrational excitations of N_2

Transition	Energy (eV)	Cross-section (cm^2)
$0 \to 1$	1.95	$5.6(-16)^a$
$0 \to 2$	2.00	$3.7(-16)$
$0 \to 3$	2.15	$3.1(-16)$
$0 \to 4$	2.22	$2.1(-16)$
$0 \to 5$	2.39	$1.3(-16)$
$0 \to 6$	2.48	$7.1(-17)$
$0 \to 7$	2.64	$3.8(-17)$
$0 \to 8$	2.82	$1.6(-17)$
$0 \to 9$	2.95	$6.1(-18)$
$0 \to 10$	3.09	$2.2(-18)$
$0 \to 11$	3.30	$6.3(-19)$
$0 \to 12$	3.87	$1.4(-19)$
$0 \to 13$	4.02	$4.5(-20)$
$0 \to 14$	4.16	$1.3(-20)$
$0 \to 15$	4.32	$3.6(-21)$
$0 \to 16$	4.49	$9.1(-22)$
$0 \to 17$	4.66	$2.4(-22)$

Maximum cross-sections with the corresponding electron energy, measured by Allan [5], are given for the transitions from the ground to the excited ($v = 1, 2, \ldots, 17$) states. [a] $5.6(-16) = 5.6 \times 10^{-16}$.

excited molecule behaves differently from the molecule in the ground state. Through collisions with other particles in a plasma, they release their internal energy and start other (secondary) collision processes (see Sect. 5.13).

5.6 Excitation of Electronic State

First we deal with a diatomic molecule. An electronic energy of a diatomic molecule depends on the internuclear distance of the molecule. Any transition between two electronic states is accompanied by a transition of rotational and vibrational ones. We have to consider a transition like

$$\mathrm{AB}(n,\, v,\, J) \;\to\; \mathrm{AB}(n',\, v',\, J'), \tag{5.41}$$

where n and n' denote the electronic states before and after the collision, and $(v,\, J)$ and $(v'\, J')$ indicate the associated vibrational and rotational states. As is stated in Sect. 4.3, we can apply the Franck–Condon factor approximation

to the electron-impact transition of the electronic states of a molecule. Then we can write the cross-section for the transition (5.41) in the form

$$Q(n, v \rightarrow n', v') = F_{vv'}^{nn'}\, Q_{\mathrm{exc}}(n \rightarrow n'). \tag{5.42}$$

Strictly speaking, this relation holds under the fixed-nuclei approximation (see Sect. 4.3). For simplicity of notation, however, we ignore the suffix FN here. In (5.42), we do not consider rotational transitions, because, in most of the experiments, it is impossible to resolve the rotational transition. The quantity F in (5.42) is the Franck–Condon factor introduced in Sect. 4.3. It is given by

$$F_{vv'}^{nn'} = \left| \int \mathrm{d}R\, \chi_{v'}^{n'}(R)^*\, \chi_v^n(R) \right|^2, \tag{5.43}$$

where χ_v^n is the vibrational wave function of the state v associated with the electronic state n. In most of the literature, Q_{exc} is given simply as the cross-section for the excitation of electronic state. In particular, almost all the theoretical calculations so far are based, explicitly or implicitly, on the fixed-nuclei assumption, so that they produce Q_{exc}.

To see how to experimentally determine Q_{exc}, the experiment with H_2 by Wrkich et al. [166] is shown here. They employed a standard method of measurement of EELS. They made the experiment at room temperature, so that the hydrogen molecule is in the vibrationally and electronically ground state. Their measurement was done at an energy resolution of 25–40 meV. They did not resolve rotational states. Upon collisions with electrons, H_2 is excited to an electronic state n and one of the associated vibrational states v. The measured EELS has a number of peaks corresponding to the excitation of the states designated with a certain pair (n, v).

One example of the EELS obtained by Wrkich et al. is shown in Fig. 5.19. This shows the region of energy loss from 11.0 to 14.5 eV. This was obtained at the collision energy of 20 eV and the scattering angle of 20°. Several different states n are excited at this collision energy. Each transition $0 \rightarrow n$ accompanies a number of different vibrational transitions $v = 0 \rightarrow v$. The measured spectrum is shown in the lowest panel of the figure (black dots). It was interpreted as a superposition of excitations of six electronic states (B $^1\Sigma_u^+$, c $^3\Pi_u$, a $^3\Sigma_g^+$, C $^1\Pi_u$, E, F $^1\Sigma_g^+$, and e $^3\Sigma_g^+$). With the use of the Franck–Condon factors, Wrkich et al. decomposed the spectrum into six sets of spectra shown in the upper panels of the figure. Each spectrum corresponds to the cross-section (actually the DCS at 20°) for the transition $(0, 0) \rightarrow (n, v)$. The peaks of each panel correspond to the vibrational states v of the electronic state indicated. The relative heights of the peaks are proportional to the Franck–Condon factors F_{0v}^{0n} with different v. With the relative flow technique for normalization (see Sect. 3.5), the absolute values of the DCS were derived. The resulting values of the DCS for the four representative states are shown in Fig. 5.20. The measurement was done over the scattering angles from 5° to 130°.

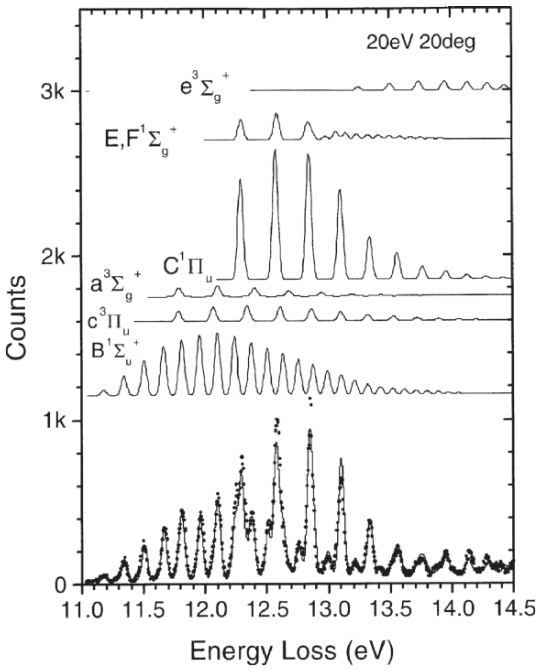

Fig. 5.19. Electron energy loss spectra of H_2 at the collision energy of 20 eV and the scattering angle of 20°, reproduced from [166]

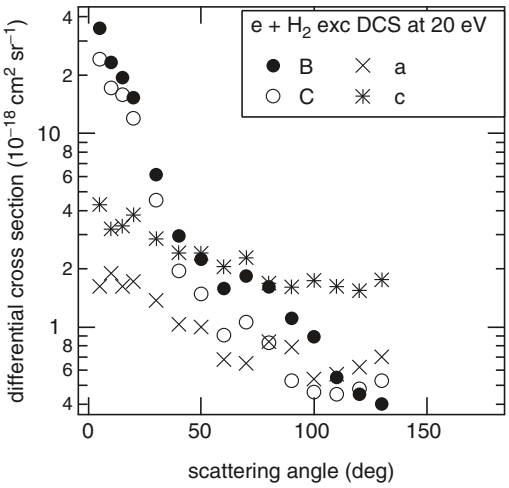

Fig. 5.20. Differential cross-sections for the excitations of the electronic states (B $^1\Sigma_u^+$, c $^3\Pi_u$, a $^3\Sigma_g^+$, C $^1\Pi_u$) of H_2, measured by Wrkich et al. [166] at the collision energy of 20 eV

Extrapolating the DCS in the forward and the backward directions, the integral cross-sections Q_{exc} were obtained. Wrkich et al. measured the cross-section at three points of energy (17.5, 20, and 30 eV). Their Q_{exc} for the B $^1\Sigma_u^+$ and C $^1\Pi_u$ states are shown in Figs. 5.21 and 5.22, respectively. For these states, Liu et al. [104] derived Q_{exc} from an emission measurement (for the method, see Sect. 5.9). Figures 5.21 and 5.22 compare the results of Wrkich et al. with those of Liu et al. The agreement of the two sets of cross-sections is very good.

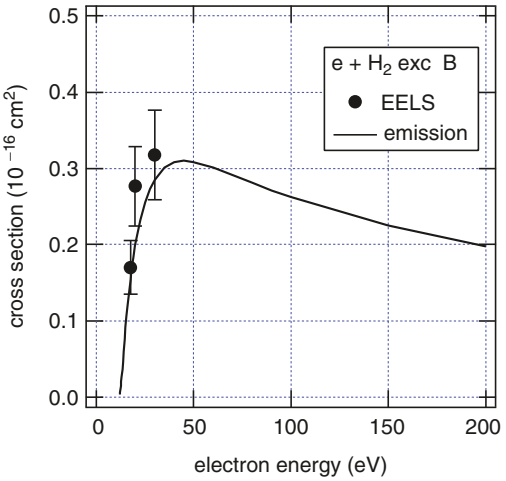

Fig. 5.21. Excitation cross-sections for the B $^1\Sigma_u^+$ state of H_2, obtained by an EELS measurement [166] and an emission measurement [104]

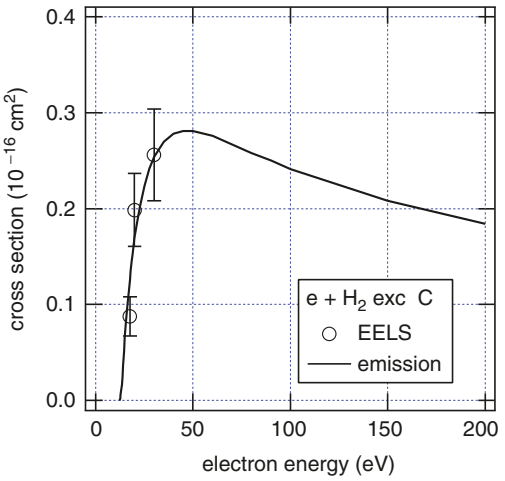

Fig. 5.22. Same as Fig. 5.21, but for the state C $^1\Pi_u$

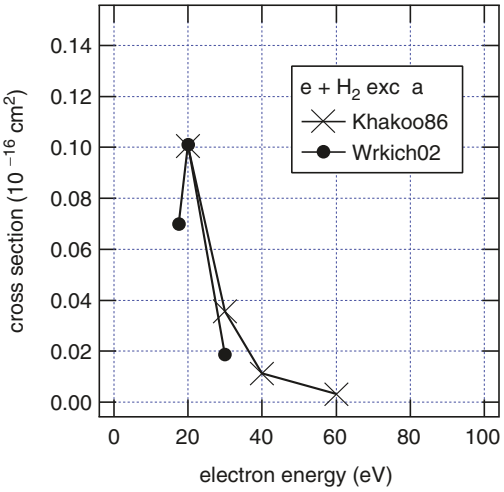

Fig. 5.23. Excitation cross-sections for the a $^3\Sigma_g^+$ state of H_2, obtained with an EELS measurement by Wrkich et al. [166] and Khakoo and Trajmar [89]

Figure 5.23 shows the cross-section for the excitation of the a $^3\Sigma_g^+$ state of H_2. The result of Wrkich et al. is compared with the measurement of the same group in 1986 [89]. The latter measurement was done at the energies 20–60 eV. The two sets of cross-sections are in good agreement. One specific feature of the excitation of the a $^3\Sigma_g^+$ state is that the cross-section decays rapidly with increasing energy. In other words, the cross-section has a sharp peak immediately above the threshold. The optical transition between the ground (X $^1\Sigma_g^+$) and a $^3\Sigma_g^+$ states is dipole forbidden. Usually cross-sections for the electron-impact excitation of dipole-forbidden transitions have a sharp peak above the threshold and decay rapidly with increasing energy. On the other hand, cross-sections for the dipole-allowed transitions (e.g., X-B and X-C transitions) have a broad peak and decay slowly (see Figs. 5.21 and 5.22).

As is seen from the above procedure, the derivation of $Q_{\rm exc}$ from the measured EELS usually relies on the deconvolution of the measured spectra with the use of the Franck–Condon (FC) factors. To do that, we need an accurate knowledge of the FC factor. In the experiment of Wrkich et al. [166], they theoretically obtained the FC factors by themselves. They collected accurate potential curves for the electronic states of H_2. From them, accurate vibrational wave functions were determined to be inserted into the formula (5.43). Even with reliable FC factors, ambiguity often accompanies the deconvolution procedure. Uncertainty arises also from the method of extrapolation of the measured DCS to the region where experimental data are not available. One should be careful about these problems when using the experimental data on $Q_{\rm exc}$.

An excitation of electronic states of polyatomic molecules is not much different from that of diatomic ones. In principle, the FC factor approximation

like (5.42) can also be used for polyatomic molecules. Since a polyatomic molecule has multiple modes of vibration, the FC factor depends on the vibrational quantum numbers in a complicated manner. Correspondingly the EELS has a complicated fine structure arising from the vibrational transitions. In reality it is almost impossible to decompose the EELS into each vibrational component, because of finite experimental resolution of the electron energy. The excitation cross-sections obtained for polyatomic molecules are mostly the one summed over the final vibrational states (sometime called *manifold cross-section*).

As an example, Fig. 5.24 shows an electron energy loss spectrum of H_2O. The spectrum was obtained at the collision energy of 100 eV and the scattering angle of 3°. It is known that H_2O has at least 13 electronic states with the excitation energy below 10.75 eV (i.e., the region shown in Fig. 5.24) [81]. It is, however, difficult to identify all of those states in the measured spectrum. This is partly because the experimental resolution of the electron energy is not sufficiently high to resolve the vibrational structure of those electronic states. Furthermore, many of the electronic states are unstable against dissociation. Those states have a broad peak, which overlaps with other peaks. For example, the very broad peak at 7–8 eV of the energy loss in Fig. 5.24 corresponds to the excitation of the lowest triplet ($1\ ^3B_1$) and singlet ($1\ ^1B_1$) states. These two states are thought to contribute to the dissociation process, $H_2O \rightarrow H + OH(X)$ [56]. With a deconvolution of their measured EELS, Tanaka and his colleagues obtained the $Q_{\rm exc}$ for several electronically excited states of H_2O [157, 158]. One of them is shown in Fig. 5.25. This is the cross-section for the excitation of $1\ ^1B_1$ (or in other notation, $\tilde{A}\ ^1B_1$) state of H_2O.

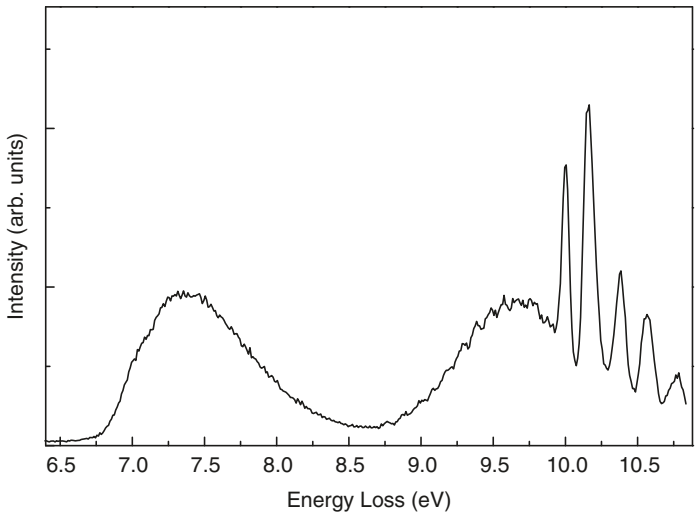

Fig. 5.24. Electron energy loss spectrum of H_2O, measured by Tanaka and his group at the collision energy of 100 eV and the scattering angle of 3° (kindly provided by Tanaka)

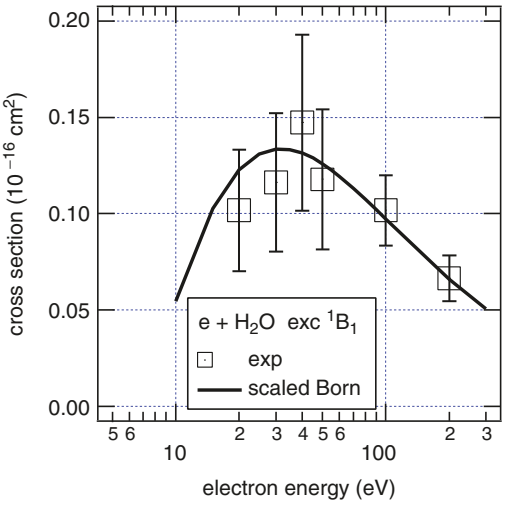

Fig. 5.25. Excitation cross-sections for the 1 $^1B_1$ state of H_2O, obtained with an EELS measurement by Thorn et al. [157]. A scaled Born cross-section is also shown

In the figure, a scaled Born cross-section (proposed by Kim [91]) is shown for a comparison. The latter well reproduces the experimental data.

Finally we mention the fate of the electronically excited molecules. They decay either through emission of radiation or through dissociation. If neither of the two decay processes has a considerable probability to occur, they change their states via collisions with other plasma particles or by hitting to the wall of the apparatus. For the radiative decay to occur, the excited state has to be connected with lower states through dipole-allowed transitions. The lifetime against such a radiative decay is of the order of 10^{-10} to 10^{-8} s. The dissociative decay of a molecule proceeds through two different manners (for more details, see Sect. 5.10). If the excited state is repulsive, the molecule dissociates promptly after excitation (direct dissociation). If the excited state is attractive but crossed with a repulsive state, dissociation occurs with a finite probability. This is called a *predissociation*. The lifetime against the dissociation is normally 10^{-15} to 10^{-14} s.

5.7 Ionization

An ionization of molecules produces several different ion products. We show this for a diatomic molecule:

1. Production of parent molecule ion

$$\mathrm{e} + \mathrm{AB} \rightarrow \mathrm{AB}^+ + 2\mathrm{e}.$$

2. Dissociative ionization

$$\mathrm{e} + \mathrm{AB} \rightarrow \mathrm{A}^+ + \mathrm{B} + 2\mathrm{e},$$

$$\mathrm{A}^+ + \mathrm{B}^+ + 3\mathrm{e}.$$

As is easily expected, various kinds of ions are produced in the ionization of polyatomic molecules (see Fig. 5.28). In some polyatomic molecules (e.g., CF_4), no parent molecule ions are produced. Whenever any electron is picked out from such a molecule, it dissociates.

Here we denote the ionization cross-section for a specific product by $Q_{\mathrm{ion}}(\mathrm{M}^+)$ (e.g., in a diatomic molecule, M = AB, A, or B). These cross-sections are called *partial ionization cross-sections*. Each partial cross-section is measured by a detection of the specific ion. When electron energies increase, multiply charged ions (e.g., A^{2+}) appear. A special caution is needed for multiply charged molecular ions. Many of the multiply charged molecular ions (particularly those of simple molecules) are unstable and have a finite lifetime. Whether they can be detected, therefore, depends on the experimental procedure. If the ion reaches the detector within its lifetime, it is detected. When use is made of the experimental cross-section for the multiply charged molecular ion like AB^{2+}, this point should be taken into account (see the discussion about N_2^{2+} below).

The total ionization cross-section is defined by the sum of all the partial cross-sections in such a way that

$$\begin{aligned} Q_{\mathrm{ion}}(\mathrm{tot}) &= Q_{\mathrm{ion}}(\mathrm{AB}^+) + Q_{\mathrm{ion}}(\mathrm{A}^+) + \cdots \\ &\quad + Q_{\mathrm{ion}}(\mathrm{AB}^{2+}) + Q_{\mathrm{ion}}(\mathrm{A}^{2+}) + \cdots . \end{aligned} \tag{5.44}$$

The easiest way to experimentally obtain the ionization cross-section is a measurement of ion current. In this method, we count ionic charge and hence obtain a cross-section defined by

$$\begin{aligned} Q_{\mathrm{ion}}(\mathrm{tot.count}) &= Q_{\mathrm{ion}}(\mathrm{AB}^+) + Q_{\mathrm{ion}}(\mathrm{A}^+) + \cdots \\ &\quad + 2Q_{\mathrm{ion}}(\mathrm{AB}^{2+}) + 2Q_{\mathrm{ion}}(\mathrm{A}^{2+}) + \cdots . \end{aligned} \tag{5.45}$$

Here each partial cross-section is multiplied by the number of the ionic charge. This is called the *total counting cross-section*. Since the ionization cross-sections for the production of multiply charged ions are usually small, the difference between the two cross-sections, $Q_{\mathrm{ion}}(\mathrm{tot})$ and $Q_{\mathrm{ion}}(\mathrm{tot.count})$, is not of practical significance.

Examples of ionization cross-sections are shown in Figs. 5.26 (N_2), 5.27 (CO), and 5.28 (CF_4). In all the figures, both the partial and the total ionization cross-sections are shown. For CF_4, no parent molecule ion (i.e., CF_4^+) is known to be produced. All of the Q_{ion} shown in the figures are those recommended by Lindsay and Mangan [103]. The partial cross-sections have been obtained by a detection of the respective product ions. In such experiments,

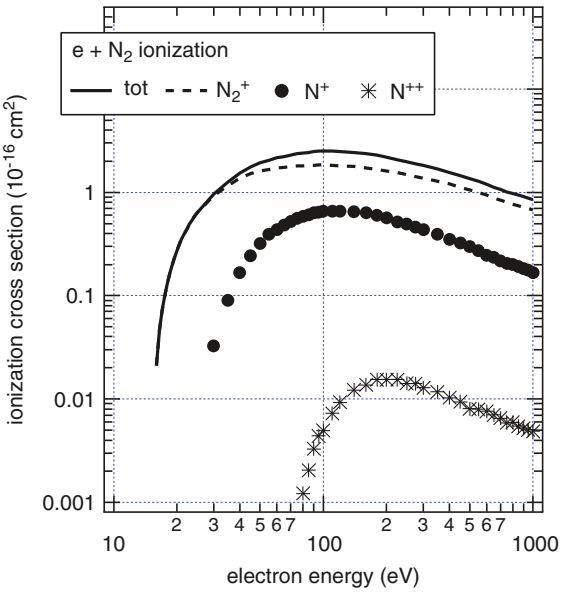

Fig. 5.26. Ionization cross-sections for N_2. Partial cross-sections for the production of N_2^+, N^+, and N^{2+} and total ionization cross-section are shown. The partial cross-section for N^+ may include a contribution of N_2^{2+} (see text)

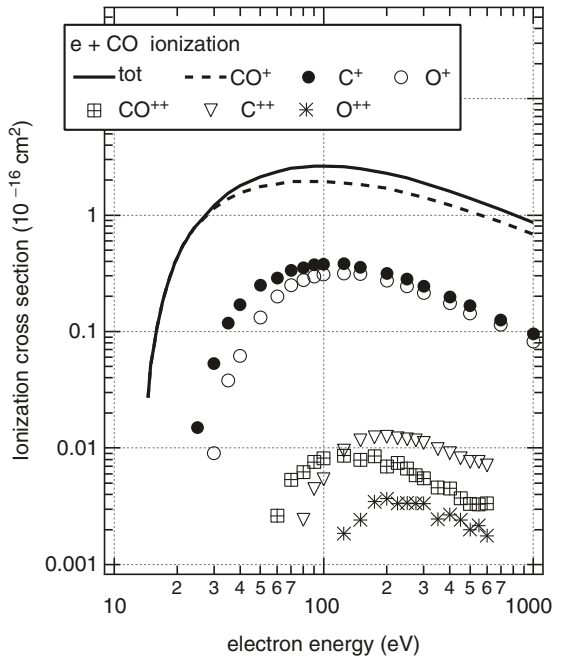

Fig. 5.27. Ionization cross-sections for CO. Partial cross-sections for the production of CO^+, C^+, O^+, CO^{2+}, C^{2+}, and O^{2+} and total ionization cross-section are shown

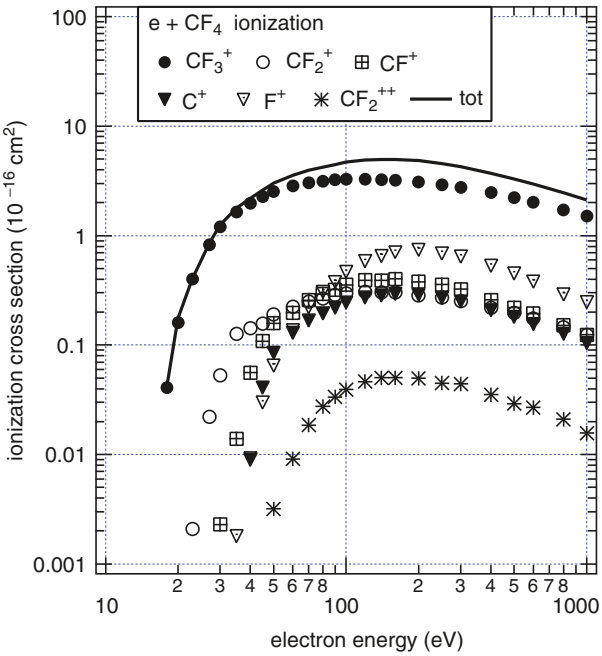

Fig. 5.28. Ionization cross-sections for CF_4. Partial ionization cross-sections for CF_3^+, CF_2^+, CF^+, C^+, F^+, and CF_2^{2+} and total ionization cross-section are shown. Cross-section for CF^+ may have a contribution of CF_3^{2+}. No other multiply charged ions than CF_2^{2+} and CF_3^{2+} are detected

a special care should be taken to have all the product ions detected. This is important because most of the fragment ions have a significant kinetic energy and tend to elude detection. Also important is to confirm that the $Q_{\rm ion}$(tot) obtained as a sum of the partial cross-sections is consistent with the $Q_{\rm ion}$(tot.count) derived from the measurement of total ion current. Lindsay and Mangan surveyed all the available experimental data and evaluated them particularly from these points of view.

Experimental data on partial ionization cross-sections need a special caution. Spectrometrical detection cannot distinguish the ions with the same (or close) charge-to-mass ratio. For example, the signal of N^+ includes that of N_2^{2+}. Therefore, the partial cross-section for N^+ in Fig. 5.26 includes that for N_2^{2+}, although the latter contribution should be small. For the same reason, $Q_{\rm ion}(CF^+)$ in Fig. 5.28 has a contribution of CF_3^{2+}.

As is stated above, a multiply charged molecular ion is often unstable and dissociates promptly into fragments. As a result, we sometime have two (or more) fragment ions simultaneously:

$$\mathrm{e} + \mathrm{AB} \rightarrow \mathrm{A}^+ + \mathrm{B}^+ + 3\mathrm{e}.$$

The measured quantity $Q_{\rm ion}(A^+)$ includes a contribution of this process. Tian and Vidal [159, 160] measured A^+ and B^+ in coincidence and thus distinguished the above process from

$$e + AB \rightarrow A^+ + B + 2e.$$

Their results for N_2 and CO are tabulated in Tables 5.2 and 5.3, respectively. Tian and Vidal measured the cross-sections up to 600 eV. Here samples of their values are shown at 100 and 200 eV. As is stated above, the signals of N^+ and N_2^{2+} cannot be distinguished from each other. The ground electronic state of N_2^{2+} supports several vibrational states. If the N_2^{2+} is produced in one of such vibrational states (particularly lower ones), it has a long lifetime against dissociation and can be detected as it is. Although Table 5.2 has no entry for N_2^{2+}, some amount of such metastable N_2^{2+} may be actually produced and mixed in the signal of N^+. (Note that, due to the finite lifetime, the actual detection of N_2^{2+} may depend on the apparatus.) If N_2^{2+} are produced in other states, they are unstable and immediately dissociate. The experiment showed that a symmetric breaking of N_2^{2+} ($\rightarrow N^+ + N^+$) is much more likely than an asymmetric one ($\rightarrow N^{2+} + N$). The table also shows that about 60% of N^+

Table 5.2. Cross-sections (in $10^{-19}\,{\rm cm}^2$) for different channels in the ionization of N_2, measured by Tian and Vidal [159]

	Products	At 100 eV	At 200 eV
Single ionization	N_2^+	1,961	1,741
	$N^+ + N$	471	380
Double ionization	$N^+ + N^+$	119	114
	$N^{2+} + N$	6	11
Triple ionization	$N^{2+} + N^+$	1	6

Table 5.3. Cross-sections (in $10^{-19}\,{\rm cm}^2$) for different channels in the ionization of CO, measured by Tian and Vidal [160]

	Products	At 100 eV	At 200 eV
Single ionization	CO^+	1.82×10^3	1.54×10^3
	$C^+ + O$	218	157
	$C + O^+$	138	109
Double ionization	CO^{2+}	8.21	6.97
	$C^+ + O^+$	118	118
	$C^{2+} + O$	5.36	8.14
	$C + O^{2+}$	1.15	2.78
Triple ionization	$C^{2+} + O^+$	0.99	4.82
	$C^+ + O^{2+}$	0.15	1.32

comes from the dissociation of N_2^+. The dissociation of N_2^{2+} contributes to the remaining 30%.

In the ionization of CO, CO^{2+} can be discriminated from other ions. A part of CO^{2+} produced, however, is unstable and dissociates. From Table 5.3, less than 10% of CO^{2+} produced are detected and other CO^{2+} dissociates, mostly into $C^+ + O^+$. This is consistent with the picture shown in Fig. 5.27. At its maximum, the partial cross-section, $Q_{\mathrm{ion}}(CO^{2+})$, is less than 1% of the total ionization cross-section. Tian and Vidal [160] also reported quadruple ionizations of CO (but not shown here, because of very small cross-sections).

Ionization cross-sections are used in many application fields. It is very helpful to have any simple formula to calculate them. The essential part of the mechanism of ionization is the impact of the incident electron on the molecular electrons. If the molecular electron acquires enough energy to break its bond to the nucleus, it can come out from the molecule. On the basis of this idea, various kinds of approximate formulas have been proposed for the calculation of the ionization cross-section. Two of them are shown here:

1. *Binary Encounter-Bethe (BEB) model*
   Kim and his colleagues (see [71]) combined the classical two-body collision (binary encounter) theory with an asymptotic form of the quantum mechanical cross-section in the limit of high-energy collision (i.e., the Bethe formula). They assumed that the Coulomb collision between the incident and the molecular electrons can be well described by the classical theory. The resulting formula, however, shows no correct behavior at high energy. At the high energy of collision, the quantum mechanical perturbation theory can be applied to the cross-section calculation. Kim et al. corrected the high-energy part of the classical binary encounter theory with the Bethe asymptote obtained quantum mechanically. To take into account the characteristics of each molecule, they incorporated into their formula the binding and kinetic energies of the molecular electrons. Those molecular properties are obtained from quantum chemical calculation of the molecule.
2. *Semiclassical Deutsch–Märk model*
   Deutsch and Märk (see [33]) also used the classical theory for the collisions between the incident and the molecular electrons. They sum up the contribution of each bound electron with taking a weighting factor. The weighting factor has been determined empirically from comparisons of the model cross-sections with the available experimental data.

In most (not all) cases, these model calculations can reasonably well reproduce the experimental cross-sections.

When an electron ionizes a molecule, we have two free electrons after the collision. (Here we ignore a multiple ionization for simplicity.) In principle, we cannot distinguish those two electrons. By convention, we call the fast one

the primary electron and the slow one the secondary electron. The balance of energy before and after the collision is written as

$$E_0 = I_\mathrm{p} + E_1 + E_2 \quad (E_1 > E_2). \tag{5.46}$$

Here E_0 is the energy of the incident electron, E_1 and E_2 are the energies of the primary and the secondary electrons, respectively, and I_p is the ionization potential of the molecule. We define the excess energy E_x by

$$E_\mathrm{x} = E_0 - I_\mathrm{p}. \tag{5.47}$$

The two outgoing electrons share the excess energy

$$E_\mathrm{x} = E_1 + E_2. \tag{5.48}$$

The problem is *how* the two electrons share the excess energy.

Now we consider the energy distribution of the secondary electron. Once the energy of the secondary electron (i.e., E_2) is known, the energy of the primary electron (i.e., E_1) is obtained from the relation (5.48). The energy distribution of the secondary electron is expressed as the differential cross-section $q(E_0, E_2)$, which is defined by

$$Q_\mathrm{ion}(E_0) = \int_0^{E_\mathrm{x}/2} \mathrm{d}E_2\, q(E_0, E_2). \tag{5.49}$$

The quantity $q(E_0, E_2)$ is called the singly differential cross-section (SDCS). (It is contrasted with the doubly differential cross-section, which represents the angular, as well as energy, dependence of the secondary electron.) The upper limit of the integral on the right-hand side of (5.49) is taken as a half of the excess energy, because, by definition, E_2 should be smaller than E_1.

Experimental data on SDCS are available for a number of molecular species. Opal et al. [127] measured the angular and energy distribution of the secondary electrons. From the measurements, they derived the SDCS for N_2, O_2, H_2, CO, NO, H_2O, CO_2, NH_3, CH_4, and C_2H_2. For N_2 and O_2, the measurements were done with the incident electron beam of 50–2,000 eV, but only the beam of 500 eV was used for other molecules. (Numerical values of the measured data are tabulated in [128].) Figure 5.29 shows the SDCS for N_2 measured at $E_0 = 50$, 100, and 200 eV.

The quantity actually measured is the energy of the electrons coming out after the ionizing collision. The curves shown in the figure above $E_\mathrm{x}/2$ (e.g., 17.2 eV in the case of $E_0 = 50$ eV) correspond with the energy distributions of the primary electrons. If the excess energy is shared symmetrically by the two electrons, we have $E_1 = E_2 = E_\mathrm{x}/2$. But the energy sharing is very asymmetric. Most of the secondary electrons have energies of a few tens of eV or less. Accordingly a large portion of the excess energy goes to the primary

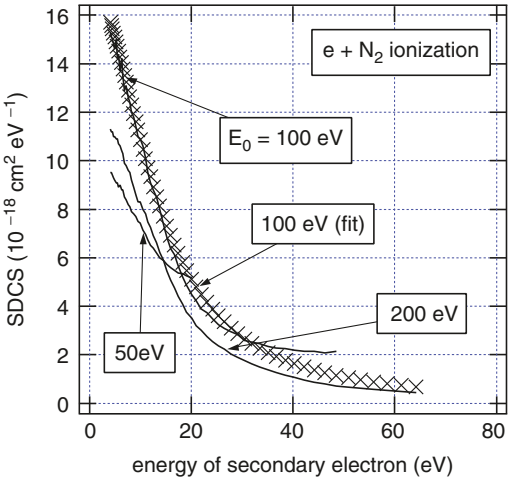

Fig. 5.29. Singly differential cross-sections for the ionization of N_2 [128]. The incident electron energy (E_0) is indicated. At $E_0 = 100\,\mathrm{eV}$, a *fitted curve* is also shown (see text)

electron. Opal et al. found that the measured SDCS can be fitted to an analytic function such as

$$q = \frac{C(E_0)}{1 + (E_2/D)^{\alpha}}. \tag{5.50}$$

Three fitting parameters are included in the function. Among them, α and D are almost independent of the incident energy, and C is the normalization constant depending on the incident energy. In Fig. 5.29, we fit the SDCS of N_2 at $E_0 = 100\,\mathrm{eV}$ with

$$q(E_0 = 100\,\mathrm{eV}) = \frac{17.3}{1 + (E_2/13)^2} \times 10^{-18}\,\mathrm{cm}^2\,\mathrm{eV}^{-1}. \tag{5.51}$$

Here E_2 is expressed in eV. The fitting is good for the secondary electron energies below about 30 eV.

Bolorizadeh and Rudd [15] measured the energy and angular distribution of the ejected electrons for H_2O. Their measurements were done with the incident electron energies 50–2,000 eV. At 500 eV, their result agrees with the measurement by Opal et al. [127]. In Fig. 5.30, we show the SDCS obtained by Bolorizadeh and Rudd at the incident electron energies of 50, 100, and 200 eV. In each curve, the part on the right side of the minimum is the energy distribution of the corresponding primary electrons.

Finally we should mention the energy loss of the incident electron in the ionizing collision. By definition, the energy loss is given by

$$(\Delta E)_{\mathrm{ion}} = E_0 - E_1 = I_{\mathrm{p}} + E_2. \tag{5.52}$$

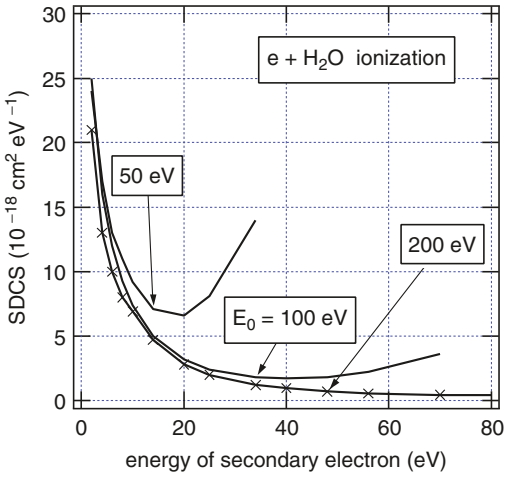

Fig. 5.30. Singly differential cross-sections for the ionization of H_2O [15]. The incident electron energy (E_0) is indicated

The energy loss is not a constant value, but continuously distributed according to the function $q(E_0, E_2)$. If we observe an electron energy loss spectrum (EELS), the contribution of ionization appears as a broad peak. The shape of the peak depends on the incident energy. The mean energy loss is calculated as

$$\begin{aligned}\langle(\Delta E)_{\text{ion}}\rangle &= \frac{1}{Q_{\text{ion}}}\int_0^{E_{\text{x}}/2} \mathrm{d}E_2\ (I_{\text{p}} + E_2)\ q(E_0,\, E_2) \\ &= I_{\text{p}} + \frac{1}{Q_{\text{ion}}}\int_0^{E_{\text{x}}/2} \mathrm{d}E_2\, E_2\, q(E_0,\, E_2). \end{aligned} \tag{5.53}$$

5.8 Electron Attachment

Some (not all) atoms and molecules can bind one more electron to form a negative ion. Those atoms and molecules are said to have a positive electron affinity (EA). In electron–molecule collisions, there are three different processes of electron attachment:

1. Radiative attachment

$$\mathrm{e} + \mathrm{AB} \rightarrow \mathrm{AB}^- + h\nu.$$

2. Three-body attachment

$$\mathrm{e} + \mathrm{AB} + \mathrm{M} \rightarrow \mathrm{AB}^- + \mathrm{M}.$$

3. Dissociative attachment (DA)

$$\mathrm{e} + \mathrm{AB} \rightarrow \mathrm{A} + \mathrm{B}^-.$$

Since the radiative attachment has a very small cross-section, we describe here only the other two processes.

Negative ions play particular roles in molecular plasmas. In the lower region (below about 90 km) of Earth's ionosphere, most of the ions are negative ones. Atmospheric pollution involves a complicated scheme of negative ion reactions. Electron-attaching gas (e.g., SF_6) is commonly used as an insulator in high-voltage technology. An electronegative plasma is a source of negative ion beams, which are then converted into beams of neutral particles. The presence of negative ions alters the discharge operation. The dominance of negative ions much distorts the electron energy distribution and particularly the structure of plasma sheath. Thus, it is a fundamental issue to know what kind of, and how many, negative ions are present in the molecular plasma considered. Electron attachment has been reviewed many times (for example, [27, 72]).

5.8.1 Dissociative Attachment

Dissociative attachment is a kind of resonance process. It proceeds through a (doubly) excited state of the negative molecular ion in such a way as

$$\mathrm{e} + \mathrm{AB} \rightarrow (\mathrm{AB}^-)^{**} \rightarrow \mathrm{A} + \mathrm{B}^-.$$

One typical example of the potential diagram for a DA process is illustrated in Fig. 5.31. In this case the negative ion state is repulsive and crosses the ground state of the neutral molecule at the internuclear distance $R = R_x$. When R is smaller than R_x, the negative ion is unstable against the autodetachment of electron (i.e., $\mathrm{AB}^- \rightarrow \mathrm{AB} + \mathrm{e}$). Once R exceeds R_x, the dissociation to $\mathrm{A} + \mathrm{B}^-$ occurs automatically. When the neutral molecule AB is initially in its vibrationally ground state, the attachment takes place only for the electron

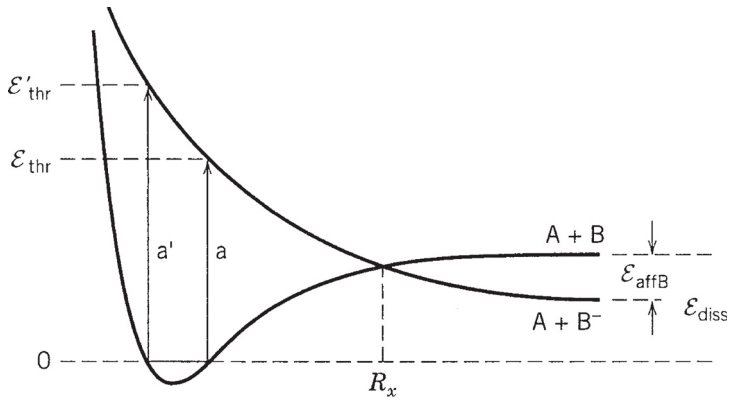

Fig. 5.31. Potential diagram of a diatomic molecule for the mechanism of dissociative attachment, reproduced from [100]

energies in the region from $\mathcal{E}_{\rm thr}$ to $\mathcal{E}'_{\rm thr}$. The width of the energy range depends on the steepness of the repulsive potential curve. Sometimes the dissociative attachment has a finite value of cross-section only in a very narrow range of electron energy. When the negative ion state has an attractive potential, DA can occur through the excitation to the vibrational continuum of the negative ion (i.e., the state located above the dissociation limit of AB^-).

A measurement of the DA cross-section is rather easy. It is suffice to detect negative ions. As in the case of positive ion production (see Sect. 5.7), we have two kinds of cross-sections: partial and total. The partial cross-section is defined for the production of a specific negative ion. The total cross-section is the sum of all the partial ones. To obtain partial cross-sections, an identification of the product ion has to be made spectrometrically. The total cross-section can be independently determined by the measurement of the negative ion current. Since no multiply charged negative ions are produced in electron–molecule collisions, we have no counting cross-section in this case. When one evaluates the quality of the experimental data on the DA cross-section, care should be taken particularly about the following points. First, as is in other cases of resonance, cross-sections may have fine structure as a function of electron energy. Any beam-type experiment should be made with energy resolution high enough to resolve the structure. Secondly, the product negative ion, particularly light one (e.g., H^-), often has a significant speed. In that case, one should be careful to have all the product ions detected. Otherwise the resulting cross-section may be too small.

As an example, we show in Fig. 5.32 the DA cross-sections for H_2O. When an electron collides with H_2O, three different negative ions (H^-, O^-, and OH^-) are produced. In the figure, the DA cross-section is shown separately

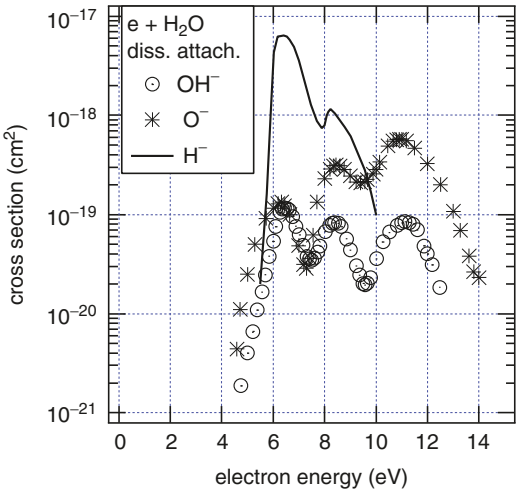

Fig. 5.32. Dissociative attachment cross-sections for H_2O. Partial cross-sections for the production of H^-, O^-, and OH^- are shown

for the production of each ion. These are the recommended values reported in a compilation by Itikawa [79]. They are the result of a beam-type experiment. DA cross-sections are also obtained with a swarm method. A small amount of the electron-attaching gas is added in an ordinary swarm experiment. From the measurement of the effect of the attachment process on the electron current, the DA cross-section is derived. With this method, only the total DA cross-section is determined. Figure 5.33 gives the cross-section for HCl recommended by Itikawa [79]. That was originally obtained with a swarm method by Petrović et al. [129]. From HCl, we can have two different negative ions: H^- and Cl^-. Because of a large EA, Cl^- can appear at very low collision energies of electrons. The cross-section shown in Fig. 5.33 must correspond to the production of Cl^- (see [79]). DA cross-sections for other molecules can be found in Itikawa's compilation [79].

Dissociative electron attachment has a special practical importance. The threshold energy of DA is lower than that of ordinary dissociation by the amount of the binding energy of the negative ion (i.e., electron affinity). That is, the threshold of DA is given by

$$\Delta E(\mathrm{AB} \rightarrow \mathrm{A} + \mathrm{B}^-) = D(\mathrm{AB} \rightarrow \mathrm{A} + \mathrm{B}) \; - \; E_{\mathrm{aff}}(\mathrm{B} \rightarrow \mathrm{B}^-). \tag{5.54}$$

Here D and E_{aff} are the dissociation energy and the electron affinity, respectively. If EA of B is sufficiently large, DA can occur even at zero-energy of electrons. In the case of $CCl_4 \rightarrow Cl^-$, for example, we have $D(CCl_4 \rightarrow CCl_3 + Cl) = 3.17\,\mathrm{eV}$ and $E_{\mathrm{aff}}(Cl) = 3.61\,\mathrm{eV}$. Then the threshold of DA is $-0.44\,\mathrm{eV}$ (see [72]). Reflecting this fact, the DA cross-section for $CCl_4 \rightarrow CCl_3 + Cl^-$ increases with decreasing energy and reaches $4.6 \times 10^{-13}\,\mathrm{cm}^2$ at $0.001\,\mathrm{eV}$ (see [79]). Thus molecules can be dissociated at relatively low collision energies, if a dissociative attachment is possible. Since a large fragment

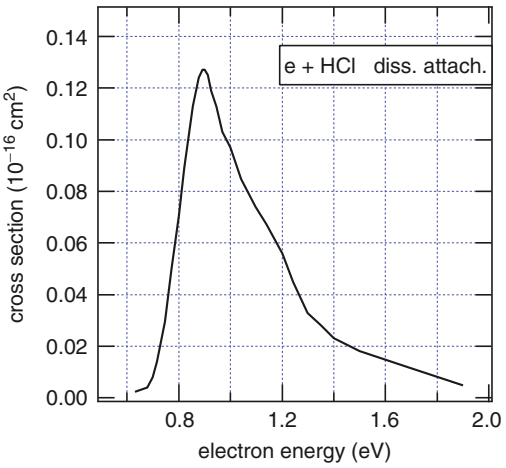

Fig. 5.33. Total dissociative attachment cross-section for HCl

molecule has a possibility to have a large EA, the dissociation via DA is a hot issue in the study of electron collisions with large biomolecules.

5.8.2 Three-Body Attachment

When a molecule AB itself has a positive EA, a negative ion of the parent molecule, AB^-, can be formed. In principle, a two-body collision, $e + AB$, cannot produce AB^-, because the conservation of energy and momentum is violated. (For an exceptional case, see Sect. 5.8.3.) But if a third body is participated in the collision and takes away the excess energy from the colliding two-body system, the product AB^- is stabilized to appear. The rate of the electron attachment is proportional to the number density of the third body, M, as

$$k_{3\text{-att}} = \kappa^{(3)} N[\mathrm{M}]. \tag{5.55}$$

At room temperature, $\kappa^{(3)}$ has a value of $\sim 10^{-31}\,\mathrm{cm}^6\,\mathrm{s}^{-1}$ (see [72]). When we consider a gas with the standard temperature and pressure (i.e., $N \sim 10^{19}\,\mathrm{cm}^{-3}$), the rate coefficient for the three-body attachment is given by

$$k_{3\text{-att}} \sim 10^{-12}\,\mathrm{cm}^3\,\mathrm{s}^{-1}. \tag{5.56}$$

This is rather small compared with the rate coefficient for other collision processes (see Appendix A). It should be noted, however, this is the only effective process to produce a negative ion of the parent molecule (but see Sect. 5.8.3).

5.8.3 Metastable Negative Ion

In some cases of large polyatomic molecules, an incoming electron can be captured with no third body present. Such molecules have a large number of normal modes of vibration. The energy gained by the attachment of electron is spent on the excitation of those vibrational motions. The energy is distributed widely over the vibrational modes, so that it is difficult to recover the energy to return to the state before the collision (i.e., detachment of electron). The resulting negative ion of the parent molecule is not stable, but has a rather long lifetime. Two examples are SF_6 and C_6F_6. The lifetimes of the negative ions SF_6^- and $C_6F_6^-$ are 1×10^{-5} and $1.3 \times 10^{-5}\,\mathrm{s}$, respectively (see [72]). In an ordinary system of experiment, those negative ions survive to detect. Figure 5.34 shows the attachment cross-section for SF_6 recommended by Christophorou and Olthoff [25]. Note that the cross-section increases with decreasing energy. The data are mainly based on the experiment by Hotop and his group [92] with an electron beam produced by a laser photoionization of rare gas atoms. By tuning the photon energy to be slightly above the ionization threshold, they succeeded to have a very low-energy electron beam with a high resolution of energy.

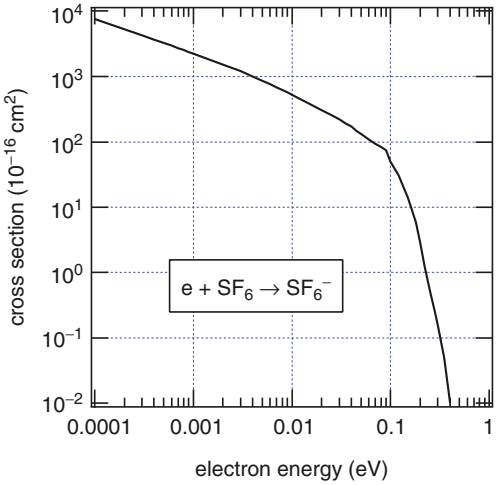

Fig. 5.34. Attachment cross-section for $SF_6 \rightarrow SF_6^-$

5.9 Emission

When molecules are excited, many of them emit radiation to decay to the lower states. The process is schematically expressed as

$$\mathrm{e} + \mathrm{AB}(0) \rightarrow \mathrm{e} + \mathrm{AB}^*(n)$$

followed by

$$\mathrm{AB}^*(n) \rightarrow \mathrm{AB}^*(m) + h\nu(\lambda_{nm}),$$

where the molecule is assumed to be in the ground state (denoted by 0) before the collision. The state m is not necessarily the ground state. The wavelength of the emitted radiation is related to the energies of the initial and final states of the transition

$$\lambda_{nm} = \frac{h\,c}{E_n - E_m}. \tag{5.57}$$

We introduce an emission cross-section, Q_{emis}, which is defined for the emission of radiation upon collision with electrons.

Emission of radiation from a plasma is one of the main mechanisms of energy loss (i.e., cooling) of the plasma. It plays an important role in the energy balance of the plasma. Emission is also important in the diagnostics of a plasma [39]. Detection of radiation with a specific wavelength implies the presence of a specific atom or molecule. The spectrum of the radiation provides us with the information of the emission mechanism. From the spectroscopic measurement, we obtain the data on the plasma parameters, such as density and temperature. The knowledge of collisional emission is fundamental in the analysis of emissions from a plasma.

Since the detection of radiation is rather easy, Q_{emis} has been measured many times. Many of early measurements of cross-sections were done with this method. Emission measurement has several difficulties, however, to obtain reliable quantitative data. First it is not easy to determine the absolute magnitude of the intensity of radiation. The standard method is to normalize the measured intensity with an emission source of known intensity. The resulting cross-section relies on the quality of the standard source used. In principle, we should detect all the radiation of the specific wavelength emitted. We need to correct the loss of the radiation, if any, between the emitter and the detector. Detection of radiation is made from one direction (often at the right angle to the direction of the incident electron beam). If the emission is anisotropic, we need a correction for that. An emission of radiation from a molecule is not an instantaneous process. It has a short, but finite, lifetime. The detector may miss the radiation, if the emitter moves fast (e.g., an emission from a dissociation fragment). Considering these difficulties, the experimental data on Q_{emis} (particularly old ones) need a careful scrutiny.

To see the magnitude of the emission cross-section, we show in Fig. 5.35 the Q_{emis} for the electron collision with N_2. Each cross-section is specified by the transition

$$(n,\, v^{(n)}) \rightarrow (m,\, v^{(m)})$$

and the wavelength of the radiation. Spectroscopically it is possible to resolve rotational states. When dealing with the emission cross-section, however, we simply ignore the rotational states. The state energies E_n and E_m in (5.57) are meant to include the respective vibrational energies. Figure 5.35 shows

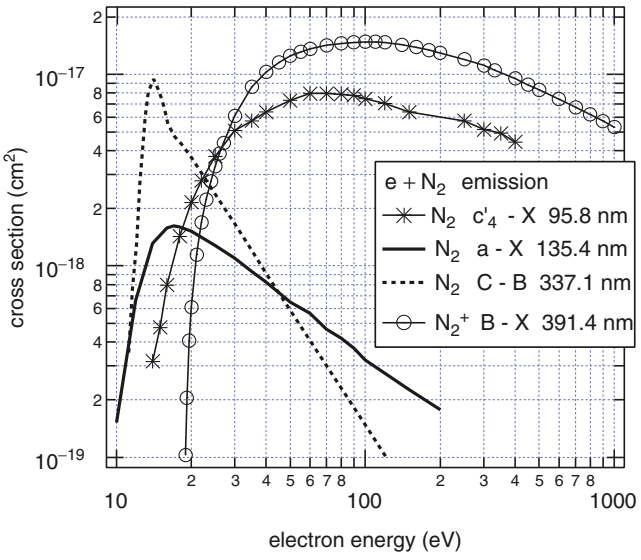

Fig. 5.35. Emission cross-sections for N_2

three strong emissions from N_2 (and one from N_2^+, which is discussed later). They are:

1. $c_4' \, {}^1\Sigma_u^+ \rightarrow X \, {}^1\Sigma_g^+$ (0,0) band at 95.8 nm
2. $a \, {}^1\Pi_g \rightarrow X \, {}^1\Sigma_g^+$ (3,0) band at 135.4 nm
3. $C \, {}^3\Pi_u \rightarrow B \, {}^3\Pi_g$ (0,0) band at 337.1 nm

The numbers in the brackets are $(v^{(n)}, v^{(m)})$. Those cross-sections are taken from the data compilation for the process $e + N_2$ by Itikawa [83]. There are many other emissions reported for N_2, but their cross-sections are small (of the order of $10^{-19}\,\mathrm{cm}^2$ or less) (see [83]).

We have a close relation between the Q_{emis} and Q_{exc}. There are two different ways of the emission of radiation of a certain wavelength λ_{nm}:

(a) Direct excitation

$$\mathrm{e} + \mathrm{AB}(0,0) \rightarrow \mathrm{e} + \mathrm{AB}^*(n, v^{(n)})$$

followed by

$$\mathrm{AB}^*(n, v^{(n)}) \rightarrow \mathrm{AB}^*(m, v^{(m)}) + h\nu(\lambda_{nm}).$$

(b) Cascade

$$\mathrm{e} + \mathrm{AB}(0,0) \rightarrow \mathrm{e} + \mathrm{AB}^*(p, v^{(p)})$$

followed first by

$$\mathrm{AB}^*(p, v^{(p)}) \rightarrow \mathrm{AB}^*(n, v^{(n)}) + h\nu(\lambda_{pn})$$

and then by

$$\mathrm{AB}^*(n, v^{(n)}) \rightarrow \mathrm{AB}^*(m, v^{(m)}) + h\nu(\lambda_{nm}).$$

The state p is one of those states which are located above the state n and connected to n with a dipole-allowed transition. The emission cross-section is given by

$$Q_{\mathrm{emis}}(\lambda_{nm}) = \frac{A^{nm}(v^{(n)}, v^{(m)})}{A^n(v^{(n)})} \, Q_{\mathrm{app}}(n, v^{(n)}), \tag{5.58}$$

where Q_{app} is the so-called *apparent cross-section* and defined by

$$Q_{\mathrm{app}}(n, v^{(n)}) = Q(0, 0 \rightarrow n, v^{(n)}) + Q_{\mathrm{cascade}}(n, v^{(n)}), \tag{5.59}$$

with

$$Q_{\mathrm{cascade}}(n, v^{(n)}) = \sum_p \sum_{v^{(p)}} \frac{A^{pn}(v^{(p)}, v^{(n)})}{A^p(v^{(p)})} \, Q(0, 0 \rightarrow p, v^{(p)}). \tag{5.60}$$

In the above equations, $A^{nm}(v^{(n)}, v^{(m)})$ is the transition probability for $(n, v^{(n)}) \rightarrow (m, v^{(m)})$ and $A^n(v^{(n)})$ is the sum of $A^{nm}(v^{(n)}, v^{(m)})$ over all possible states (m) below n, i.e.,

$$A^n(v^{(n)}) = \sum_{s<n} \sum_{v^{(s)}} A^{ns}(v^{(n)}, v^{(s)}). \tag{5.61}$$

If we can ignore the cascade contribution in (5.59), we have

$$Q_{\text{emis}}(\lambda_{nm}) = \frac{A^{nm}(v^{(n)}, v^{(m)})}{A^n(v^{(n)})}\, Q(0, 0 \to n, v^{(n)}). \tag{5.62}$$

With the Franck–Condon factor approximation (see (5.42)), we can derive Q_{exc} from Q_{emis} in such a way as

$$Q_{\text{exc}}(0 \to n) = \left(\frac{A^{nm}(v^{(n)}, v^{(m)})}{A^n(v^{(n)})}\, F^{0n}_{0,v^{(n)}} \right)^{-1} Q_{\text{emis}}(\lambda_{nm}). \tag{5.63}$$

One example is shown in Fig. 5.36. In the figure, two sets of Q_{exc} for the C $^3\Pi_u$ state of N_2 are compared with each other. One is Q_{exc} derived from the measurement of radiation C $^3\Pi_u \to$ B $^3\Pi_g$ (shown in Fig. 5.35), with the relation (5.63) (i.e., under the assumption of no cascade contribution). The other is the cross-section recommended by Itikawa [83], who determined that from the measurements of EELS. The agreement between the two is good. The difference in the peak region arises probably from the uncertainties of the two experiments (see [83]). Another example is shown in Figs. 5.21 and 5.22. In those figures, the Q_{exc} deduced from the emission measurement is compared with the result of an EELS measurement. In that case the cascade effects were carefully taken into account in the derivation of the excitation cross-section. (See, for the emission measurement, [104].) Again the agreement of the two sets of cross-sections is very good. One of the advantages of the emission measurement is that the experiment is easily done over a wide range of collision energy.

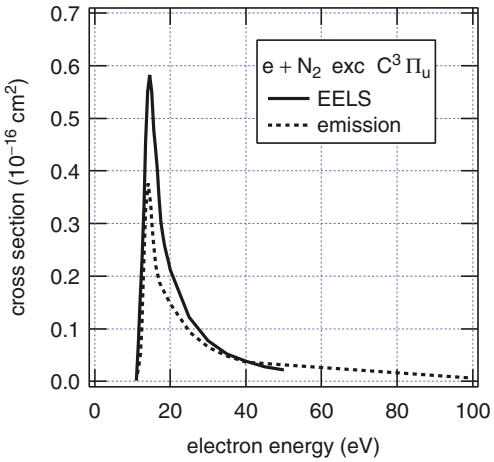

Fig. 5.36. Excitation cross-sections for the state C $^3\Pi_u$ of N_2 (from [83]). Two sets of measurement are compared: EELS measurement and emission measurement

When an electron collides with a molecule, radiation can be emitted simultaneously with ionization or dissociation. It means that the product of ionization or dissociation emits radiation. One example is an emission accompanied by ionization of N_2

$$e + N_2(X) \rightarrow e + N_2^+(B\ ^2\Sigma_u^+) + e$$

followed by

$$N_2^+(B) \rightarrow N_2^+(X\ ^2\Sigma_g^+) + h\nu.$$

The Q_{emis} for the (0,0) band of this transition at 391.4 nm is shown in Fig. 5.35. This emission is rather intense and one of the main features of the aurora (see Sect. 2.1).

An example of emission from a dissociation fragment is given in Fig. 5.37. This is the emission following dissociation of methane:

(1)

$$e + CH_4 \rightarrow H(n)$$

followed by

$$H(n = 3) \rightarrow H(n = 2) + h\nu\ (656.28\,\text{nm}) \quad (H_\alpha\ )$$

and

$$H(n = 4) \rightarrow H(n = 2) + h\nu\ (486.13\,\text{nm}) \quad (H_\beta\ )$$

and

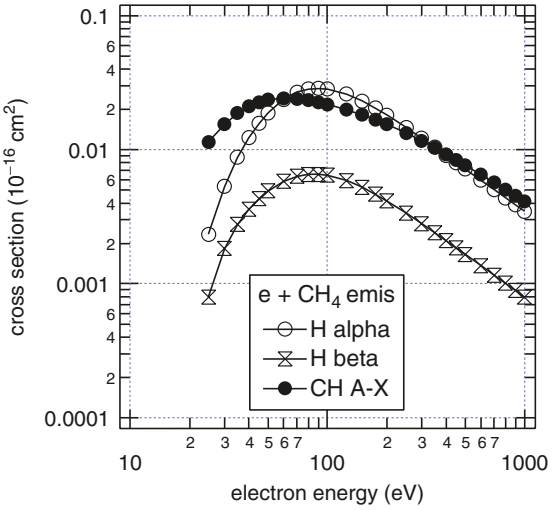

Fig. 5.37. Cross-sections for the emission from H and CH upon electron collisions with CH_4 [116]

(2)

$$\mathrm{e} + \mathrm{CH_4} \rightarrow \mathrm{CH(A\ ^2\Delta)}$$

followed by

$$\mathrm{CH(A\ ^2\Delta)} \rightarrow \mathrm{CH(X\ ^2\Pi)} + h\nu\ (420\text{–}440\,\mathrm{nm}).$$

The experiment was done by Motohashi et al. [116]. Since these radiations are in the visible range of wavelength, they are useful for the diagnostics of CH_4 plasma. From the emission measurement alone, it is impossible to know the fragmentation pattern. For example, the dissociation partner of CH (A) may be $H_2 + H$ or 3H or their ions. Motohashi et al. studied the fragmentation scheme with the detailed measurement of the appearance potentials of each emission.

5.10 Dissociation

Dissociation is a process specifically associated with a molecular target. It is of practical importance, because most of the dissociation products are active species (e.g., radicals) and have a considerable kinetic energy. Dissociation of a molecule is a transition to the continuum state of energy of molecular vibration. When an electron collides with a molecule in its electronically and vibrationally ground state, AB(X, $v^{(\mathrm{X})} = 0$), different schemes of dissociation are possible:

(1) Transition to the vibrational continuum of the electronically ground state

$$\mathrm{AB} \rightarrow \mathrm{AB(X,}\ v^{(\mathrm{X})}\mathrm{=continuum)}$$

(2) Transition to the vibrational continuum of an electronically excited state

$$\mathrm{AB} \rightarrow \mathrm{AB^*}(n,\ v^{(n)}\mathrm{=continuum})$$

(3) Transition to a repulsive electronically excited state

$$\mathrm{AB} \rightarrow \mathrm{AB^*(repulsive)}$$

(4) Predissociation through the coupling of bound and repulsive excited states

$$\begin{aligned}\mathrm{AB} &\rightarrow \mathrm{AB^*}(p,\ v^{(p)})\\ &\rightarrow \mathrm{AB^*(repulsive)}\end{aligned}$$

(5) Two-step process through the radiative decay of the excited state

$$\begin{aligned}\mathrm{AB} &\rightarrow \mathrm{AB^*}(p,\ v^{(p)})\\ &\rightarrow \mathrm{AB^*}(n,\ v^{(n)} = \mathrm{continuum}) + h\nu\end{aligned}$$

Here the excited molecule AB* is assumed to include a molecular ion in its excited state, AB^{+*}. Process (1) is an extension of the vibrational excitation of a molecule in its electronically ground state. It has a small cross-section. Since the radiative transition needs a finite time ($\approx 10^{-8}$ s), process (5) is very slow compared with other processes. In most textbooks, it is not regarded as a *collisional* dissociation. But it plays an important role in the production of radical fragments. In the present section, we deal only with the processes (2)–(4) and a mix of them.

Some of the dissociation fragments have a (positive or negative) charge. The charged particles are easy to detect and separately treated in other sections (dissociative ionization in Sect. 5.7 and dissociative attachment in Sect. 5.8). The subject of the present section is, therefore, concentrated on the production of neutral species, particularly those in the ground or metastable state. Figure 5.38 shows a general feature of dissociation. A comparison is shown there for

$$\begin{aligned} e + H_2O &\rightarrow H^+ + OH + 2e \\ &\quad H^- + OH \\ &\quad H + OH + e. \end{aligned}$$

The corresponding cross-sections are taken from a review of Itikawa and Mason [81]. Dissociative ionization has a higher threshold. Dissociative attachment takes place in a limited range of electron energy and normally has a small cross-section. As is stated below, it is difficult to detect neutral fragments. The process shown in the figure (i.e., $H_2O \rightarrow H + OH$) is one of the exceptional cases for which experimental cross-section is available.

There is no standard method of detection of neutral particles, except for a detection of emission from excited particles. (Dissociative emission is not the

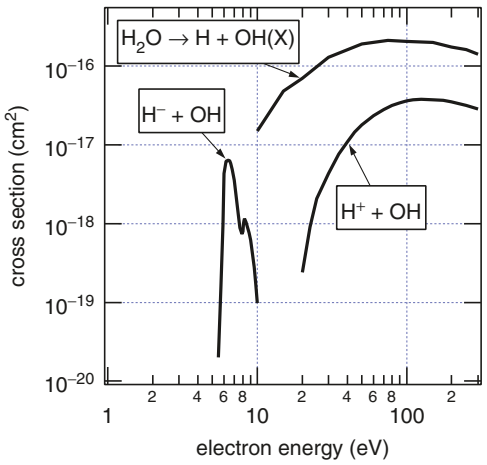

Fig. 5.38. Dissociation cross-sections for H_2O

subject of this section but dealt with in Sect. 5.9.) Various attempts, depending on the processes, have been made to experimentally obtain the dissociation cross-section for neutral products. Several of them, particularly those having a possibility of wide applications, are described below:

(A) *Measurement of total dissociation cross-section*
A total dissociation cross-section is defined here as the sum of the cross-sections for the ionic and neutral products. The cross-section for the production of neutral fragments is denoted by "neutral dissociation cross-section". Consider an experiment where an electron beam is injected into a box filled with molecules to dissociate. If a special metal or metallic compound is chosen as the surface of the box, the dissociation fragments (being active) are adsorbed on the surface. Then the gaseous pressure in the box is reduced. By the measurement of the pressure change, we can deduce the total dissociation cross-section. Subtracting the ionic contribution from the result, we can determine the neutral dissociation cross-section. Two examples are shown in Figs. 5.39 (H_2) and 5.40 (N_2).
Corrigan [29] obtained the dissociation cross-section for H_2. He determined the cross-section (shown in Fig. 5.39) by the measurement of pressure decrease in a closed system where the dissociation fragments are trapped on a getter (MoO_3) surface. He claimed that his result includes ionization cross-section. Yoon et al. [167] subtracted their recommended values of ionization cross-section from the Corrigan's original result to obtain the contribution of neutral fragments. The result is also plotted in Fig. 5.39. A similar experiment was done by Winters [165] for N_2. He measured the pressure decrease by the adsorption of the dissociation

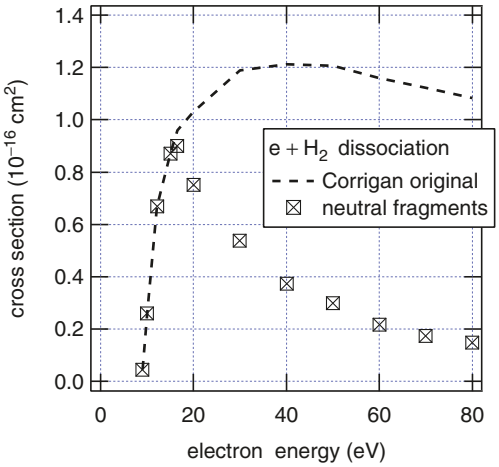

Fig. 5.39. Dissociation cross-sections for H_2. The *dotted line* indicates the total dissociation cross-section measured by Corrigan [29] and *squares* the contribution of neutral fragments (see text)

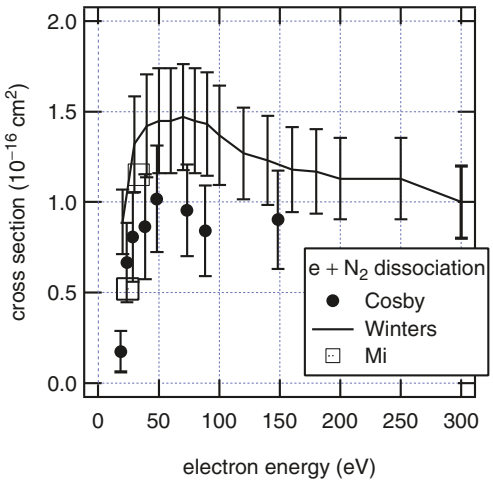

Fig. 5.40. Neutral dissociation cross-sections for N_2, measured by Winters [165], Cosby [31], and Mi and Bonham [111]

fragments on a metallic surface. He derived the dissociation cross-section of N_2, but, as he reported, the result includes the cross-section for the dissociative ionization of N_2. We subtract the dissociative ionization cross-section from the result of Winters. The resulting values are plotted in Fig. 5.40. Winters and his colleagues applied the same method to the measurement of dissociation cross-section for several hydrocarbon and fluoroalkane molecules (see the recent paper on C_2F_6 and references therein [45]).

(B) *Measurement of energy loss spectrum*

A dissociation process appears as a broad peak in an electron energy loss spectrum (EELS). If it is certain that no other peaks overlap with the broad peak, we can derive dissociation cross-section from the measurement of EELS. This is the case of the excitation of b $^3\Sigma_u^+$ state of H_2. The b state is repulsive (i.e., process (3) in the above list). Yoon et al. [167] confirmed that the $Q_{\rm exc}$ obtained from an EELS measurement for the b $^3\Sigma_u^+$ state agrees with the neutral dissociation cross-section obtained by Corrigan (see Fig. 5.39) in the energy range below the peak. In the energy region above the peak, some highly excited states also have a contribution to the dissociation.

From all the inelastic peaks in an EELS, we can determine a total inelastic cross-section, $Q_{\rm tot.inel}$, defined by

$$Q_{\rm tot.inel} = Q_{\rm ion} + Q_{\rm dis} + \sum Q_{\rm exc}. \tag{5.64}$$

If we know the total cross-section for the ionization, $Q_{\rm ion}$, and the sum of all the excitation cross-section, $Q_{\rm exc}$, then we can derive the neutral

dissociation cross-section, Q_{dis}, from $Q_{\mathrm{tot.inel}}$. This is the principle taken by Mi and Bonham [111] when they determined the dissociation cross-section of N_2. Their result is shown in Fig. 5.40. They obtained the cross-section only at two points of energy. Their cross-sections agree well with other data. It should be noted that, in this case, rather detailed data were available for Q_{exc}. The same authors applied the technique to the electron collision with CF_4 [112]. In the case of CF_4, it is known that all the excitations of electronic state lead to dissociation. Hence Q_{exc} in (5.64) can be ignored.

(C) *Detection of fast neutral particles*
If having a sufficient kinetic energy, even a neutral particle can be detected. Cosby [31] produced a fast N_2 beam (3–5 keV) with a charge exchange of N_2^+. With using an electron beam crossed with the fast N_2 beam, he dissociated N_2 into two nitrogen atoms. Since the product N atoms almost keep the velocity of the N_2 beam, they can be detected with a detector sensitive to a high speed particle. Cosby measured the two atoms in coincidence to confirm that they come from the dissociation of N_2. Thus he obtained the neutral dissociation cross-section for N_2, which is also plotted in Fig. 5.40. The cross-section of Cosby agrees with the cross-section measured by Winters (corrected with the ion contribution) within the uncertainties of the two experiments. He applied the same method to the dissociation of CO [30].

(D) *Laser-induced fluorescence*
With a laser of a proper wavelength, we can excite a neutral particle (atom or molecule) to an excited state. The excited particle immediately emits radiation to decay. With detecting the radiation, we can identify the particle. The intensity of radiation is proportional to the number density of the emitting particles. This is the principle of the laser-induced fluorescence (LIF). To determine the *absolute* value of the number density, we need to resort to some normalization procedure. Detecting OH radicals in the ground state with the LIF, Harb et al. [60] determined the dissociation cross-section for the process, $H_2O \rightarrow H + OH(X)$. The result is shown in Fig. 5.41 (and Fig. 5.38). Below the threshold of neutral dissociation ($\rightarrow H + OH$), the dissociative attachment ($\rightarrow H^- + OH$) occurs. In that energy region, the absolute number of OH can be obtained by a comparison to the DA cross-section, which is already known (see Sect. 5.8). The resulting calibration of the apparatus can be used at other energies.
Another example of the LIF method is the detection of $Si(^1S)$ from the dissociation of SiH_4. For the system, Abramzon et al. [2] did the experiment and obtained a peak cross-section of $4.5 \times 10^{-17}\,\mathrm{cm}^2$ at 60 eV. The LIF method seems useful for any dissociation process, but we need a laser with the wavelength corresponding to the excitation energy, and a reliable normalization method.

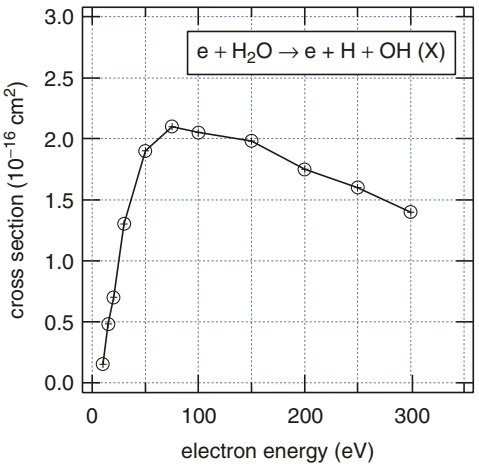

Fig. 5.41. Dissociation cross-section for $H_2O \rightarrow H + OH(X)$, measured by Harb et al. [60] with a LIF method

(E) *Threshold ionization method*
Another method to detect neutral particles is an ionization of them and detection of the charged product. If the ionization cross-section is known, an absolute number of the neutral particles can be determined with this method. For example, we consider the following process

$$e + CH_4 \rightarrow CH_3 + H + e.$$

We can detect CH_3 by the electron-impact ionization

$$e + CH_3 \rightarrow CH_3^+ + 2e.$$

If we know the ionization cross-section of the latter process, we can determine the number of CH_3. In the present case, CH_3^+ is also produced from the ionization of CH_4 (i.e., dissociative ionization). The threshold of the dissociative ionization (14.3 eV) is above the ionization threshold of CH_3 (9.8 eV). If we tune the energy of the electron beam for the dissociation to be below the threshold of the dissociative ionization, we can exclude the CH_3^+ from the parent molecule. This method was applied by Makochekanwa et al. [105] to obtain the dissociation cross-section for the process $CH_4 \rightarrow CH_3 + H$. The result is shown in Fig. 5.42. It is noted that the cross-section was made absolute without resorting to any normalization procedure. The cross-section has peaks at around 9.6 and 11.5 eV. The authors concluded that these peaks are caused by the excitation of different electronic states of CH_4, which lead to the production of CH_3.

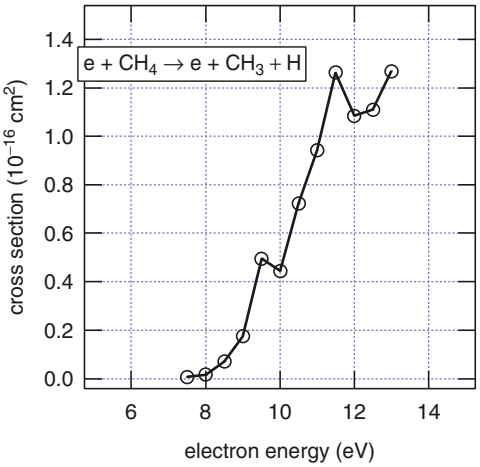

Fig. 5.42. Dissociation cross-section for $CH_4 \rightarrow CH_3 + H$, measured by Makochekanwa et al. [105]

5.11 Total Scattering Cross-Section

The total scattering cross-section is defined by

$$\begin{aligned} Q_{\mathrm{tot}} &= \sum_s Q_s \\ &= Q_{\mathrm{elas}} + Q_{\mathrm{ion}}(\mathrm{tot}) + Q_{\mathrm{dis}}(\mathrm{tot}) + \sum_{\mathrm{exc}} Q, \end{aligned} \tag{5.65}$$

where the last term on the right-hand side means the sum of all the excitation (i.e., rotational, vibrational, and electronic) cross-sections. Some of the excitation processes are known to lead to dissociation. Those excitation processes should be excluded in the summation of excitation cross-sections. When an electron attachment process is possible, (total) attachment cross-section should be included on the right-hand side of (5.65). But usually it has a minor contribution. The Q_{tot} can be measured directly with the beam attenuation method (see Sect. 3.5). Since the method is simple and rather easy to perform, Q_{tot} has been measured since 1930s. As a result, reasonably accurate cross-sections are available over a wide range of energy (see the review and compilation by Karwasz et al. [87]).

The importance of Q_{tot} is twofold. First it serves as the upper limit of cross-section of any process (except for the momentum–transfer cross-section). If any cross-section exceeds the Q_{tot} (after consideration of the respective uncertainties), the experimental method to obtain the former cross-section must be unreliable. One of the advantages of the beam attenuation method is that the absolute value of the cross-section is directly obtained (i.e., without

Table 5.4. Cross-section set for electron collisions with CH_4 [86]

Energy	Q_{elas}	Q_{vib}	Q_{exc}	Q_{ion}	Q_{dis}	Summed	Q_{tot}
1.0	1.66	0.24				1.90	2.13
2.0	5.61	0.21				5.82	5.24
3.0	9.25	0.46				9.71	9.06
5.0	18.0	0.83				18.8	18.9
8.0	26.3	1.33				27.6	26.4
10	23.0	1.02			0.31	24.3	25.9
20	14.4	0.31	1.75	1.22		17.7	20.0
30	11.3		1.75	2.56		15.6	16.5
50	6.57		1.2	3.60		11.4	13.3
100	3.2		0.67	3.92		7.79	9.56
200	2.56		0.37	3.17		6.10	6.31
300	1.63		0.26	2.55		4.44	4.76
500	1.33		0.17	1.85		3.35	3.18

Energy is given in eV and cross-sections are in $10^{-16}\,\mathrm{cm}^2$.

any normalization procedure). The total scattering cross-section, therefore, is used to normalize other cross-sections. Secondly, when we have a set of cross-sections for a specific molecule, the relation (5.65) is used to test the consistency of the member cross-sections of the set. Such a test has been made when the recommended cross-section sets in Appendix D were determined. As is stated in Appendix E, Zecca and his group made an extensive data compilation for a number of molecules. When possible, they summed their selected cross-section values to compare with the available data on the Q_{tot}. One example of such a comparison is shown in Table 5.4. This is a set of cross-sections for CH_4. These cross-sections are taken from the table in the data compilation of Zecca's group [86] and shown only for illustration of the comparison. They are not exactly the same as the corresponding cross-sections presented in other places of the present chapter, but the difference is not significant.

In the case of Table 5.4, the summed values of the individual cross-sections agree well with the total scattering cross-section, except in the region 50–100 eV. At 50 and 100 eV, the summed values are notably smaller than Q_{tot}, which, according to the compilation [86], may be ascribed to the underestimate of the elastic cross-section.

An extensive data compilation of Q_{tot} has been made by Karwasz et al. [87]. After carefully evaluating the available data, they determined the best values of Q_{tot} for a large number of molecules. Figure 5.43, for example, gives their Q_{tot} for O_2 and CF_4. The cross-section for CF_4 has a sharp peak at around 9 eV. This arises from a resonance scattering. At the

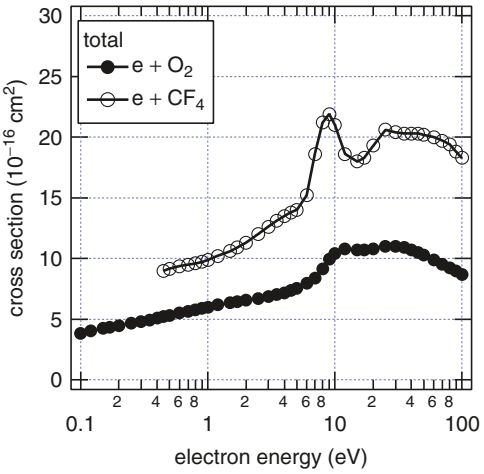

Fig. 5.43. Total scattering cross-sections for O_2 and CF_4

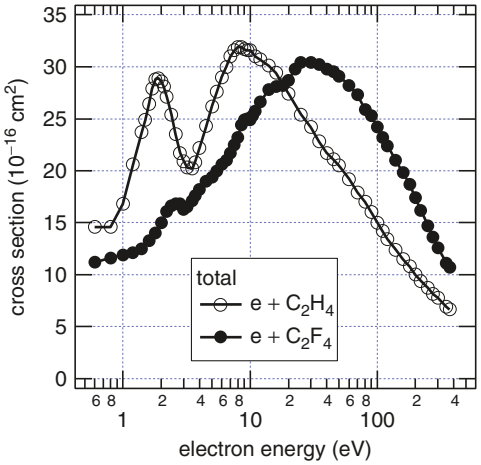

Fig. 5.44. Total scattering cross-sections for C_2H_4 and C_2F_4

peak, Q_{tot} for CF_4 is much larger than the corresponding elastic cross-section shown in Fig. 5.4. The difference comes from the vibrational excitation, which has a large resonance cross-section at the same energy (see the review by Christophorou et al. [24]). Figure 5.44 compares the Q_{tot} for C_2H_4 and C_2F_4 measured by Szmytkowski et al. [151]. In the energy range above 100 eV, Q_{tot} for any molecule has a similar trend. It decreases with increasing energy. In the lower energy range (i.e., < 100 eV), Q_{tot} reflects the characteristics of each molecule. The cross-section of C_2H_4 has a sharp peak at around 2 eV. This may be due to a resonance. C_2F_4 has a larger number of electrons than C_2H_4.

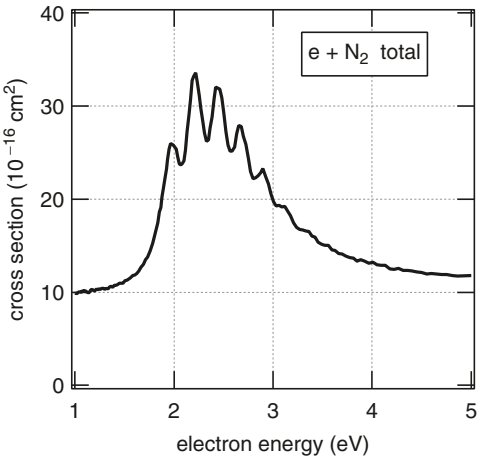

Fig. 5.45. Total scattering cross-section for N_2 in the resonance region

This may be reflected in the cross-section at the higher collision energies. That is, the $Q_{\rm tot}$ for C_2F_4 is larger than that for C_2H_4 in the high-energy region. At the lower energies, the magnitude of $Q_{\rm tot}$ seems to have no relation to the number of molecular electrons.

The beam attenuation method directly determines the energy dependence of the integral cross-section. It is suitable to study fine structure in the energy dependence of the cross-section. One example is the detailed structure caused by a resonant scattering. Figure 5.45 shows the $Q_{\rm tot}$ of N_2 in the resonance region (1–5 eV). This is a part of the cross-section recommended by Itikawa [83]. The cross-section was originally determined by Kennerly [88] with a beam attenuation experiment. The corresponding cross-sections for the elastic scattering and the rotational and vibrational excitations are shown in the respective sections (i.e., $Q_{\rm elas}$ in Fig. 5.1, $Q_{\rm rot}$ in Fig. 5.9, and $Q_{\rm vib}$ in Fig. 5.18). The mechanism of the structure formation is described in Sect. 5.5 in relation to the vibrational cross-section.

5.12 Stopping Cross-Section

Stopping cross-section, defined below, gives a measure of energy transfer during a collision, in the same way as the momentum–transfer cross-section gives a measure of momentum–transfer. The stopping cross-section is defined by

$$S(E) = \Delta E\, Q(E), \tag{5.66}$$

where ΔE is the energy transferred to the target molecule and $Q(E)$ is the corresponding cross-section. For ionization, we have to take into account the

secondary electron, which takes away an energy E_2 (see Sect. 5.7). The stopping cross-section for ionization is given by

$$S_{\rm ion}(E) = \int_0^{E_{\rm x}/2} {\rm d}E_2 \; (I_{\rm p} \, + \, E_2) \; q(E, \, E_2), \tag{5.67}$$

where $q(E, E_2)$ is the energy distribution of the secondary electrons (i.e., the singly differential cross-section for the ionization), $I_{\rm p}$ is the ionization potential of the molecule, and $E_{\rm x} = E - I_{\rm p}$. In the case of elastic scattering, the energy transfer is given by (3.76) in Sect. 3.4. Then the stopping cross-section is written as

$$S_{\rm elas}(E) = \frac{2m_{\rm e}}{M} \, E \, Q_{\rm m}(E), \tag{5.68}$$

where $Q_{\rm m}$ is the (elastic) momentum–transfer cross-section defined in Sect. 5.3.

Using the stopping cross-section, the mean energy loss of an electron per unit path-length in the molecular gas is given by

$$-\frac{{\rm d}E}{{\rm d}x} = \sum N \, S(E), \tag{5.69}$$

where N is the number density of the gaseous molecule and the summation is taken over all the possible collision processes. This is also called the *stopping power* of the gas, leading to the name of the quantity S. It should be noted that the stopping cross-section is not the ordinary cross-section introduced in Sect. 3.1. It has the dimension of energy times area.

When the target molecule is in its excited state, a deexcitation process can occur. In that case ΔE should be negative. Molecules are populated in rotationally excited states even at room temperature. The stopping cross-section for rotational transition is thus calculated by

$$S_{\rm rot} = \sum_{J_0} \sum_{J} F_{J_0} \, \Delta E(J_0 \rightarrow J) \, Q_{\rm rot}(J_0 \rightarrow J), \tag{5.70}$$

where F_{J_0} is the fraction of the molecule in the rotational state J_0.

We show examples of stopping cross-sections in Figs. 5.46 (N_2) and 5.47 (H_2O). Above the threshold of the excitation of the lowest electronically excited state (called the *first excitation threshold*), the stopping cross-section is governed by the excitation of electronic states. (In the higher energy region, ionization also has a significant contribution.)

Here we show the energy region below the first excitation threshold, where electron–molecule collisions have a special feature (see below). Figures 5.46 and 5.47 show the stopping cross-sections for elastic scattering, and rotational and vibrational excitations. To show an example of electronic state excitation, the stopping cross-sections for the excitation of the lowest excited states (A $^3\Sigma_u^+$ state for N_2 and 1 $^3B_1$ state of H_2O) are also presented there. All the stopping cross-sections shown in the figures have been calculated with the

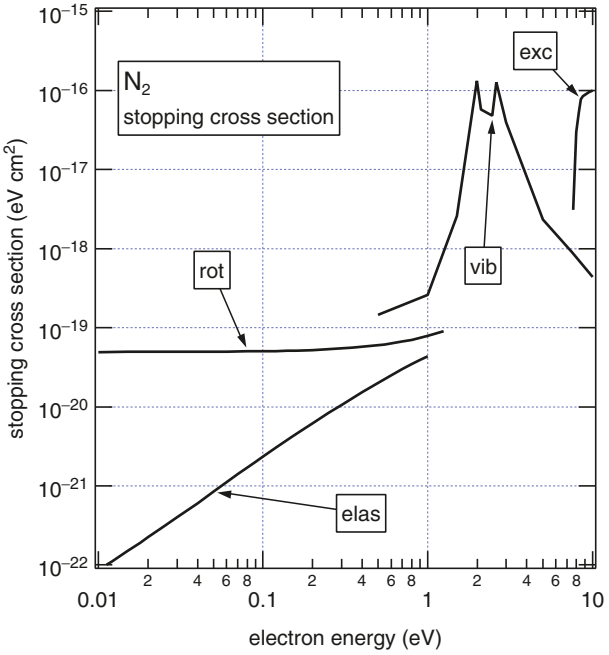

Fig. 5.46. Stopping cross-sections for N_2

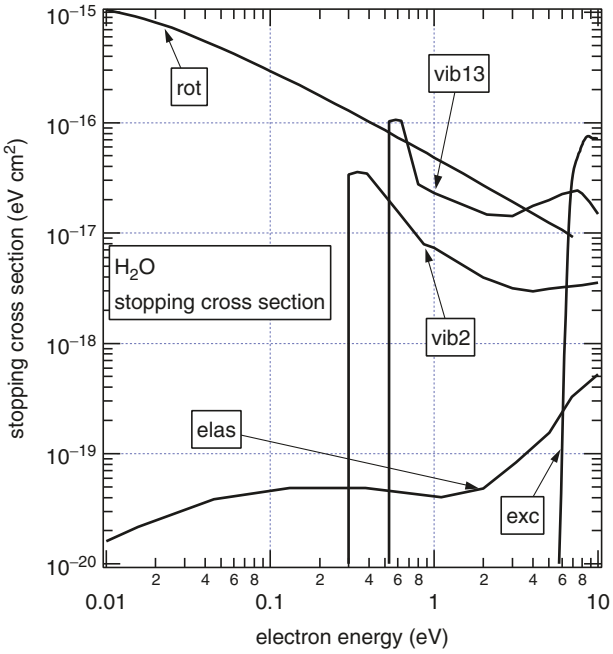

Fig. 5.47. Stopping cross-sections for H_2O

recommended values of the relevant cross-sections (see [83] for N_2 and [81] for H_2O). In Fig. 5.47, vibrational cross-sections for H_2O are shown separately for the bending mode (vib2) and the sum of stretching modes (vib13). Since no experimental data are available for the excitation of 1 $^3B_1$ state of H_2O, theoretical values have been adopted for them [56]. From these two figures, we draw the following conclusions:

1. In the case of electron–molecule collisions, the stopping cross-sections below the first excitation threshold are dominated by the rotational and vibrational excitations. The contribution of elastic scattering is negligibly small (except in the very low-energy region below the threshold of rotational excitation, which is not shown here). Accordingly electrons lose a significant amount of their energy even when the energy is very low (say, much less than 1 eV). This is in clear contrast to the case of atomic targets.
2. In the case of polar molecules, the contribution of rotational transition is very large to the electron energy loss. It even increases with decreasing electron energy. Once in its rotationally excited state, a polar molecule emits microwave radiation to decay to the lower state. This means that a gas of polar molecules is very effective for cooling low-energy electrons.

5.13 Collisions with Excited Molecules

Most of the experiments for electron–molecule collisions are carried out at room temperature. It is implicitly assumed that the target molecules are in their ground state of energy. All of the previous sections in this chapter deal with the electron collisions with molecules in ground state (except for rotational states), although not necessarily say so. In a real plasma, however, we often have a considerable number of molecules in their excited states. In that case, we need information of the electron collisions with those excited molecules.

Consider a collision process

$$\mathrm{e} + \mathrm{AB}(1) \rightarrow \mathrm{e} + \mathrm{AB}(2)$$

and its reverse one

$$\mathrm{e} + \mathrm{AB}(2) \rightarrow \mathrm{e} + \mathrm{AB}(1).$$

We have the following relation of the cross-sections for the two processes

$$g_1 \, E \, Q(1 \rightarrow 2|E) = g_2 \, E' \, Q(2 \rightarrow 1|E'). \tag{5.71}$$

Here g_1 and g_2 are the statistical weights of the initial (1) and the final (2) states, respectively, and E and E' are the electron energies before and after the collision of the process $1 \rightarrow 2$. We have a relation $E = E' + \Delta E(1 \rightarrow 2)$, where

$\Delta E(1 \to 2)$ is the transition energy of the process $1 \to 2$. The relation (5.71) is called "the principle of detailed balancing". Once we have the cross-section for the excitation process, $1 \to 2$, then we can evaluate the cross-section for the deexcitation process, $2 \to 1$, from the relation (5.71). This is one simple way to obtain cross-sections for the excited targets.

In a plasma we have two ways of production of excited molecules: thermal excitation and electron-impact excitation. When a molecular gas is in thermal equilibrium, the energy state of the molecule is distributed according to the Maxwell–Boltzmann distribution function. If the excitation energy of the lowest excited state is large compared with the thermal energy (i.e., $k_{\mathrm{B}}T_{\mathrm{gas}}$), only the ground state is populated. At room temperature, therefore, molecules are almost in the vibrationally and electronically ground states. However, rotational states are widely distributed even at room temperature (see Sect. 4.1). Furthermore, it is usually impossible to experimentally resolve each rotational state. Any cross-section measured should be regarded as an average over the rotational states

$$\langle Q \rangle = \sum_{J_0} F_{J_0}\, Q^{J_0}, \tag{5.72}$$

where Q^{J_0} is the cross-section for the target molecule in its rotational state J_0, the fraction of which is given by F_{J_0}. The fraction is a function of the gas temperature. In this sense, any cross-section measured depends on T_{gas}. No information of the J_0 dependence of a cross-section is available, except for the dissociative attachment (which is discussed later). Most of the processes in the electron–molecule collision are believed to depend slightly on the rotational state of the target.

When the gas temperature increases, vibrational states are also thermally excited. Collisions with the vibrationally excited molecules are of particular importance for polyatomic molecules. Large polyatomic molecules often have vibrational modes with small excitation energy. Those modes are excited even at room temperature (see Table 4.2). Upon excitation, some vibrational modes of polyatomic molecules significantly change the nuclear configuration from that of the ground state. Simply saying, the shape of the molecule is changed by the vibrational excitation. In such cases, collision mechanism might be different for the targets in excited state and those in ground one. One of the experimental evidence is shown in Fig. 5.48. Ferch et al. [44] measured the total scattering cross-section for CO_2 at two values of T_{gas} (250 and 520 K). At 250 K almost all the molecules are in the vibrationally ground state. At 520 K, 69% of CO_2 is in the ground state, but 27% is in the first excited state of bending vibration (its excitation energy being 82.8 meV). The remaining (a few percentage) molecules are in the excited states of other modes. From the analysis of their experimental result, Ferch et al. derived the total scattering cross-section for the ground state, $Q_{\mathrm{tot}}(\mathrm{g})$, and that for the excited state, $Q_{\mathrm{tot}}(\mathrm{v})$. Figure 5.48 shows them. Over the energy range considered, the $Q_{\mathrm{tot}}(\mathrm{v})$ is larger than $Q_{\mathrm{tot}}(\mathrm{g})$. This may be simply due to the difference in

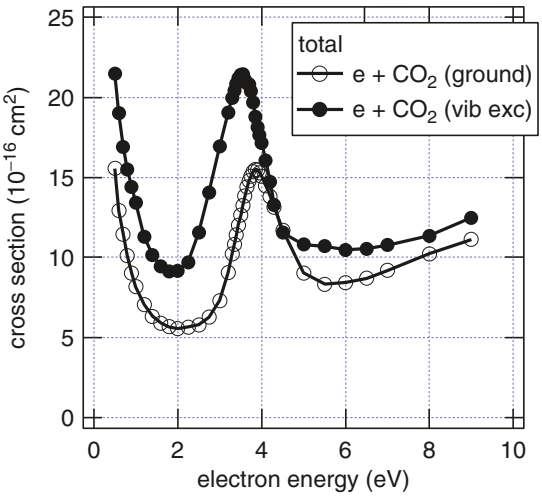

Fig. 5.48. Total scattering cross-sections for CO_2 in its vibrationally excited and ground states, measured by Ferch et al. [44]

the electrostatic interaction, caused by the change in the molecular shape. The peak position of the shape resonance is shifted by about 0.3 eV. Shape resonance is sensitive to the symmetry of the collision system. The difference in the resonance peaks may arise from the change in the symmetry.

Electron impact itself can excite molecules. In a plasma, we usually have a condition that electron temperature is much higher than the gas temperature. As long as the power supply from outside continues, electrons keep exciting molecules. Most of the excited molecules emit radiation to decay to the ground state, or dissociate. Some of the excited molecules (called metastable ones) have a long lifetime. One example is the electronic state A $^3\Sigma_u^+$ of N_2. It has a lifetime of 1.9 s. Armentrout et al. [7] made an experiment of an electron collision with $N_2(A\ ^3\Sigma_u^+)$. They produced the metastable molecule by a charge exchange collision between N_2^+ and NO. About half of the N_2 produced were in the metastable state. Then they hit an electron beam to the resulting N_2 to ionize them. They obtained the ionization cross-section for

$$e + N_2^*(A) \rightarrow N_2^+ + 2e\ .$$

The resulting cross-section is shown in Fig. 5.49. In the figure, the ionization cross-section for the production of N_2^+ from the ground-state nitrogen is also shown (see Fig. 5.26). The ionization threshold is decreased for $N_2^*(A)$ by its internal energy. The absolute magnitude of the ionization cross-section for $N_2^*(A)$ is much smaller than that for the ground state. This difference may be ascribed to the change in the molecular orbitals participating in the ionization process.

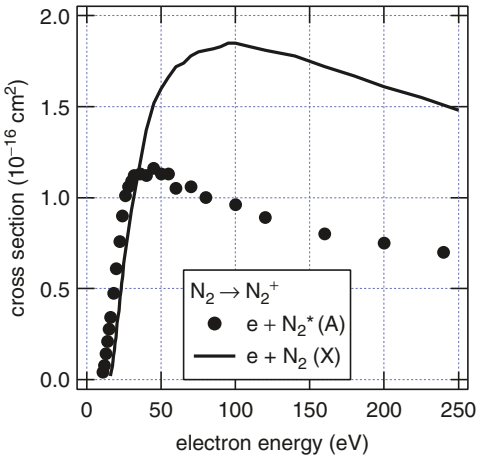

Fig. 5.49. Ionization cross-section for excited nitrogen molecule $N_2^*(A)$, compared with that for the ground-state molecule [7]

When electrons excite vibrations of IR-active mode, the excited molecules immediately emit IR radiation to decay to the ground state. When the vibration is not IR-active (e.g., in the case of homonuclear diatomic molecules), the vibrationally excited molecules have a long lifetime. Electron collisions with those excited molecules are expected to play significant roles in a molecular plasma. At least at present, however, no experimental data are available for the process (except for those shown in Fig. 5.48).

Finally we show one special process which is known to depend strongly on the internal state of the molecule. It is the dissociative electron attachment (DA) (see Sect. 5.8 for the general feature of DA). One typical case is the electron collision with a hydrogen molecule:

$$\mathrm{e} + \mathrm{H}_2(v) \rightarrow \mathrm{H}^- + \mathrm{H}.$$

Allan and Wong [4] measured the yield of the negative ion with varying the temperature of the hydrogen gas from 300 to 1,600 K. With increasing temperature, the ion yield increased enormously, when the electron energy was in the range of 1–5 eV. They attributed this enhancement of ion yield to the vibrational excitation of the hydrogen molecules (and rotational excitations to some extent). From the analysis of their experimental result, Allan and Wong derived the relative magnitudes of the DA cross-sections over the vibrational states from $v = 0$ to 4. The ratio of the DA cross-sections for the molecule in $v = 4$ to $v = 0$ was found to be as much as 4×10^4. It is not easy, however, to experimentally determine the absolute value of the DA cross-section for each vibrational state. On the other hand, there have been many theoretical attempts to obtain the cross-section. Figure 5.50 shows the result of one such calculation by Horáček et al. [69]. They reported a similar dependence of the

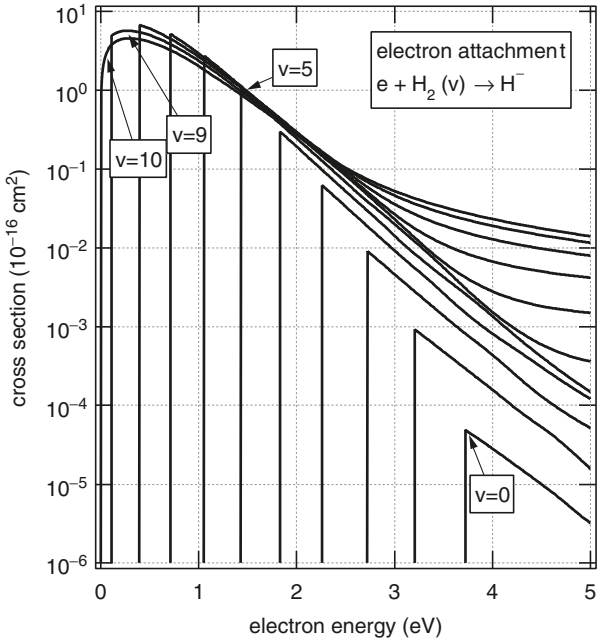

Fig. 5.50. Cross-sections for dissociative electron attachment to vibrationally excited hydrogen molecules, calculated by Horáček et al. [69]

DA cross-sections on the rotational states. But the rotational states have a much less effect than the vibrational ones. They claimed that, using their theoretical result, they could reproduce the temperature dependence of the ion yield observed by Allan and Wong. However, the individual cross-sections shown in Fig. 5.50 have never been confirmed by experiment. When H_2 is vibrationally excited, the internuclear distance has more probability of having a large value. Then the resonance (negative ion) state has a larger chance of dissociation to produce H^- (see the potential diagram in Fig. 5.31). This is a simple qualitative argument for the enhancement of the DA cross-section for high vibrational states of initial molecule. This enhancement of the DA cross-section is now being used for the construction of an efficient H^- source. An electron attachment to other excited molecules is summarized in a review by Christophorou and Olthoff [26].

6

Ion Collisions with Molecules

6.1 Characteristics of Ion Collisions Compared with Electron Collisions

The most prominent characteristic of an ion is that its mass is much larger than the electron mass. Under the same electric field, the ion is much less accelerated than the electron. An ion loses a large fraction of its energy at a collision with neutral molecules, even in an elastic collision. Thus the ions in a molecular plasma do not much deviate from the thermal equilibrium with the neutral molecules, unless the applied field is too strong. This means that the mean energy (i.e., the temperature) of ions is often close to the gas temperature. According to the estimate by Phelps [134], the ion temperature is less than 10 eV, unless the reduced electric field, $\mathcal{E}/N$, exceeds 10^3 Td (1 Td $= 10^{-17}\,\mathrm{V\,cm^2}$). In the present chapter, we mostly deal with the ion–molecule collisions at the ion energies below about 10 eV.

Another characteristic of an ion is the availability of a wide range of species. This is in contrast to the case of electrons (i.e., only one species of electron being available). Most of the ions in a molecular plasma are produced by the electron collisions with molecules. According to Sect. 5.7, an ionization process of AB gives not only the parent molecule ion, AB^+, but also dissociation products A^+ or B^+ or both. High-energy electrons, if any, can produce multiply charged ions (A^{2+}, etc.). Multiply charged molecular ions (AB^{2+}, etc.) are also possible. But most of them are unstable or metastable and have a finite lifetime. An electron attachment process (Sect. 5.8) results in negative ions (AB^-, A^-, etc.). For such processes to occur, the relevant molecules or atoms must have a positive electron affinity. The specific importance of those negative ions is discussed in Sect. 5.8 in relation to the process of electron attachment.

One of the particular features of the ion–molecule collision is its ability of transformation of one species of ion into another species. It is possible through a charge-transfer (charge-changing) collision or a rearrangement one. Because

of the presence of these processes, we have to consider a wider range of ions than those we expect from the constituent molecules of a plasma. For example, as is shown later, we have to consider H_3^+, in addition to H_2^+ and H^+, in a H_2-plasma.

In the present chapter, we separate the ion–molecule collisions into three categories:

1. Momentum–transfer collision
2. Inelastic collision with no change of the incident ion
3. Rearrangement (including charge changing) collision

Each category is described in the following three sections, respectively. The categories (1) and (2) are essentially the same as those in the case of electron–molecule collisions. The category (3) is specific to the ion collisions. For the purpose of illustration, only the collision with positive ions are considered in the following. Very similar processes, however, are possible also for negative ions.

When we consider cross-sections for ion–molecule collisions, we should be careful particularly about the following two points: the definition of the collision energy and the details of the collision products. Unlike in the case of electron collisions, we have to specify the frame of reference where we consider the collision system. The collision energy in the laboratory frame is different from the relative energy (or the energy in the center of mass (CM) frame) (see Sect. 3.4). For a collision between Particle 1 (with mass m_1) and Particle 2 (with mass m_2), the relative energy or the energy in the CM frame, is obtained as

$$E_{\mathrm{CM}} = \frac{1}{2}\mu_{12}v^2, \tag{6.1}$$

where $\boldsymbol{v}$ is the relative velocity between the two particles and $\mu_{12} = m_1m_2/(m_1+m_2)$ is the reduced mass. The laboratory energy, E_{lab}, depends on the laboratory system. Here we consider the system where a beam of particle (Particle 1) collides with a fixed target (Particle 2). The laboratory energy is given by

$$E_{\mathrm{lab}} = \frac{1}{2}m_1v_1^2, \tag{6.2}$$

where $\boldsymbol{v}_1$ is the velocity of Particle 1 (projectile). In this particular case of laboratory system, we have $\boldsymbol{v} = \boldsymbol{v}_1$ and hence

$$E_{\mathrm{CM}} = \frac{m_2}{m_1+m_2}E_{\mathrm{lab}}. \tag{6.3}$$

The CM energy is more important in understanding the physics involved. The laboratory energy is more suitable to express experimental results. Whenever we see cross-section data, we should note which energy is used to specify the data. (In the case of electron collisions with molecules, we have $m_1 \ll m_2$ and hence no significant difference between E_{CM} and E_{lab}.)

Another point to be noted is the collision product. Take a simple system for illustration. When a molecular ion A_2^+ collides with a molecule B_2, we have

$$\begin{aligned} A_2^+ + B_2 \rightarrow & \\ & A_2B^+ + B \quad \text{(a)} \\ & AB_2^+ + A \quad \text{(b)} \\ & AB^+ + AB \quad \text{(c)} \\ & A_2^+ + B_2 \quad \text{(d)} \\ & A_2^+ + B_2^+ + e \quad \text{(e)} \\ & A_2 + B_2^+ \quad \text{(f)} \\ & A_2^+ + B + B \quad \text{(g)} \\ & A + A + B_2^+ \quad \text{(h)} \\ & A^+ + A + B_2 \quad \text{(i)} \\ & A_2 + B^+ + B \quad \text{(j)} \end{aligned}$$

Here any collision product can be in its excited state, although it is not shown explicitly. Then Process (d) means a simple elastic scattering or an excitation of the target molecule or projectile ion. Process (e) is the ionization of the target molecule. Processes (g) and (i) are dissociations of the target and projectile, respectively. All others are a rearrangement, a charge transfer, or a mix of them. In principle we need to indicate the details of the collision products when we specify any of the cross-sections. To make a matter more complicated, a sort of degeneracy arises when A = B. For example, the process

$$H_2^+ + H_2 \rightarrow H_3^+ + H$$

can be either the process (a) or (b) (i.e., a transfer of H or H^+). The two processes are physically different, but difficult to experimentally distinguish. Similarly

$$H_2^+ + H_2 \rightarrow H_2 + H_2^+$$

is a mix of the three processes (c), (d), and (f). We should take into account this kind of degeneracy, when we interpret the experimental result.

As in the case of electron collisions (see Sect. 5.13), an excitation of internal states affects the collision process. Besides the target molecule, the incident molecular ion may be in its excited state. The distribution of the internal (particularly the vibrational) states of the ion strongly depends on the method of production of the ion. When ions are formed by electron impact, their population of vibrational states is usually determined by the Franck–Condon principle similarly to those in the case of excitation of electronic states. Ions are often generated through charge-transfer collisions. In this case, the Franck–Condon rule does not necessarily hold and a more careful analysis is needed. Accordingly the experimental cross-section depends, in principle, on the ion

source used in the experiment. In the evaluation of experimental data for ion collisions, this point should be taken into account.

Because of the complexity and the wide variety of the collision system, it is very difficult to do any comprehensive study of ion–molecule collisions. There are very few systematic compilations of cross-section data for ion–molecule collisions. The cross-sections shown in the following sections are not necessarily the best available ones. In many cases, the cross-section is selected only for the illustration of typical behavior of the collision process.

6.2 Momentum–Transfer

As is in the case of electrons, the velocity distribution of ions in a plasma satisfies the Boltzmann equation. Since the mass of ions is not small compared with the mass of molecules, it is difficult to solve the equation. On the other hand, ions do not deviate much from the thermal equilibrium with molecules, unless a very strong field is applied. In many cases of molecular plasmas, therefore, the velocity distribution of ions can be taken to be Maxwellian. More details of ion kinetics are found in the text book of Mason and McDaniel [107].

In the kinetic or transport phenomena of ions in a plasma, the momentum–transfer cross-section Q_{m} plays a central role, in such a way as in the case of electrons (see Sect. 5.3). There are three different ways to determine Q_{m} for ions. They are

1. Theoretical calculation
2. Estimate from the measured values of transport coefficients
3. Integration of the differential cross-sections (see (5.9))

Since reliable experimental data on the differential cross-section for ion–molecule collisions are available only at high energies (say, $> 1\,\mathrm{keV}$), the last method is not mentioned here.

A calculation of Q_{m} for ion–molecule collisions is a rather complicated problem. We have various levels of approximation. In the simplest way, the ion–molecule collision is assumed as a potential scattering. A spherical model potential is mostly used, but in some cases a more realistic (i.e., anisotropic) model is adopted. To choose a potential scattering means that any inelastic process is ignored in the collision. But, in reality, inelastic collisions (particularly rotational and vibrational transitions) may affect momentum–transfer. The effect of inelastic processes arises in two ways. First, an inelastic collision itself accompanies momentum–transfer. Secondly, a possibility of inelastic processes has to be taken into account when elastic cross-sections are calculated. Furthermore, charge transfer and rearrangement collisions may also have an effect on the momentum–transfer. All of these effects can be taken into account only in the quantum mechanical calculation. But semiclassical or classical theories are often used for the calculation of Q_{m}.

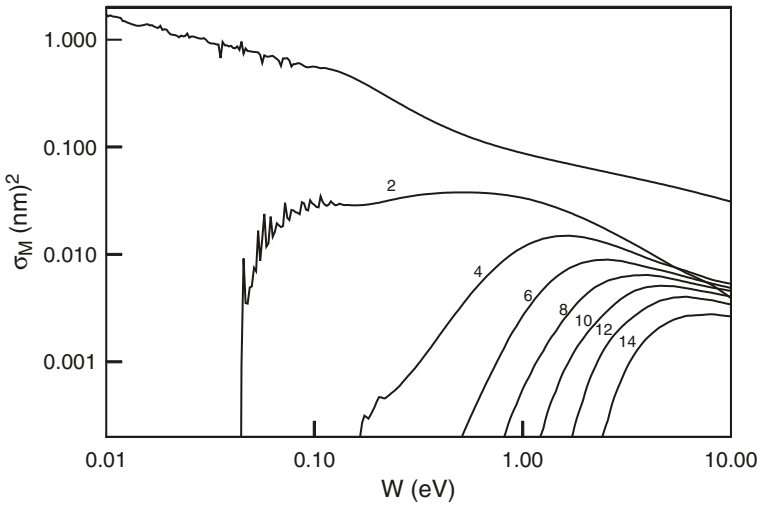

Fig. 6.1. Momentum–transfer cross-sections (in $(\mathrm{nm})^2 = 10^{-14}\,\mathrm{cm}^2$) for $Li^+ + H_2$ (as functions of relative energy) for the rotational transitions $J = 0 \rightarrow J'$ with $J' = 0, 2, \ldots, 14$, calculated by Røeggen et al. [139] (kindly provided by Skullerud)

Figure 6.1 is the result of one elaborate calculation. It shows Q_m for $Li^+ + H_2$ calculated by Røeggen et al. [139]. They made a quantum mechanical calculation with taking transitions among rotational states of H_2 into account. They constructed the interaction between Li^+ and H_2 as accurately as possible. They calculated Q_m for each rotational transition $J = 0 \rightarrow J'$. The figure presents the result for $J' = 0, 2, \ldots, 14$. The elastic process ($J = 0 \rightarrow 0$) has the cross-section much larger than those for inelastic processes. With using their own cross-sections, Røeggen et al. evaluated the mobility of Li-ions in a hydrogen gas. To take an account of inelastic processes more correctly, they did not take a simple method based on Q_m, but took a more detailed method using differential cross-sections for angular distribution. Furthermore they measured the corresponding ion mobility by themselves. Figure 6.2 shows the comparison of the theory and experiment. (The figure shows the reduced mobility, i.e., the mobility normalized to the standard temperature and pressure.) At least at the values of $\mathcal{E}/N$ below 220 Td ($1\,\mathrm{Td} = 10^{-17}\,\mathrm{V\,cm}^2$), the agreement between theory and experiment was very good. They measured the mobility up to 400 Td (not shown in the figure). Above 220 Td, the agreement becomes worse. The disagreement may be ascribed, at least partly, to the neglect of vibrational motion in the theory. They tested the effects of (1) anisotropy of the interaction and (2) inelasticity of the collision. The curve A in Fig. 6.2 is the result obtained using only the isotropic part of the interaction potential. The curve B is the result of the calculation in which the correct form of the interaction is used in the cross-section calculation but the inelastic loss of the energy is ignored in the transport calculation. The anisotropy of the interaction has a significant effect all over the values of $\mathcal{E}/N$. The inelastic effect is important only at high $\mathcal{E}/N$.

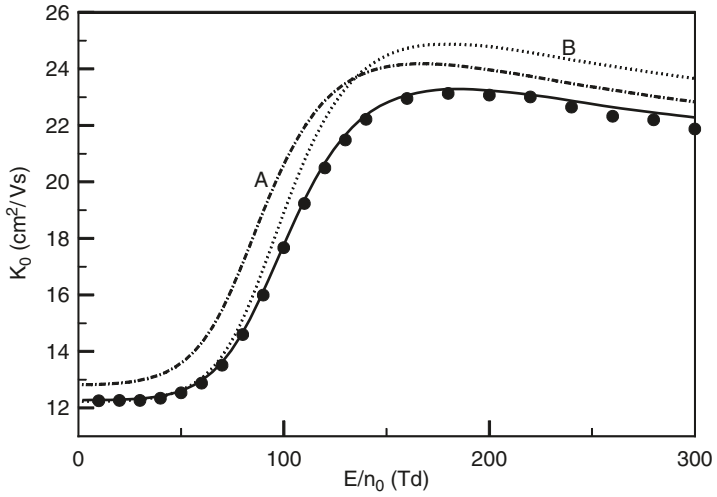

Fig. 6.2. The reduced mobility of Li^+ ions in H_2 at 295 K (reproduced from [139]). Theoretical values (*solid line*) are compared with measurement (*filled circles*). *Curve A* shows the effect of the anisotropy of the interaction and *curve B* the inelastic effect on the mobility (see text)

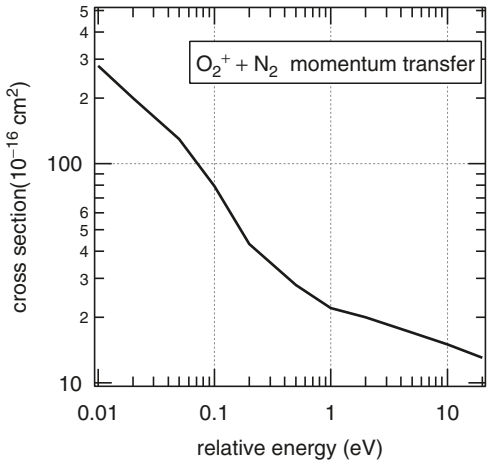

Fig. 6.3. Momentum–transfer cross-section for O_2^+ in N_2, calculated by Nelson et al. [121]

For molecular ions, the interaction potential is so complicated that any elaborate calculation is very difficult to do. Nelson et al. [121] made a simple calculation to obtain Q_m for $O_2^+ + N_2$. They assume a spherical potential for the interaction and employed a semiclassical approach to calculate the cross-section. Figure 6.3 shows the result. They calculated Q_m also for several other systems (e.g., $H_2O^+ + H_2O$, $CO_2^+ + N_2$, etc. [13,120]). With the use of these

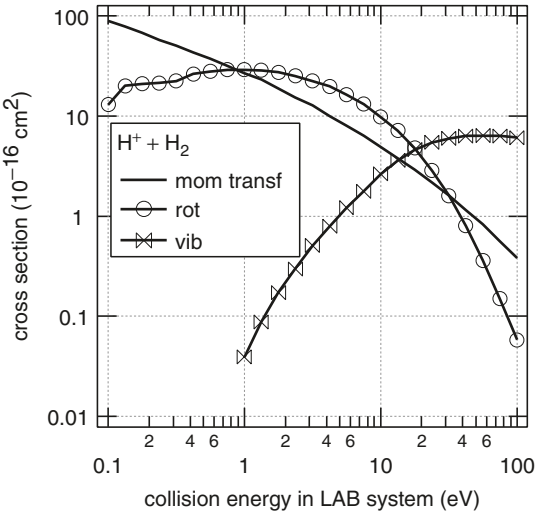

Fig. 6.4. Momentum–transfer cross-section for $H^+ + H_2$. A comparison is made with the rotational ($J = 0 \to 2$) and vibrational ($v = 0 \to 1$) cross-sections

cross-sections, they calculated mobilities and other transport coefficients for those ion–molecule systems by a Monte Carlo method.

Phelps [133] took a simpler method to obtain Q_{m}. He derived the cross-section from experimental data on ion mobility with the use of an approximate relation between Q_{m} and mobility (see, for such relations, [107]). The experimental data on ion mobility was taken from the compilation by Ellis et al. [35]. (Data on ion mobility are available also from [36], [37].) Figure 6.4 presents Q_{m} for $H^+ + H_2$ thus determined by Phelps [133]. In the figure, cross-sections for rotational and vibrational excitations of H_2 are shown for comparison. The validity of these cross-sections is discussed in Sect. 6.3.

In the low-energy limit, we have one universal formula for Q_{m}. When the ion energy is very low, the polarization interaction dominates in the ion–molecule collision. It is the interaction of the incoming ion and the dipole moment induced by the ion in the molecule. The interaction potential is written in the form

$$U_{\mathrm{pol}}(r) = -\frac{\alpha q e^2}{2r^4}, \tag{6.4}$$

where qe is the ionic charge, α is the polarizability of the target molecule, and r is the distance of the ion from the target. Here we consider, for simplicity, only the spherical part of the polarizability. In principle, (6.4) can be used also for the scattering of negative ions. But in that case qe should be the absolute value of the ionic charge. Consider scattering of an ion from the polarization potential. To obtain a representative value of the cross-section, we employ a classical theory, where the motion of the ion is specified with its

impact parameter, b, and incident velocity, v_0 (i.e., the relative velocity of the collision system). The ion motion is governed by an effective potential

$$U_{\text{eff}} = U_{\text{pol}} + U_{\text{c}}. \tag{6.5}$$

Here U_{c} is the centrifugal potential given by

$$U_{\text{c}} = \frac{\mu b^2 v_0^2}{2r^2} = \frac{E_{\text{CM}} b^2}{r^2}, \tag{6.6}$$

where μ and E_{CM} are the reduced mass and the relative kinetic energy of the collision system. The effective potential (6.5) has a maximum value

$$U_{\text{eff}}(\text{max}) = \frac{(E_{\text{CM}} b^2)^2}{2\alpha q e^2}. \tag{6.7}$$

When $E_{\text{CM}} < U_{\text{eff}}(\text{max})$, the ion is repelled by the potential, but, when $E_{\text{CM}} > U_{\text{eff}}(\text{max})$, the incident ion can hit the target. The relation $E_{\text{CM}} = U_{\text{eff}}(\text{max})$ defines a critical impact parameter b_0, which is given by

$$b_0 = \left(\frac{2\alpha q e^2}{E_{\text{CM}}}\right)^{1/4}. \tag{6.8}$$

Any trajectory with the impact parameter $b < b_0$ goes to the scattering center. The incident ion with this trajectory must collide with the molecule. Now we introduce the Langevin cross-section defined by

$$Q^{\text{L}} = \pi b_0^2 = \pi \left(\frac{2\alpha q e^2}{E_{\text{CM}}}\right)^{1/2}. \tag{6.9}$$

We can easily assume that any cross-section for the ion–molecule collision at very low energies has the value of the order of Q^{L}. Heiche and Mason [61] made a rigorous calculation of an ion scattering from the potential U_{pol} in the semiclassical theory. They obtained the momentum–transfer cross-section of the form

$$Q_{\text{m}}^{\text{pol}} = 2.2137\pi \left(\frac{\alpha q e^2}{\mu v_0^2}\right)^{1/2}. \tag{6.10}$$

In practical units, it is rewritten as

$$Q_{\text{m}}^{\text{pol}} = 18.7 \times 10^{-16}\,\text{cm}^2 \left(\frac{q\alpha\,(\text{Å}^3)}{E_{\text{CM}}\,(\text{eV})}\right)^{1/2}. \tag{6.11}$$

As an example, the formula (6.11) is applied to the collision systems shown in Figs. 6.1, 6.3, and 6.4.

$$\begin{aligned}
&\text{For } \text{Li}^+ + \text{H}_2, \quad Q_{\text{m}}^{\text{pol}} = 168 \times 10^{-16}\,\text{cm}^2 \quad \text{at } E_{\text{CM}} = 0.01\,\text{eV},\\
&\text{For } \text{O}_2^+ + \text{N}_2, \quad Q_{\text{m}}^{\text{pol}} = 247 \times 10^{-16}\,\text{cm}^2 \quad \text{at } E_{\text{CM}} = 0.01\,\text{eV},\\
&\text{For } \text{H}^+ + \text{H}_2, \quad Q_{\text{m}}^{\text{pol}} = 64.8 \times 10^{-16}\,\text{cm}^2 \quad \text{at } E_{\text{lab}} = 0.1\,\text{eV}\\
&\qquad\qquad\qquad\qquad\qquad\qquad\qquad\qquad\qquad\qquad (\text{i.e., } E_{\text{CM}} = 0.067\,\text{eV}).
\end{aligned}$$

Compared with the more realistic results shown in the figures, the formula (6.10) or (6.11) gives fairly reasonable (within a factor of two) values of Q_{m} at the low energies of ion.

Finally we mention the effect of charge-transfer collision on the momentum–transfer cross-section. When an ion moves in its parent gas, a symmetric (or sometimes called resonant) charge-transfer process

$$\mathrm{AB}^+ + \mathrm{AB} \rightarrow \mathrm{AB} + \mathrm{AB}^+$$

can occur. In principle, this cannot be distinguished from the simple elastic scattering of AB^+ from AB. Hence this process affects much the momentum–transfer cross-section. To illustrate the effect, we evaluate Q_{m} in a simple semiclassical theory. In the theory, the nuclear motions are assumed to follow classical trajectories. For each trajectory (specified with the impact parameter b), the electron transfer takes place with a probability P_{ex}. Then the momentum–transfer cross-section is written in the form (see [107])

$$Q_{\mathrm{m}} = 4\pi \int_0^\infty P_{\mathrm{ex}} b \, \mathrm{d}b + 2\pi \int_0^\infty (1 - 2P_{\mathrm{ex}})(1 - \cos\theta) b \, \mathrm{d}b, \tag{6.12}$$

where θ is the scattering angle of the incident ion. If P_{ex} is small, this formula gives the conventional definition (in the semiclassical theory) of the momentum–transfer cross-section. Essentially an electron exchange is a result of a close collision. If a long-range interaction dominates, the probability P_{ex} is small. As is stated above, the long-range polarization interaction dominates at low energies of ion–molecule collision. In that case, the charge-transfer process has a minor effect on the momentum–transfer. On the other hand, the second integral in (6.12) is small when electron exchange is dominant. It is because $P_{\mathrm{ex}} \approx 1/2$ for small impact parameters and $\cos\theta \approx 1$ for large impact parameters. (In a close collision, the processes with and without charge transfer can be assumed to occur with equal probability. In a distant collision, the interaction is so weak that the ions slightly deflect.) As a result, when electron exchange is dominant, we have an approximate relation

$$Q_{\mathrm{m}} \approx 2Q_{\mathrm{ex}}, \tag{6.13}$$

where the charge-transfer cross-section Q_{ex} is calculated from

$$Q_{\mathrm{ex}} = 2\pi \int_0^\infty P_{\mathrm{ex}} b \, \mathrm{d}b. \tag{6.14}$$

When the ion energy is fairly large and the charge-transfer process has a significant probability, we have to use the expression (6.13) for the evaluation of the momentum–transfer cross-section. In such a case, the velocity of the incident ion is high and, hence, the slow ion produced by the charge-transfer process can be distinguished from the incident one. Thus the charge-transfer cross-section Q_{ex} can be experimentally determined. More detailed treatment of the charge-transfer process (particularly in the quantum mechanical theory) is given in the text book by Mason and McDaniel [107].

6.3 Inelastic Scattering

The processes dealt with in Chap. 5 for electron–molecule collisions (except for electron attachment) are also possible in the ion–molecule collisions. The essential features of those collision processes are the same in both the collision systems, although the ion–molecule collision is more complicated. Since we concentrate our discussion on the collisions at low energies of ions, we consider here only the ion-impact rotational and vibrational excitations of molecules. For other processes, useful information and typical examples are found in the review papers by Phelps for the collisions H^+, H_2^+, H_3^+ + H_2 [133] and N^+, N_2^+ + N_2 [134]. On the basis of the review by Phelps [133] and other original literature, Tabata and Shirai produced their recommended cross-sections in analytic forms for the collisions of H^+, H_2^+, H_3^+, H, H_2, and H^- with H_2 [152].

First we consider the simplest case, H^+ + H_2. Figure 6.4 presents the cross-sections for the rotational ($J = 0 \rightarrow 2$) and the vibrational ($v = 0 \rightarrow 1$) transitions in H_2 by H^+-impact. They are the values recommended by Phelps [133]. He determined the cross-sections from the theoretical and experimental data available at that time. To understand the behavior of these cross-sections, we compare them, in Figs. 6.5 and 6.6, with the corresponding values for the electron collisions with H_2. The electron cross-sections are taken from Chap. 5 (i.e., the rotational cross-section from Fig. 5.8 and the vibrational cross-section from Fig. 5.13). For the rotational excitation, the H^+ impact has a much larger cross-section than the electron impact. At the low energies, the electron–molecule collision is dominated by a (weak) long-range interaction of the electron with the molecular multipole moment (see Sect. 4.2).

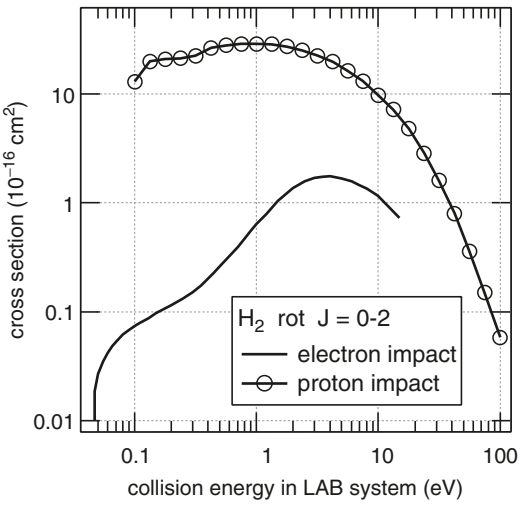

Fig. 6.5. Rotational excitation of H_2. A comparison of the electron-impact excitation and H^+-impact one is shown

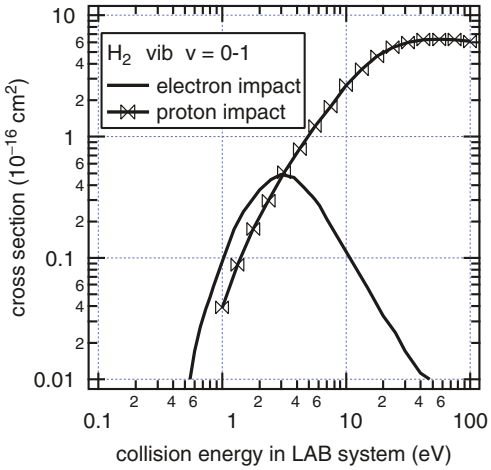

Fig. 6.6. Vibrational excitation of H_2. A comparison of the electron-impact excitation and H^+-impact one is shown

In the ion–molecule collision, the (strong) short-range part of the interaction dominates even at such low energies. The ion–molecule interaction is also strongly anisotropic. (Recall the molecular shape of H_3^+.) These are the reasons why the ion impact rotational excitation has a large cross-section at the low energies.

The mechanism of vibrational excitation of a molecule (except for a resonant process) is as follows. First the incoming charged particle distorts the electron cloud of the molecule. Then the nuclei in the molecule move to adjust their positions to the new configuration of the electron cloud. This results in the excitation of vibrational motion of the molecule. Crudely speaking the distortion of the electron cloud depends on the speed of the incident particle. If it is too fast, the distortion is too small to excite vibrational motion. On the other hand, if the ion speed is too slow, the distortion is caused adiabatically and recovered after the collision. In the present case of vibrational excitation, the most effective energy of ions is around 100 eV. Because of strong short-range interaction, the ion-impact vibrational excitation has a large cross-section. In the e + H_2 system, the broad peak in the vibrational cross-section is thought to be due to a shape resonance.

Šimko et al. [147] made a Monte Carlo simulation of hydrogen plasmas. On the basis of the recommended cross-sections of Phelps, they calculated the transport coefficients (i.e., mobilities and diffusion coefficients) for the ions (H^+ and H_3^+) in the plasma and compared them with measurements. They obtained a good agreement between the calculated and the measured values. In this sense, the cross-sections shown in Fig. 6.4 (rotational and vibrational cross-sections, as well as momentum–transfer one) were confirmed to be reliable.

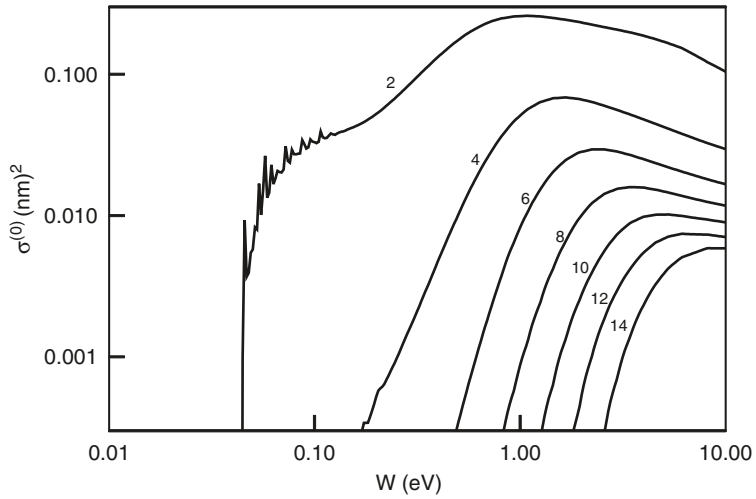

Fig. 6.7. Cross-sections (in $(\mathrm{nm})^2 = 10^{-14}\,\mathrm{cm}^2$) of rotational excitation of H_2 by the collision of Li^+, as functions of relative energy. Calculated values for the transitions $J = 0 \to J'$ with $J' = 2, \ldots, 14$ are shown (reproduced from [139])

As is described in Sect. 6.2, Røeggen et al. [139] made a quantum mechanical calculation of the rotational transitions in the system $Li^+ + H_2$. Besides the momentum–transfer cross-sections shown in Sect. 6.2, they obtained the cross-section for the rotational transitions $J = 0 \to J'$. Figure 6.7 presents their result for $J' = 2, \ldots, 14$. The magnitude of the cross-section for $J = 0 \to 2$ is very large. It is comparable to that of the rotational cross-sections for $H^+ + H_2$, shown in Fig. 6.5. Probably the same mechanism of rotational excitation works for the two collision systems.

The general behavior of the cross-section for a complex (molecular) ion may be much different from the case of atomic ions presented above. When a molecular ion collides with molecules, the ion itself can be excited rotationally and vibrationally. We show one example. That is the vibrational transitions in the collision of N_2^+ and N_2

$$N_2^+(v_1) + N_2(v_2) \to N_2^+(v_1') + N_2(v_2'),$$

where v_1 and v_2 are the vibrational quantum numbers of the two molecules before collision. Even if we restrict the initial states to the ground one (i.e., $v_1 = 0$, $v_2 = 0$), many sets of final states (v_1', v_2') are possible. Figure 6.8 shows the cross-section summed over all possible final states. This cross-section is taken from the review by Phelps [134]. He based this on the calculation by Moran et al. [114]. According to the calculation, the largest contribution comes from the sets (v_1', v_2')=(1, 0) and (0, 1). The cross-sections for the two final sets have a comparable magnitude. Moran et al. made a similar calculation for other systems such as $O_2^+ + O_2$, $CO^+ + CO$, and $NO^+ + NO$.

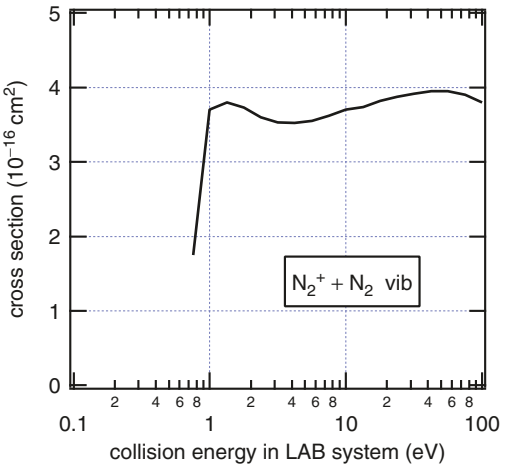

Fig. 6.8. Cross-section for the vibrational transition in the collision, $N_2^+ + N_2$. Initially both the N_2 and N_2^+ are in their ground vibrational states

To show one difficulty in treating a collision of molecular ions, we mention some details of the above process. The same combination of products can be obtained in two ways

$$N_2^+(\text{fast}, v_1) + N_2(\text{slow}, v_2) \rightarrow N_2^+(\text{fast}, {v_1}') + N_2(\text{slow}, {v_2}') \quad \text{(direct)}$$
$$N_2^+(\text{fast}, v_1) + N_2(\text{slow}, v_2) \rightarrow N_2(\text{fast}, {v_2}') + N_2^+(\text{slow}, {v_1}') \quad \text{(charge transfer)}$$

Here we distinguish the charge-transfer process by the difference in the ion speed after the collision. The theoretical calculation providing the cross-section shown in Fig. 6.8 took account of the possibility of both the processes. When the incident ion is fast, charge-transfer cross-sections can be measured. The total (i.e., summed over all the vibrational transitions) charge-transfer cross-sections obtained in the present calculation were compared with the experimental data at the ion energies 30–2,200 eV [46]. A fairly good agreement was obtained between the theoretical and experimental results. This is an indirect confirmation of the reliability of the cross-section shown in Fig. 6.8.

6.4 Reaction

In ion–molecule collisions, electric charge can be transferred and atomic composition of molecules can be changed. In some cases, both the processes (i.e., charge transfer and rearrangement) take place simultaneously, as is shown in Sect. 6.1. We categorically call them "ion–molecule reactions". Depending on the collision system, a wide variety of reactions are possible to occur. A large number of theoretical and experimental studies have been performed for the

reaction processes (see, for example, a review by Lindinger et al. [102]). It is impossible to summarize them here. In the present section, we show only a few characteristic features of the process. For readers' convenience, available compilations of cross-sections (or rate coefficients) are listed in Appendix G.

In most of the reactions among neutral particles, an energy is needed to activate the reactions. This is called an activation energy. Even for the exothermic processes we need an activation energy. It is spent to overcome the potential barrier between the initial and final states of the collision system. In the ion–molecule reactions, however, we normally need no activation energy, because ions are already active (i.e., in the state of high internal energy). This means that an ion–molecule reaction is possible even at a very low temperature.

First we approximately estimate the rate coefficient of ion–molecule reactions at low temperature, with the use of the so-called Langevin model. As is stated in Sect. 6.2, the interaction between an ion and a molecule at the low collision energy is dominated by the polarization interaction. We employ the classical theory of collisions, as in Sect. 6.2. Each collision is specified with an impact parameter b. We compare this with the critical value, b_0, defined by (6.8). When $b > b_0$, the incident ion is scattered away by the target, but, when $b < b_0$, the ion comes into the center of the target to make a reaction possible. Thus the Langevin cross-section Q^{L} (6.9) can be regarded as a representative value (more precisely an upper limit) of the reaction cross-section at low energies. We evaluate the corresponding rate coefficient (called the Langevin rate coefficient) by

$$k^{\mathrm{L}} = \langle v Q^{\mathrm{L}} \rangle, \tag{6.15}$$

where the brackets mean an average over the distribution of relative velocity. Since Q^{L} is inversely proportional to v, the product vQ^{L} becomes independent of v. Then we do not need to know any details of the velocity distribution and have

$$k^{\mathrm{L}} = 2.34 \times 10^{-9}\,\mathrm{cm^3\,s^{-1}} \left(\frac{q\alpha\,(\mathrm{\AA}^3)}{\mu\,(\mathrm{amu})} \right)^{1/2}. \tag{6.16}$$

This rate coefficient does not depend on temperature and gives the value of the order of 10^{-9}–$10^{-10}\,\mathrm{cm^3\,s^{-1}}$, even in the limit $T \to 0$.

In the following, we show a few examples of ion–molecule reactions. First example is the process in which the atomic composition is changed (a rearrangement process). That is

$$\mathrm{H_2^+ + H_2 \rightarrow H_3^+ + H}$$

Due to this reaction, the most abundant ion species in a plasma of hydrogen molecules is $\mathrm{H_3^+}$, instead of $\mathrm{H_2^+}$. Upon collisions with $\mathrm{H_2}$, the plasma electrons produce $\mathrm{H_2^+}$ first. But soon the above process transforms $\mathrm{H_2^+}$ into $\mathrm{H_3^+}$.

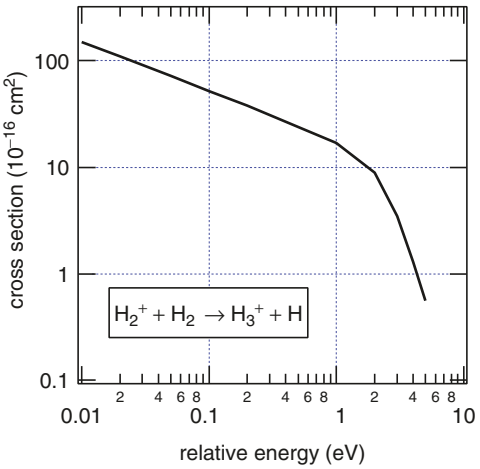

Fig. 6.9. Reaction cross-section for $H_2^+ + H_2 \rightarrow H_3^+ + H$

Figure 6.9 shows the cross-section recommended by Linder et al. [101]. They determined this after a survey of available experimental data. With the use of this cross-section, Stancil et al. [149] evaluated the rate coefficient to be

$$k = 2.24 \times 10^{-9}\,\mathrm{cm^3\,s^{-1}} \left(\frac{T}{300}\right)^{0.042} \exp\left(-\frac{T}{46,600}\right). \tag{6.17}$$

Here T is expressed in K. This equation gives

$$k = 2.23 \times 10^{-9}\,\mathrm{cm^3\,s^{-1}} \quad \text{at } 300\,\mathrm{K},$$

which is compared with the Langevin rate coefficient in this case

$$k^{\mathrm{L}} = 2.10 \times 10^{-9}\,\mathrm{cm^3\,s^{-1}}.$$

Unlike the Langevin rate coefficient, the value (6.17) decreases slowly with decreasing temperature. For the low-energy cross-section, Linder et al. took the experimental result of Gentry et al. [50]. With a merged-beam method, they obtained the cross-section down to the relative energy of 0.01 eV. In the low-energy region, their cross-sections have an energy dependence of $E^{-0.46}$. This is slightly different from the Langevin's formula, $E^{-0.5}$. This difference may be the effect of the interaction other than the polarization.

As mentioned in Sect. 6.1, the above reaction can proceed by two ways. If two hydrogen atoms are distinguished by H_A and H_B, we have

$$\begin{aligned} (H_A)_2^+ + (H_B)_2 &\rightarrow (H_A)_2^+ H_B + H_B \quad \text{(a)} \\ (H_A)_2^+ + (H_B)_2 &\rightarrow H_A^+ (H_B)_2 + H_A \quad \text{(b)} \end{aligned}$$

The process (a) is the atom (H) transfer and (b) is the proton transfer. If both the reactants are in the ground vibrational state before collision, the latter

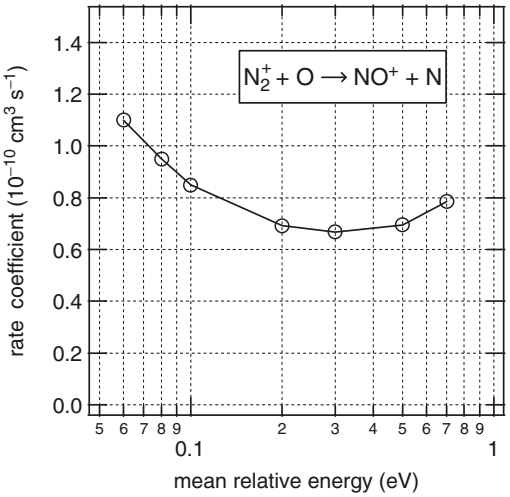

Fig. 6.10. Reaction rate coefficient for $N_2^+ + O \rightarrow NO^+ + N$ [108]

process has a larger exothermicity. Accordingly the proton transfer process must contribute much to the present reaction. However, any experimental confirmation of that is difficult.

As is stated in Sect. 2.1, the most abundant ion species in the lower region of the Earth's ionosphere is NO^+. The most abundant neutral molecule in the region is N_2 and, hence, the solar radiation produces N_2^+ most. But due to the reaction process

$$N_2^+ + O \rightarrow NO^+ + N,$$

the ion N_2^+ is quickly changed into NO^+. McFarland et al. [108] measured the rate coefficient for this process with a drift tube method. In the experiment, the reaction proceeded while the ions were drifting in the tube filled with the reactant molecules. The measured value of the rate coefficient is shown in Fig. 6.10 as a function of mean relative kinetic energy (equivalent to the temperature). In this case we have the Langevin rate coefficient

$$k^{\mathrm{L}} = 6.56 \times 10^{-10}\,\mathrm{cm}^3\,\mathrm{s}^{-1}.$$

This seems too large compared with the measured value. But, if the temperature decreases further, the measured rate coefficient probably reaches somewhere around the Langevin value. In this collision system, a charge-transfer process

$$N_2^+ + O \rightarrow N_2 + O^+.$$

is also possible. McFarland et al. measured the branching ratio of the products and found that 93% of the process goes to $NO^+ + N$.

Finally we show an example of reaction in which the final set of the collision system looks completely the same as the initial one. It is a symmetric charge

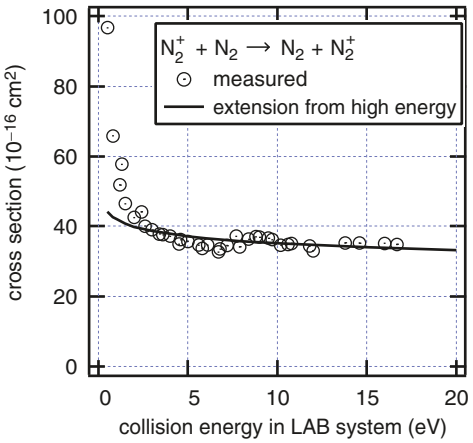

Fig. 6.11. Cross-section for the symmetric charge transfer $N_2^+ + N_2 \rightarrow N_2 + N_2^+$. Measured values are compared with the extension from the high-energy beam data [122]

transfer. For example, Fig. 6.11 shows the cross-section for

$$N_2^+ + N_2 \rightarrow N_2 + N_2^+.$$

This cross-section was obtained by Nichols and Witteborn [122] with shooting a beam of N_2^+ into a nitrogen gas. The product ion is slow compared with the incident one. Then the charge-transfer process can be separated from the elastic collision. If the ion energy is sufficiently high, the measurement of the charge-transfer cross-section is easy to perform. Stebbings et al. [150] measured the cross-section at the ion energy 30–1,000 eV. Nichols and Witteborn fitted the cross-section with a formula

$$Q_{\mathrm{CT}} = (6.48 - 0.24 \ln E(\mathrm{eV}))^2 \times 10^{-16}\,\mathrm{cm}^2. \tag{6.18}$$

An extension of the formula to the lower energies gives the solid line in Fig. 6.11. Above about 3 eV, the measured values agree with the fitted formula. At the lower energies, the experimental data may have a large uncertainty, because it is difficult to produce such a low energy ion beam. Phelps [134] determined his recommended cross-section for the same charge-transfer process, on the basis of his own extrapolation of the result of the high-energy experiment. His values are not much different from the data shown in Fig. 6.11. Another comment is concerned with theoretical calculation. In relation to the data shown in Fig. 6.8, we have mentioned the calculation of the charge-transfer cross-section by Flannery et al. [46]. Since they reported no results in the low energy region, their calculation cannot be compared with the values in Fig. 6.11.

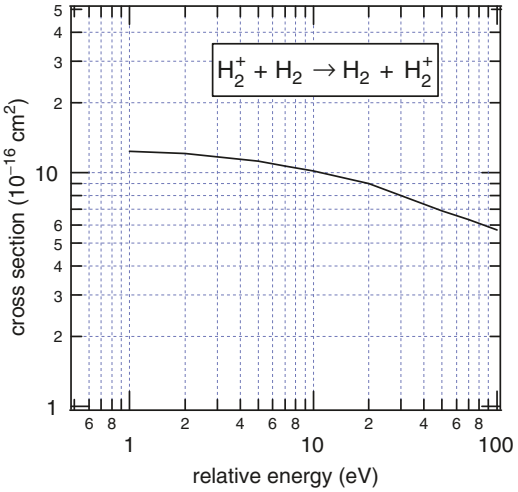

Fig. 6.12. Cross-section for the symmetric charge transfer $H_2^+ + H_2 \rightarrow H_2 + H_2^+$

Another example of the symmetric charge transfer is

$$H_2^+ + H_2 \rightarrow H_2 + H_2^+ .$$

We show in Fig. 6.12 the cross-section recommended by Linder et al. [101]. At the relative energy of 1 eV or less, the collision $H_2^+ + H_2$ also leads to $H_3^+ + H$ (see Fig. 6.9). Considering a possible interference between the two processes, Phelps [133] suggested that the cross-section for the charge transfer (i.e., $H_2^+ + H_2 \rightarrow H_2 + H_2^+$) decreases with decreasing energy below about 5 eV. If we take into account the symmetry of the charge-transfer process, however, the cross-section might increase with decreasing energy. In any case, we have no clear experimental information about the cross-section of the charge transfer in the energy region below 1 eV.

Ion–molecule reactions are affected by the internal degrees of motions (i.e., rotational and vibrational states) of the molecule. When molecular ions are involved, cross-sections are dependent also on the rotational and vibrational states of the ion. There is a fairly large amount of information of the effects of rotational and vibrational excitations on the rate coefficients or cross-sections of ion–molecule reactions [12,102,164]. Rotational energy is efficient at driving endothermic reactions. Exothermic reactions are affected by the rotational motion, only when the collision partner has a large rotational constant. Vibrational effects are much sensitive to the collision systems. In some cases, the vibrational energy has a large effect, but in other cases it does not. Vibrational effects are often significant in charge-transfer collisions.

7

Electron Collisions with Molecular Ions

7.1 General Remarks

In the present chapter, an electron collision with positive molecular ions is considered. If ignoring negative ions, the density of ions is equal to the electron density. Since the electron density is much smaller than the density of neutral molecules in most of molecular plasmas, the electron collision with ions is much less frequent than the electron collision with molecules. Accordingly the electron–ion collisions are less important in molecular plasmas. Furthermore it is difficult to do any experiment of electron–ion collisions, because ions cannot be accumulated enough to serve as the collision target. In fact, very few experimental data are available for the electron–ion collisions. One exception is the electron–ion recombination. It is separately described in Sect. 7.2. In a plasma, the production of ions is balanced with the annihilation of them. In a laboratory plasma, ions attach the surface of the apparatus or electrodes to disappear. In a space plasma, ions annihilate through the recombining collisions with electrons. For example, the ionosphere on the Earth is maintained by the balance of the ionization by solar radiation and the recombination by electron–ion collision. As is shown in Sect. 7.2, most of the molecular ions recombine with electrons through dissociative processes. The recombination process, therefore, produces radicals and reactive atoms. That is, the electron–ion recombination may play a significant role in the production of active species.

Electron–ion collisions can be important in a plasma with high density of ions (e.g., the edge plasma in fusion devices). Mechanism of electron–ion collisions is essentially the same as that of the electron collisions with neutral particles. Here we show some features specific to the electron–ion collisions.

Although no experimental data are available, there are several calculations of vibrational excitation of molecular ions. Figure 7.1 shows the result of calculation by Sarpal and Tennyson [140]. It is the cross-section for the electron-impact vibrational excitation $v = 0 \rightarrow 1$ of H_2^+. The excitation cross-section has a peak at the threshold (i.e., 0.2713 eV). This kind of threshold

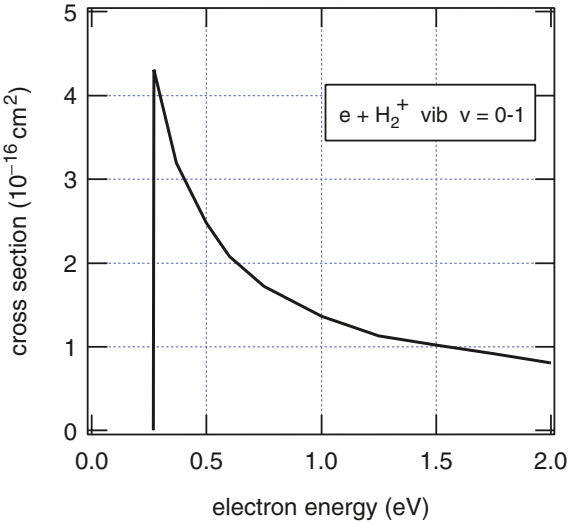

Fig. 7.1. Cross-section for the electron-impact vibrational excitation of H_2^+, calculated by Sarpal and Tennyson [140]

peak is seen in most of the cross-sections for the electron-impact excitation of ions. That is caused by an acceleration of the incoming electron due to the attractive Coulomb force of the ion. The same group of authors made a similar calculation for the excitation of NO^+ [135]. In this case, the cross-section was found to have fine structure due to a resonance. This resonance is caused by a temporary capture of the electron by NO^+ to form a highly excited neutral molecule NO*. Because of the attractive interaction between the electron and ion, this kind of resonance must be common in the electron–ion collisions.

Ionization (or dissociative ionization) of molecular ions has been experimentally studied for a number of ion species. Experimental results for N_2^+ are shown in Fig. 7.2. They are the cross-sections for

$$\begin{aligned} e + N_2^+ \rightarrow\ & N_2^{2+} + 2e \qquad (SI) \\ & N^+ + N + e \qquad (DE) \\ & N^+ + N^+ + 2e \quad (DI) \end{aligned}$$

Here SI, DE, and DI mean single ionization, dissociative excitation, and dissociative ionization, respectively. These were measured by Bahati et al. [11] with a 4 keV-beam of N_2^+ crossed with an electron beam. Spectrometrically N_2^{2+} cannot be distinguished from N^+ (see Sect. 5.7). But, with an analysis of the kinetic energy distribution of the product ions, they could separate each ionization channel. For example, N_2^{2+} in SI has almost the same kinetic energy

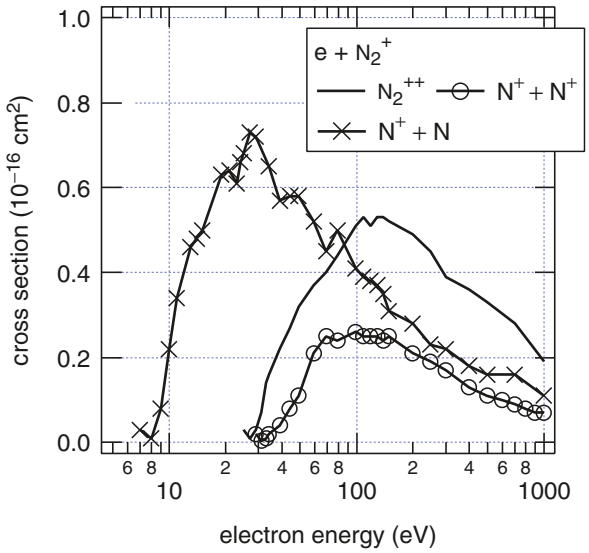

Fig. 7.2. Electron-impact ionization of N_2^+. Cross-sections for three different sets of products, N_2^{2+}, N^++N, N^++N^+ are shown [11]

as the incident ion, but the dissociation fragments (N^+) have a wide range of additional kinetic energies. The DE has the lowest threshold (8.4 eV) and a large peak in the low energy region around 20–30 eV. The SI has the threshold at 27.9 eV. This has the largest cross-section at the energies above 100 eV. Finally the DI has the threshold at 31.2 eV and the smallest cross-section among the three processes. The measured threshold of the N_2^{2+} production was 43.5 eV above the ground state of N_2. The minimum energy to produce $N^+ + N^+$ from N_2 is 38.8 eV (calculated from the ionization potential of nitrogen atom (14.5 eV) and the dissociation energy of N_2 (9.8 eV)). Thus the N_2^{2+} produced is energetically unstable against dissociation to $N^+ + N^+$ (an asymmetric dissociation, $N_2^{2+} \rightarrow N + N^{2+}$, being known to be negligible compared with others). But the experiment did not show such an evidence. This may mean a long lifetime of N_2^{2+}.

Lecointre et al. [97, 98] made a similar ionization experiment of CO^+. Figure 7.3 shows their result for

$$\begin{aligned} e + CO^+ \rightarrow\ & CO^{2+} + 2e \quad (SI) \\ & C^+ + O + e \quad (DE) \\ & C + O^+ + e \quad (DE) \\ & C^+ + O^+ + 2e \quad (DI) \end{aligned}$$

In contrast to the case of N_2^+, the dissociative ionization has the largest cross-section at the collision energy of about 60 eV and above. The cross-section for SI is the smallest all over the energies considered. This means that

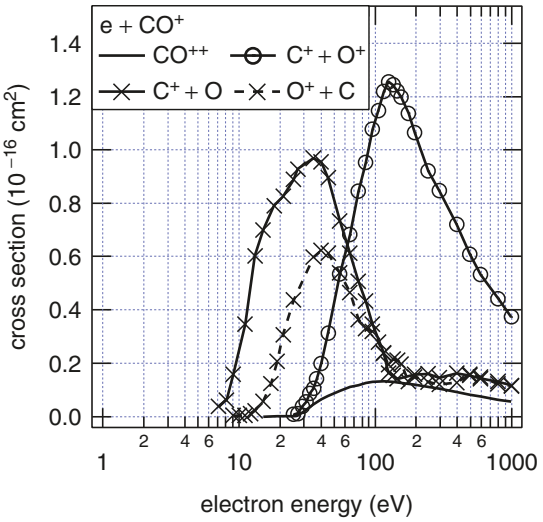

Fig. 7.3. Electron-impact ionization of CO^+. Cross-sections for four different sets of products, CO^{2+}, C^++O, C+O^+, C^++O^+ are shown [97, 98]

CO^{2+} has a short lifetime and mostly dissociates into C^+ and O^+. (Asymmetric dissociations (e.g., $CO^{2+} \rightarrow C^{2+} + O$) were found negligible.) The experimental studies of ionization of molecular ions have been done also for H_2^+ [1], $CO_2{}^+$ [10], and O_2^+ [23].

7.2 Electron–Ion Recombination

7.2.1 Three-Body Recombination

Consider an electron-impact ionization of a molecule

$$e + M \rightarrow e + e + M^+.$$

The inverse process of this is

$$e + e + M^+ \rightarrow e + M.$$

This is called a three-body recombination.

Three-body collisions can occur only when the particle density (i.e., the electron density in this case) is high. In a molecular plasma, this process is dominated by the dissociative recombination, unless the electron density is very high. To estimate the role of the three-body recombination, the rate of the process is evaluated as follows (mostly following Smirnov [148]).

First an electron interacts strongly with an ion. Then a third body (i.e., the second electron) comes close to the colliding system and takes away the

excess energy arising from the recombination process ($e + M^+ \rightarrow M$). The probability of the first process is given by

$$P^{(1)} = N_{\text{ion}} b^3 \,, \tag{7.1}$$

where b is the distance of the incoming electron from the ion and N_{ion} is the number density of the ions. It is assumed that N_{ion} is equal to the number density of electrons (N_{e}). The rate coefficient of the second process is estimated with

$$R^{(2)} = vb^2, \tag{7.2}$$

where v is the relative velocity of the electron and the ion. The effective cross-section for the collision of the second electron with the colliding system ($e + M^+$) is estimated by b^2. The rate coefficient of the three-body recombination is obtained as the product of (7.1) and (7.2),

$$\alpha = P^{(1)} R^{(2)} = vb^5 N_{\text{ion}}. \tag{7.3}$$

Now we estimate b from the relation

$$b \sim \frac{e^2}{T}. \tag{7.4}$$

Here T is the plasma temperature in energy units and the thermal equilibrium is assumed. The formula (7.4) means that the kinetic energy of the plasma particles is balanced with the Coulomb energy of the electron and the ion. Then we have

$$\alpha \sim e^{10} m_{\text{e}}^{-1/2} T^{-9/2} N_{\text{e}}. \tag{7.5}$$

There are several papers reporting the rate coefficient quantitatively. All of them show the rate for the 3-body recombination in the form

$$\alpha_{\text{3-body}} = C \left(\frac{300}{T_{\text{e}}} \right)^{4.5} N_{\text{e}} \times 10^{-20}\,\text{cm}^3\,\text{s}^{-1}, \tag{7.6}$$

where T_{e} and N_{e} are expressed in K and cm^{-3}, respectively. In (7.6), C is a numerical constant having a value between 1 and 10. For instance, Flannery [47] gives $C = 2.7$.

Now we compare the three-body recombination to the dissociative recombination (DR, see Sect. 7.2.2). At 300 K, we have

$$\alpha_{\text{3-body}} \approx 10^{-20} N_{\text{e}}\,\text{cm}^3\,\text{s}^{-1}$$

and

$$\alpha_{\text{DR}} \approx 10^{-7}\,\text{cm}^3\,\text{s}^{-1}.$$

From these relations, the 3-body process is dominant if $N_{\text{e}} > 10^{13}\,\text{cm}^{-3}$ when $T_{\text{e}} = 300\,\text{K}$. From (7.6), the 3-body recombination rate decreases rapidly

with increasing temperature. That decrease is much faster than the rate of DR. The 3-body recombination, therefore, is completely negligible at a high temperature (say, $T_e > 1{,}000\,\mathrm{K}$).

7.2.2 Dissociative Recombination

In a two-body collision, we have two different processes of recombination

$$\begin{aligned} &e + AB^+ \rightarrow AB + h\nu \quad \text{radiative recombination} \\ &e + AB^+ \rightarrow A + B \quad\;\; \text{dissociative recombination (DR)} \end{aligned}$$

The radiative process is very slow compared with the DR. We only deal with DR here. Details of DR processes can be found, for example, in the review articles by Florescu-Mitchell and Mitchell [48] and Adams et al. [3].

In principle, DR is a resonance process and written in the form

$$e + AB^+ \rightarrow AB^{**} \rightarrow A + B^{(*)}$$

That is, it takes place through a temporary capture of the incident electron into an excited state of the target molecule. This mechanism is similar to that of the dissociative attachment (see Sect. 5.8.1). Unlike the attachment, recombination occurs also through an indirect mechanism, where the electron is captured into one of the highly excited (the so-called Rydberg) states of the neutral molecule. There are a large number of Rydberg states converging to the ground state of the molecular ion. The dissociation is possible, when we have a coupling of excited vibrational states of the Rydberg states and the resonant state of the molecule. As is easily understood, nuclear motion of the molecule is involved in the DR process in a complicated manner. The DR rate or cross-section depends sensitively on the rotational and vibrational states of the molecular ion. To understand the mechanism, extensive theoretical studies have been done for, at least, simple molecules (see the reviews cited above).

Experiments of recombination have two intrinsic difficulties. First it is difficult to have sufficient number of ions collected together for targets. Another difficulty is to produce an electron beam of very low energy, at which the DR cross-section has a sizable magnitude. Despite these difficulties, measurements of DR cross-sections have been carried out for many kinds of ions.

Experimental studies of DR are mainly based on two different approaches: afterglow techniques and merged-beam methods. The early experimental study of recombination was made with a stationary afterglow. In the method, the recombination rate was determined from the time dependence of the electron density. No identification was made of the ion species involved. Later the method was replaced with a flowing afterglow. In this method, desired ions are produced with chemical means. These ions and accompanying electrons are put into a flow of buffer gas (e.g., He). The spatial (i.e., along the flow) dependence of the electron density is analyzed in terms of recombination. The ion

is identified spectrometrically. With controlling the temperature of the flow tube, the rate coefficient of DR is determined as a function of temperature.

DR cross-sections as a function of the collision energy are determined with a merged-beam technique (see Sect. 3.5). A fast ion beam is merged with a fast electron beam to enable a sufficient number of collisions between them. After running for a while, the beams of ions and electrons are separated from each other. The method has several advantages. A chance of collision is increased compared with the crossed-beam experiment. By tuning the velocities of the two beams, we can achieve a low relative velocity, which is favorable to the recombination process. The neutral product resulting from the collision has the same velocity as the primary ion beam and is easy to detect. There are two different merged beam methods: single pass and multipass measurements. The multipass measurement is performed with an ion storage ring (see, e.g., [96]), where a high energy ion beam is injected into a quasicircular path consisting of bending magnets. When the pressure in the ring is kept at extremely high vacuum, the ion can be stored there for a long time (up to tens of seconds). Ion storage rings have been developed for use in nuclear physics. A part of the ion beam is usually merged with an electron beam. The main purpose of this is the reduction of the thermal motion of ions (called electron cooling). But it can also be used for an electron–ion collision experiment. More details of these and other experiments can be found, for instance, in the two review articles mentioned above [3, 48].

DR cross-sections and rate coefficients are summarized in several review articles. Only a few examples are shown here. Sheehan and St.-Maurice [145] extensively surveyed the experimental results for the ions of atmospheric molecules (N_2^+, O_2^+, and NO^+). From the survey, they determined the recommended values of rate coefficient. Those are

$$\alpha = 2.2 \times 10^{-7} \left(T_\mathrm{e}/300\right)^{-0.39} \mathrm{cm^3\,s^{-1}} \qquad N_2^+(v=0) \text{ at } T_\mathrm{e} < 1,200\,\mathrm{K}$$
$$\alpha = 1.95 \times 10^{-7} \left(T_\mathrm{e}/300\right)^{-0.70} \mathrm{cm^3\,s^{-1}} \qquad O_2^+(v=0) \text{ at } T_\mathrm{e} < 1,200\,\mathrm{K}$$
$$\alpha = 3.5 \times 10^{-7} \left(T_\mathrm{e}/300\right)^{-0.69} \mathrm{cm^3\,s^{-1}} \qquad NO^+(v=0) \text{ at } T_\mathrm{e} < 1,200\,\mathrm{K}$$

Here the electron temperature, T_e, is expressed in K. These rate coefficients are shown in Fig. 7.4. The above values were determined under the assumption that the initial ion is in the vibrationally ground state. Sheehan and St.-Maurice also estimated the rate coefficient for vibrationally excited molecular ions. Figures 7.5 and 7.6 compare the rate coefficients for $v = 0$ and $v > 0$ in the cases of N_2^+ and O_2^+, respectively. For these ions (and also for NO^+), vibrational excitation of ions yields lower rate coefficients than the value for the ground-state ions. Furthermore Sheehan and St.-Maurice discussed the rate coefficient at the higher temperature (i.e., $T_\mathrm{e} > 1{,}200\,\mathrm{K}$).

In the recombination of ions of polyatomic molecules, different sets of neutral products are possible to appear. The branching ratio of each product is of practical importance. As is shown in Sect. 2.2, for example, an electron recombination with H_3O^+ plays a role in the formation of interstellar molecules.

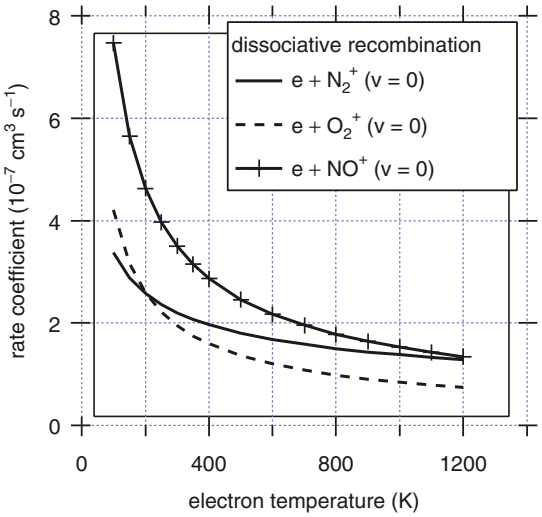

Fig. 7.4. Rate coefficients for dissociative recombination of N_2^+, O_2^+, and NO^+ in their ground vibrational states

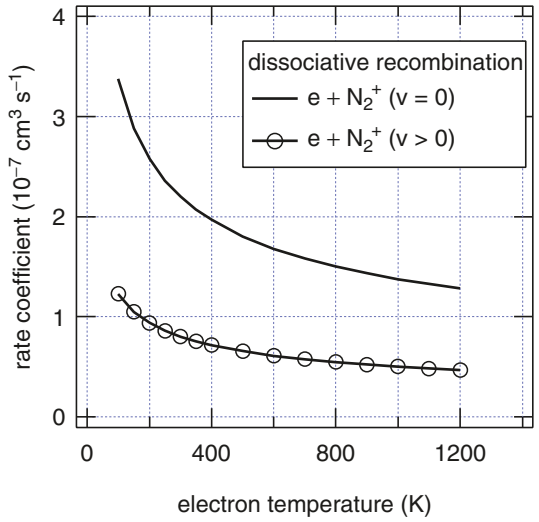

Fig. 7.5. Rate coefficients for dissociative recombination of $N_2^+(v)$, for $v=0$ and $v>0$

The recombination of H_3O^+ results in

$$\begin{aligned} e + H_3O^+ \rightarrow\ & H_2O + H \quad (a)\\ & OH + H_2 \quad (b)\\ & OH + H + H \quad (c)\\ & O + H + H_2 \quad (d) \end{aligned}$$

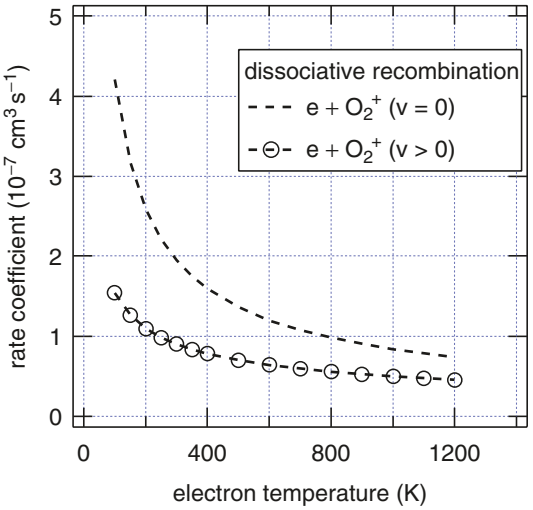

Fig. 7.6. Rate coefficients for dissociative recombination of $O_2^+(v)$, for $v=0$ and $v>0$

With the use of the ion storage ring, ASTRID, Jensen et al. [84] determined the branching ratio of the above process to be (at the collision energy of 0 eV)

$$(a) : (b) : (c) : (d) = 0.25 : 0.14 : 0.60 : 0.01$$

Within uncertainties, this result is in reasonable agreement with the values obtained by another storage-ring (CRYRING) experiment by Neau et al. [119]. But there is a disagreement between these results and the measurement with a flowing afterglow technique (see the review articles [3, 48]).

Another process assigned for the formation of interstellar molecules is

$$\begin{aligned} e + HCO^+ \rightarrow\ & CO + H \\ & O + HC \\ & C + OH \end{aligned}$$

Geppert et al. [51] determined the branching ratio with the ion-storage ring, CRYRING. Their result gives

$$CO : HC : OH = 0.92 : 0.01 : 0.07.$$

The production of three atoms (H + C + O) is too much endothermic to occur.

Other data on the branching ratio are summarized also in the review articles [3, 48].

8

Summary of the Roles of the Molecular Processes in Plasmas

As a conclusion of the present volume, molecular processes are summarized according to the roles they play in molecular plasmas. In principle, all the processes occur simultaneously in the plasma and are intrinsically coupled with each other. In the following, the processes listed in each category are those which directly contribute to the role of the category. Comments on other possible processes are given, when necessary.

1. Generation and maintenance of plasmas
   - Electron-impact ionization (Sect. 5.7)
   - Electron attachment (Sect. 5.8)
   - Electron–ion recombination (Sect. 7.2)

   Ions produced can be converted into other ions through charge transfer and rearrangement processes (Sect. 6.4).
2. Establishment of electron energy distribution function (EEDF)
   - Electron momentum–transfer (Sect. 5.3)
   - Electron-impact excitations of rotational, vibrational, and electronic states (Sects. 5.4–5.6)
   - Electron-impact dissociation (Sect. 5.10)

   Electron attachment (Sect. 5.8) and ionization (Sect. 5.7) induce a change of electron density. But they have a minor effect on the EEDF, unless the electron temperature is too high.
3. Electron transport
   - Electron momentum–transfer (Sect. 5.3)

   Electron-impact excitations of rotational and vibrational states (Sects. 5.4 and 5.5) may have a minor contribution.
4. Production of active species
   (a) For the production of excited molecules
      - Electron-impact excitation (Sect. 5.6)

   (b) For the production of ions
      - Electron-impact ionization (for positive ions) (Sect. 5.7)
      - Electron attachment (for negative ions) (Sect. 5.8)

(c) For the production of active neutral species (i.e., radicals and reactive atoms)
- Electron-impact dissociative ionization (Sect. 5.7)
- Electron-impact dissociative attachment (Sect. 5.8)
- Electron-impact dissociation (Sect. 5.10)
- Dissociative recombination (for neutral fragments) (Sect. 7.2)

(d) For the production of high-energy photons
- Electron-impact emission (Sect. 5.9)

5. Ion transport
   - Ion momentum–transfer (Sect. 6.2)

   Ion-impact excitations of rotational and vibrational states (Sect. 6.3) may have a minor contribution.
6. Conversion of active species
   - Charge changing and rearrangement collisions (Sect. 6.4)

A

Order of Magnitude of Macroscopic Quantities

In a study of kinetic or transport phenomena of electrons or ions in a plasma, it is useful to have an idea about the magnitudes of fundamental macroscopic quantities directly involving cross-sections. Here we consider electron collisions with molecules in a plasma. A recipe of conversion of the resulting values to the ion collision is also given. We assume a typical value ($10^{-16}\,\mathrm{cm}^2$) of collision cross-section and evaluate such macroscopic quantities as mean free path, collision frequency, and mean collision time. We also estimate typical values of rate coefficient. Since we show the formulas for the quantities, it is easy to evaluate them for other values of cross-section. The following symbols are used:

v = electron velocity

Q = cross-section ($= 10^{-16}$ cm^2 as an assumption)

N = number density of the gaseous molecules

T = temperature of the molecular gas

Energies of electrons are indicated in units of eV. In the case of electrons with a thermal distribution of energies, it is convenient to express the mean energy in temperature units. All the tables have an entry for 300 K (corresponding to 0.0259 eV).

1. Rate coefficient
   The magnitude of rate coefficient is represented by vQ, whose typical values are given in Table A.1. Rate coefficient in any real situation is given by vQ averaged over the velocity distribution of electrons (see (3.19) in the text). If the cross-section varies much as a function of velocity, the magnitude of the rate coefficient may be much different from the values shown in Table A.1.

Table A.1. Representative values of rate coefficient, vQ, for electron collisions with molecules, with an assumption, $Q = 10^{-16}\,\mathrm{cm}^2$

Energy	Velocity ($\mathrm{cm\,s^{-1}}$)	Rate coefficient ($\mathrm{cm^3\,s^{-1}}$)
10 eV	1.88×10^8	2×10^{-8}
1 eV	5.93×10^7	6×10^{-9}
300 K[a]	9.54×10^6	1×10^{-9}

[a]Mean electron energy.

Table A.2. Mean free path, collision frequency, and mean collision time for electron collisions with molecules, with an assumption, $Q = 10^{-16}\,\mathrm{cm}^2$

Energy	Pressure	Mean free path (cm)	Collision frequency ($\mathrm{s^{-1}}$)	Mean collision time (s)
10 eV	1 atm.	4.08×10^{-4}	4.60×10^{11}	2.18×10^{-12}
	1 torr	3.11×10^{-1}	6.04×10^8	1.66×10^{-9}
1 eV	1 atm.	4.08×10^{-4}	1.45×10^{11}	6.88×10^{-12}
	1 torr	3.11×10^{-1}	1.91×10^8	5.24×10^{-9}
300 K[a]	1 atm.	4.08×10^{-4}	2.34×10^{10}	4.28×10^{-11}

[a]Mean electron energy.

2. Mean free path, collision frequency, and mean collision time
   According to (3.8), (3.6), and (3.9) in Sect. 3.1, mean free path, collision frequency, and mean collision time are given by

   $$\text{Mean free path} = (NQ)^{-1}$$
   $$\text{Collision frequency} = NvQ$$
   $$\text{Mean collision time} = (NvQ)^{-1}.$$

   Here we evaluate these quantities for two cases of pressure of the molecular gases: 1 atm. and 1 torr. The gaseous temperature is assumed to be 300 K. Then the corresponding number densities of the gaseous molecules are:

   $$N = 2.45 \times 10^{19}\,\mathrm{cm^{-3}} \quad \text{for 1 atm. and 300 K},$$
   $$N = 3.22 \times 10^{16}\,\mathrm{cm^{-3}} \quad \text{for 1 torr and 300 K}.$$

   The resulting values of mean free path, etc. are presented in Table A.2.
3. Conversion to the case of ion collisions
   The above formulas are also applied to the ion–molecule collision. In that case, however, the velocity v should be taken as the relative velocity v_{rel} between the ion and the molecule. That is given by

   $$v_{\mathrm{rel}} = (2E_{\mathrm{CM}}/\mu)^{1/2},$$

where E_{CM} is the collision energy in the center-of-mass frame and μ is the reduced mass of the collision system. Or, in practical units, we have

$$v_{\mathrm{rel}}\,[\text{in cm s}^{-1}] = 1.389 \times 10^{6} (E_{\mathrm{CM}}\,[\text{in eV}]/\mu\,[\text{in amu}])^{1/2}.$$

When the ion energy (i.e., E_{CM}) takes the same value as the electron energy, the ratio of the ion (relative) velocity to the electron velocity (v_{e}) is given by

$$v_{\mathrm{rel}}/v_{\mathrm{e}} = 2.342 \times 10^{-2} (\mu\,[\text{in amu}])^{-1/2}.$$

Then the rate coefficient and collision frequency for ion collisions are obtained by those quantities in the above tables multiplied by this velocity ratio. The mean collision time for ions is the value in Table A.2 divided by this ratio. Mean free path is the same in the two cases.

B

Molecular Properties

An understanding of collision processes involving molecules needs the knowledge of properties of those molecules. Information on the molecular properties can be obtained from handbooks, data compilations, or review articles. Even online databases are available these days. Sometime, however, it takes much time to find proper information. In the present appendix, numerical data are collected for the molecular properties necessary to understand the cross-sections shown in the preceding chapters. All of the values in Tables B.1–B.4, except for a few with notes, are taken from

CRC Handbook of Chemistry and Physics, ed. by D.R. Lide, 86th Edition (Taylor & Francis, London, 2005)

When the same information is needed for other molecules than those listed here, one should consult this reference. Another useful reference for the molecular properties is

S.V. Khristenko, A.I. Maslov, and V.P. Shevelko, Molecules and Their Spectroscopic Properties (Springer, Berlin, 1998)

Useful data are also available online from

NIST Chemistry Webbook, NIST Standard Reference Database Number 69, Eds. P.J. Linstrom and W.G. Mallard, June 2005, National Institute of Standards and Technology, Gaithersburg, MD 20899, USA (http://webbook.nist.gov).

Table B.5 is based on the data reported in

D.M. Bishop, L.M. Cheung, J. Phys. Chem. Ref. Data 11, 119 (1982)

Table B.1. Ionization potential, dissociation energy, and electron affinity

Molecule	Ionization potential (eV)	Dissociation energy (eV)	Electron affinity (eV)
H_2	15.426	H–H[a] 4.516	
N_2	15.581	N–N 9.798	
O_2	12.070	O–O 5.165	0.450
Cl_2	11.480	Cl–Cl 2.514	2.38
CO	14.014	C–O 11.156	
NO	9.2644	N–O 6.535	0.026
HF	16.044	H–F 5.906	
HCl	12.749	H–Cl 4.470	
H_2O	12.621	H–OH 5.152	
N_2O	12.886	O–N_2 1.735	-0.03 ± 0.1
CO_2	13.773	O–CO 5.45[b]	
O_3	12.43	O–O_2 1.105	2.1028
NH_3	10.070	H–NH_2 4.665	
CF_4	14.7[c]	F–CF_3 5.667	
CH_4	12.61	H–CH_3 4.553	
SiH_4	11.00	H–SiH_3 3.977	
C_2H_4	10.514	H–HC=CH_2 4.822	
SF_6	15.32	F–SF_5 4.059	1.05

[a]Dissociating bond indicated.
[b]From Y. Itikawa, J. Phys. Chem. Ref. Data 31, 749 (2002).
[c]From L.G. Christophorou, J.K. Olthoff, J. Phys. Chem. Ref. Data 28, 967 (1999).

Table B.2. Dipole moment and dipole polarizability

Molecule	Dipole moment (D)[a]	Dipole polarizability[b] ($Å^3$)
H_2		0.8042
N_2		1.7403
O_2		1.5812
Cl_2		4.61
CO	0.1098	1.95
NO	0.1587	1.70
HF	1.8262	0.80
HCl	1.1086	2.63
H_2O	1.8546	1.45
N_2O	0.1608	3.03
CO_2		2.911
O_3	0.5337	3.21
NH_3	1.4718	2.26

Molecule	Dipole moment (D)[a]	Dipole polarizability[b] ($Å^3$)
CF_4		3.838
CH_4		2.593
SiH_4		5.44
C_2H_4		4.252
SF_6		6.54

[a]D=Debye (1 D = 0.393430 a.u.).
[b]Isotropic component.

Table B.3. Excitation energies of the lowest rotational and vibrational states of diatomic molecules

Molecule	Lowest rotational state (10^{-3} eV)	Lowest vibrational state (eV)
H_2	(J=2)[a] 44.13	0.516
N_2	(J=2) 1.480	0.289
O_2	(J=2) 1.069	0.193
Cl_2	(J=2) 0.181	0.069
CO	(J=1) 0.477	0.266
NO	(J=1) 0.412	0.233
HF	(J=1) 5.097	0.491
HCl	(J=1) 2.589	0.358

[a]For homonuclear molecules, only even J states are accessible from the ground ($J = 0$) state.

Table B.4. Vibrational energy of polyatomic molecules (IR-active modes are indicated in Table B.5)

Molecule	Mode of vibration[a]	Lowest vibrational state (eV)
H_2O	ν_1 s-stretch	0.453
	ν_2 bend	0.198
	ν_3 a-stretch	0.466
N_2O	ν_1 NN stretch	0.276
	ν_2 bend	0.073
	ν_3 NO stretch	0.159
CO_2	ν_1 s-stretch	0.165
	ν_2 bend	0.083
	ν_3 a-stretch	0.291
O_3	ν_1 s-stretch	0.137
	ν_2 bend	0.087

Table B.4. Continued

Molecule	Mode of vibration[a]	Lowest vibrational state (eV)
	ν_3 a-stretch	0.129
NH_3	ν_1 s-stretch	0.414
	ν_2 s-deform	0.118
	ν_3 deg.stretch	0.427
	ν_4 deg.deform	0.202
CF_4	ν_1 s-stretch	0.113
	ν_2 deg.deform	0.054
	ν_3 deg.stretch	0.159
	ν_4 deg.deform	0.078
CH_4	ν_1 s-stretch	0.362
	ν_2 deg.deform	0.190
	ν_3 deg.stretch	0.374
	ν_4 deg.deform	0.162
SiH_4	ν_1 s-stretch	0.271
	ν_2 deg.deform	0.121
	ν_3 deg.stretch	0.272
	ν_4 deg.deform	0.113
C_2H_4[b]	ν_1 CH_2 s-stretch	0.375
	ν_2 CC stretch	0.201
	ν_3 CH_2 scis	0.166
	ν_4 CH_2 twist	0.127
	ν_5 CH_2 a-stretch	0.385
	ν_6 CH_2 rock	0.153
	ν_7 CH_2 wag	0.118
	ν_8 CH_2 wag	0.117
	ν_9 CH_2 a-stretch	0.385
	ν_{10} CH_2 rock	0.102
	ν_{11} CH_2 s-stretch	0.371
	ν_{12} CH_2 scis	0.179
SF_6[c]	ν_1 s-stretch	0.096
	ν_2 deg.stretch	0.080
	ν_3 deg.stretch	0.118
	ν_4 deg.deform	0.076
	ν_5 deg.deform	0.065
	ν_6 deg.deform	0.043

[a]The following abbreviations are used: *s-stretch* symmetric stretching, *a-stretch* antisymmetric stretching, *bend* bending, *deg* degenerate, *deform* deformation, *scis* scissors, *twist* twisting, *rock* rocking, *wag* wagging.
[b]From T. Shimanouchi, *Tables of Molecular Vibrational Frequencies Consolidated Volume I* NBS Ref. Data Series 39 (US Government Printing Office, Washington, DC, 1972).
[c]From L.G. Christophorou, J.K. Olthoff, J. Phys. Chem. Ref. Data 29, 267 (2000).

Table B.5. Dipole matrix element for the lowest transition from the ground state of the IR-active mode of vibration

Molecule	Mode	IR intensity (A) ($\mathrm{km\,mol^{-1}}$)	(Dipole matrix element)$^{2\,a}$ (10^{-3} a.u.)
CO		61.2	1.76
NO		27.3	0.899
HF		77.5	1.21
HCl		33.2	0.711
H_2O	ν_1	2.93	0.0495
	ν_2	62.5	2.42
	ν_3	41.7	0.686
N_2O	ν_1	289	8.03
	ν_2	8.20	0.860
	ν_3	59.1	2.84
CO_2	ν_2	47.8	4.43
	ν_3	498.7	13.1
O_3	ν_1	2.38	0.133
	ν_2	4.4	0.39
	ν_3	85.7	5.08
NH_3	ν_1	4.9	0.091
	ν_2	148	9.62
	ν_3	3.2	0.057
	ν_4	27.1	1.03
CF_4	ν_3	935.3	45.0
	ν_4	12.3	1.20
CH_4	ν_3	65.5	1.34
	ν_4	31.8	1.50
SiH_4	ν_3	320.5	9.03
	ν_4	296.3	20.0
C_2H_4	ν_7	81.25	5.29
	ν_9	24.9	0.495
	ν_{10}	20.3	1.52
	ν_{11}	13.51	0.279
	ν_{12}	9.76	0.418
SF_6	ν_3	1,361	88.7
	ν_4	74	7.4

[a]Calculated from the IR intensity, A, with the use of the relation (5.35) in Sect. 5.5.

C

Atomic Units and Evaluation of the Born Cross-Section

In most of the theoretical papers on atomic collisions, atomic units are used for the presentation of theoretical formulas. According to the convention, the Born cross-sections in this book are also expressed in atomic units. Here the definition of atomic units is given. Examples of the evaluation of the Born cross-section are also presented.

C.1 Definition of Atomic Units

The atomic unit (a.u.) is based on the relation

$$\mathrm{e} = m_\mathrm{e} = \hbar = 1$$

and the unit of length given by the Bohr radius

$$a_0 = 4\pi\epsilon_0\hbar^2/m_\mathrm{e}e^2.$$

The unit length, energy, time, and velocity of atomic unit are given by:

Length: $a_0 = 5.292 \times 10^{-9}\,\mathrm{cm}$
Energy: E_h (hartree) $= \hbar^2/m_\mathrm{e}a_0^2 = 27.21\,\mathrm{eV}$
Time: $\hbar/E_\mathrm{h} = 2.419 \times 10^{-17}\,\mathrm{s}$
Velocity: $a_0E_\mathrm{h}/\hbar = 2.188 \times 10^{8}\,\mathrm{cm\,s^{-1}}$

The unit mass of a.u. is:

Mass : $m_\mathrm{e} = 9.109 \times 10^{-28}\,\mathrm{g}$

and 1 amu (or u) is given by

$$1\,\mathrm{amu\ (or\ u)} = 1.823 \times 10^{3}\,\mathrm{a.u.}$$

Cross-section is expressed in the units of

$$a_0^2 = 2.800 \times 10^{-17}\,\mathrm{cm}^2.$$

C.2 Example of the Calculation of the Born Cross-Section for Rotational Transitions

Consider the electron-impact rotational transition due to the electron–dipole interaction. The Born cross-section for the transition $J_0 = 0 \rightarrow J = 1$ is given by (see (5.25))

$$Q_{\mathrm{rot}}^{\mathrm{Born,dipole}}(J = 0 \rightarrow 1) \;=\; \frac{8\pi}{3k_0^2}\,\langle M_1\rangle^2\,\ln\left|\frac{k_0 + k_1}{k_0 - k_1}\right|. \tag{C.1}$$

In atomic units, the wave numbers k_0 and k_1 are obtained from the corresponding energies in such a way

$$k_0^2 = 2E_0, \tag{C.2}$$

$$k_1^2 = 2E_1 = 2(E_0 - \Delta E(0 \rightarrow 1)). \tag{C.3}$$

To evaluate the Born cross-section, we need two molecular parameters: the transition energy $\Delta E(0 \rightarrow 1)$ and the dipole moment $\langle M_1\rangle$.

Now, as an example, we calculate the cross-section of HCl at the collision energy of 1 eV. For the molecular parameters, we take the values from Appendix B. They are

$$\Delta E(0 \rightarrow 1) = 2.589 \times 10^{-3}\,\mathrm{eV} = 9.514 \times 10^{-5}\,\mathrm{a.u.}, \tag{C.4}$$

$$\langle M_1\rangle = 1.11\,\mathrm{D} = 0.437\,\mathrm{a.u.} \tag{C.5}$$

At E_0=1 eV=3.6749×10^{-2} a.u., the relations (C.2) and (C.3) give

$$k_0 = 0.27111,$$
$$k_1 = 0.27076.$$

With the use of these values and the dipole moment (C.5), the Born cross-section is calculated to be

$$Q_{\mathrm{rot}}^{\mathrm{Born,dipole}}(J = 0 \rightarrow 1) = 1.598 \times 10^2\,\mathrm{a.u.} \tag{C.6}$$

Since 1 a.u. of the cross-section is $2.800 \times 10^{-17}\,\mathrm{cm}^2$, we finally have

$$Q_{\mathrm{rot}}^{\mathrm{Born,dipole}}(J = 0 \rightarrow 1) = 4.475 \times 10^{-15}\,\mathrm{cm}^2. \tag{C.7}$$

There are different choices of the molecular parameters. In Fig. 5.11, the Born cross-section is compared with the theoretical result of Pfingst et al. [130]. In their calculation, Pfingst et al. employed the following set

$$\Delta E(0 \to 1) = 2.627 \times 10^{-3}\,\mathrm{eV}, \tag{C.8}$$

$$\langle M_1 \rangle = 0.47827\,\mathrm{a.u.} \tag{C.9}$$

(The dipole moment was their own theoretical result.) Using these parameters, we have

$$Q_{\mathrm{rot}}^{\mathrm{Born,dipole}}(J = 0 \to 1) = 5.350 \times 10^{-15}\,\mathrm{cm}^2. \tag{C.10}$$

This is shown in Fig. 5.11 to be compared with the theoretical result of Pfingst et al.

C.3 Example of the Calculation of the Born Cross-Section for Vibrational Transitions

The Born cross-section for the vibrational transition $v_0 = 0 \to v = 1$ is given by (see (5.33))

$$Q_{\mathrm{vib}}^{\mathrm{Born,dipole}}(v = 0 \to 1) = \frac{8\pi}{3k_0^2}\,|\langle 1|M_1|0\rangle|^2\,\ln\left|\frac{k_0 + k_1}{k_0 - k_1}\right|. \tag{C.11}$$

Only the dipole interaction is considered here. Similarly to the case of rotational transition, we need two molecular parameters: the transition energy $\Delta E(v = 0 \to 1)$ and the dipole matrix element squared $|\langle 1|M_1|0\rangle|^2$.

Now, as an example, we calculate the cross-section for the transition $v = 0 \to 1$ of the IR-active mode ν_3 of CH_4. The collision energy is set to be 1 eV. We take the relevant molecular parameters from Appendix B. They are

$$\Delta E(v = 0 \to 1) = 0.374\,\mathrm{eV} = 0.0137\,\mathrm{a.u.}, \tag{C.12}$$

$$|\langle 1|M_1|0\rangle|^2 = 1.34 \times 10^{-3}\,\mathrm{a.u.} \tag{C.13}$$

At $E_0 = 1\,\mathrm{eV}$, we have from (C.2) and (C.3)

$$k_0 = 0.27111,$$
$$k_1 = 0.21450.$$

The Born cross-section for the vibrational transition is calculated to be

$$\begin{aligned} Q_{\mathrm{vib}}^{\mathrm{Born,dipole}}(v = 0 \to 1) &= 0.3283\,\mathrm{a.u.} \\ &= 9.193 \times 10^{-18}\,\mathrm{cm}^2. \end{aligned} \tag{C.14}$$

In Fig. 5.17, the Born cross-section is compared with the theoretical result of Nishimura and Gianturco [123]. Nishimura and Gianturco employed the molecular parameters obtained by themselves:

$$\Delta E(v = 0 \to 1) = 0.402\,\mathrm{eV}, \tag{C.15}$$

$$|\langle 1|M_1|0\rangle|^2 = 3.37 \times 10^{-3}\,\text{a.u.} \tag{C.16}$$

Using these values, we have

$$Q_{\text{vib}}^{\text{Born,dipole}}(v = 0 \to 1) = 2.213 \times 10^{-17}\text{cm}^2. \tag{C.17}$$

This is shown in Fig. 5.17. This cross-section is much different from the value (C.14). The difference is mainly due to the difference in the dipole matrix element used. The theoretical value of the dipole matrix element (C.16) is very large compared with the experimental value (C.13). This reflects the difficulty of the calculation of the dipole matrix element.

D

Cross-Section Sets for H_2, N_2, H_2O, and CO_2

Sets of cross-sections are shown here for the electron collisions with four representative molecules: H_2 (Fig. D.1), N_2 (Fig. D.2), H_2O (Fig. D.3), and CO_2 (Fig. D.4). Those cross-sections are taken from the data reviews: [167] for H_2, [83] for N_2, [81] for H_2O, and [78] for CO_2. Cross-sections shown are listed below. Details of each cross-section are given in the respective review papers.

1. H_2 (Fig. D.1)
   tot=total scattering cross-section ($Q_{\rm tot}$)
   elas=elastic scattering cross-section ($Q_{\rm elas}$)
   mom transf=momentum–transfer cross-section ($Q_{\rm m}$)
   rot=cross-section for rotational transition ($Q_{\rm rot}$)
   vib=cross-section for vibrational transition ($Q_{\rm vib}$)
   diss=dissociation cross-section for neutral products ($Q_{\rm dis}$)
   ion (tot)=total ionization cross-section ($Q_{\rm ion}$(tot))
   H^+=partial ionization cross-section for the production of H^+
   B, E, b=cross-sections for the excitation of electronic states $B\ ^1\Sigma_{\rm u}^+$, $E\ ^1\Sigma_{\rm g}^+$, and $b\ ^3\Sigma_{\rm u}^+$
2. N_2 (Fig. D.2)
   tot = total scattering cross-section ($Q_{\rm tot}$)
   elas = elastic scattering cross-section ($Q_{\rm elas}$)
   mom transf = momentum–transfer cross-section ($Q_{\rm m}$)
   rot = cross-section for rotational transition ($Q_{\rm rot}$)
   vib = cross-section for vibrational transition ($Q_{\rm vib}$)
   diss = dissociation cross-section for neutral products ($Q_{\rm dis}$)
   ion (tot) = total ionization cross-section ($Q_{\rm ion}$(tot))
   ion (diss) = sum of all the partial ionization cross-sections for the dissociative ionization
   B, C, a = cross-sections for the excitation of electronic states $B\ ^3\Pi_{\rm g}$, $C\ ^3\Pi_{\rm u}$, and $a\ ^1\Pi_{\rm g}$

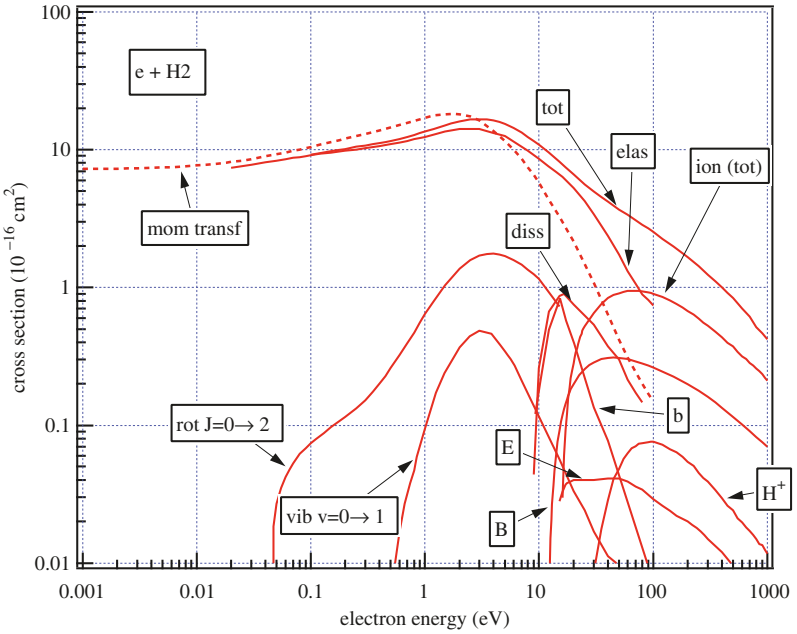

Fig. D.1. Cross-section set for e + H_2

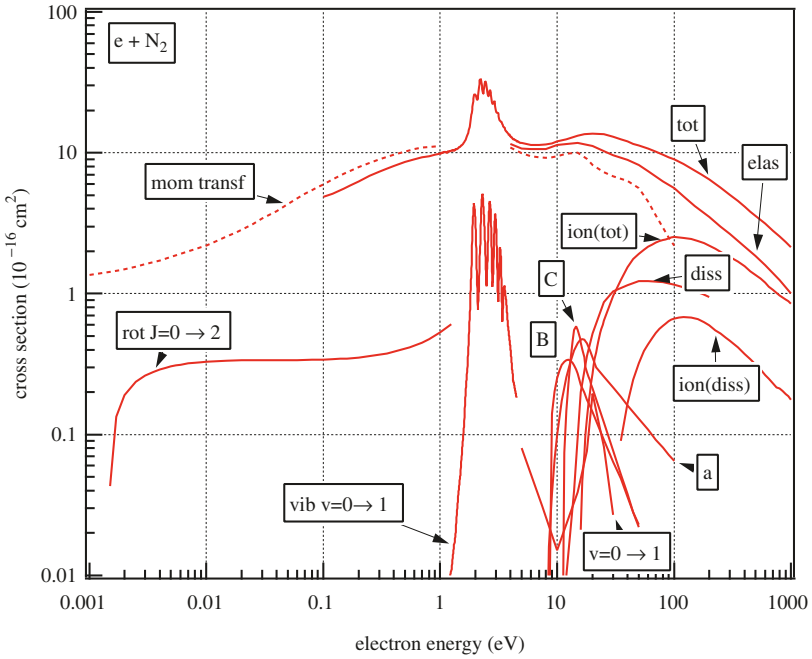

Fig. D.2. Cross-section set for e + N_2

3. H_2O (Fig. D.3)
   tot = total scattering cross-section ($Q_{\rm tot}$)
   elas = elastic scattering cross-section ($Q_{\rm elas}$)
   mom transf = momentum–transfer cross-section ($Q_{\rm m}$)
   rot = cross-section for rotational transition ($Q_{\rm rot}$)
   vib = cross-section for vibrational transition ($Q_{\rm vib}$)
      Bend is the cross-section for the first excited state of the bending mode and stretch is the sum of the corresponding cross-sections for the symmetric and antisymmetric stretching modes.
   attach = cross-section for the production of H^-
   ion (tot) = total ionization cross-section ($Q_{\rm ion}$(tot))
   OH(X) = cross-section for the production of OH(X)
   OH A–X = emission cross-section for the radiation A–X from OH
   H ($n = 2 - 1$) = emission cross-section of the Lyman α radiation from H
   H ($n = 3 - 2$) = emission cross-section of the Balmer α radiation from H
4. CO_2 (Fig. D.4)
   tot = total scattering cross-section ($Q_{\rm tot}$)
   elas = elastic scattering cross-section ($Q_{\rm elas}$)
   mom transf = momentum–transfer cross-section ($Q_{\rm m}$)

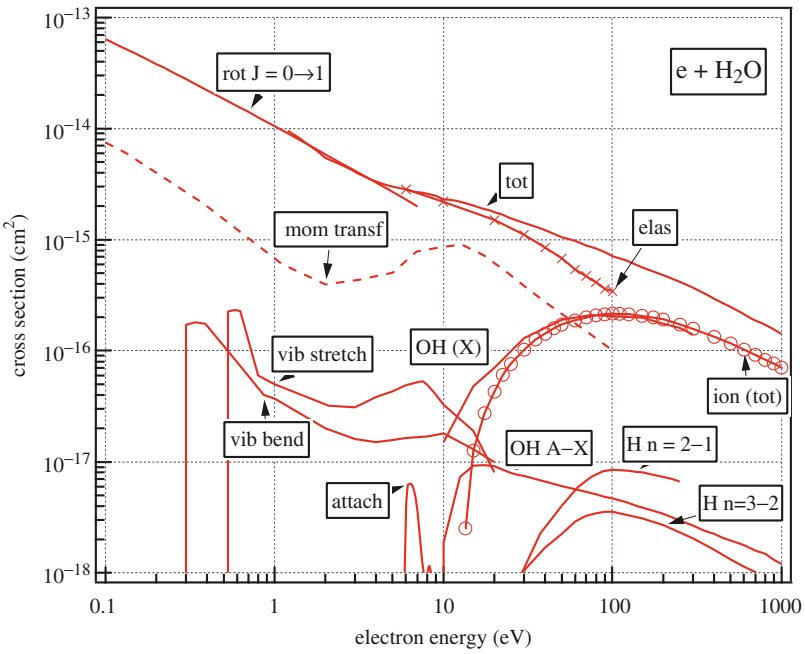

Fig. D.3. Cross-section set for e + H_2O

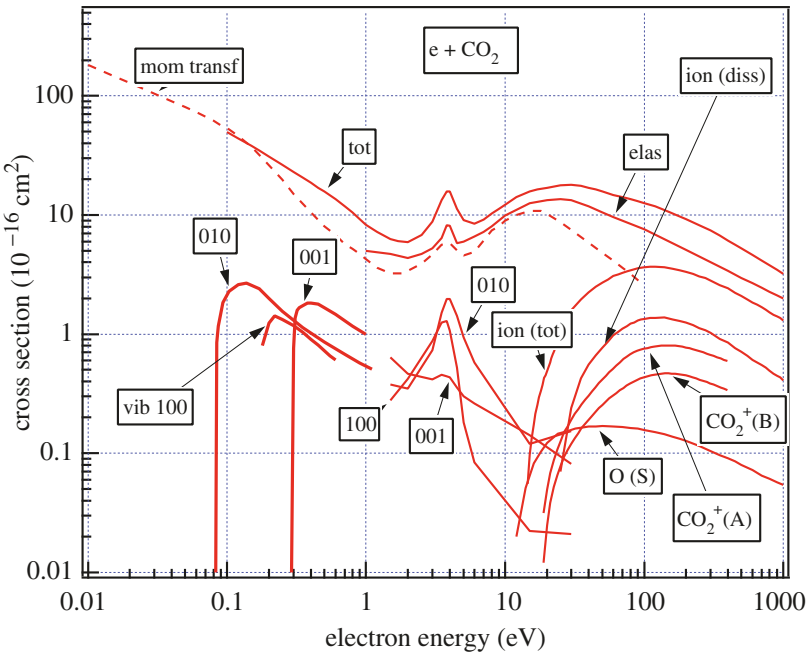

Fig. D.4. Cross-section set for e + CO_2

vib = cross-section for vibrational transition (Q_{vib})
(100), (010), and (001) are the excitation of the first excited state of symmetric, bending, and antisymmetric modes, respectively. Cross-sections below 1 eV were obtained by the method different from those above 1 eV.
ion (tot) = total ionization cross-section (Q_{ion}(tot))
ion (diss) = sum of all the partial ionization cross-sections for the dissociative ionization
O(S) = cross-section for the production of O(^{1}S)
CO_2^+ (A,B) = emission cross-sections for the radiations A–X and B–X from CO_2^+.

E

How to Find Cross-Section Data

There is no universal method to find cross-section data. Only through an extensive survey of literature, we can reach the cross-section data we want. Collision cross-sections are the basic knowledge in many fields of science and technology. They are reported in quite a wide range of literature. Cross-sections are found in papers of astrophysics, atmospheric science, atomic and molecular physics, plasma physics, nuclear fusion, gaseous electronics, physical chemistry, radiation physics and chemistry, and biological science. It is not easy, therefore, to find appropriate values of cross-sections. The following materials may help the survey of cross-section data. This is not a complete list of items useful for a data search. Depending on the subjects, there may be many other means for that.

E.1 Data Compilations in Printed Form

The simplest way to obtain cross-section data is to consult a data compilation or data book. For electron–molecule collisions, the most comprehensive compilation of cross-section data is

> Y. Itikawa, ed. Landolt-Börnstein, vol. I/17, *Photon and Electron Interactions with Atoms, Molecules and Ions*, subvolume C, *Interactions of Photons and Electrons with Molecules* (Springer, Berlin Heidelberg New York, 2003)

This volume includes numerical data on the cross-section for

> Ionization
>
> Electron attachment

Total scattering

Elastic scattering

Momentum–transfer

Excitations of rotational, vibrational, and electronic states

The recommended values of the cross-sections are tabulated for 71 molecular species, but only for the cases where reliable experimental data are available. An attached index is helpful to find the relevant data.

For diatomic molecules, another extensive data compilation is available:

M.J. Brunger, S.J. Buckman, Phys. Rep. 357, 215 (2002) Electron–molecule scattering cross-sections. I. Experimental techniques and data for diatomic molecules

This paper includes detailed information of the differential, as well as integral, cross-section for elastic scattering and various excitation processes. It also reports total scattering and momentum–transfer cross-sections, but nothing for ionization and dissociation.

An extensive data compilation was also made by Zecca et al. Their result was published in a series of papers.

A. Zecca, G.P. Karwasz, R.S. Brusa, La Rivista del Nuovo Cimento 19(3), 1 (1996) One century of experiments on electron–atom and molecule scattering: A critical review of integral cross-sections I. Atoms and diatomic molecules

G.P. Karwasz, R.S. Brusa, A. Zecca, La Rivista del Nuovo Cimento 24(1), 1 (2001) One century of experiments on electron–atom and molecule scattering: A critical review of integral cross-sections II. Polyatomic molecules

G.P. Karwasz, R.S. Brusa, A. Zecca, La Rivista del Nuovo Cimento 24(4), 1 (2001) One century of experiments on electron–atom and molecule scattering: A critical review of integral cross-sections III. Hydrocarbons and halides

These papers deal with not only diatomic but also polyatomic molecules. When no experimental data are available, the authors estimated the cross-section by a simple theory.

Other data compilations available for electron–molecule collisions are listed in Appendix F. Those for ion–molecule collisions are presented in Appendix G.

E.2 Journals Exclusively Focused on Atomic and Molecular Data

The following two journals publish papers on compilations or reviews of atomic and molecular data, including cross-sections.

> Atomic Data and Nuclear Data Tables, published bimonthly by Elsevier, Inc.
>
> and
>
> Journal of Physical and Chemical Reference Data, published quarterly by the American Institute of Physics

Through the index of papers, one can reach the data tables needed.

E.3 Online Database

Online databases for collision cross-sections are still in the developing stage. The up-to-date information about the online database is occasionally available at the International Conference on Atomic and Molecular Data and Their Applications (ICAMDATA), which is described below.

One example of the online database is available at

> National Institute for Fusion Science (NIFS), Atomic and Molecular Data Research Center, Toki, Japan (URL= http://dbshino.nifs.ac.jp/)

They maintain databases separately for electron–molecule and ion–molecule collisions. The latter is mainly concerned with charge transfer collisions. They also have a database on bibliographic information for atomic and molecular physics. Their databases can be accessed freely, but users need to register first.

International organization often offers online databases. One of them is

> International Atomic Energy Agency (IAEA), Nuclear Data Section/Atomic and Molecular Data Unit, Vienna, Austria (URL=http://www-amdis.iaea.org/)

Their databases are mainly concerned with fusion plasmas.

Both the NIFS and IAEA web sites have links to other related databases.

E.4 Review Papers

Review papers often report cross-section data. Although its coverage of data is not comprehensive, many useful information are available from those review articles. There are journals and periodic publications occasionally reporting review articles in the field of atomic and molecular physics. One of them is

Advances in the Atomic, Molecular, and Optical Physics, published every year by Academic Press

In particular, its volume 33 (published in 1994) is a special volume for atomic data. The volume was intended to provide a guide to those who need to use cross-section data. For example, the following two chapters of the volume were written directly for the purpose

J.W. Gallagher, Adv. At. Mol. Opt. Phys. vol. 33, p. 373 (1994) Guide for Users of Data Resources

E.W. McDaniel, E.J. Mansky, Adv. At. Mol. Opt. Phys. vol. 33, p. 389 (1994) Guide to Bibliographies, Books, Reviews, and Compendia of Data on Atomic Collisions

The latter paper is a continuation of the paper by the same group of authors

E.W. McDaniel, M.R. Flannery, E.W. Thomas, S.T. Manson, Atomic Data Nucl. Data Tables 33, 1 (1985) Selected Bibliography on Atomic Collisions: Data Collections, Bibliographies, Review Articles, Books, and Papers of Particular Tutorial Value

Other examples of review papers on atomic data are

W.M. Huo, Y.-K. Kim, IEEE Trans. Plasma Sci. 27, 1225 (1999) Electron Collision Cross-Section Data for Plasma Modeling

W.L. Morgan, Adv. At. Mol. Opt. Phys. vol. 43, p. 79 (2000) Electron Collision Data for Plasma Chemistry Modeling

L.G. Christophorou, J.K. Olthoff, Adv. At. Mol. Opt. Phys. vol. 44, p. 59 (2001) Electron Collision Data for Plasma-Processing Gases

Although mainly for processing plasmas, the following book reviews the electron collisions with molecules. In particular, the book gives the detailed information of the cross-section data for ten specific molecules (CF_4, C_2F_6, C_3F_8, CHF_3, CCl_2F_2, Cl_2, SF_6, CF_3I, c-C_4F_8, and BCl_3). Those information are based on the data compilations published by the authors in J. Phys. Chem. Ref. Data (see Appendix F).

L.G. Christophorou, J.K. Olthoff. Fundamental Electron Interactions with Plasma Processing Gases (Plenum Press, New York, 2004)

E.5 Conference

Since 1997, a special international conference is held every 2 or 3 years on atomic and molecular data. It is called

The International Conference on Atomic and Molecular Data and Their Applications (ICAMDATA)

It was held at

I. National Institute of Standards and Technology, Maryland, USA in 1997
II. Keble College, Oxford, UK in 2000
III. Gatlinburg, Tennessee, USA in 2002
IV. Toki, Gifu-prefecture, Japan in 2004
V. Meudon, France in 2006

Invited talks at the Conference have been published as

I. P.J. Mohr, W.L. Wiese, eds. *Atomic and Molecular Data and their Applications*, AIP Conf. Proc. 434 (American Institute of Physics, Woodbury, NY, 1998)
II. K.A. Berrington, K.L. Bell, eds. *Atomic and Molecular Data and their Applications*, AIP Conf. Proc. 543 (American Institute of Physics, Melville, NY, 2000)
III. D.R. Schultz, P.S. Krstić, F. Ownby, eds. *Atomic and Molecular Data and their Applications*, AIP Conf. Proc. 636 (American Institute of Physics, Melville, NY, 2002)
IV. T. Kato, H. Funaba, D. Kato, eds. *Atomic and Molecular Data and their Applications*, AIP Conf. Proc. 771 (American Institute of Physics, Melville, NY, 2005)
V. E. Roueff, ed. *Atomic and Molecular Data and their Applications*, AIP Conf. Proc. 901 (American Institute of Physics, Melville, NY, 2007)

F

Data Compilations for Electron–Molecule Collisions

A list of the compilations of cross-section data for electron–molecule collisions is presented here. The compilations published since 1980 are listed. The list includes only those compilations publicly available. Institution reports, for instance, are not included there. The listings are arranged in groups by year of publication and, within each group, alphabetically by the name of the first author. For readers' convenience, an index is given in Table F.1 for the principal molecules dealt with in the preceding chapters.

1. S. Trajmar, D.F. Register, A. Chutjian. Phys. Rep. 97, 219 (1983) Electron scattering by molecules II. Experimental methods and data
2. Y. Itikawa, M. Hayashi, A. Ichimura, K. Onda, K. Sakimoto, K. Takayanagi, M. Nakamura, H. Nishimura, T. Takayanagi. J. Phys. Chem. Ref. Data 15, 985 (1986) Cross-sections for collisions of electrons and photons with nitrogen molecules
3. Y. Itikawa, A. Ichimura, K. Onda, K. Sakimoto, K. Takayanagi, Y. Hatano, M. Hayashi, H. Nishimura, S. Tsurubuchi. J. Phys. Chem. Ref. Data 18, 23 (1989) Cross-sections for collisions of electrons and photons with oxygen molecules
4. H. Tawara, Y. Itikawa, H. Nishimura, M. Yoshino. J. Phys. Chem. Ref. Data 19, 617 (1990) Cross-sections and related data for electron collisions with hydrogen molecules and molecular ions
5. W.L. Morgan. Plasma Chem. Plasma Process. 12, 449 (1992) A critical evaluation of low-energy electron impact cross-sections for plasma processing modeling. I: Cl_2, F_2, and HCl
6. W.L. Morgan. Plasma Chem. Plasma Process. 12, 477 (1992) A critical evaluation of low-energy electron impact cross-sections for plasma processing modeling. II: CF_4, SiH_4, and CH_4
7. I. Kanik, S. Trajmar, J.C. Nickel. J. Geophys. Res. 98, 7447 (1993) Total electron scattering and electronic state excitations cross-sections for O_2, CO, and CH_4

Table F.1. Index by molecule

Molecule	Reference
H_2	[1, 4, 13, 27, 32]
N_2	[1, 2, 9, 13, 16, 27, 30, 32, 36, 38]
O_2	[1, 3, 7, 9, 13, 16, 27, 30, 32]
Cl_2	[5, 19, 27, 32]
CO	[1, 7, 10, 13, 26, 27, 32]
NO	[1, 13, 27, 32, 33]
HF	[1, 27, 32]
HCl	[1, 5, 24, 27, 32]
H_2O	[1, 24, 26, 32, 35]
N_2O	[1, 24, 32, 33]
CO_2	[1, 24, 26, 29, 30, 32]
O_3	[24, 32]
NH_3	[1, 24, 32]
CF_4	[6, 8, 11, 20, 25, 30, 32]
CH_4	[1, 6, 7, 24, 31, 32]
SiH_4	[6, 12, 24, 30, 32]
C_2H_4	[1, 25, 31, 32, 34]
SF_6	[1, 21, 25, 30, 32]

8. R.A. Bonham. Jpn. J. Appl. Phys. 33, 4157 (1994) Electron impact cross-section data for carbon tetrafluoride
9. Y. Itikawa. Adv. At. Mol. Opt. Phys. 33, 253 (1994) Electron collisions with N_2, O_2, and O: What we do and do not know
10. W. Liu, G.A. Victor. Astrophys. J. 435, 909 (1994) Electron energy deposition in carbon monoxide gas
11. L.G. Christophorou, J.K. Olthoff, M.V.V.S. Rao. J. Phys. Chem. Ref. Data 25, 1341 (1996) Electron interactions with CF_4
12. J. Perrin, O. Leroy, M.C. Bordage. Contrib. Plasma Phys. 36, 3 (1996) Cross-sections, rate constants and transport coefficients in silane plasma chemistry
13. A. Zecca, G.P. Karwasz, R.S. Brusa. La Rivista del Nuovo Cimento 19(3), 1 (1996) One century of experiments on electron-atom and molecule scattering: A critical review of integral cross-sections I. Atoms and diatomic molecules
14. L.G. Christophorou, J.K. Olthoff, M.V.V.S. Rao. J. Phys. Chem. Ref. Data 26, 1 (1997) Electron interactions with CHF_3
15. L.G. Christophorou, J.K. Olthoff, Y. Wang. J. Phys. Chem. Ref. Data 26, 1205 (1997) Electron interactions with CCl_2F_2

16. T. Majeed, D.J. Strickland. J. Phys. Chem. Ref. Data 26, 335 (1997) New survey of electron impact cross-sections for photoelectron and auroral electron energy loss calculations
17. L.G. Christophorou, J.K. Olthoff. J. Phys. Chem. Ref. Data 27, 1 (1998) Electron interactions with C_2F_6
18. L.G. Christophorou, J.K. Olthoff. J. Phys. Chem. Ref. Data 27, 889 (1998) Electron interactions with C_3F_8
19. L.G. Christophorou, J.K. Olthoff. J. Phys. Chem. Ref. Data 28, 131 (1999) Electron interactions with Cl_2
20. L.G. Christophorou, J.K. Olthoff. J. Phys. Chem. Ref. Data 28, 967 (1999) Electron interactions with plasma processing gases: An update for CF_4, CHF_3, C_2F_6, and C_3F_8
21. L.G. Christophorou, J.K. Olthoff. J. Phys. Chem. Ref. Data 29, 267 (2000) Electron interactions with SF_6
22. L.G. Christophorou, J.K. Olthoff. J. Phys. Chem. Ref. Data 29, 553 (2000) Electron interactions with CF_3I
23. L.G. Christophorou, J.K. Olthoff. J. Phys. Chem. Ref. Data 30, 449 (2001) Electron interactions with c-C_4F_8
24. G.P. Karwasz, R.S. Brusa, A. Zecca. La Rivista del Nuovo Cimento 24(1), 1 (2001) One century of experiments on electron-atom and molecule scattering: A critical review of integral cross-sections II. Polyatomic molecules
25. G.P. Karwasz, R.S. Brusa, A. Zecca. La Rivista del Nuovo Cimento 24(4), 1 (2001) One century of experiments on electron-atom and molecule scattering: A critical review of integral cross-sections III. Hydrocarbons and halides
26. T. Shirai, T. Tabata, H. Tawara. Atomic Data Nucl. Data Tables 79, 143 (2001) Analytic cross-sections for electron collisions with CO, CO_2, and H_2O relevant to edge plasma impurities
27. M.J. Brunger, S.J. Buckman. Phys. Rep. 357, 215 (2002) Electron–molecule scattering cross-sections. I. Experimental techniques and data for diatomic molecules
28. L.G. Christophorou, J.K. Olthoff. J. Phys. Chem. Ref. Data 31, 971 (2002) Electron interactions with BCl_3
29. Y. Itikawa. J. Phys. Chem. Ref. Data 31, 749 (2002) Cross-sections for electron collisions with carbon dioxide
30. Y. Sakai. Appl. Surface Sci. 192, 327 (2002) Database in low temperature plasma modeling
31. T. Shirai, T. Tabata, H. Tawara, Y. Itikawa. Atomic Data Nucl. Data Tables 80, 147 (2002) Analytic cross-sections for electron collisions with hydrocarbons: CH_4, C_2H_6, C_2H_4, C_2H_2, C_3H_8, and C_3H_6
32. Y. Itikawa, ed. Landolt–Börnstein, vol. I/17, *Photon and Electron Interactions with Atoms, Molecules and Ions*, subvolume C, *Interactions of Photons and Electrons with Molecules* (Springer, Berlin Heidelberg New York, 2003) (See Appendix E for details)

33. A. Zecca, G.P. Karwasz, R.S. Bursa, T. Wróblewski. Int. J. Mass Spectrom. 223–224, 205 (2003) Low–energy electron collisions in nitrogen oxides: a comparative study
34. R.K. Janev, D. Reiter Phys. Plasmas 11, 780 (2004) Collision processes of $C_{2,3}H_y$ and $C_{2,3}H_y^+$ hydrocarbons with electrons and protons
35. Y. Itikawa, N. Mason. J. Phys. Chem. Ref. Data 34, 1 (2005) Cross-sections for electron collisions with water molecules
36. Y. Itikawa. J. Phys. Chem. Ref. Data 35, 31 (2006) Cross-sections for electron collisions with nitrogen molecules
37. I. Rozum, P. Limão-Vieira, S. Eden, J. Tennyson, N.J. Mason. J. Phys. Chem. Ref. Data 35, 267 (2006) Electron interaction cross-sections for CF_3I, C_2F_4, and CF_x (x=1–3) radicals
38. T. Tabata, T. Shirai, M. Sataka, H. Kubo. Atom. Data Nucl. Data Tables 92, 375 (2006) Analytic cross-sections for electron impact collisions with nitrogen molecules

G

Data Compilations for Ion–Molecule Reactions and Related Processes

There are not so many data compilations for ion–molecule collisions, particularly those publicly available. Because of a wide variety of collision systems, it is difficult to make a comprehensive survey of the data compilations for ion collisions. Only for illustration, here we present two categories of data compilations. One is the list of papers published in J. Phys. Chem. Ref. Data and Atomic Data Nucl. Data Tables, and the other is the list of other compilations.

(I) Papers published in J. Phys. Chem. Ref. Data and Atomic Data Nucl. Data Tables
(I.1) Ion–molecule reactions

1. E.E. Ferguson. Atomic Data Nucl. Data Tables 12, 159 (1973) Rate constants of thermal energy binary ion–molecule reactions of aeronomic interest
2. D.L. Albritton. Atomic Data Nucl. Data Tables 22, 1 (1978) Ion-neutral reaction-rate constants measured in flow reactors through 1977
3. V.G. Anicich. J. Phys. Chem. Ref. Data 22, 1469 (1993) Evaluated bimolecular ion–molecule gas phase kinetics of positive ions for use in modeling planetary atmospheres, cometary comae, and interstellar clouds

(I.2) Chemical reactions of neutral species

1. D.L. Baulch, R.A. Cox, R.F. Hampson Jr., J.A. Kerr, J. Troe, R.T. Watson. J. Phys. Chem. Ref. Data 9, 295 (1980) Evaluated kinetic and photochemical data for atmospheric chemistry
   Followed by

   Supplement I. J. Phys. Chem. Ref. Data 11, 327 (1982)
   Supplement II. J. Phys. Chem. Ref. Data 13, 1259 (1984)
   Supplement III. J. Phys. Chem. Ref. Data 18, 881 (1989)

Supplement IV. J. Phys. Chem. Ref. Data 21, 1125 (1992)
Supplement V. J. Phys. Chem. Ref. Data 26, 521 (1997)
Supplement VI. J. Phys. Chem. Ref. Data 26,1329 (1997)
Supplement VII. J. Phys. Chem. Ref. Data 28, 191 (1999)
Supplement VIII. J. Phys. Chem. Ref. Data 29, 167 (2000)

2. N. Cohen, K.R. Westberg. J. Phys. Chem. Ref. Data 12, 531 (1983) Chemical kinetic data sheets for high–temperature chemical reactions
3. N. Cohen, K.R. Westberg. J. Phys. Chem. Ref. Data 20, 1211 (1991) Chemical kinetic data sheets for high–temperature chemical reactions. Part II
4. D.L. Baulch, C.J. Cobos, R.A. Cox, C. Esser, P. Frank, Th. Just, J.A. Kerr, M.J. Pilling, J. Troe, R.W. Walker, J. Warnatz. J. Phys. Chem. Ref. Data 21, 411 (1992) Evaluated kinetic data for combustion modelling
Followed by

Supplement I. J. Phys. Chem. Ref. Data 23, 847 (1994)
Supplement II. J. Phys. Chem. Ref. Data 34, 757 (2005)

(II) Others (for specific applications)

1. H. Mätzing. Adv. Chem. Phys. 80, 315 (1991) Chemical kinetics of flue gas cleaning by irradiation with electrons
2. I.A. Kossyi, A.Yu. Kostinsky, A.A. Matveyev, V.P. Silakov. Plasma Sources Sci. Technol. 1, 207 (1992) Kinetic scheme of the nonequilibrium discharge in nitrogen–oxygen mixtures
3. T.J. Millar, P.R.A. Farquhar, K. Willacy. Astron. Astrophys. Suppl. 121, 139 (1997) The UMIST database for astrochemistry 1995
4. Y.H. Le Teuff, T.J. Millar, A.J. Markwick. Astron. Astrophys. Suppl. 146, 157 (2000) The UMIST database for astrochemistry 1999
5. L.W. Sieck, J.T. Herron, D.S. Green. Plasma Chem. Plasma Process. 20, 235 (2000) Chemical kinetics database and predictive schemes for humid air plasma chemistry. Part I: Positive ion–molecule reactions

References

1. M.O. Abdellahi, El Ghazaly, J. Jureta, X. Urbain, P. Defrance, J. Phys. B **37**, 2467 (2004)
2. N. Abramzon, K.E. Martus, K. Becker, J. Chem. Phys. **113**, 2250 (2000)
3. N.G. Adams, V. Poterya, L.M. Babcock, Mass Spectrom Rev. **25**, 798 (2006)
4. M. Allan, S.F. Wong, Phys. Rev. Lett. **41**, 1791 (1978)
5. M. Allan, J. Phys. B **18**, 4511 (1985)
6. D.A. Alman, D.N. Ruzic, J.N. Brooks, Phys. Plasmas **7**, 1421 (2000)
7. P.B. Armentrout, S.M. Tarr, A. Dori, R.S. Freund, J. Chem. Phys. **75**, 2786 (1981)
8. O. Ashihara, K. Takayanagi, Planet. Space Sci. **22**, 1201 (1974)
9. M. Bacal, A. Hatakeyama, J. Peters, IEEE Trans. Plasma Sci. **33**, 1845 (2005)
10. E.M. Bahati, J.J. Jureta, D.S. Belic, S. Rachafi, P. Defrance, J. Phys. B **34**, 1757 (2001)
11. E.M. Bahati, J.J. Jureta, D.S. Belic, H. Cherkani-Hassani, M.O. Abdellahi, P. Defrance, J. Phys. B **34**, 2963 (2001)
12. K.H. Becker, M. Schmidt, A.A. Viggiano, R. Dressler, S. Williams, in *Non-Equilibrium Air Plasmas at Atmospheric Pressure*, ed. by K.H. Becker, U. Kogelschatz, K.H. Schoenbach, R.J. Barker (Institute of Physics Publishing, Bristol, 2005), p. 124
13. M. Benhenni, M. Yousfi, A. Bekstein, O. Eichwald, N. Merbahi, J. Phys. D **39**, 4886 (2006)
14. D.M. Bishop, L.M. Cheung, J. Phys. Chem. Ref. Data **11**, 119 (1982)
15. M.A. Bolorizadeh, M.E. Rudd, Phys. Rev. A **33**, 882 (1986)
16. A.L. Broadfoot, D.B. Hartfield, E.R. Anderson, T.C. Stone, B.R. Sandel, J.A. Gardner, E. Murad, D.J. Knecht, C.P. Pike, R.A. Viereck, J. Geophys. Res. **102A**, 11567 (1997)
17. M.J. Brunger, S.J. Buckman, Phys. Rep. **357**, 215 (2002)
18. M.J. Brunger, S.J. Buckman, M.T. Elford, in *Photon and Electron Interactions with Atoms, Molecules and Ions*, ed. by Y. Itikawa. Landolt– Börnstein, vol. I/17, Subvolume C (Springer, Berlin Heidelberg New York, 2003)
19. S.J. Buckman, M.J. Brunger, M.T. Elford, in *Photon and Electron Interactions with Atoms, Molecules and Ions*, ed. by Y. Itikawa. Landolt– Börnstein, vol. I/17, Subvolume C (Springer, Berlin Heidelberg New York, 2003)

20. L. Campbell, M.J. Brunger, D.C. Cartwright, P.J.O. Teubner, Planet. Space Sci. **52**, 815 (2004)
21. M. Capitelli, M. Dilonardo, C. Gorse, Chem. Phys. **56**, 29 (1981)
22. M. Capitelli, M. Cacciatore, R. Celiberto, O. De Pascale, P. Diomede, F. Esposito, A. Gicquel, C. Gorse, K. Hassouni, A. Laricchiuta, S. Longo, D. Pagano, M. Rutigliano, Nucl. Fusion **46**, S260 (2006)
23. H. Cherkani-Hassani, D.S. Belic, J.J. Jureta, P. Defrance, J. Phys. B **39**, 5105 (2006)
24. L.G. Christophorou, J.K. Olthoff, M.V.V.S. Rao, J. Phys. Chem. Ref. Data **25**, 1341 (1996)
25. L.G. Christophorou, J.K. Olthoff, J. Phys. Chem. Ref. Data **29**, 267 (2000)
26. L.G. Christophorou, J.K. Olthoff, Adv. Atom. Mol. Opt. Phys. **44**, 155 (2001)
27. A. Chutjian, A. Garscadden, J.M. Wadehra, Phys. Rep. **264**, 393 (1996)
28. R.E.H. Clark, D.H. Reiter (eds.), *Nuclear Fusion Research, Understanding Plasma– Surface Interactions* (Springer, Berlin Heidelberg New York, 2005)
29. S.J.B. Corrigan, J. Chem. Phys. **43**, 4381 (1965)
30. P.C. Cosby, J. Chem. Phys. **98**, 7804 (1993)
31. P.C. Cosby, J. Chem. Phys. **98**, 9544 (1993)
32. R.W. Crompton, Adv. Atom. Mol. Opt. Phys. **33**, 97 (1994)
33. H. Deutsch, K. Becker, S. Matt, T.D. Märk, Int. J. Mass Spectrom. **197**, 37 (2000)
34. M.T. Elford, S.J. Buckman, M.J. Brunger, in *Photon and Electron Interactions with Atoms, Molecules and Ions*, ed. by Y. Itikawa. Landolt– Börnstein, vol. I/17, Subvolume C (Springer, Berlin Heidelberg New York, 2003)
35. H.W. Ellis, R.Y. Pai, E.W. McDaniel, E.A. Mason, L.A. Viehland, Atomic Data Nucl. Data Tables **17**, 177 (1976)
36. H.W. Ellis, E.W. McDaniel, D.L. Albritton, L.A. Viehland, S.L. Lin, E.A. Mason, Atomic Data Nucl. Data Tables **22**, 179 (1978)
37. H.W. Ellis, M.G. Thackston, E.W. McDaniel, E.A. Mason, Atomic Data Nucl. Data Tables **31**, 113 (1984)
38. J.P. England, M.T. Elford, R.W. Crompton, Aust. J. Phys. **41**, 573 (1988)
39. U. Fantz, Plasma Sources Sci. Technol. **15**, S137 (2006)
40. A. Faure, J.D. Gorfinkiel, J. Tennyson, Mon. Not. R. Astron. Soc. **347**, 323 (2004)
41. H. Feng, W. Sun, M.A. Morrison, Phys. Rev. A **68**, 062709 (2003)
42. J. Ferch, W. Raith, K. Schröder, J. Phys. B **13**, 1481 (1980)
43. J. Ferch, B. Granitza, W. Raith, J. Phys. B **18**, L445 (1985)
44. J. Ferch, C. Masche, W. Raith, L. Wiemann, Phys. Rev. A **40**, 5407 (1989)
45. D.W. Flaherty, M.A. Kasper, J.E. Baio, D.B. Graves, H.F. Winters, C. Winstead, V. McKoy, J. Phys. D **39**, 4393 (2006)
46. M.R. Flannery, P.C. Cosby, T.F. Moran, J. Chem. Phys. **59**, 5494 (1973)
47. M.R. Flannery, in *Molecular Processes in Space*, ed. by T. Watanabe, I. Shimamura, M. Shimizu, Y. Itikawa (Plenum, New York, 1990), Chap. 7.
48. A.I. Florescu-Mitchell, J.B.A. Mitchell, Phys. Rep. **430**, 277 (2006)
49. L.S. Frost, A.V. Phelps, Phys. Rev. **127**, 1621 (1962)
50. W.R. Gentry, D.J. McClure, C.H. Douglass, Rev. Sci. Instrum. **46**, 367 (1975)
51. W.D. Geppert, R.D. Thomas, A. Ehlerding, F. Hellberg, F. Österdahl, M. Hamberg, J. Semaniak, V. Zhaunerchyk, M. Kaminska, A. Källberg, A. Paal, M. Larsson, J. Phys.: Conf. Ser. **4**, 26 (2005)

52. F.A. Gianturco, A. Jain, Phys. Rep. **143**, 347 (1986)
53. F.A. Gianturco, J.A. Rodrigues-Ruiz, N. Sanna, J. Phys. B **28**, 1287 (1995)
54. F.A. Gianturco, D.G. Thompson, A. Jain, in *Computational Methods for Electron–Molecule Collisions*, ed. by W.M. Huo, F.A. Gianturco (Plenum, New York, 1995), p. 75
55. F.A. Gianturco, S. Meloni, P. Paioletti, R.R. Lucchese, N. Sanna, J. Chem. Phys. **108**, 4002 (1998)
56. J.D. Gorfinkiel, L.A. Morgan, J. Tennyson, J. Phys. B **35**, 543 (2002)
57. M. Gote, H. Ehrhardt, J. Phys. B **28**, 3957 (1995)
58. P.T. Greenland, Proc. R. Soc. Lond. A **457**, 1821 (2001)
59. G.J.M. Hagelaar, L.C. Pitchford, Plasma Sources Sci. Technol. **14**, 722 (2005)
60. T. Harb, W. Kedzierski, J.W. McConkey, J. Chem. Phys. **115**, 5507 (2001)
61. G. Heiche, E.A. Mason, J. Chem. Phys. **53**, 4687 (1970)
62. E. Herbst, W. Klemperer, Astrophys. J. **185**, 505 (1973)
63. E. Herbst, Chem. Soc. Rev. **30**, 168 (2001)
64. E. Herbst, J. Phys. Chem. A **109**, 4017 (2005)
65. D. Herrebout, A. Bogaerts, M. Yan, R. Gijbels, W. Goedheer, E. Dekempeneer, J. Appl. Phys. **90**, 570 (2001)
66. G. Herzberg, *Molecular Spectra and Molecular Structure*, vol. 1, *Spectra of Diatomic Molecules*, 2nd ed. (Van Nostrand, New York, 1950)
67. G. Herzberg, *Molecular Spectra and Molecular Structure*, vol. 2, *Infrared and Raman Spectra of Polyatomic Molecules* (Van Nostrand, New York, 1945)
68. G. Herzberg, *Molecular Spectra and Molecular Structure*, vol. 3, *Electronic Spectra and Electronic Structure of Polyatomic Molecules* (Van Nostrand, New York, 1966)
69. J. Horáček, M. Čížek, K. Houfek, P. Kolorenč, W. Domcke, Phys. Rev. A **70**, 052712 (2004)
70. H. Hotop, M.-W. Ruf, M. Allan, I.I. Fabrikant, Adv. Atom. Mol. Opt. Phys. **49**, 85 (2003)
71. W. Hwang, Y.-K. Kim, M.E. Rudd, J. Chem. Phys. **104**, 2956 (1996)
72. E. Illenberger, B.M. Smirnov, Physics-Uspekhi **41**, 651 (1998)
73. M. Inokuti (ed.), *Advances in Atomic, Molecular, and Optical Physics*, vol. 33 (Academic, New York, 1994)
74. W.A. Isaacs, C.W. McCurdy, T.N. Rescigno, Phys. Rev. A **58**, 309 (1998)
75. Y. Itikawa, Phys. Fluids **16**, 831 (1973)
76. Y. Itikawa, J. Phys. Soc. Jpn. **36**, 1121 (1974)
77. Y. Itikawa, Int. Rev. Phys. Chem. **16**, 155 (1997)
78. Y. Itikawa, J. Phys. Chem. Ref. Data **31**, 749 (2002)
79. Y. Itikawa, in *Photon and Electron Interactions with Atoms, Molecules and Ions*, ed. by Y. Itikawa. Landolt–Börnstein, vol. I/17, Subvolume C (Springer, Berlin Heidelberg New York, 2003)
80. Y. Itikawa, J. Phys. B **37**, R1 (2004)
81. Y. Itikawa, N. Mason, J. Phys. Chem. Ref. Data **34**, 1 (2005)
82. Y. Itikawa, N. Mason, Phys. Rep. **414**, 1 (2005)
83. Y. Itikawa, J. Phys. Chem. Ref. Data **35**, 31 (2006)
84. M.J. Jensen, R.C. Bilodeau, C.P. Safvan, K. Seiersen, L.H. Andersen, H.B. Pedersen, O. Heber, Astrophys. J. **543**, 764 (2000)
85. C.Y. Johnson, J. Geophys. Res. **71**, 330 (1966)
86. G.P. Karwasz, R.S. Brusa, A. Zecca, La Rivista del Nuovo Cimento **24**(1), 1 (2001)

87. G.P. Karwasz, R.S. Brusa, A. Zecca, in *Photon and Electron Interactions with Atoms, Molecules and Ions*, ed. by Y. Itikawa. Landolt– Börnstein, vol. I/17, Subvolume C (Springer, Berlin Heidelberg New York, 2003)
88. R.E. Kennerly, Phys. Rev. A **21**, 1876 (1980)
89. M.A. Khakoo, S. Trajmar, Phys. Rev. A **34**, 146 (1986)
90. S.V. Khristenko, A.I. Maslov, V.P. Shevelko, *Molecules and Their Spectroscopic Properties* (Springer, Berlin Heidelberg New York, 1998)
91. Y.-K. Kim, J. Chem. Phys. **126**, 064305 (2007)
92. D. Klar, M.-W. Ruf, H. Hotop, Aust. J. Phys. **45**, 263 (1992)
93. S.I. Krasheninnikov, Phys. Scr. **T96**, 7 (2002)
94. H. Kubo, H. Takenaga, K. Sawada, T. Nakano, S. Kobayashi, S. Higashijima, N. Asakura, K. Shimizu, J. Nucl. Mater. **337–339**, 161 (2005)
95. H. Kutz, H.-D. Meyer, Phys. Rev. A **51**, 3819 (1995)
96. M. Larsson, Rep. Prog. Phys. **58**, 1267 (1995)
97. J. Lecointre, D.S. Belic, H. Cherkani-Hassani, J.J. Jureta, P. Defrance, J. Phys. B **39**, 3275 (2006)
98. J. Lecointre, D.S. Belic, J.J. Jureta, K.H. Becker, H. Deutsch, J. Limtrakul, T.D. Märk, M. Probst, P. Defrance, J. Phys. B **40**, 85 (2007)
99. J.S. Lee, J.P. Doering, T.A. Potemra, L.H. Brace, Planet. Space Sci. **28**, 947 (1980)
100. M.A. Lieberman, A.J. Lichtenberg, *Principles of Plasma Discharges and Materials Processing* (Wiley, New York, 1994)
101. F. Linder, R.K. Janev, J. Botero, in *Atomic and Molecular Processes in Fusion Edge Plasmas*, ed. by R.K. Janev (Plenum, New York, 1995), p. 397
102. W. Lindinger, A. Hansel, Z. Herman, Adv. Atom. Mol. Opt. Phys. **43**, 243 (2000)
103. B.G. Lindsay, M.A. Mangan, in *Photon and Electron Interactions with Atoms, Molecules and Ions*, ed. by Y. Itikawa. Landolt–Börnstein, vol. I/17, Subvolume C (Springer, Berlin Heidelberg New York, 2003)
104. X. Liu, D.E. Shemansky, S.M. Ahmed, G.K. James, J.M. Ajello, J. Geophys. Res. **103**, 26739 (1998)
105. C. Makochekanwa, K. Oguri, R. Suzuki, T. Ishihara, M. Hoshino, M. Kimura, H. Tanaka, Phys. Rev. A **74**, 042704 (2006)
106. A. Mann, F. Linder, J. Phys. B **25**, 533 (1992)
107. E.A. Mason, E.W. McDaniel, *Transport Properties of Ions in Gases* (Wiley, New York, 1988)
108. M. McFarland, D.L. Albritton, F.C. Fehsenfeld, E.E. Ferguson, A.L. Schmeltekopf, J. Geophys. Res. **79**, 2925 (1974)
109. P. McNaughten, D.G. Thompson, A. Jain, J. Phys. B **23**, 2405S (1990)
110. R.R. Meier, Space Sci. Rev. **58**, 1 (1991)
111. L. Mi, R.A. Bonham, J. Chem. Phys. **108**, 1904 (1998)
112. L. Mi, R.A. Bonham, J. Chem. Phys. **108**, 1910 (1998)
113. T.J. Millar, P.R.A. Farquhar, K. Willacy, Astron. Astrophys. Suppl. **121**, 139 (1997)
114. T.F. Moran, K.J. McCann, M.R. Flannery, J. Chem. Phys. **63**, 3857 (1975)
115. M.A. Morrison, R.W. Crompton, B.C. Saha, Z.L. Petrovic, Aust. J. Phys. **40**, 239 (1987)
116. K. Motohashi, H. Soshi, M. Ukai, S. Tsurubuchi, Chem. Phys. **213**, 369 (1996)
117. N.F. Mott, H.S.W. Massey, *The Theory of Atomic Collisions*, 3rd ed. (Oxford University Press, Oxford, 1965)

118. R. Müller, K. Jung, K.-H. Kochem, W. Sohn, H. Ehrhardt, J. Phys. B **18**, 3971 (1985)
119. A. Neau, A. Al Khalili, S. Rosén, A. Le Padellec, A.M. Derkatch, W. Shi, L. Vikor, M. Larsson, J. Semaniak, R. Thomas, M.B. Någård, K. Andersson, H. Danared, M. af Ugglas, J. Chem. Phys. **113**, 1762 (2000)
120. D. Nelson, M. Benhenni, M. Yousfi, O. Eichwald, J. Phys. D **34**, 3247 (2001)
121. D. Nelson, M. Benhenni, O. Eichwald, M. Yousfi, J. Appl. Phys. **94**, 96 (2003)
122. B.J. Nichols, F.C. Witteborn, Measurements of Resonant Charge Exchange Cross-Sections in Nitrogen and Argon between 0.5 and 17 eV, NASA Technical Note, NASA TN D-3265 (1966)
123. T. Nishimura, F.A. Gianturco, J. Phys. B **35**, 2873 (2002)
124. T.F. O'Malley, L. Rosenberg, L. Spruch, Phys. Rev. **125**, 1300 (1962)
125. T.F. O'Malley, Phys. Rev. **130**, 1020 (1963)
126. K. Onda, M. Ejiri, Y. Itikawa, J. Geophys. Res. **104**, 27991 (1999)
127. C.B. Opal, W.K. Peterson, E.C. Beaty, J. Chem. Phys. **55**, 4100 (1971)
128. C.B. Opal, E.C. Beaty, W.K. Peterson, Atomic Data **4**, 209 (1972)
129. Z.Lj. Petrović, W.C. Wang, L.C. Lee, J. Appl. Phys. **64**, 1625 (1988)
130. K. Pfingst, H.T. Thümmel, S.D. Peyerimhoff, J. Phys. B **25**, 2107 (1992)
131. R.A. Phaneuf, C.C. Havener, G.H. Dunn, A. Müller, Rep. Prog. Phys. **62**, 1143 (1999)
132. A.V. Phelps, L.C. Pitchford, Phys. Rev. A **31**, 2932 (1985)
133. A.V. Phelps, J. Phys. Chem. Ref. Data **19**, 653 (1990)
134. A.V. Phelps, J. Phys. Chem. Ref. Data **20**, 557 (1991)
135. I. Rabadán, J. Tennyson, J. Phys. B **32**, 4753 (1999)
136. M. Rädle, G. Knoth, K. Jung, H. Ehrhardt, J. Phys. B **22**, 1455 (1989)
137. F.H. Read, J.M. Channing, Rev. Sci. Instrum. **67**, 2372 (1996)
138. A.G. Robertson, M.T. Elford, R.W. Crompton, M.A. Morrison, W. Sun, W.K. Trail, Aust. J. Phys. **50**, 441 (1997)
139. I. Røeggen, H.R. Skullerud, T.H. Løvaas, D.K. Dysthe, J. Phys. B **35**, 1707 (2002)
140. B.K. Sarpal, J. Tennyson, Mon. Not. R. Astron. Soc. **263**, 909 (1993)
141. K. Sawada, T. Fujimoto, J. Appl. Phys. **78**, 2913 (1995)
142. G.J. Schulz, Phys. Rev. **135**, A988 (1964)
143. G.J. Schulz, Rev. Mod. Phys. **45**, 423 (1973)
144. R.W. Schunk, A.F. Nagy, *Ionospheres* (Cambridge University Press, Cambridge, 2000)
145. C.H. Sheehan, J.-P. St.-Maurice, J. Geophys. Res. **109**, A03302 (2004)
146. M. Shimoi, Y. Itikawa, J. Phys. B **32**, 65 (1999)
147. T. Šimko, V. Martišovitš, J. Bretagne, G. Gousset, Phys. Rev. E **56**, 5908 (1997)
148. B.M. Smirnov, *Physics of Ionized Gases* (Wiley, New York, 2001)
149. P.C. Stancil, S. Lepp, A. Dalgarno, Astrophys. J. **509**, 1 (1998)
150. R.F. Stebbings, B.R. Turner, A.C.H. Smith, J. Chem. Phys. **38**, 2277 (1963)
151. C. Szmytkowski, S. Kwitnewski, E. Ptasinska-Denga, Phys. Rev. A **68**, 032715 (2003)
152. T. Tabata, T. Shirai, Atomic Data Nucl. Data Tables **76**, 1 (2000)
153. K. Tachibana, M. Nishida, H. Harima, Y. Urano, J. Phys. D **17**, 1727 (1984)
154. K. Takayanagi, Y. Itikawa, Adv. Atom. Mol. Phys. **6**, 105 (1970)
155. K. Takayanagi, Y. Itikawa, Space Sci. Rev. **11**, 380 (1970)

156. J. Tennyson, in *Handbook of Molecular Physics and Quantum Chemistry*, ed. by S. Wilson, vol. 3 (Wiley, Chichester, 2003), p. 356
157. P.A. Thorn, M.J. Brunger, P.J.O. Teubner, N. Diakomichalis, T. Maddern, M.A. Bolorizadeh, W.R. Newell, H. Kato, M. Hoshino, H. Tanaka, H. Cho, Y.-K. Kim, J. Chem. Phys. **126**, 064306 (2007)
158. P.A. Thorn, M.J. Brunger, H. Kato, M. Hoshino, H. Tanaka, J. Phys. B **40**, 697 (2007)
159. C. Tian, C.R. Vidal, J. Phys. B **31**, 5369 (1998)
160. C. Tian, C.R. Vidal, Phys. Rev. A **59**, 1955 (1999)
161. S. Trajmar, J.W. McConkey, Adv. Atom. Mol. Opt. Phys. **33**, 63 (1994)
162. A. Vallance Jones, R.L. Gattinger, J. Geomagn. Geoelectr. **42**, 1385 (1990)
163. R.J. Vidmar, IEEE Trans. Plasma Sci. **18**, 733 (1990)
164. A.A. Viggiano, R.A. Morris, J. Phys. Chem. **100**, 19227 (1996)
165. H.F. Winters, J. Chem. Phys. **44**, 1472 (1966)
166. J. Wrkich, D. Mathews, I. Kanik, S. Trajmar, M.A. Khakoo, J. Phys. B **35**, 4695 (2002)
167. J.-S. Yoon, M.-Y. Song, J.-M. Han, S.H. Hwang, W.-S. Chang, B.J. Lee, Y. Itikawa, submitted to J. Phys. Chem. Ref. Data (2007)

Index

Springer Series on

ATOMIC, OPTICAL, AND PLASMA PHYSICS

Springer Series on

ATOMIC, OPTICAL, AND PLASMA PHYSICS

10 **Film Deposition by Plasma Techniques**
By M. Konuma

11 **Resonance Phenomena in Electron–Atom Collisions**
By V.I. Lengyel, V.T. Navrotsky, and E.P. Sabad

12 **Atomic Spectra and Radiative Transitions**
2nd Edition
By I.I. Sobel'man

13 **Multiphoton Processes in Atoms**
2nd Edition
By N.B. Delone and V.P. Krainov

14 **Atoms in Plasmas**
By V.S. Lisitsa

15 **Excitation of Atoms and Broadening of Spectral Lines**
2nd Edition, By I.I. Sobel'man, L. Vainshtein, and E. Yukov

16 **Reference Data on Multicharged Ions**
By V.G. Pal'chikov and V.P. Shevelko

17 **Lectures on Non-linear Plasma Kinetics**
By V.N. Tsytovich

18 **Atoms and Their Spectroscopic Properties**
By V.P. Shevelko

19 **X-Ray Radiation of Highly Charged Ions**
By H.F. Beyer, H.-J. Kluge, and V.P. Shevelko

20 **Electron Emission in Heavy Ion–Atom Collision**
By N. Stolterfoht, R.D. DuBois, and R.D. Rivarola

21 **Molecules and Their Spectroscopic Properties**
By S.V. Khristenko, A.I. Maslov, and V.P. Shevelko

22 **Physics of Highly Excited Atoms and Ions**
By V.S. Lebedev and I.L. Beigman

23 **Atomic Multielectron Processes**
By V.P. Shevelko and H. Tawara

24 **Guided-Wave-Produced Plasmas**
By Yu.M. Aliev, H. Schlüter, and A. Shivarova

25 **Quantum Statistics of Nonideal Plasmas**
By D. Kremp, M. Schlanges, and W.-D. Kraeft

26 **Atomic Physics with Heavy Ions**
By H.F. Beyer and V.P. Shevelko

27 **Quantum Squeezing**
By P.D. Drumond and Z. Ficek

28 **Atom, Molecule, and Cluster Beams I**
Basic Theory, Production and Detection of Thermal Energy Beams
By H. Pauly

29 **Polarization, Alignment and Orientation in Atomic Collisions**
By N. Andersen and K. Bartschat

30 **Physics of Solid-State Laser Physics**
By R.C. Powell
(Published in the former Series on Atomic, Molecular, and Optical Physics)

31 **Plasma Kinetics in Atmospheric Gases**
By M. Capitelli, C.M. Ferreira, B.F. Gordiets, A.I. Osipov

32 **Atom, Molecule, and Cluster Beams II**
Cluster Beams, Fast and Slow Beams, Accessory Equipment and Applications
By H. Pauly

33 **Atom Optics**
By P. Meystre

34 **Laser Physics at Relativistic Intensities**
By A.V. Borovsky, A.L. Galkin, O.B. Shiryaev, T. Auguste

35 **Many-Particle Quantum Dynamics in Atomic and Molecular Fragmentation**
Editors: J. Ullrich and V.P. Shevelko